HYDROGEN FUELLING

OF AN

INTERNAL COMBUSTION ENGINE

A thesis submitted for the Degree of

Doctor of Philosophy

by

Neil Glasson

Department of Mechanical Engineering

University of Canterbury

Christchurch

NEW ZEALAND

1992

To Mum and Dad

RELATED PUBLICATIONS

The following papers were published during the course of this investigation.

GREEN, R.K. GLASSON, N.D. Direct injector development for hydrogen fuelled internal combustion engines. *Proceedings of the 8th World Hydrogen Energy Conference.* **vol.3** 1990. pp.1285-1294.

GLASSON, NEIL. GREEN, ROGER. TINNION, GREGORY. Hydrogen - a future transport fuel for New Zealand. *Choosing the Future. Proceedings - annual conference, The Institute of Professional Engineers New Zealand.* **vol.2** 1991. pp.227-238.

GLASSON, NEIL. GREEN, ROGER. High pressure hydrogen injection. *Proceedings of the 9th World Hydrogen Energy Conference.* **vol.2** 1992. pp.1285-1294.

GREEN, R.K. GLASSON, N.D. High-pressure hydrogen injection for internal combustion engines. *International Journal of Hydrogen Energy.* **vol.17 no.11** 1992. pp.895-901.

CONTENTS

LIST OF FIGURES

LIST OF PLATES

LIST OF TABLES

ABSTRACT

This thesis traces and critically reviews recent developments in hydrogen fuelling of internal combustion engines. It reports the development of an improved fuelling system that has been tested on a Ricardo E6 variable compression spark ignition engine, in the Thermodynamics laboratory, Department of Mechanical Engineering at the University of Canterbury.

The introduction of hydrogen to an internal combustion engine via the inlet manifold (external mixture formation), often results in the occurrence of pre-ignition. This is because hydrogen, with its low ignition energy and extreme lean limit of flammability, is easily ignited by residual gases or hot spots in an engine cylinder. If pre-ignition occurs before inlet valve closure, the mixture may burn back through pre-mixed gases in the inlet manifold. Another serious disadvantage with external mixture formation is that hydrogen displaces a large volume of air, effectively reducing the volumetric efficiency of the engine.

To overcome these problems hydrogen may be injected directly into an engine combustion chamber during the compression stroke, although if injection commences too early in the stroke pre-ignition may still occur. It is thus considered that the most desirable system for fuelling an internal combustion

engine on hydrogen is to employ direct gaseous injection at high pressure late in the compression stroke.

There are a number of problems involved with the design and development of a suitable high pressure hydrogen direct injector. In particular the injector must actuate rapidly and be controllable to a high degree of accuracy to consistently meter precise quantities of fuel at each injection. Leakage of hydrogen through the injector when closed must be minimised in order to avoid unnecessary fuel wastage and to prevent the build up of a flammable pre-mixed mixture that could lead to pre-ignition.

A suitable injector has been designed and tested. The injector is electro-magnetically actuated for electronic control of injection timing and duration (control of injection duration being necessary to vary the quantity of fuel delivered). The injector has a nominal lift distance of 0.2 mm and can be opened for durations as short as 1 ms. A fluorocarbon elastomer Quad-ring was used in the seat of the valve to provide a leak free seal for the high pressure hydrogen.

Engine testing was conducted to determine the performance of the valve. The engine was tested on hydrogen for compression ratios of 8:1, 10:1 and 12:1 over a range of operating conditions. Results of engine performance, complete with combustion chamber pressure traces and exhaust gas emission analysis are presented.

The design concept has proven to be successful with satisfactory operation of the engine on hydrogen without any combustion related problems. The elastomeric seal, although providing leak free operation, had an average lifetime of about 30 minutes. Future injector development work should focus on devising a highly durable injector seat seal which minimises leakage.

NOMENCLATURE

ATDC	After top dead centre
A/D	Analogue to digital
A/F	Air to fuel ratio
A/F_{stoic}	Stoichiometric air to fuel ratio
AWG	American wire gauge
BDC	Bottom dead centre
BP	Brake power
$BP_{corrected}$	Brake power corrected for ambient temperature and barometric pressure
BTDC	Before top dead centre
CA_{inj}	Length of injection in degrees of crank angle
CNG	Compressed natural gas
CO	Carbon monoxide
CO_2	Carbon dioxide
dc	Direct current
EGR	Exhaust gas recirculation
e.m.f.	Electro-motive force
$F_{pre\text{-}load}$	Pre-load force holding valve open
GH_2	Gaseous hydrogen
H_2	Hydrogen
H_2O_2	Hydrogen peroxide

HC	Unburnt hydrocarbons
LH_2	Liquid hydrogen
LPG	Liquified petroleum pas
MH_2	Hydrogen stored in metal hydride
MOSFET	Metal oxide semiconductor field effect transistor
MBT	Minimum advance for best torque
mfr_{air}	Mass flow rate of air
mfr_{inj}	Mass flow rate of fuel during the injection
mfr_{fuel}	Mass flow rate of fuel
mpc_{fuel}	Mass of fuel required per firing cycle
NO_x	Oxides of nitrogen NO and NO_2
NTP	Normal temperature and pressure
P	Pressure
$P_{barometric}$	Barometric pressure
PEI	Polyether imide
$\Delta P_{snapshut}$	Pressure differential at which valve snaps shut
PTFE	Polytetrafluoroethylene (Teflon)
PVT	Pressure, volume and temperature
R	Gas constant
SOS	Slotted optical switch
T	Temperature
$T_{ambient}$	Ambient temperature
TDC	Top dead centre
WOT	Wide open throttle

bsfc	Brake specific fuel consumption
ppm	Parts per million
rpm	Revolutions per minute
rps	Revolutions per second
V	Volts or volume
v	Specific volume
vfr_{air}	Volume flow rate of air
vol.	On a volume basis
vpc_{air}	Volume of air (at NTP) induced per firing cycle
γ	Ratio of specific heats c_p/c_v
η_{bt}	Brake thermal efficiency
λ	Relative air fuel ratio = (Actual air delivered)/(Stoichiometric air requirement)

CHAPTER 1 INTRODUCTION

1.1 Hydrogen as an energy carrier

Hydrogen is considered by many researchers to be the ideal energy carrier of the future[1,2,3,4]. That is, hydrogen can be utilised as the medium for storing and distributing energy for final use in a wide variety of applications. The range of production, storage, distribution and utilisation strategies that have been investigated in recent years has been extremely diverse, indicating the tremendous scope for hydrogen as an energy carrier [5,6].

There are many advantages to be gained from the application of hydrogen as an energy carrier. The three major advantages are:

a. Hydrogen is an environmentally friendly fuel. Utilisation of hydrogen as a fuel liberates mainly water. Hydrogen, produced from water, thus represents a closed cycle energy carrier system. When hydrogen is burnt in air, the only potentially harmful pollutants are oxides of nitrogen (NO_x) and hydrogen peroxide (H_2O_2). Attention to the design of hydrogen utilisation systems can minimise or eliminate the production of these pollutants.

b. Hydrogen can be produced from water and any primary energy source. Hydrogen can therefore be manufactured independent of supplies of non-renewable primary energy sources (petroleum, coal, natural gas, nuclear energy). Renewable energy sources (solar, wind, hydro-electric, ocean) used to produce hydrogen from water represent a potentially sustainable source of fuel for the future.

c. Hydrogen can be used as a means of storing energy, thereby providing a buffer between energy production and demand. This is particularly significant for those primary energy sources where there are problems in matching production to demand. For example, hydrogen from solar energy could be stored in a distribution pipeline for utilisation during times when fuel demand exceeds possible production.

Opponents of the developing concept of large scale use of hydrogen as an energy carrier, cite safety problems and the shorter term alternative energies which can be used before any transition to hydrogen is necessary.

Hydrogen is hazardous by definition of being a fuel. But it has been demonstrated that hydrogen can be handled safely, comparing well with other fuels[7].

The fuels which are likely to become more dominant before hydrogen is accepted as a future fuel are natural gas, coal and the alcohols (ethanol and methanol).

All of these shorter term alternatives produce polluting exhaust emissions. Natural gas and coal are subject to depletion in the long term. Coal requires expensive refining in order to be suitable for transport fuelling applications. The manufacture of methanol currently relies on carbon based fuel feedstocks which are liable to become depleted in the future. Methanol produced from biomass and ethanol production require the use of land that may otherwise be devoted to growing food crops.

Having recognised a perceived need for the transition to a hydrogen based energy system, the task remains to develop the required technology to a standard whereby transition to hydrogen may be carried out when required, as a result of economic, social, technological or political changes. Research has been conducted into many aspects of the proposed 'hydrogen economy' [†,8]. One area that has received much attention is the use of hydrogen as an automotive fuel.

1.2 Introduction to the investigation

The purpose of this study is to investigate the use of hydrogen as a fuel for internal combustion engines. The major application in terms of which the topic

---

† 'Hydrogen economy' is a phrase which arose in the early 1970's to describe the future large scale use of hydrogen as a means of storing and transporting energy.

is discussed is with regard to automotive power. The requirements of the hydrogen fuelled automotive internal combustion engine include high engine performance, low emission levels, moderate capital cost, long life, good reliability and driveability (the ability to be controlled accurately and responsively under different operating conditions). Implicit under the term "engine performance" is the desirable feature of good low load operation. This is because automotive engines typically spend a large proportion of their operating life at part load (cruising, idling or decelerating). In this study the emphasis is on the performance and exhaust emission characteristics of a hydrogen engine operated over a range of loads.

This investigation has lead to the operation of a spark ignited internal combustion engine on hydrogen. The initial emphasis of the thesis was to investigate the use of high pressure direct injection of hydrogen into the combustion chamber late in the compression stroke. This method was considered the best approach in terms of power, efficiency and elimination of hydrogen related combustion problems.

In the development of an experimental fuelling system for a hydrogen internal combustion engine, it is important to realise that there are many features of present day engines, designed to run on gasoline or diesel, that may not be ideal when fuelling with hydrogen. For example, with the late injection of hydrogen it may be desirable to employ a higher level of turbulence in the combustion chamber to ensure adequate mixing of injected hydrogen with the induced air.

Although this project clearly shows the applicability of direct injection of hydrogen for an internal combustion engine, future internal combustion engines designed specifically for hydrogen may well provide greatly enhanced performance.

CHAPTER 2 LITERATURE REVIEW OF HYDROGEN AS A FUTURE FUEL

2.1 Hydrogen fuel and atmospheric pollution

There are many adverse effects of emissions from large scale fossil fuel combustion. The three main areas of concern are health problems due to urban smog[9], regional acid precipitation[10] and on a global scale the possible increase in the average temperature of the earths atmosphere (the enhanced greenhouse effect[11]). In 1990 it was estimated that the damage caused by the world-wide consumption of fossil fuels amounted to more than US$460 per capita each year[12].

The utilization of hydrogen as a fuel produces none of the carbon or sulphur based pollutants which are emitted by fossil fuel combustion[†] (no unburnt hydrocarbons, carbon monoxide, carbon dioxide, sulphur dioxide or particulate matter). If hydrogen (produced from clean energy sources) were to displace fossil fuels as the major form of energy then the adverse effects of fossil fuel use could be greatly reduced[10,13,14,15]. Plass *et al*[16] suggest that by the year 2000 hydrogen (produced from solar energy) may become cost competitive with

---

† If the utilization system consumes lubricating oil, then small levels of carbon based emissions may be apparent. The current discussion is considering the consumption of hydrogen and air only.

gasoline as a fuel for surface transportation. This study was based on the combined costs of the environmental and societal impact of the production and burning of fuel.

Although hydrogen utilisation produces none of the carbon or sulphur based pollutants it can produce harmful emissions of oxides of nitrogen (NO_x) and hydrogen peroxide (H_2O_2).

2.1.1 Oxides of nitrogen (NO_x)

When hydrogen is burnt in air the main pollutant that can result is nitric oxide (NO)[17]. In atmospheric reactions the nitric oxide is oxidised to form nitrogen dioxide (NO_2). These two main nitrogen oxide pollutants are described collectively as NO_x[18]. The emission of NO_x has become recognised as a major factor in the formation of photochemical smog[19].

The formation of nitric oxide from nitrogen and oxygen has been studied in detail and is quite well understood[19]. Nitric oxide formation is usually considered to proceed mainly by the following reactions (known as the extended Zeldovich mechanism):

$$O_2 \rightleftharpoons 2O \qquad (2.1)$$

$$O + N_2 \rightleftharpoons NO + N \qquad (2.2)$$

$$N + O_2 \rightleftharpoons NO + O \qquad (2.3)$$

$$NO + OH \rightleftharpoons NO + H \qquad (2.4)$$

This mechanism and various enhancements of it have been used to predict the concentration of NO in exhaust emissions[19]. From experimental and theoretical investigations, Newhall and Shahed[20] concluded that NO formation from high pressure hydrogen air flames occurs largely as a result of post-flame reactions and that NO formation is thus well represented by Equations (2.2) and (2.3) only. The reaction in Equation (2.2) requires a lot of energy to break the strong nitrogen bond. This reaction is highly temperature dependant and is thought to limit the rate of formation of NO[18]. The reverse reactions occur at a very much slower rate than the forward reactions. NO is formed at high temperature, and if rapidly cooled the reverse reactions have insufficient time for completion. The factors favouring the emission of nitric oxide are:

a. ample quantities of reactants (oxygen and nitrogen)

b. high temperature and sufficient time to form NO

c. rapid cooling from the high temperature, halting the reverse reactions and "freezing out" NO

For most hydrogen fuelled systems it is impractical to use pure oxygen instead of air as the oxidiser. In order to minimise NO emissions the temperature must be low and/or cooling must be at a slow rate. Some hydrogen fuelled systems operate at sufficiently low temperatures to preclude the formation of NO (catalytic burners[17] and low temperature fuel cells[1]). Hydrogen fuelled internal combustion engines may be operated very lean (reducing the peak temperature) to produce negligible NO[21].

2.1.2 Hydrogen peroxide (H_2O_2)

In 1974 Griffith[22] demonstrated that hydrogen peroxide could be present in the exhaust gases of a hydrogen fuelled engine. Hydrogen peroxide is highly toxic[23] and can form hydroxyl radicals in the atmosphere which react with NO in the formation of photochemical smog[24].

The claims of Griffith have been largely discredited due to the method used to measure the level of hydrogen peroxide. Griffith used a potassium permanganate ($KMnO_4$) titration to measure the concentration of hydrogen peroxide in an exhaust. Swain *et al*[25] describe their earlier work[26] in which they demonstrated that potassium permanganate is also affected by nitric oxide. The use of potassium permanganate to determine the concentration of hydrogen peroxide in the exhaust is thus prone to error due to the possible presence of nitric oxide. Studies which have more reliably measured hydrogen peroxide [24,25] (with a

phenol-ferrous sulphate titration) demonstrate that emissions of hydrogen peroxide correlated well with emissions of unburnt hydrogen. A system which is designed to use hydrogen efficiently will produce little or no unburnt hydrogen or hydrogen peroxide[25].

2.2 Production of hydrogen

Hydrogen is easily produced in school classrooms by electrolysis of water, using a Hofmann voltameter[27]. Students learn from this simple experiment that water is made up of two parts hydrogen and one part oxygen[28]. Hydrogen exists in abundance in nature but being very reactive it seldom appears naturally as pure hydrogen gas[29]. For hydrogen to be considered as a viable alternative fuel for the future the technology to economically produce pure hydrogen must be developed.

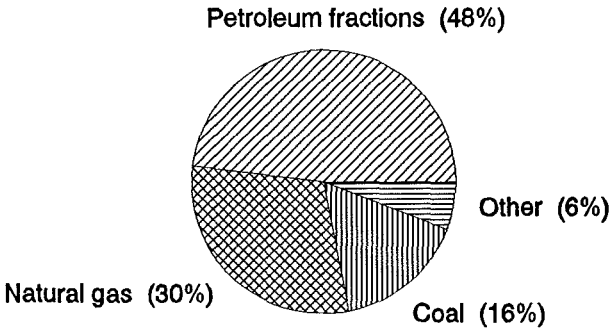

Figure 2.1 Current worldwide hydrogen production from various primary energy sources.

Much of the hydrogen currently used is produced commercially from fossil fuels as shown in Figure 2.1[30]. There are numerous processes for the production of hydrogen from fossil fuels[31]. They typically involve the high temperature chemical splitting of water to form hydrogen and carbon monoxide or carbon dioxide[30]. The basic reactions involved are:

$$CH_4 + H_2O \rightarrow CO + 3H_2 \qquad (2.5)$$

$$CO + H_2O \rightarrow CO_2 + H_2 \qquad (2.6)$$

If the future hydrogen economy is to reduce carbon based gaseous emissions, the hydrogen must either be produced independently of carbon based fuels, or from carbon based fuels using 'clean' technologies. A number of recent studies have considered strategies for producing hydrogen from hydrocarbon fuels with low or zero emissions of carbon dioxide to the atmosphere[32,33].

The production of hydrogen from water using electricity as the primary energy source accounts for less than 1% of the worldwide market share[30]. There are two main processes for the production of hydrogen by electrolysis.

a. Electrolysis of brine

In this process an electric current is passed through an aqueous solution of sodium chloride to produce hydrogen and chlorine gases[34]. Currently the chlorine produced by this process is often the desired product with hydrogen being a by-product. The brine solution gradually

turns to sodium hydroxide, another useful by-product. The hydrogen and chlorine from the electrolysis of brine is often used to produce hydrochloric acid. Tennaknoe[35] introduces a modification to this process for the possible large scale production of hydrogen.

b. Electrolysis of water†

Hydrogen and oxygen are produced by passing a current through an electrolyte solution. This is the most ideal of current technologies for the large scale production of hydrogen. If the electricity used is produced from clean, renewable energy sources then the production of the hydrogen involves no emissions of pollutants. Winter and Fuchs[36] describe a number of hydrogen production projects where solar energy is used to produce the electricity required for electrolysis.

Many different scenarios have been considered for the large scale production of hydrogen for use as a fuel. One of the more ambitious studies considers the floating of solar hydrogen production platforms on the oceans. Escher[37] suggests that in the extreme case, the projected total world energy demand for the year 2000 could be met using 22100 $1km^2$, floating modules. These hydrogen production platforms would be located near the equator for the highest solar irradiance and the resultant hydrogen and oxygen could be shipped as liquids to the worldwide energy markets[38]. A similar concept has been studied by Hiraoka

---

† The hydrogen used for this project was supplied from New Zealand Industrial Gases, and was produced from water by electrolysis. The composition of the hydrogen supplied was specified as 99.8% H_2, <0.1% O_2, <0.1% N_2 and smaller amounts of CO, CO_2 and water.

et al[39,40] for the supply of liquid hydrogen to replace all the petroleum used for transportation in Japan. The proposed system was evaluated in terms of petroleum conservation and CO_2 emission. It was assumed that the system would be implemented using conventional energy sources. The conclusions reached by Hiraoka *et al* were that at the present time the system would consume more conventional energies than does the current petroleum energy system. They predict that future technologies would enable the system to conserve conventional energies and reduce CO_2 emissions.

A recent feasibility study on the production and transmission of hydrogen over long distances has been carried out in the Euro-Quebec Hydro-Hydrogen Pilot Project (EQHHPP)[41]. This comprehensive project proposes the production of hydrogen in Quebec by electrolysis using hydro-electric power. The hydrogen would be shipped to Europe as either liquid hydrogen or bound chemically as methylcyclohexane. In Europe it is proposed that the hydrogen would be used to fuel a bus fleet, airbus service, and electricity cogeneration. This pilot project is ongoing[42,43].

German aerospace (DFVLR) have studied the feasibility of producing hydrogen for use in Europe from solar energy in the Sahara desert[44]. The sahara desert was chosen for its high solar irradiance and large area of low cost land. Either solar thermal or photovoltaic power generation would provide the electricity required for electrolysis. The water required would be desalinated and piped in from the Mediterranean. Hydrogen would be liquified and transported by pipeline

or tanker to Germany. Such a scheme would make good use of otherwise unproductive land.

2.3 Storage and distribution of hydrogen

Hydrogen is currently used in food, chemical and petrochemical processing and a variety of manufacturing industries. In the United States 99.5% of hydrogen consumed is produced on the site where it is used (captive hydrogen)[45]. Almost all of the hydrogen produced in the US is used for the production of ammonia and methanol and in the refining of fossil fuels[6]. The small proportion of hydrogen that is used for purposes other than ammonia, methanol and refining fossil fuels is supplied mostly as merchant hydrogen (hydrogen produced for sale directly)[45]. With much of the current hydrogen usage being from captive hydrogen, the networks for storing and distributing hydrogen over larger distances have not been extensively developed.

The three main modes considered for the storage and distribution of hydrogen are as:

a. High pressure gas

b. Metal hydrides

c. Liquid hydrogen

Other storage options have been investigated (for example cryoadsorbents[46] and chemical storage as methylcyclohexane[47]) and may be developed to better suit particular applications. Various systems have been developed specifically for automotive application, where low storage system mass and volume are very important. These will be discussed in chapter 3.

Carpetis[48] describes the alternatives for the large scale storage of hydrogen and calculates the various costs associated with each system. Selection of an appropriate storage mode depends largely on the hydrogen storage capacity, storage time and throughput requirements for a given application.

2.3.1 High pressure gas

The small quantities of hydrogen handled as merchant hydrogen are easily dealt with using conventional gas handling technology (high pressure gas cylinders)[6,49].

The large scale distribution of hydrogen as a compressed gas could be most efficiently accomplished via a gas pipeline[50]. A gas pipeline offers the distinct advantage that it can provide a large storage facility in itself (line packing). Pipeline storage of hydrogen could act as the required buffer between production of hydrogen from renewable resources (which are typically difficult to match with demand) and end use. The technology to successfully distribute hydrogen via

a pipeline has been demonstrated in facilities such as Air Products and Chemicals' Houston, Texas pipeline[51]. This pipeline network is used to distribute merchant hydrogen to sixteen individual customers. A number of other hydrogen pipelines exist including a 210 km pipeline network in West Germany and a 16 km pipeline network at Imperial Chemical Industries' (ICI) Teesside facility in England[6].

Garat[52] details a survey of existing natural gas pipelines in France and concludes that the steels currently in use for natural gas piping are compatible with the transmission of hydrogen (with regard to hydrogen embrittlement). The efficient distribution of hydrogen could be handled by the existing natural gas pipelines when natural gas supplies are exhausted[3].

Large quantities of hydrogen have been stored as a high pressure gas by ICI, underground in three large man-made salt caverns[53]. This facility in England utilises brine from surface ponds to pump into the caverns and displace the hydrogen at a pressure of 50 bar. Large quantities of gas have also been stored underground in natural aquifers[53]. Such underground storage systems depend on the availability of suitable underground sites and are therefore unlikely to find widespread application.

2.3.2 Metal hydrides[54]

Hydrogen molecules are so small that they can easily exist within the lattice molecular structure of metals. A metal hydride storage container consists of a pressure vessel/heat exchanger which houses a powdered metal alloy (such as FeTi or Mg_2Ni). The storage tank is charged by supplying hydrogen at pressure and removing heat generated by the ensuing exothermic reaction. To liberate the hydrogen from the hydride heat must be supplied. Metal hydride storage systems are generally very safe as the hydrogen is not released until the hydride is heated. Thus a puncture in a metal hydride storage vessel will not leak large quantities of gaseous hydrogen.

The mass of a metal hydride storage system is comparable to the mass of a compressed gas storage system but the volume is considerably smaller. A given mass of hydrogen can take up less volume when bound in metal hydride form than in liquid form[55]. The large mass of metal hydride storage systems is not particularly prohibitive for stationary storage, but does render them unsuitable for the large scale transmission of hydrogen.

One serious disadvantage with metal hydride storage is the need for very pure hydrogen with which to charge the hydride, as any impurities can act cumulatively to reduce the capacity of such a storage system[56].

Metal hydride storage systems require high pressure hydrogen and a heat sink in order to be charged with hydrogen, and a heat source to liberate the hydrogen. This makes the control of hydrogen in and out of the storage unit more complex than that of a high pressure hydrogen storage vessel.

2.3.3 Liquid hydrogen

Hydrogen can be stored as a liquid in specially constructed insulated storage vessels[57]. Hydrogen is kept at a very low temperature (20 K) rather than high pressure in order to maintain the liquid state. Liquid hydrogen offers low mass and low volume storage. Current uses for liquid hydrogen are as an aerospace fuel and in research such as super-conductivity as a cryogenic coolant. It is envisaged that liquid hydrogen will have an important role in aviation where it is unequalled as a fuel in terms of energy content per unit mass[5,58]. Storage of hydrogen as a liquid is expensive both in terms of the energy required to liquify the hydrogen[59] and the technology required to store the hydrogen at low temperature with minimal heat gain[54]. Hydrogen stored as a liquid poses a problem with regard to the boil off hydrogen (due to heat leakage) which must be released from the vessel[60,61]. Such venting is wasteful of hydrogen and must be controlled in order to circumvent a potential explosion hazard.

2.4 Safety considerations

A common public perception is that hydrogen is a dangerously explosive gas, with often quoted examples of the destructive power of hydrogen being the hydrogen bomb and the Hindenburg disaster. The hydrogen bomb bares no relevant comparison to the "conventional" use of hydrogen as an energy carrier and any fear of hydrogen arising from this association is a result of ignorance. The Hindenburg disaster is however undeniably linked to the dangers of hydrogen as a highly flammable gas. An important point to note however is that out of the 97 passengers and crew on board, 62 survived[62]. A very positive safety aspect of hydrogen combustion is that the flame radiates little heat (see Appendix A). Unless directly in the flame, there is little chance of being burnt from a hydrogen fire. The hydrogen in the Hindenburg was stored above the people on board and as it burnt the hydrogen fire rose away from the passengers as the Hindenburg sank to the ground. This disaster contrasts with more recent airliner disasters such as the Canary Island airport collision of 1977[62]. A refuelled KLM 747 was taking off when it collided with a Pan Am 747 in it's path on the runway. The fuel tanks of the KLM jet exploded causing an intense fire that killed all 249 people aboard. 333 of the Pan Am's 394 passengers and crew were also killed. The heat radiated from a petroleum fuelled fire is very much greater than that from a hydrogen fire and has the potential to cause much greater damage to property and life.

The major safety hazard associated with hydrogen arises from the properties of a low minimum ignition energy and low lean limit of flammability (see Appendix A). The consequence of these two properties is that a very small leak of hydrogen in an enclosed space can pose a danger. The ignition energy of hydrogen is such that even the rapid venting of hydrogen into the air can create enough energy to cause ignition[64]. It is safest always to assume that if a combustible hydrogen - air mixture occurs, there will always be a source of ignition available. The safety problem then becomes one of preventing an undesired combustible hydrogen - air mixture from occurring.

When hydrogen is contained under pressure, special attention must be paid to ensure that fittings do not leak. Hydrogen has small molecules compared to other fuel gases and is therefore much harder to contain. Hydrogen will even leak through the walls of PTFE† lined flexible high pressure hose[63].

Hydrogen leaks are very much more dangerous in confined spaces than outdoors[64]. A hydrogen leak indoors can quickly lead to a combustible mixture. A hydrogen leak outdoors will rapidly rise and diffuse away from any possible ignition sites. The exception to this is the case of a large spill of liquid hydrogen. The gas that boils off from a liquid hydrogen spill will remain denser than air until it gains sufficient heat from the surroundings.

---

† Polytetrafluoroethylene (Teflon)

Being odourless and colourless hydrogen is difficult to detect without the aid of special equipment[65]. Hydrogen detection in a school classroom is done by the pop test, but this is hardly practical for determining if a room is filled with hydrogen! The safe application of hydrogen in confined spaces therefore depends on high integrity containment of the hydrogen and/or some reliable means of detecting leakage. Isolating and venting a confined space in the event of hydrogen leakage must also be considered.

Numerous researchers have analyzed the safe use of hydrogen as a fuel[7,66,67,68]. The general conclusion is that safety can be achieved with the careful development of suitable systems. The development of the hydrogen economy should not be greatly hampered by safety problems.

CHAPTER 3 LITERATURE REVIEW OF HYDROGEN ENGINE RESEARCH

Many researchers have contributed to the current wide body of knowledge relating to the fuelling of internal combustion engines on hydrogen[68,69,70]. Internal combustion engines designed for fuelling with diesel or gasoline, can be fuelled on hydrogen with few modifications. The simplest hydrogen engine fuelling systems (external mixture formation applied to a spark ignition engine), suffer from low power output and combustion problems when compared to equivalent gasoline operation[71,72]. If hydrogen as a fuel for internal combustion engines is to be accepted, then hydrogen engines must be developed which demonstrate significant advantages over present day engines.

One of the greatest advantages of hydrogen as a fuel for internal combustion engines is the potential for operation over a wide range of air/fuel ratios[71]. This allows charge quality regulation as the primary means of load control, eliminating the pumping losses associated with throttling in a conventional spark ignition engine[24]. In practice λ has an upper limit of about 2.5[73,†] due to reduced brake thermal efficiency[74] and hydrogen peroxide emissions[24,25]. Hence for low load operation, a throttle is required.

---

† Much leaner operation has been demonstrated[24,71].

3.1 Review of hydrogen fuelling techniques

The performance characteristics of hydrogen fuelled internal combustion engines are usually expressed in terms of output power, pollutant emission and fuel consumption for various engine speeds, compression ratios and relative air fuel ratios (λ). Hydrogen fuelling technology for internal combustion engines can be classified as[75]:

a. external mixture formation using a gas carburettor or manifold injection system
b. internal mixture formation early in the compression stroke by means of low pressure direct injection
c. internal mixture formation late in the compression stroke by means of high pressure direct injection

3.1.1 External mixture formation

External mixture formation provides a simple means of fuelling internal combustion engines on gaseous fuels. Many gaseous fuelled external mixture formation systems have been successfully installed in New Zealand cars for fuelling on indigenous compressed natural gas (CNG) and liquified petroleum gas (LPG). Hydrogen too can be introduced to an engine in this manner, but not

without some serious problems[76]. The major problems with the external mixture formation of hydrogen are:

a. Low volumetric efficiency. Hydrogen displaces a large proportion of the air on the induction stroke[77]. A stoichiometric hydrogen/air mixture contains 29.53% hydrogen (by volume), compared with about 1.76% for gasoline† in air[7]. From these proportions and the fuel densities (83.764 g/m^3 and ≈4400 g/m^3 respectively - see Appendix A) the mass of each fuel per unit induced volume can be calculated.

Mass of hydrogen = 24.7 g/m^3

Mass of gasoline = 77.4 g/m^3

Using these masses and the lower calorific values of each fuel (119.93 kJ/g and 44.5 kJ/g respectively) we can determine the overall heat input (per unit induced volume).

Hydrogen heat input = 2962 kJ/m^3

Gasoline heat input = 3444 kJ/m^3

---

† This assumes gasoline to be in the gaseous phase. In reality, some of the gasoline would in the wet vapour phase and would take up less volume in the induced charge.

This result indicates that when operating at stoichiometric mixture strengths, an external mixture formation hydrogen engine should deliver about 86% of the power of a similar gasoline fuelled engine (assuming similar thermal efficiencies). Further comparisons with CNG and LPG[78] for both induction (external mixture formation) and injection (internal mixture formation) are presented in Figure 3.1. The graph represents the comparative energy of stoichiometric charges. Of the fuels represented, hydrogen suffers the greatest detriment in input charge energy due to decreased volumetric efficiency when using external mixture formation techniques. However, hydrogen also offers the most significant increase in charge energy available when using direct injection.

b. Pre-ignition and back-firing into the inlet manifold. Hydrogen has a low lean limit of flammability and a very low ignition energy[79]. These two properties enable a hydrogen/air charge to pre-ignite very easily[80]. Pre-ignition can occur when the hydrogen/air mixture enters the combustion chamber and comes into contact with hot residual gases or hot spots in the combustion chamber. If pre-ignition occurs before the inlet valve closes it can result in a violent back-firing of the hydrogen/air mixture into the inlet manifold. This is particularly alarming in the case of a carburetted multi-cylinder engine, where such a back-firing will consume the entire gaseous contents of the manifold.

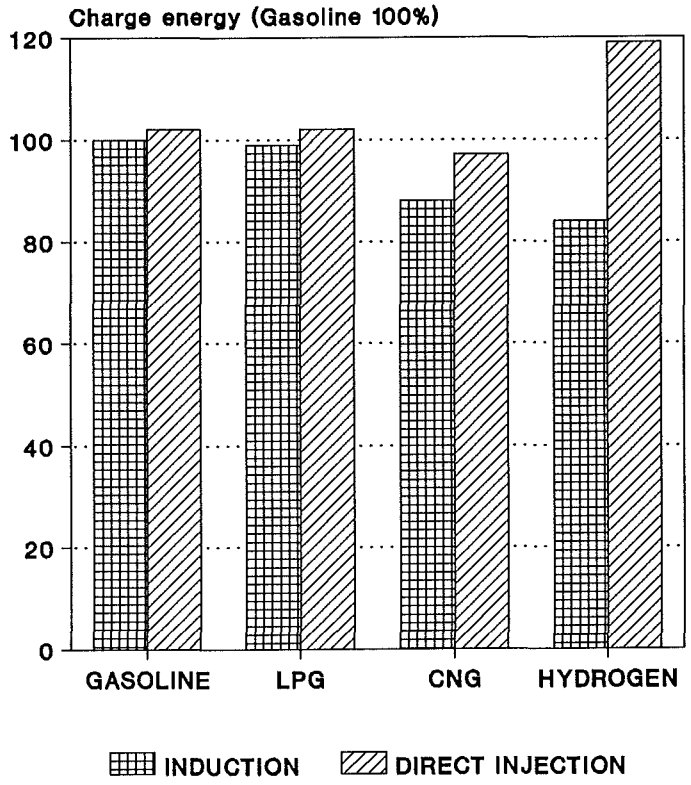

Figure 3.1 Theoretical charge energy comparison - induction vs direct injection.

Much work has been done to identify the mechanisms causing pre-ignition and back-firing[81]. Lucas and Morris[82] suggest that although pre-ignition and back-firing may be induced by hot spots on combustion chamber walls, the dominant cause may well be a chemical effect from hot residual gases in the combustion chamber. In their work it was found that a cycle in which back-firing was experienced was immediately preceded by several cycles of decreasing combustion pressure. Research conducted by Yamaguchi *et al*[83] supports the conclusion of Lucas and Morris that hot residual gases in the combustion chamber are

the major source of pre-ignition in an external mixture formation hydrogen engine. Yamaguchi *et al*[83] established that the hot exhaust valve and spark plug were not sites of initiation for abnormal combustions (pre-ignition and back-firing). Watson and Milkins[76] describe the earlier work of Hii[84] where it was found that back-firing could occur independent of pre-ignition, although the exact mechanism of this is not well understood.

c. A "knocking" sound is apparent when operating pre-mixed charge hydrogen engines at conditions approaching stoichiometric. The mechanism thought to be causing the noise is auto-ignition[21,85,86]. Auto-ignition is defined as the spontaneous combustion of unburnt gas ahead of the flame front, due to reactions caused by high temperature and pressure conditions.

For hydrogen/air mixture strengths approaching stoichiometric the combustion rate is very high with a corresponding high rate of pressure rise[87,88]. Some researchers consider that the knocking sound may possibly be due to detonation[80,89] or some other phenomenon termed

combustion pressure vibration[87,90] as well as (or instead of) auto-ignition†.

Irrespective of the exact mechanisms of knocking combustion in hydrogen engine operation, it is commonly accepted to be an undesirable feature of engine operation related to the rate of combustion[80,90,91]. Takiguchi *et al*[90] concluded that combustion pressure vibration had no obvious detrimental effect on engine performance or durability, but that the noise produced was reason enough to avoid knocking combustion.

Many attempts have been made to alleviate the numerous problems associated with external mixture formation systems.

The drop in power due to the decreased volumetric efficiency has been countered with such measures as supercharging[92,93] and turbocharging[81,94]. Such forced aspiration improves engine performance but also adds complexity and heightens some other problems. Supercharging can increase NO_x emissions and enhance knocking combustion due to increased charge temperature[92].

---

† Detonation is the propagation of the flame front with a shock wave which reflects from the combustion chamber walls, resulting in a high frequency noise[177]. Some researchers use the term detonation for the phenomenon described above as auto-ignition[85,87].

Combustion pressure vibration is thought to be the high frequency component of a very rapid rate of pressure rise[87].

Lynch[94] found that with turbocharging, the increased charge temperatures also promoted the occurrence of pre-ignition.

Another technique for improving the volumetric efficiency is to fuel with cold hydrogen from liquid storage and rely on the cooling effect of the hydrogen to increase the induced air density[75]. Cooling the inlet charge with cold hydrogen has the added advantages of decreasing the production of NO_x[95] and inhibiting pre-ignition and knocking combustion[75]. Supplying cold hydrogen to the inlet charge may cause moisture from the air to freeze on the walls of the inlet manifold[75].

Reducing the occurrence of pre-ignition and back-firing with external mixture formation systems relies on eliminating the possible ignition sites.

In order to prevent hot residual gases or hot spots from igniting the incoming charge a number of strategies have been tried to cool the combustion chamber prior to hydrogen induction. Water induction has been used with limited success[96] and has the added advantage of decreasing NO_x production by reducing the combustion chamber temperature. Water induction has also been shown to control knocking combustion[75,97]. Problems with water induction include a drop in brake thermal efficiency, contamination of the lubricating oil[98] and possible freezing of the water supply during winter.

Another method used for cooling the combustion chamber is the induction of air prior to the timed port injection of hydrogen[99,100,101,102]. This has been shown to be most effective in eliminating back-fire[98].

Increasing the compression ratio of a hydrogen engine promotes more effective gas exchange processes, reducing the possibility of pre-ignition due to hot residual gases in the combustion chamber[103]. Reducing valve overlap has also been shown to reduce the occurrence of pre-ignition and back-firing[75].

One possible solution to the problems of pre-ignition, back-firing, NO_x emissions and knocking combustion is to limit engine operation to mixture strengths much leaner than stoichiometric. This approach is impractical because the maximum power output is severely restricted. A similar solution to lean operation has been achieved using exhaust gas recirculation[75]. EGR has the same effect but offers no practical advantages over other methods of controlling NO_x emissions[104], pre-ignition, back-firing[105] and knocking combustion[98].

Prabhukumar *et al*[97] describe the use of water induction to combat knocking combustion in a hydrogen engine with pilot diesel injection. Water induction serves to cool the end gas and slow the rate of combustion, thereby reducing the tendency for knocking combustion. This allows higher full load power output but reduces the brake thermal efficiency at part loads. The reduction in brake thermal efficiency was attributed to the water induction affecting the temperature at the end of the compression stroke, thereby extending the ignition delay period

and reducing the combustion rate. Increased wall quenching is also cited as a possible mechanism for the reduction of break thermal efficiency due to water induction.

3.1.2 Low pressure injection - internal mixture formation

The low pressure injection† of hydrogen into the combustion chamber after the closure of the inlet valve eliminates the problems of low volumetric efficiency and back-firing associated with external mixture formation[106]. Pre-ignition and knocking combustion may still occur[102,107].

Internal mixture formation requires an additional port into the combustion chamber in which to mount an injector. The injector must seal hydrogen under pressure and also seal against back-flow of gases from the combustion chamber[102].

---

† Low pressure injection refers to injection into the combustion chamber immediately after inlet valve closure, when the combustion chamber pressure is "low". A low pressure injector would require a hydrogen supply pressure in the order of 10 bar. High pressure injection refers to injection of hydrogen towards the end of the compression stroke when the combustion chamber pressure is "high". The hydrogen supply pressure required for high pressure injection is in the order of 100 bar. The exact hydrogen supply pressure required for a specific application is a function of fuel delivery requirement, compression ratio, engine speed, injector design and injection timing.

The control of the air/fuel ratio may be achieved by either injection pressure variation or injection duration variation (or a combination of both[102]).

- Injection pressure variation. This method is implemented by either throttling the hydrogen flow before the injector[108] or by varying the injector lift[109]. Reducing the injection pressure (to increase the air/fuel ratio) will be detrimental to the charge mixing process[110].

- Injection duration variation. By varying the duration of the injection, while supplying hydrogen at constant pressure, the amount of fuel can be regulated whilst still delivering it at the maximum flow rate possible[106,111,112]. This is most desirable for consistent rapid mixing of the injected hydrogen with air[89,110].

Rapid and consistent injector actuation is required for the precise metering of hydrogen[102].

During the compression stroke, the injection must be completed before the combustion chamber pressure approaches the supply pressure[102]. Thus the higher the supply pressure, the later in the compression stroke the injection can occur.

3.1.3 High pressure injection - internal mixture formation

Many of the features of low pressure injection are equally applicable to high pressure injection. The major advantages of high pressure hydrogen injection late in the compression stroke are that pre-ignition is eliminated and knocking combustion may be controlled[111,113]. The control of knocking combustion is achieved by injecting hydrogen towards the source of ignition, over a period including the time of ignition[111]. This promotes the combustion of a heterogenous charge, reducing the rate of pressure rise, thereby eliminating knocking combustion.

Takiguchi and Furuhama reduced the occurrence of knocking combustion by inducing a very lean hydrogen/air mixture through the inlet valve and supplying most of the hydrogen through a high pressure injector late in the compression stroke[89]. The induced hydrogen was supplied from the boil off from liquid storage and was too lean to allow pre-ignition. The effect of this method is to provide a stratified charge that will ignite easily but burn more slowly than a homogenous mixture.

A disadvantage of very late injection and combustion of a heterogenous charge is a possible reduction in thermal efficiency due to inadequate mixing[110]. This loss may be compensated for by the slight enhancement in power output with a high pressure injection due to the reduced compression work requirement of the

engine (Furuhama and Azuma[107] describe a theoretical 6% increase in indicated power by late injection compared to early injection).

High pressure direct hydrogen injection late in the compression stroke is widely recognised as the most promising means of improving performance and overcoming the combustion related problems associated with the operation of an internal combustion engine on hydrogen[75,111,114,115]. The main problems with high pressure injection lie with the design of a suitable fuel supply and injection system.

3.2 Hydrogen vehicle storage options

The storage of hydrogen on board a vehicle is a major consideration when designing a fuelling system. Binder and Withalm[75] describe the three main storage technologies and the interaction of these with the possible fuelling methods. The three storage options considered are†:

a. High pressure gas

b. Metal hydride

c. Liquid hydrogen

---

† An introduction to the principles behind each of these storage options is given in section 2.3.

Other storage methods have been studied and could possibly be developed to provide advantages over the three options discussed here[116].

Comparisons of the mass and volume characteristics of these storage options are presented in Figure 3.2[117]. The data represented is for the complete storage system. The stored hydrogen makes up only a small proportion of the storage vessel mass. Gasoline storage is superior to all hydrogen storage systems in terms of the system mass and volume for equivalent energy storage.

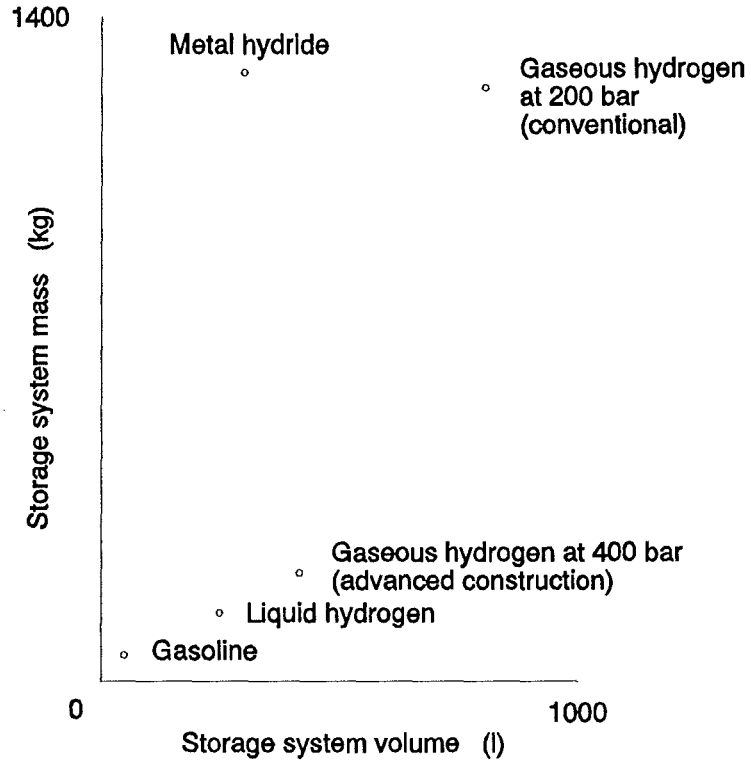

Figure 3.2 Mass - volume comparisons for various hydrogen vehicle storage options

3.2.1 High pressure gas storage

Storage of hydrogen as a high pressure gas has the advantage of being simple to implement in providing a high pressure supply to an engine[63]. The development of advanced composite high pressure storage vessels is predicted to bring the storage system mass and volume down to levels approaching those for liquid hydrogen storage[118]. One serious disadvantage of high pressure gas storage is that if the gas is required at high pressure for the fuelling system, then the hydrogen can only be used down to this pressure. For example, if hydrogen is stored at 690 bar (as predicted[118]) and supplied to the engine at 80 bar, then when the tank is depleted to 80 bar, about 12% of the gas originally stored in the tank remains unusable. This means the tank must be designed larger and/or the vehicle must travel less distance per fill. Very high pressure gas storage on board a vehicle could represent a considerable hazard in the event of a collision.

3.2.2 Metal hydride storage

Metal hydride storage provides a favourable means of storing hydrogen on a vehicle with regard to the volume of the storage vessel (Figure 3.2). However, the excessive mass of the storage vessel is a major disadvantage in the use of metal hydrides for hydrogen storage on a vehicle. A Mercedes-Benz 280 TE passenger vehicle used for fleet testing required a low temperature metal hydride storage system with a mass of 280 kg[119,120]. This storage system held an

energy equivalent of 11 l of gasoline which translates to 13% of the original gasoline storage (85 l) on the 280 TE. Thus for metal hydride storage systems, the inherently high mass has a detrimental effect on the vehicle design mass and/or range.

The heat required to release hydrogen from a metal hydride storage tank is typically supplied from the waste heat in the exhaust. High temperature metal hydrides have been developed which are lighter than the low temperature hydrides[121,122]. The heat input required to release the hydrogen is however too high to be supplied by engine exhaust heat alone. Complex systems combining both high and low temperature hydrides have been investigated to optimize hydride storage system performance[123,124].

The minimum time required to refill a practical vehicular metal hydride storage tank is in the order of 10 minutes[56,119].

Metal hydride storage systems are not suitable for supplying hydrogen at high pressures. Binder and Withalm[75] report the theoretical possibility of supplying hydrogen at a pressure of 60 bar from a Ti-Fe hydride heated to temperatures of at least 350K. In practice, the problem of heating the metal hydride from cold (when starting) renders metal hydride storage unsuitable for supplying hydrogen for high pressure direct injection[125].

3.2.3 Liquid hydrogen storage

Hydrogen stored as a low temperature liquid represents the best method of storing pure hydrogen on board a vehicle with regard to the system mass and volume. Hydrogen can be efficiently pumped as a liquid to high pressure and is thus compatible with fuelling systems requiring high pressure hydrogen[113,126]. The low temperature of the hydrogen gas that comes from the liquid hydrogen supply could be used to cool the charge in order to improve volumetric efficiency, reduce NO_x emissions[127] and reduce the combustion problems of pre-ignition, back-firing and knocking[127] (see section 3.1). The cost of hydrogen liquefaction is high and this must be considered when evaluating the overall cost of hydrogen fuelling[75,128]. The refuelling of liquid hydrogen storage containers often involves the release of quite considerable amounts of gas as the vessel cools[129]. Some means of using or venting this gas is necessary. The safe disposal of gaseous hydrogen vented during refuelling has been attempted by means of a catalyst to combine the hydrogen with oxygen to produce water[130].

One of the important safety concerns with the storage of hydrogen as a liquid, is the release of the hydrogen which boils off due to ingress of heat into the vessel. The factors influencing the boil off of hydrogen have been studied in detail[131] and current designs of tank for automotive use provide minimum boil off rates as low as 1.7% of the contents per day[132].

The refuelling time for a vehicular liquid hydrogen storage vessel is similar to that for metal hydrides. Stewart[129] gives a minimum refuelling time of 9 minutes for a 110 l dewar.

3.3 Ignition systems

The ignition of the hydrogen/air mixture requires careful consideration. Three main methods have been attempted by various researchers. These are spark ignition, compression ignition and hot surface ignition.

3.3.1 Spark ignition

Spark ignition has been demonstrated as an efficient and reliable means of ignition for numerous projects on hydrogen fuelling[73,85,106,133,134].

It is claimed by De Boer *et al*[21] that in order to get the best performance in a spark ignited hydrogen engine, the spark gap should be set to about ½-⅓ of the gap used for a gasoline engine. The main reason for this reduction is to compensate for the high ionization potential† of hydrogen/air mixtures (particularly with high compression ratios and lean mixtures)[96,135]. Other

† Ionization potential of hydrogen is 15.4 electron volts. This compares with 12.6 eV for iso-octane and 9.86 eV for methane.

researchers[82] have found it necessary to increase the spark plug gap in order to prevent water from condensing on the electrodes and impeding cold starting. Withalm and Gelse[125] describe a special spark plug which overcomes this problem by drawing water away from the electrodes using a capillary effect.

3.3.2 Compression ignition

Compression ignition of hydrogen fuelled internal combustion engines has been attempted[136,137,138]. Although having a low ignition energy requirement, hydrogen has a very high self-ignition temperature (858 K compared to 525 K for diesel[139]). As a result, extremely high compression ratios must be used in order to generate the temperature required to ignite the hydrogen-air mixture. Homan *et al*[137] could not achieve compression ignition of hydrogen-air mixtures even with a compression ratio of 29:1. The long ignition delay associated with hydrogen-air mixtures is another reason given for the difficulty in attaining consistent compression ignition[136]. Pilot diesel injection can be used to provide a reliable means of compression ignition[139]. This approach suffers from the increased complexity of requiring two fuel supply and control systems as well as producing additional undesirable exhaust emissions.

3.3.3 Hot surface ignition

Hot surface ignition has been attempted as a simple means of igniting hydrogen-air mixtures[90,137,140,141]. Typically the hot surface consists of a glow plug type arrangement positioned in the path of the hydrogen jet supplied from a high pressure direct injection system[142]. The timing of the ignition is controlled by adjusting the timing of the injection. Furuhama describes the major disadvantages with hot surface ignition are the high electrical power consumption to heat the hot surface and the limited durability of the hot surface igniter[113].

CHAPTER 4 DEVELOPMENT OF THE PROPOSED FUELLING SYSTEM

In this chapter the optimum configuration of a hydrogen fuelling system for an internal combustion engine is proposed. Theoretical calculations are performed to determine the key parameters for the hydrogen fuelling system to suit a Ricardo E6 research engine.

A summary of the compressible flow theory relevant to the design of a high pressure gaseous injector is given.

The first stage of injector development is described, where an injector needle and nozzle is designed and tested to verify suitable open flow and closed leakage performance. The requirements of the injector actuator are detailed.

4.1 Optimum configuration

The proposed optimum hydrogen fuelling system for an internal combustion engine comprises a high pressure direct injection valve capable of delivering precisely metered quantities of hydrogen to the combustion chamber late in the compression stroke. Injection early in the compression stroke could promote

pre-ignition while injection very late in the compression stroke may not allow sufficient time to achieve adequate mixing of the hydrogen with air. The optimum timing of injection would be determined experimentally.

The operation of the injection valve would be electronically controlled to enable interfacing with an engine management computer. The injection duration would be varied to adjust the quantity of hydrogen injected. The engine load would be adjustable by varying mixture quality in the range $1 < \lambda < 2.5$. For engine loads lower than that obtained at $\lambda = 2.5$, intake air throttling would be employed. This would avoid the problems of hydrogen peroxide emission and cyclic pressure variation which are related to very lean hydrogen-air mixtures.

Spark ignition would be utilised in order to provide a reliable, efficient and controllable combustion initiation.

The hydrogen supply on a vehicle would conceivably be from a cryogenic hydrogen storage system via a pump to deliver hydrogen at the required pressure. The hydrogen would receive heat to convert to gaseous form before injection.

4.2 Calculated operating parameters for hydrogen fuelling of the Ricardo E6 engine.

The development of a suitable hydrogen fuelling system for the Ricardo E6 engine begins with a calculation of the fuel delivery requirement. The overall fuel requirement is calculated and this is used to determine the specification for the injector.

The equations given in this section were programmed with MathCAD so that the effects of modifying various operating parameters could be assessed. The results were analyzed in an array corresponding to the range of engine speeds.

4.2.1 Assumptions made for theoretical calculations.

There were a number of assumptions made as the basis for the following calculations.

a. The volumetric efficiency of the engine was assumed to be a constant 85% (obtained from previous engine testing on gasoline)[†].

[†] This assumption proved to be quite valid. All hydrogen engine testing was done with the throttle wide open and for engine speeds ranging from 20 to 33.3 rps. Volumetric efficiency ranged from 81 to 91% with a mean of 87% and a standard deviation of 2%.

b. The design compression ratio was 12:1 (based on the work of Furuhama[90]).

c. The calculations were performed for the case of stoichiometric operating conditions.

d. The maximum injection opening duration was specified as 90° crank angle. Such a large angle for injection was specified to provide a conservative initial valve design. To maintain similar engine operation with a smaller angle of injection a higher mass flow rate of hydrogen during the injection would be necessary. It was reasoned that the higher the mass flow rate through the valve, the more difficult it would be to consistently meter a precise amount of hydrogen per injection.

e. The relevant hydrogen fuel properties used for the calculations are given in Table 4.1†. The hydrogen pressure given in Table 4.1 was calculated to ensure sonic flow through the injector into the combustion chamber (see section 4.3).

f. Standard atmospheric properties of air were assumed as detailed in Table 4.2[143].

---

† See appendix A for a description of properties of hydrogen, including detail on the variation of γ with temperature.

Table 4.1 Hydrogen fuel properties used in engine fuelling calculation

Property	Symbol	Value	Units
Ratio of specific heats	γ	1.4	
Stoichiometric air fuel ratio	A/F_{stoic}	34.3	kg/kg
Fuel supply pressure	P_{fuel}	80	bar
Fuel supply temperature	T_{fuel}	293.15	K
Fuel gas constant	R_{fuel}	4.1243	kJ/kgK

Table 4.2 Air properties used in engine fuelling calculation

Property	Symbol	Value	Units
Ratio of specific heats	γ	1.4	
Atmospheric pressure	P_{air}	1.01325	bar
Air temperature	T_{air}	293.15	K
Air gas constant	R_{air}	0.2871	kJ/kgK

4.2.2 Engine fuel requirement

The mass flow rate of hydrogen required to fuel the Ricardo E6 (see Appendix G) engine was calculated by considering the mass flow rate of air and the stoichiometric air/fuel ratio of a hydrogen air mixture.

Firstly the volume of air induced per engine cycle is calculated.

$$vpc_{air} = \text{swept volume} \times \text{volumetric efficiency} \quad (4.1)$$

The volume flow rate of air is then determined.

$$vfr_{air} = vpc_{air} \times \frac{\text{engine speed}}{2} \quad (4.2)$$

Multiplying the volume flow rate of air by the density of air at standard conditions gives the mass flow rate of air into the engine.

$$mfr_{air} = \frac{P_{air} \times vfr_{air}}{R_{air} \times T_{air}} \quad (4.3)$$

The required mass flow rate of fuel into the engine is then calculated for the case of a stoichiometric air/fuel ratio.

$$mfr_{fuel} = \frac{mfr_{air}}{A/F_{stoic}} \quad (4.4)$$

From the above assumptions and equations the maximum mass flow rate of hydrogen required to fuel the engine was calculated as 1.36 kg/hr for stoichiometric operation at 50 r.p.s.

4.2.3 Mass flow rate of hydrogen through injector

The required mass flow rate of hydrogen through the injector during injection is determined by considering the maximum duration of valve open (specified in degrees crank angle) and the mass of hydrogen injected per firing cycle.

$$\text{injection duration} = \frac{CA_{inj}}{360 \times \text{engine speed}} \tag{4.5}$$

$$mpc_{fuel} = \frac{mfr_{fuel} \times 2}{\text{engine speed}} \tag{4.6}$$

$$mfr_{inj} = \frac{mpc_{fuel}}{\text{injection duration}} \tag{4.7}$$

The required mass flow rate of hydrogen during the injection was thus calculated to be 3.0 g/s.

4.3 Summary of relevant compressible flow theory

The theory of isentropic flow, as detailed by Shapiro[144], gives the following relationship for the maximum mass flow rate of a perfect gas through a nozzle.

$$\dot{m} = A^* \sqrt{\frac{\gamma}{R}\left(\frac{2}{\gamma+1}\right)^{\frac{\gamma+1}{\gamma-1}}} \frac{P_o}{\sqrt{T_o}} \qquad \text{for } \frac{P^*}{P_o} < \left(\frac{2}{\gamma+1}\right)^{\frac{\gamma}{\gamma-1}} \qquad (4.8)$$

Where:

γ	=	ratio of specific heats
R	=	gas constant
A	=	area of nozzle
P	=	absolute pressure
T	=	absolute temperature
*	=	value at minimum contraction of nozzle
o	=	value upstream of nozzle

For a particular gas the maximum mass flow through a given nozzle is thus proportional to the supply pressure and inversely proportional to the square root of the absolute supply temperature. Note that the maximum mass flow rate is independent of the conditions downstream of the nozzle (provided that $P^*/Po < 0.53$ for hydrogen). This property is used to advantage in the design of the

hydrogen injector by providing a constant mass flow rate when open, regardless of the range of combustion chamber conditions downstream of the nozzle.

The decision of the hydrogen supply pressure was based on ensuring that the flow of hydrogen through the injector was sonic. The peak pressure downstream of the injector during the compression stroke may be approximated by the maximum pressure due to adiabatic compression of the intake air charge.

$$PV^{\gamma} = \text{constant} \tag{4.9}$$

$$P_1V_1^{\gamma} = P_2V_2^{\gamma} \tag{4.10}$$

$$P_2 = P_1\left(\frac{V_1}{V_2}\right)^{\gamma} \tag{4.11}$$

For the design compression ratio of 12:1 and the pressure at the start of compression (condition 1) being atmospheric the pressure at the end of the compression stroke (condition 2) is:

$$\begin{aligned} P_2 &= 1.01325\ (12)^{1.4} \\ &= 33 \text{ bar} \end{aligned} \tag{4.12}$$

The lower limit of the hydrogen supply pressure is then calculated by applying this combustion chamber pressure to the limiting pressure ratio for sonic flow (P^*/P_o equation (4.8)):

$$P^* = \frac{33}{0.53} \qquad (4.13)$$

$$= 62 \text{ bar}$$

The decision to specify a hydrogen supply pressure of 80 bar was to allow a margin for error in the above calculated pressure. A hydrogen supply pressure of 80 bar would also be sufficient to prevent the possibility of a back-flow of combustion chamber gases into the injector in the case of injector failure†.

† The peak combustion chamber pressure recorded during hydrogen engine testing was 72 bar (at 12:1 compression ratio). No problems of combustion chamber gas back-flow were encountered in spite of numerous injector failures.

4.4 High pressure hydrogen injector development

This section details the initial development of the high pressure hydrogen injector used for fuelling the Ricardo E6 engine. The procedures and results of testing to determine various parameters of the injector design are described along with the design specifications.

A two stage approach was adopted for the development of the injector. In the first stage a simple manually adjustable injector was designed. This injector was used to determine a suitable injection nozzle configuration in order to provide for a satisfactory mass flow rate of hydrogen when open and minimal leakage when closed. Further tests were devised to determine the forces on the injector needle due to the high pressure hydrogen, for both flow and no-flow situations. The results from these tests were then applied in the second stage of development - the design of an actuated injector suitable for engine testing. This stage is described in the following chapter.

4.5 Injector specification

The hydrogen injector must be able to accurately meter hydrogen at a rate of approximately 3.0 g/s (when open) from a supply pressure of 80 bar into the combustion chamber of the Ricardo E6 research engine. The quantity of hydrogen injected will be controlled by varying the injection duration. The

actuation of the injector must therefore allow a very consistent adjustable injection duration.

The main operational requirements for the injector are:

a. Rapid response. Response time of the injector actuator is defined as the period of time between the initiation of the actuation and the start of the travel of the needle. Thus the response time has an upper limit approaching the period of one engine cycle. A very slow response time will not allow application to higher speed or two stroke engines.

b. Short travel time. The travel time of an injector is defined as the time required for the injector needle to move from one extreme position to the other. The upper limit on travel time is not so easily defined as for the response time. In order to maximize the average mass flow rate during injection (and thereby enhance internal mixture formation), it is desirable to minimise the period of low flow injection (during valve opening and closing). It has been argued (MacCarley[145]) that a short travel time is required based on the premise that a linear relationship between injection duration and injected quantity is desirable. This may be the case for a simple mechanically controlled system, but in the case of an electronic control system, compensation may be made for any non-linearity.

c. Accurately controllable injection duration. In order to use injection duration variation as the means of controlling the air/fuel ratio the duration must be accurately regulated. An electronic control system would be most desirable considering the trend towards optimizing engine management using microprocessor control[146].

d. Accurately controllable injection timing. It is considered essential to be able to experiment with the precise timing of the injection. Variable injection timing could most easily be incorporated into an electrical actuation system.

e. Minimal leakage when closed. The upper limit for injection valve leakage is constrained by the possibility of pre-ignition during the induction or compression phases if leakage is excessive. Valve leakage during the induction stroke will reduce the volumetric efficiency. Valve leakage during the exhaust stroke is a waste of hydrogen. For a practical system, consideration must be given to preventing leakage when the engine is stopped. This could perhaps be achieved with a fail safe shut-off valve which isolates the injector.

Valve leakage has been cited as beneficial by way of slight pre-mixing which smooths the combustion process[136]. In this work it is considered best to have a zero leakage valve. In this way, any spurious effects of a possibly variable pre-mixing due to injector leakage will be avoided.

If desired, further work could be done to test the effect of pre-mixing by induction.

f. Resistance to high temperature. The injector must be able to withstand the high temperature associated with injection directly into the combustion chamber.

g. Durability. The injector is required to actuate at a frequency in the order of 50 Hz and the requirement for a short travel time means that the sealing and travel limit faces must endure high impact loadings. The valve must be designed to withstand this high impact loading while maintaining consistent flow and leakage performance.

h. Low power consumption - The injector actuator should not use too much power. In the case of electrical actuation, consideration must be paid to the power consumption with regard to overheating of the solenoid.

There are obvious trade-offs between many of the above requirements. A high needle lift to ensure a sufficient flow rate will conflict with the aim for a short travel time. Flexible seating materials to ensure minimized leakage may limit durability and be susceptible to deterioration from high temperature. Considering the above requirements, the next design decision was the specification of a suitable injector actuation method.

4.5.1 Injector actuation methods

Various methods of actuation have been considered. They may be grouped into the categories of mechanical, electrical and fluidic (hydraulic or pneumatic).

a. A mechanical hydrogen direct injection system has been successfully demonstrated[142]. A notable problem with employing a mechanical actuation is the complexity involved with controlling both injection duration and injection timing. Other problems with a mechanical system are lubrication, control of wear, back-lash and thermal expansion.

b. Electrical actuation of a hydrogen direct injection valve has been attempted with some degree of success[72,102,109,147]. The key advantages are independence from a mechanical drive from the engine and simple control of injection duration and timing. The travel time of the valving component must be minimized by considering both inductive and inertial delays in valve actuation.

c. Fluidic actuation systems can offer advantages of fast response, short travel time and consistent control of the injector. Adjustment of the injection duration and timing may not be as simple as for electrical actuation but fluidic actuation has advantages over a mechanical system that wear, backlash and thermal expansion are not severe problems.

- Hydraulic actuation of a hydrogen injector has been demonstrated a number of times[148,149]. A hydraulic actuation system typically embodies a diesel injection pump used to actuate a plunger via a closed circuit of hydraulic fluid. The plunger is connected to the hydrogen injector needle. The control of injection duration and timing may be achieved by using the same mechanisms used to control diesel injection[150]. Hydraulic actuation systems allow rapid response and accurate control of injection using well developed Diesel injection technology, but suffer from the added complexity of a hydraulic system to drive the actuator.

- Pneumatic actuation. It is conceivable that a satisfactory valve actuator could be designed which uses the high pressure hydrogen to perform the primary actuation of the valve. Such a valve is described by May[151]. A small fast acting solenoid valve vents some of the high pressure gas from behind a piston, thus causing the piston to lift the main valve needle. When the solenoid valve is closed a small bleed port equalizes the pressure on both sides of the piston, allowing the valve to close. This system suffers from a loss of hydrogen through venting. The vented hydrogen could be perhaps recovered by pre-mixing with the intake air. Pneumatic actuation of a hydrogen direct injection valve has been attempted by MacCarley and van

Vorst[73]. They found that the opening and closing times were too large for practical application.

Considering the relative merits of the above actuation methods it was decided to proceed with the design of an injection valve based on an electrical actuator. Two important considerations for an injector design to suit an electrical actuation system are:

a. The mass of the valve needle must be as small as possible in order to minimize the inertial delay.

b. The travel distance must be minimized in order to allow a short travel time. Electro-magnetic actuators (solenoids) are suitable to very fast acting application only over short travel distances[152].

4.6 Initial non-actuated injector design

Two valving configurations are considered for high pressure direct injection. The methods are shown in Figure 4.1.

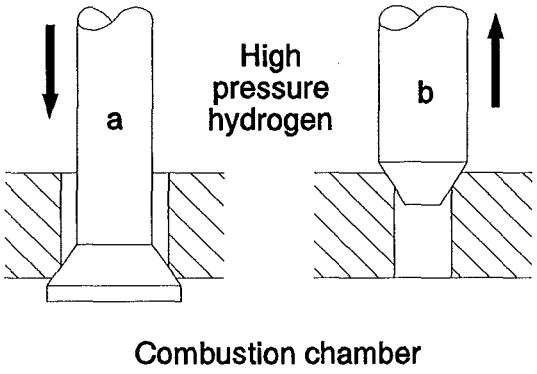

Figure 4.1 Injection valve configuration alternatives.

In Figure 4.1 (a) the injector needle movement during valve opening is towards the combustion chamber. This approach gives good protection from back flow of combustion chamber gases into the injector. Whenever the combustion chamber pressure is higher than the injector supply pressure, the resultant force on the valve due to gas pressure is acting to close the valve. This feature is irrelevant for the proposed design, as the injector supply pressure is designed to be considerably higher than the combustion chamber pressure. The major disadvantage with this layout is that the valve takes up a large area of the combustion chamber. Not only does this mean that there will be a high heat transfer into the valve and seat, but also that the potential for efficient cylinder head design may be greatly reduced.

In Figure 4.1 (b) the injector needle lifts off the seat and moves away from the combustion chamber to open the valve. With this configuration the needle and seating faces are not exposed to the high combustion chamber temperature and the valve seating area can be lower. As the hydrogen supply pressure will be higher than the peak combustion chamber pressure, the net force due to gas pressure always acts to close the valve and makes it impossible for a back-flow of combustion chamber gases into the injector. An added advantage of this method is that the valve moving element can be made smaller and lighter, aiding a major requirement of fast travel.

Option b. was thus adopted for the injector configuration.

A suitable injector was designed to allow the testing of hydrogen mass flow rate and leakage through various injector needle and seat configurations. The final form of the hydrogen injector has a spatial restriction defined by the cylinder head and camshaft housing surrounding the auxiliary spark plug hole on the Ricardo E6 engine (see Figure 4.2), where the injector was to be mounted. The initial non-actuated injector was originally intended as a base upon which to mount a suitable actuator, and was thus designed to fit within this space envelope also.

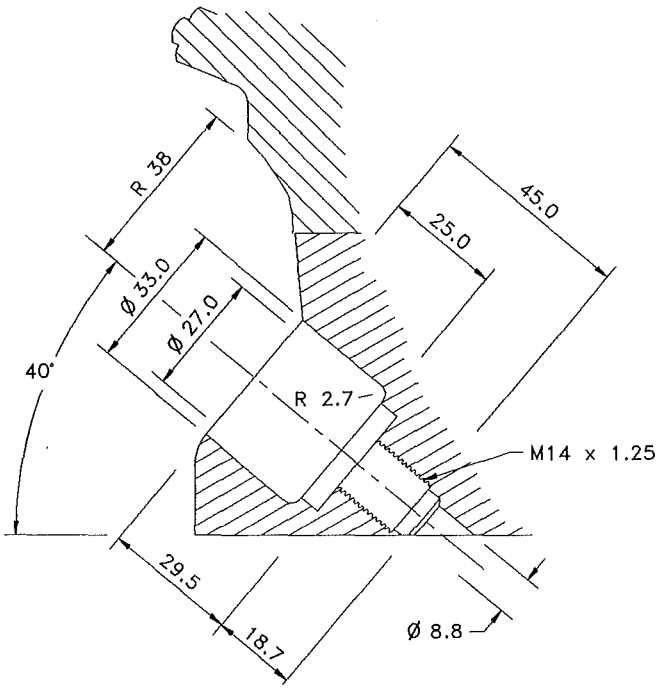

Figure 4.2 Detail of spatial restriction to injector design

The manually adjustable non-actuated injector is shown in Figure 4.3.

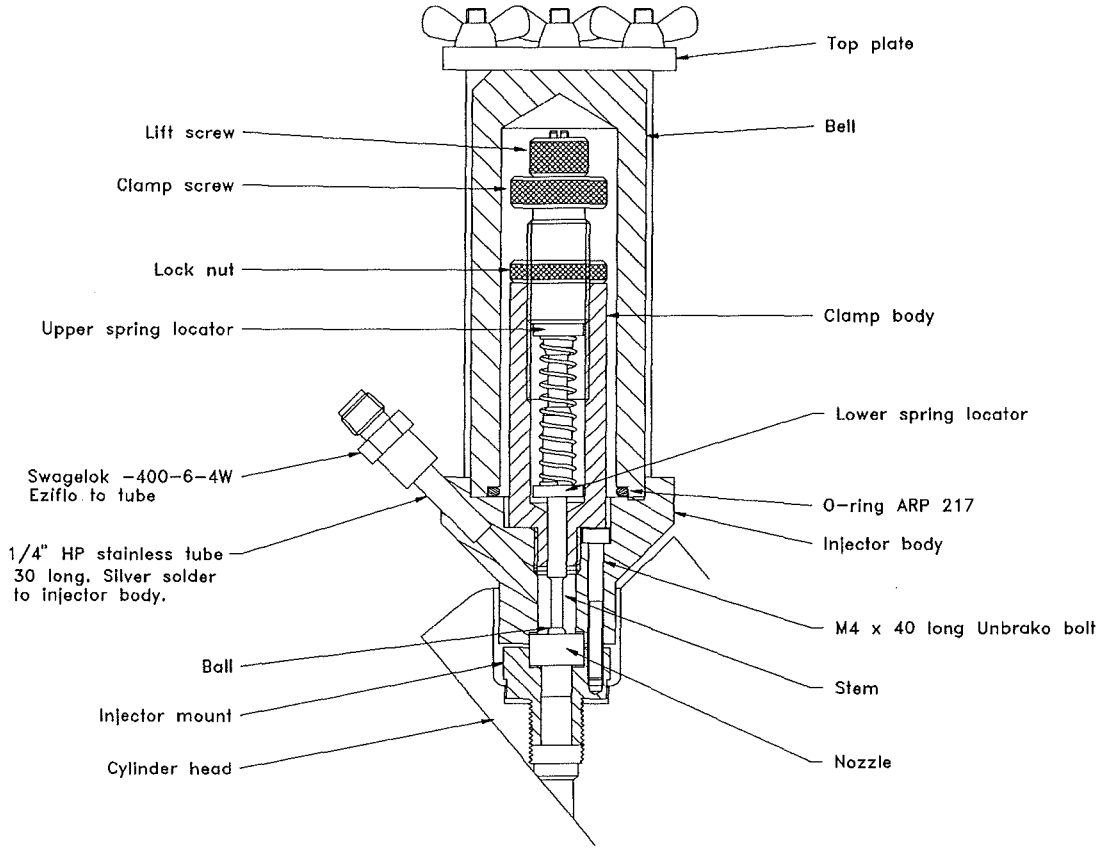

Figure 4.3 Manually adjustable, non-actuated test injector

Main features of the design are:

- A mounting which enables the valve to be located close to the combustion chamber. Any extra volume between the valve and the combustion chamber would result in a delay between injection and the gas entering the combustion chamber, and any hydrogen in this volume may also not mix with air sufficiently well to burn completely.

- Side entry of the high pressure hydrogen supply. This allows hydrogen flow tests to be directly applicable to the next stage of development - the actuated injector. If the hydrogen was fed in through the top of the injector, the hydrogen flow characteristics could be influenced by the subsequent actuator design. This feature also enables the dismantling of the upper part of the injector without removing the high pressure hydrogen connection.

- Manual adjustment of the needle lift distance and valve seating force. These two parameters could be altered by adjusting the lift screw and clamp screw respectively. The spring constant was determined so that the extent of spring compression could be used to calculate the needle seating force.

- Housing for a standard nozzle element. Being one of the key components under investigation the nozzle was designed to be removable so that different nozzles could easily be tested. The nozzle designs tested are detailed in Appendix D. The original nozzle design (Figure 4.4) was based on an optimum profile for a sonic nozzle given by Stratford[153]. The nozzle element was sealed in place using loctite† master gasket sealing compound.

---

† Loctite is a registered trade mark of Loctite Corp. U.S.A.

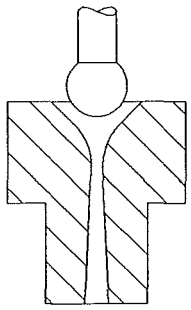

Figure 4.4 Original injector needle and nozzle configuration.

Leakage through high pressure hydrogen injection valves has been an ongoing problem in previous studies[136,145]. An effective solution to the leakage problem was employed by MacCarley[145] in which the needle sealed on an elastomeric seat. MacCarley used a neoprene O-ring in his electronically controlled manifold hydrogen injection system to obtain leakage rates of only 0.75 cm^3/min (with a supply pressure of 4.46 bar). Watson *et al*[100] have also demonstrated the successful application of elastomers to seal a delayed port admission system. Elastomeric seals seem ideal for manifold injection systems where both operating temperature and supply pressure are not high. For a direct injection valve that actuates away from the combustion chamber it is conceivable that advanced high

temperature elastomers (such as Viton[154] or Kalrez†[155]) may be suitable for sealing the valve.

The initial injector needle and nozzle design employed a metal to metal seal (see Figure 4.4). It was considered that a spherical needle on a conical seat would alleviate the problem of misalignment experienced by MacCarley with his original metal to metal seat design, which resulted in an unacceptable leakage rate. A 3/16" carbon chrome steel ball bearing was seated on a phosphor bronze 90° included angle conical seat. The ball was mated onto the bronze seat by light tapping to produce a uniform 1 mm wide indentation.

4.6.1 Leakage mass flow rate testing

The rate of leakage through the closed injector was determined by timing the displacement of water in an inverted measuring cylinder while supplying the closed injector with hydrogen at 80 bar (see Figure 4.5).

---

† Viton and Kalrez are registered trademarks of DuPont.

Viton is a fluorocarbon elastomer with a maximum service temperature of 230°C.

Kalrez is a perfluorocarbon elastomer with a maximum service temperature of 316°C.

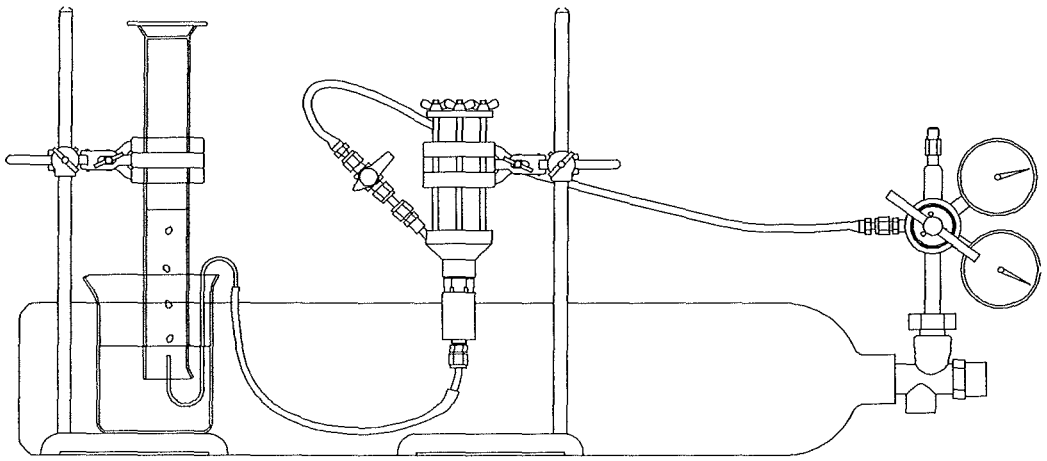

Figure 4.5 Injector leakage test set-up.

Other than errors of measurement and timing, two possible errors associated with this test are those due to:

a. hydrogen dissolving in the water.

b. water vaporizing into the hydrogen.

The potential magnitude of these errors is calculated below.

a. Hydrogen is only very slightly soluble in water. The Bunsen coefficient is defined as the volume of gas (corrected to 0°C and 1 atmosphere pressure) dissolved per unit volume of solvent at system temperature T and partial pressure of solute - one atmosphere[156]. The Bunsen coefficient can be determined for a particular temperature from its relationship to the Ostwald coefficient.

$$\text{Bunsen} = \frac{\text{Ostwald} \times 273}{T} \qquad (4.14)$$

The Ostwald coefficient for hydrogen in water at 25°C and one atmosphere is 0.01913[157]. Using the above relationship the Bunsen coefficient is 0.01752. This means that for every litre of water, up to 17.5 cm^3 may be dissolved. For the leakage tests performed, up to 0.3 l of hydrogen was bubbled through 1 l of water. If the water was hydrogen free before a test and completely saturated with hydrogen after a test then the maximum possible error due to hydrogen dissolving in the water would be:

$$\frac{0.01752}{0.3} = 6\% \qquad (4.15)$$

This potential error could be reduced by using as little water as possible. In practice the error would be expected to be much lower than the above calculation suggests due to saturation of the water with hydrogen after the first few tests.

b. The maximum possible error associated with the vaporization of water into the hydrogen would occur if hydrogen was free of water before bubbling and was completely saturated with water vapour afterwards. The saturation vapour pressure of water at 25°C is 3166 Pa[143]. The total pressure of the gas in the measuring cylinder at the end of the test is

approximately one atmosphere (101325 Pa). Applying the Gibbs-Dalton law, the partial pressure of hydrogen is 98159 Pa. The volume of this mixture of hydrogen and water vapour is 0.3 l. If the same quantity of pure hydrogen was at atmospheric pressure then the volume occupied would be:

$$0.3 \times \frac{98159}{101325} = 0.29 \text{ l} \qquad (4.16)$$

This amounts to a possible over-estimate of leakage rate of 3% due to vaporization of water in the hydrogen.

Based on the above calculations, the errors involved with this method of hydrogen leakage measurement are considered to be acceptably small.

The results of initial leakage tests on the spherical needle and conical phosphor bronze seat were disappointing. The leakage was in the order of 500 cm^3/min when the valve was held shut with a spring force of 22.1 N plus the force due to the 80 bar supply pressure. The specified volume flow rate (at NTP) of hydrogen with the valve fully open was approximately 2100 l/min. Hence a leakage of 0.5 l/min represents only 0.02% of the maximum flow. During the intake and compression strokes at a low engine speed of 900 RPM the leakage would amount to approximately 0.5 cm^3, which in a 500 cm^3 displacement engine gives

a mixture far leaner than the lean limit of flammability for hydrogen in air (0.1% vol. compared to the lean limit of flammability of 4% vol. hydrogen in air).

For reasons detailed in section 4.5 it was decided to pursue the aim of zero valve leakage. It appeared unlikely that a significantly lower leakage rate would be possible unless a completely different sealing method was used. Based on the successful work of MacCarley[145] and Watson *et al*[100] it was decided to try and incorporate an elastomeric seat to seal the high pressure injection valve.

4.6.2 Elastomeric injector seat

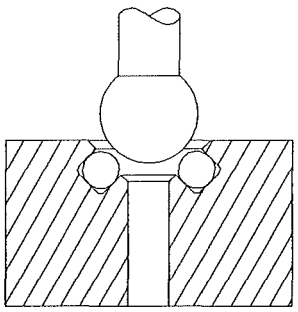

Figure 4.6 Elastomeric O-ring seat nozzle.

The use of a Viton or Kalrez O-ring was considered a simple and effective method of incorporating an elastomeric seal into the injector design. The design of a new nozzle with a 006 O-ring seal is shown in Figure 4.6. The nozzle diameter was made larger than for the previous design to allow the annulus to behave as the

critical section rather than having the minimum contraction downstream of the needle. It was considered that this would allow for a smaller lift to give the required flow rate.

The new design of valve needle and nozzle was tested as before and found to demonstrate zero leakage.

The use of an elastomer as the sealing element of a direct injection valve raised concerns about the effects of temperature on the sealing properties of the elastomer. A test was devised to assess the compatibility of a Viton[†] elastomer O-ring seat with the injector operating environment.

The injector was mounted in the auxiliary spark plug hole of the Ricardo E6 engine with the Viton O-ring seat fitted. The injector needle was secured against the O-ring seat to simulate the valve being fully closed. The engine was then operated on gasoline for a period of 24 hours. During testing the exhaust temperature was maintained higher than 660°C and the temperature immediately behind the needle ball end was measured at an average of 125°C.

After the period of engine operation the injector was dismantled to reveal that the O-ring showed no visible signs of deterioration due to the effects of temperature.

---

† Viton was used because Kalrez O-rings were too expensive. 006 size Viton O-rings were NZ$7 each whereas Kalrez O-rings were NZ$90 (Paykel Engineering Ltd. February 1990).

The test O-ring compared well with a new one. It was unknown at this stage what effect cyclic impact loadings and cooling due to hydrogen expansion would have on the elastomer.

The next test for the injector was to measure the maximum mass flow rate.

4.6.3 Hydrogen mass flow rate measurement

In order to measure the mass flow rate of hydrogen through the continuously open injector it was necessary to devise a suitable means for measuring a flow of 3.0 g/s, the calculated nominal flow requirement. This could perhaps be accomplished easily and at moderate expense by using a suitable variable area flow meter (rotameter)[158]. The final requirement of a mass flow rate measuring device was to measure a flow in the order of 0.4 g/s (during engine testing). Variable area flow meters are not suited to pulsating flow[159] (Homan *et al*[137] report actual hydrogen flow rates of 45%-85% of those indicated by a rotameter. This discrepancy was attributed to the pulsating nature of the flow.). Thus a variable area flow meter could possibly be used for continuous flow testing but could not be used for a later stage of the work, actuated flow measurement.

It was decided to calculate the mass flow rate by injecting the hydrogen into a known volume and recording the temperature and pressure in that volume over time (inferred mass flow rate measurement[159]). The mass within the volume could

be determined approximately by applying the ideal gas equation ($PV = mRT$)[†]. Thus the mass flow rate can be inferred from the change of mass in the vessel over a measured time. The vessel was based on a 0.638 l injector test rig (see Figure 4.7) which was designed for possible visualisation work to model the flow of gas within the combustion chamber. This apparatus was not used for its intended purpose in this project but was designed early for use by another postgraduate student[160,‡].

The vessel was modified for mass flow rate testing by fitting steel plates in place of the Ricardo cylinder head and windows. The vessel was connected to an NZIG[¶] hydrogen pressure vessel to give a total reference volume of 16.0 l (see Plate 4.1). The injector test rig was instrumented for pressure and temperature with a Bourdon tube pressure gauge and a K-type thermocouple with a Yokogawa 2455 digital thermometer. Before testing, the vessel was evacuated to 740 mm Hg and rinsed with hydrogen at 40 bar to effectively remove the air from the chamber. During testing the pressure in the receiver vessel was not allowed above the critical pressure for sonic flow.

---

† Use of the ideal gas equation was later shown to be inappropriate for calculating the mass flow rate. For this design stage the mass flow rates were not recalculated because the error was not large due to the moderate pressures involved (error in the order of a 3% over-estimate of the mass flow rate).

‡ Zavier used the apparatus for Schlieren flow visualization of pilot direct injection of methane.

¶ New Zealand Industrial Gases

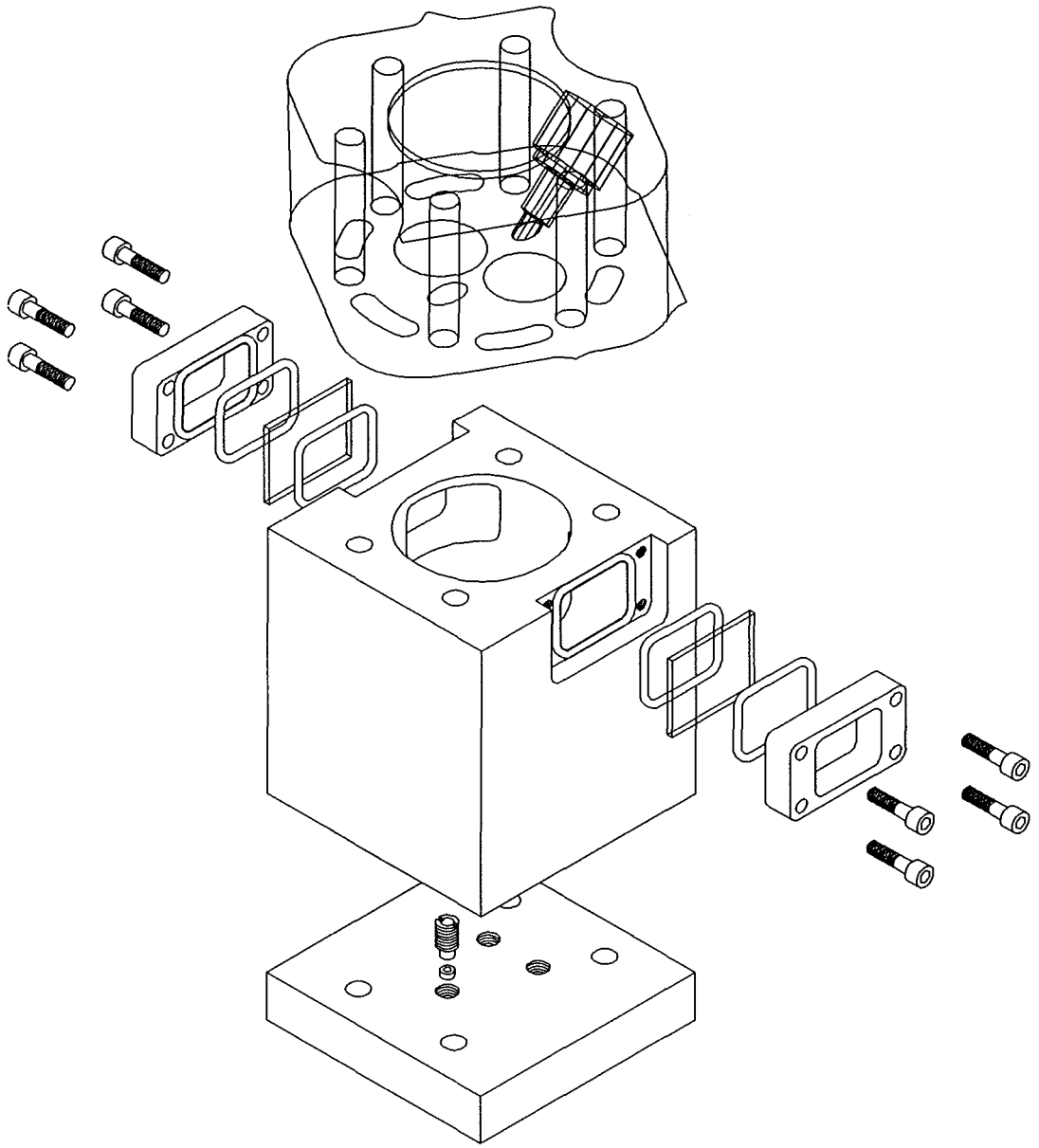

Figure 4.7 Injector test rig assembly

Note that the Ricardo E6 cylinder head is secured to the top of the test rig by four studs. The auxiliary spark plug hole which houses the injector is directed towards the space between the windows.

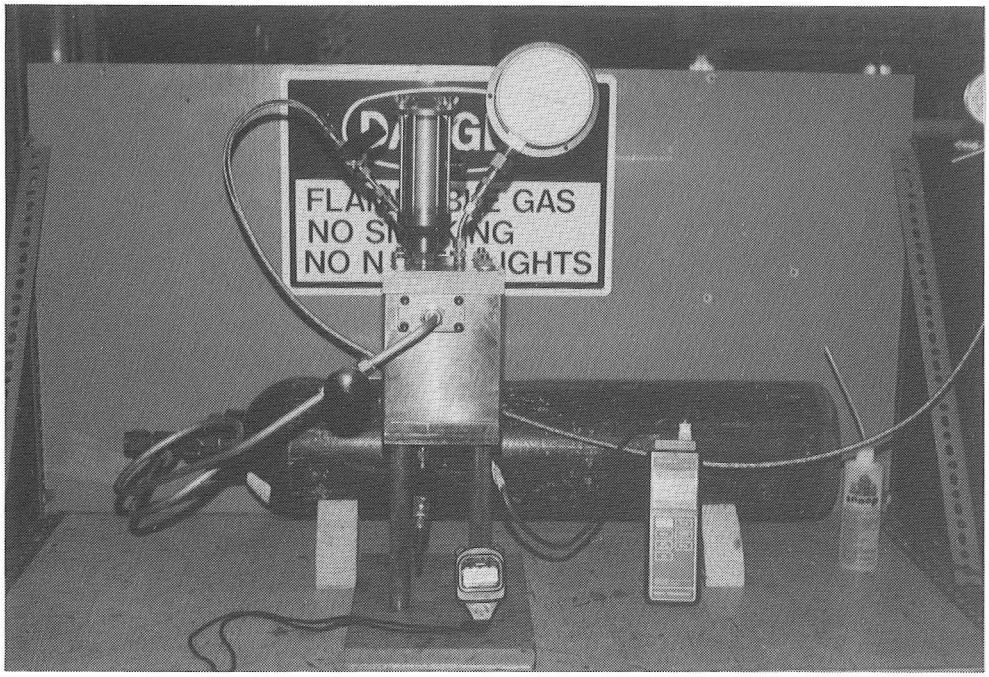

Plate 4.1 Mass flow rate measurement rig with non-actuated injector installed.

This was to ensure that the mass flow rate was constant, determined only by the upstream pressure and temperature conditions and the nozzle geometry.

To determine the relationship between valve lift and flow-rate the injector was tested over a range of lifts. The valve was assembled with the needle set to the lift to be tested. The lift was measured accurately with a vernier calliper. The valve was sealed with the bell housing and connected to the hydrogen supply. The temperature and pressure were recorded both at the start and end of a timed injection period.

Mass flow rate test results are displayed in Figure 4.8. The effective static flow area is defined as the area of the minimum contraction of the nozzle. This area was calculated from the un-deformed geometry of the elastomeric seat and the needle lift. The static flow area was calculated as the area of the frustum defined by a generatrix normal to the sphere of the needle and the torus of the nozzle. The theoretical mass flow rate shown in Figure 4.8 is calculated from sonic flow theory based on the static flow area.

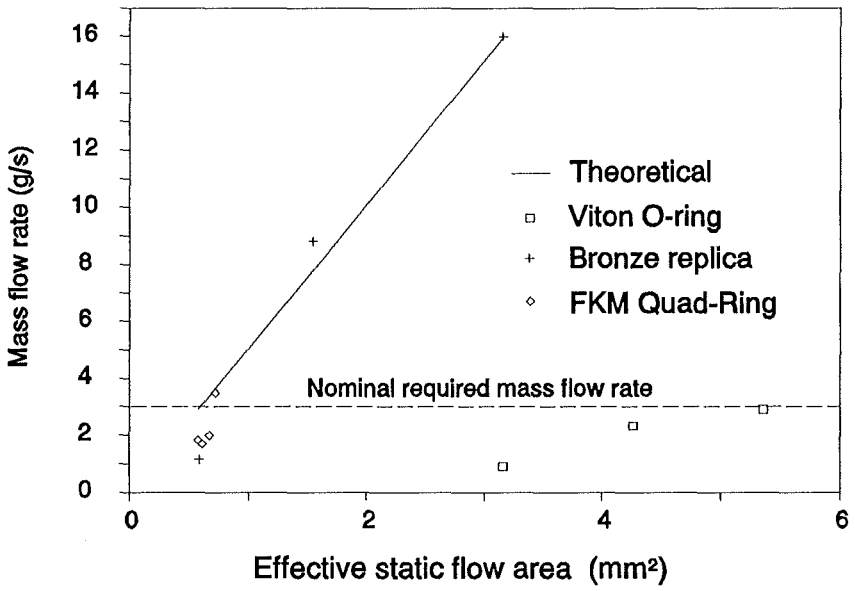

Figure 4.8 Continuous injection mass flow rate results.

The mass flow rate results for the Viton O-ring seat differed greatly from theory. A hypothesis was formulated that this discrepancy was due to the elastomer being deformed by the hydrogen flow. This was verified by measuring the mass flow rate of hydrogen through a solid phosphor bronze replica of the Viton O-ring seat. The mass flow rate results for the replica seat corresponded well to the theoretical mass flow rate.

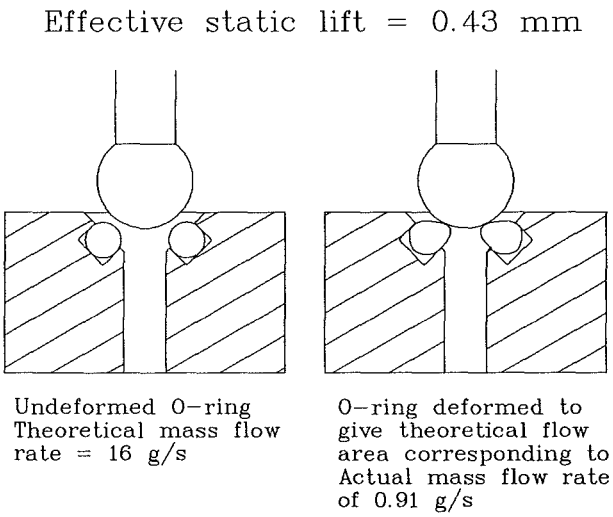

Figure 4.9 Depiction of possible Viton O-ring deformation.

The extent of deformation required to reduce the flow area of the O-ring seat is depicted in Figure 4.9. The exact mode of the deformation is unknown and may well have been unsymmetrical and/or cyclic.

The next development was to restrict the elastomer deformation by designing a more constraining seat configuration. This was achieved by using a two piece

nozzle to secure an FKM Quad-ring† so that only one lobe protruded to seal against the ball end needle (Figure 4.10). This design gave mass flow rates that closely agreed with theory.

The effective static needle lift for the required nominal mass flow rate of 3.0 g/s was 0.1 mm for the Quad-ring nozzle. This compares with a required lift of over 0.7 mm for the Viton O-ring nozzle. Tests verified that the Quad-ring nozzle design provided a zero leakage seal.

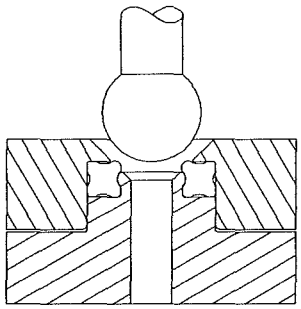

Figure 4.10 Quad-ring nozzle.

† FKM is an abbreviation of fluorocarbon elastomer.
Quad-ring is a registered trade name for the Minnesota rubber company.

4.6.4 Consideration of forces on moving element of injector

The moving element of the injector incorporates the needle, stem and solenoid armature. The forces on the moving element are due to:

a. Friction between the needle and the bearing.

b. The pressure differential between the inside of the injector and the combustion chamber.

c. The actuation force on the armature imparted by the magnetic field generated in the solenoid.

d. The force from a return spring acting to close the valve.

It is very important to select an injector layout that results in suitable net forces on the needle. If the solenoid is positioned outside the high pressure hydrogen region (Figure 4.11 (a)) then the seal friction may be considerable and the larger seal area at the top of the injector will result in a net force tending to open the valve. Friction on the seal may be eliminated by using a diaphragm instead of a moving seal (Figure 4.11 (b)). This layout suffers from the difficulty of designing a diaphragm which gives sufficient movement of the needle while still being strong enough to resist the high fatigue loading and high pressure. If the solenoid is contained within the valve (Figure 4.11 (c)) then the hydrogen pressure will act

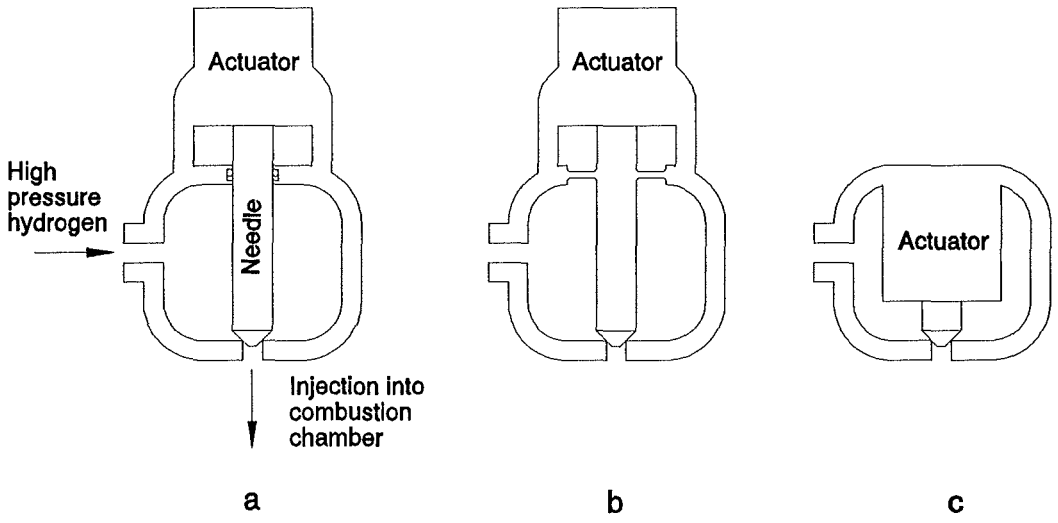

Figure 4.11 Injector actuator installation options

to hold the valve closed and bearings may be designed to offer negligible friction. It was therefore decided that the best location for the solenoid actuator was within the high pressure hydrogen region. Quite apart from the friction associated with sealing a high pressure difference across a sliding bearing, it is far easier to ensure a gas tight seal for stationary connections than it is to seal a sliding bearing.

In order to design a suitable actuator for the injector, the magnitude of the force acting against the actuator must be determined. The force exerted on the needle by gas pressure when the valve was closed could only be calculated approximately due to the uncertainty of the effective area over which the pressure

acted. It was decided to determine the force on the needle due to gas pressure with three simple tests.

a. Valve open test.

The object of this test was to determine the magnitude of the force acting to close the valve when it was open. The valve was held open (0.1 mm lift) with a spring set to a known pre-load. The hydrogen supply pressure to the valve was increased until the valve snapped shut. The pressure difference at that time was recorded and used to give an indication of the force that the gas exerts on the needle when the valve is fully open. The results of tests at various pre-loads gave an approximately linear relationship:

$$\Delta P_{snapshut} = 2.1 \times F_{pre-load} \qquad (4.17)$$

The maximum pre-load was set so that the maximum pressure differential applied during testing was in excess of 60 bar, as this was anticipated to be approximately the pressure differential encountered during injection into the engine combustion chamber.

b. Valve closed test

The force with which the needle was held closed by gas pressure was determined by another simple test whereby the valve was inverted and

a pin inserted through the nozzle to push on the needle. The pin was connected to a suspended weights holder in order to provide a force acting to open the valve against gas pressure. Hydrogen was supplied at the design pressure of 80 bar and a dial test indicator was positioned to show the relative position of the needle as weights were applied. The mass required to break the needle away from the elastomeric seat was 4.17 kg. Thus, a force of 41 N is required to overcome the gas pressure force. This value is very approximate as the effective area of the needle-seat interface may have changed significantly as the weights were added.

c. Quad-ring compression test

An approximation of the maximum force with which the needle would be held shut by gas pressure was determined by considering the maximum area over which the pressure could effectively act holding the needle down on the seat. In order to effectively estimate this area it was necessary to determine the relationship between the needle seating force and elastomer deformation. This relationship was determined using suspended weights to simulate the needle seating force and a dial test indicator to measure the displacement of the needle. The results of this test are presented in Figure 4.12. The main point to note from this graph is that the displacement of the needle varies little with forces greater than 50 N. With a hydrogen supply pressure of 80 bar the needle displacement would be in the order of 0.30 mm. The maximum

effective seating diameter was estimated from the geometry of the seat to be approximately 3.8 mm. This means that the gas pressure acts on an area of 11.3 mm^2 giving a force of 90 N (with a maximum possible pressure difference of 80 bar).

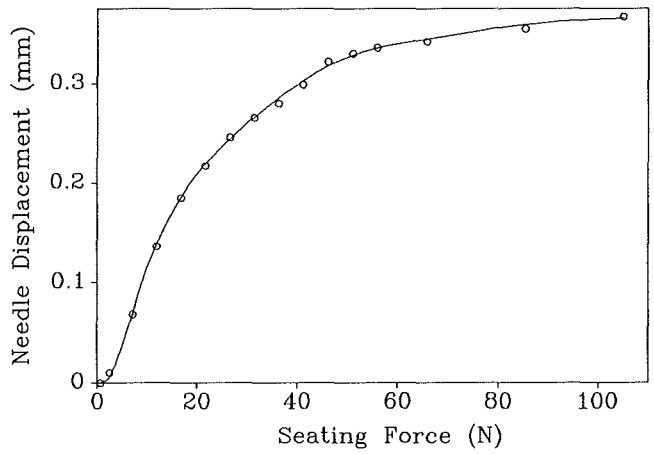

Figure 4.12 Quad-ring compression test results.

From the above tests the seating force is estimated to be between 40 and 90 N due to a pressure differential of 80 bar. In engine testing the downstream pressure will be in the order of 20 bar during injection, so the pressure differential is expected to be approximately 60 bar. A pressure differential of 60 bar acting over an area of 11.3 mm^2 gives a force requirement of the actuator of at least 68 N to open the valve and when the valve is open a force of at least 29 N (Equation (4.17)) is required to hold the valve open.

At this stage of the test programme it was decided that the solenoid actuated valve could be closed without the aid of a return spring as has been used in previous designs by other researchers [112,145,148]. A net returning force of 29 N, produced by the gas flow, was considered adequate to close the valve. The benefit of producing a design without a return spring is that all the force generated by the actuator is used to overcome the gas pressure force and the inertia of the moving element. If a return spring is used then the solenoid must be even more powerful to counter this spring force. A more powerful solenoid would generally consume more power and exhibit a higher inductive delay which would counteract the most desired feature of a short travel time.

These calculations are approximate and give estimates only of the forces involved. The force required of the actuator is considerably higher than 68 N as the travel time of the needle must be minimised by providing for high initial acceleration. For purposes of development of the solenoid a force requirement specification of 100 N was chosen.

CHAPTER 5 ACTUATED INJECTOR AND DRIVER CIRCUIT DEVELOPMENT

5.1 Solenoid design

From the results and analysis of the previous chapter an initial solenoid actuator specification was defined such that the travel distance must be in the order of 0.1 mm and the force developed in the order of 100 N. One emphasis of the design is that it should enable various parameters to be optimised experimentally rather than to rely purely on the available theory. The main reasons for this approach were the approximate nature of the results of the needle-nozzle testing programme and more importantly the current lack of knowledge and information regarding the design of suitable fast acting solenoids.

A number of solenoid configurations were considered for application to this injector (including helenoid[161], colenoid[162] and multipole[163] configurations). The Disole[164] (disk solenoid - see Figure 5.1) configuration was chosen as it is relatively simple to build, and the multiple coil layout allows a variety of wiring and armature configurations to be easily tested to optimise performance.

One of the main advantages claimed of the Disole system is that the adjacent coils can be wired in opposing directions such that the magnetic fields from

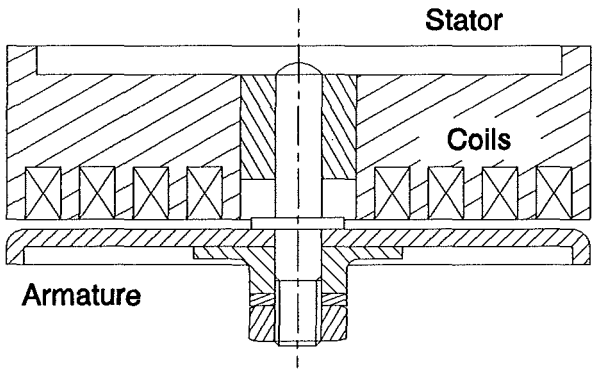

Figure 5.1 Disole (disk solenoid) arrangement

adjacent coils reinforce one another. Another advantage is that the total mass of copper wire in the coils is separated by what are effectively cooling fins. The better the heat transfer away from the coils, the more energy can be safely utilised in the coils.

The design of the Disole was estimated from Kushida[164] and Yang[165]. Yang describes a general solenoid design procedure in a graphical form. The design method is for a standard cylindrical solenoid with conical core and armature faces. Although not directly applicable to Disole design it was thought that the cylindrical solenoid design procedure would be appropriate for specifying a suitable wire gauge and the number of turns of wire.

The graphical procedure outlined by Yang was well suited to modelling on a computer as it involved numerous iterations and many of the given graphs were linear in nature. The procedure was appropriately programmed (see Appendix C). This proved far less time consuming and more accurate than working

through the graphical technique manually. The results of the computer program were that in order to develop a force of 100 N from a 12 V dc supply with a cylindrical solenoid with zero cone angle and a specified air gap of 1.5 mm, a current of 29 amps would need to flow in 96 turns of 22 AWG (0.643 mm) copper wire. This calculation is based on using 1018 steel for the armature and core, having a side gap of 0.5 mm and having a coil height to width ratio of 0.7.

The parameters used for the Disole design were the number of turns and gauge of wire. A Disole similar in proportion to that developed by Kushida[164] was designed.

5.2 Displacement transducer

To determine the performance characteristics of the injector it was necessary to incorporate a transducer to sense the displacement of the moving element. The transducer had to satisfy the following requirements:

a. Fast response

   The transducer must respond much faster than the injector moving element in order to accurately represent the displacement-time characteristic.

b. Linear response

Although a non-linear response could be linearised by computer, it would be simpler if the response was linear as this would allow direct interpretation of the results via an oscilloscope.

c. Resistance to electro-magnetic interference

The transducer output must not be affected by the high transient electro-magnetic fields in the nearby actuation coils of the injector.

d. Minimal friction

The transducer must not retard the travel of the moving element.

It was decided that an optical transducer would best suit the above requirements.

MacCarley used an optical displacement transducer in the development of a hydrogen fuel injector[145]. The system consisted of an infrared emitter directed towards a phototransistor. The light beam was interrupted by a flag attached to the tip of the injector needle. The output current of the phototransistor was proportional to the extent of interruption of the beam.

A displacement transducer similar to that used by MacCarley was devised. Rather than fabricating the transducer from discrete components, a proprietary slotted optical switch (SOS) was used. A slotted optical switch is a device which directs a narrow beam of light across a small gap to a light detector.

Slotted optical switches are usually used in applications such as limit switching and position detection[†], where the performance in a semi-switched state is of little importance. For this reason it was necessary to test the output of an assortment of slotted optical switches to find one which exhibited a suitable linear range between fully on and fully off.

Testing was performed by interrupting the beam of the SOS with a flag attached to the depth gauge of a vernier calliper. The output current of the transducer could then be plotted against the measurement from the vernier calliper. The characteristics of the General Instruments MST8 slotted optical switch were found to be suitable with a linear range of at least 0.3 mm.

An automatic calibration test rig was devised to repeatedly test the MST8 SOS in order to determine the optimum operating parameters for the circuit. Figure 5.2 shows the connections to the slotted optical switch. A program was written to control a stepper motor which turned a screw to advance a flag across the slotted optical switch beam. Voltages across the shunt resistor (corresponding to each step) were read into a computer via a Dash-8 data acquisition system[‡]. A regulated supply voltage of 1.09 V dc was found to give the widest linear range.

---

† A slotted optical switch is also used as a sensor for the injection timing circuit. See page 100.

‡ A high speed multi-channel data acquisition system manufactured by the Keithley MetraByte Corporation. This system was replaced with a higher performance DAS-20 data acquisition system from the same manufacturer prior to engine testing.

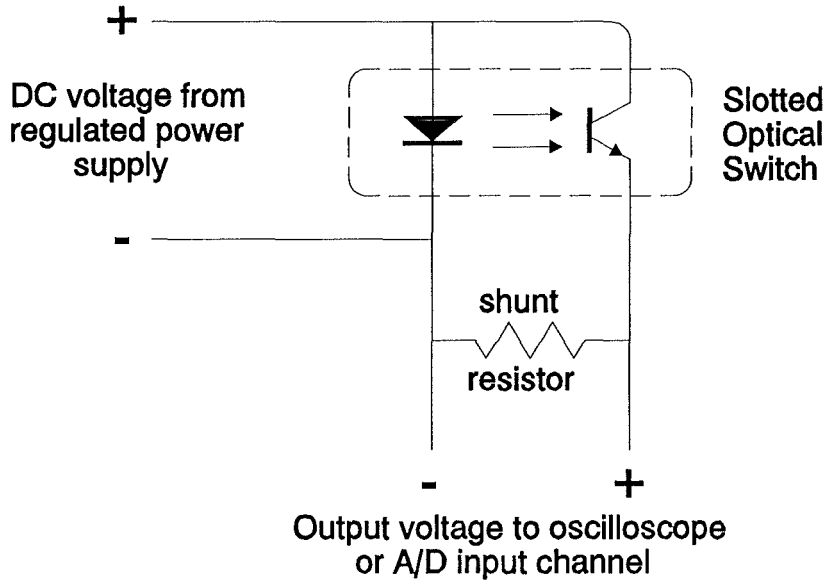

Figure 5.2 Slotted optical switch displacement transducer circuit.

A shunt resistance of 580 Ω gave an output voltage within the range, 0 to 1 volt.

5.3 Injector design features

The injector was designed to embody the previously defined features of the needle and nozzle, the Disole actuator and the SOS displacement transducer. This section describes some of the main features of the injector design.

A cross sectional arrangement drawing of the injector is shown in Figure 5.3. The detail drawings of the injector components are given in Appendix D.

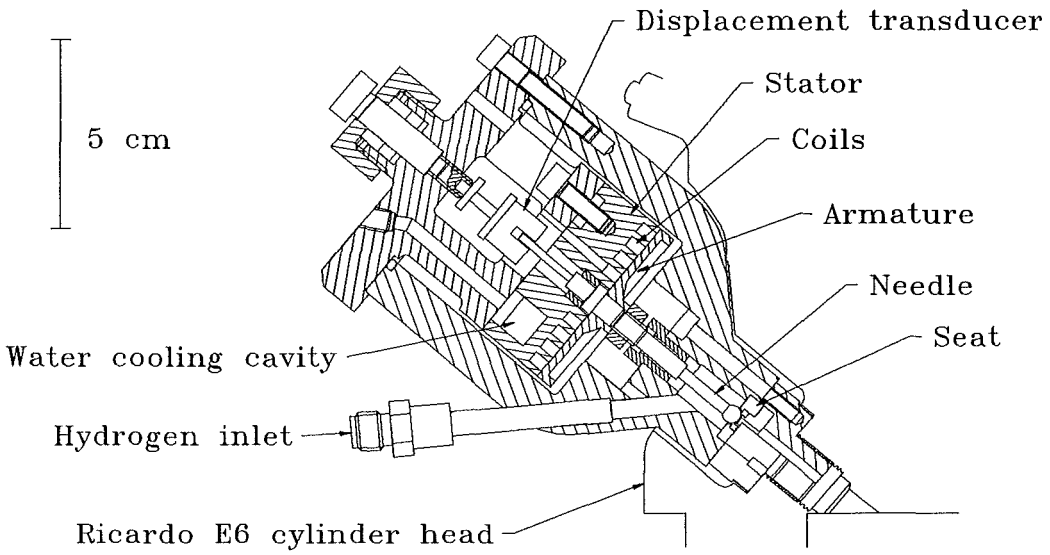

Figure 5.3 Actuated injector assembly drawing

Sealing around the nozzle element, the base securing screws and the stator/top cap interface was achieved using loctite® master gasket sealing compound. Because of the curing time required and the frequency with which the injector was dismantled, the design was later modified. The nozzle element and the base securing screws were re-designed with grooves to house suitable Viton O-rings. The stator/top cap assembly was never dismantled and so was left unmodified.

Special jigs were devised for winding and installing the Disole coils. The 4 coils were wound from 22 AWG PEI† insulated copper wire (24 turns each). Epoxy resin was applied to secure the coils into the grooves in the face of the Disole stator.

The coil cooling advantage of the Disole configuration was enhanced by incorporating water cooling in the stator behind the coils. This was not considered essential but was deemed desirable with regard to keeping the coils at a constant temperature during operation. The stator and top cap were cadmium plated to inhibit corrosion of the cooling water cavity.

A smaller alternative armature of 40.7 mm diameter was made to allow a comparison between using three and four coils of the Disole for actuation. Tests performed as in section 5.6 showed that the smaller armature, actuated by only the inner three coils wired in series, gave quicker needle travel than the original design. The smaller armature was accepted for the remaining tests.

The displacement transducer was mounted on an adjustment screw which was sealed with a PTFE gland at the top of the injector. The wires to the SOS were loosely wound around a small bobbin along the axis of the screw to allow a few turns of the adjustment screw.

---

† Polyether imide lacquer insulation.

All electrical and water cooling connections were made through the top of the injector to enable the easy removal of the displacement transducer and stator assembly. This allowed ready access to the needle for inspection and adjustment purposes. The minimum and maximum solenoid air gap was adjustable by means of appropriate shims either side of the armature disk.

Three different types of electrical feed-throughs were fitted through the top of the injector (Figure 5.4). Originally three screw connector feed-throughs (Figure 5.4 (a)) were installed. It was initially thought that the Disole actuator and the SOS displacement transducer could share a common earth connection through the body of the injector. When it became apparent that this was not possible (due to uncommon earth levels) two wire feed-throughs (Figure 5.4 (b)) were added. The final assembly used two of the screw connector feed-throughs to connect the Disole and the remaining screw connector and the wire feed-throughs to connect the SOS. One thermocouple feed-through (Figure 5.4 (c)) was installed to allow the stator temperature to be monitored.

5.4 Capacitive discharge injector driver circuit

To activate the magnetic field in the solenoid to the maximum intensity in the shortest possible time it is necessary to drive a high initial current into the solenoid. To do this, while conserving power and avoiding undue heating, it is essential to supply the peak current only for the short time required to actuate the

a.

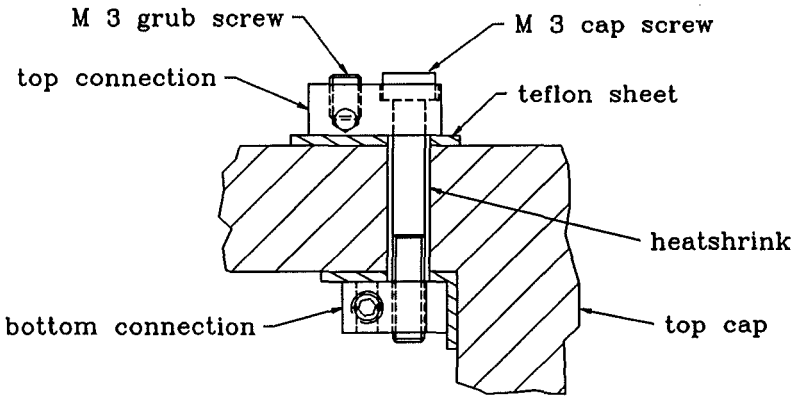

b.

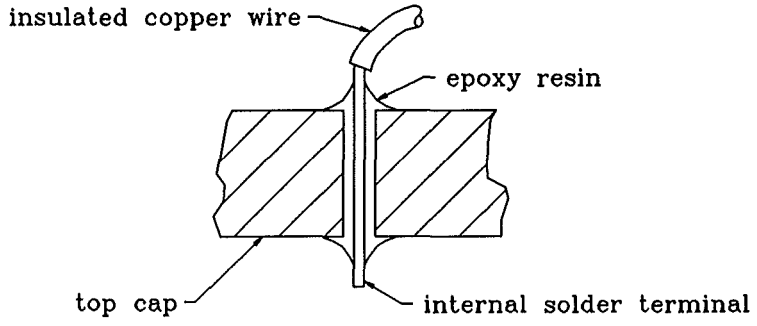

c.

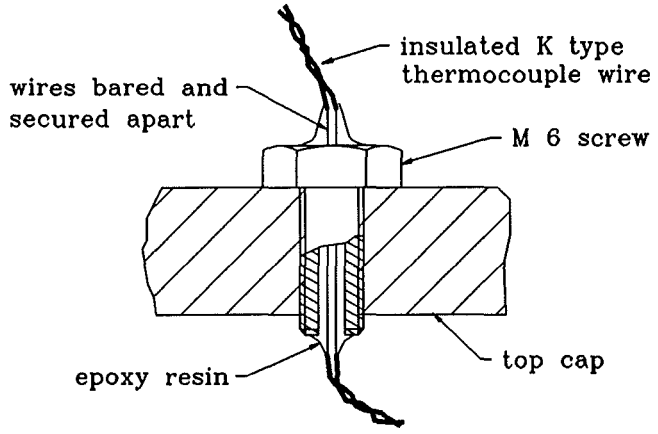

Figure 5.4 Electrical feed-through details.

injector. Once actuated, the solenoid air gap is reduced and the current required to hold the solenoid on is much smaller than the initial actuation current. The circuit to control the current to the injector must be capable of precisely timing both the start of injection and the injection duration. In a circuit described by MacCarley[145] the injection was initiated by a digital trigger pulse. The duration of injection was controlled by an analog voltage. The circuit used the discharge of a charged capacitor to supply the initial high current to the solenoid. The capacitor charging voltage was 80 volts. After the initial high current supplied from the capacitor has decayed, a lower current from a 12 volt supply acted to hold the solenoid on.

A circuit based on that used by MacCarley was described in detail by Green and Wallace[112]. This circuit was used as a model for the development of the circuit described below. Testing of the injector and circuit is described in sections 5.6 and 5.7. This circuit represents the optimum configuration determined from these tests.

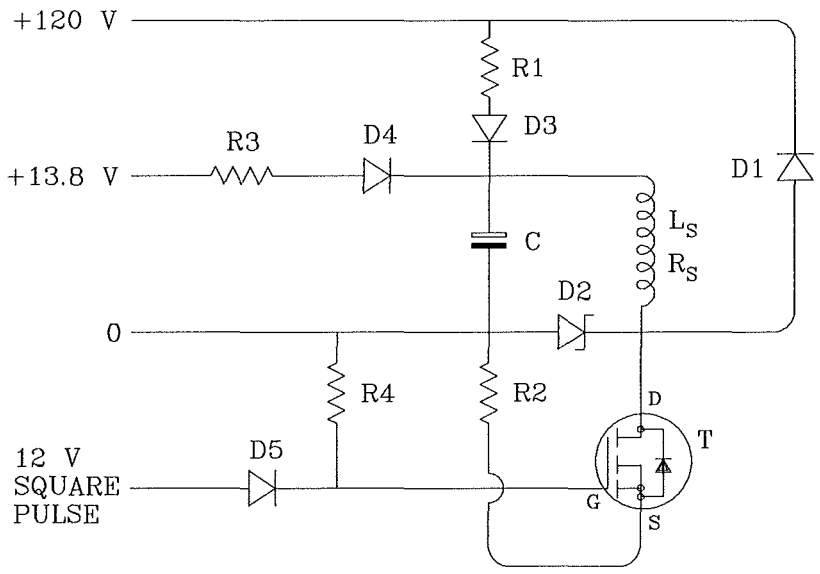

Figure 5.5 Capacitive discharge driver circuit.

The components used in the capacitive discharge driver circuit are listed below:

R1 made up of 2 x 180 Ω 10 W and 2 x 150 Ω 10 W resistors in parallel to give a resistance of 41 Ω 37 W.

R2 0.15 Ω 5 W wire wound resistor. This is used as a shunt resistor, across which a voltage proportional to the solenoid current can be measured. A voltage record could be displayed on an oscilloscope and then transferred to a computer.

R3 3.3 Ω 10 W

R4 1 kΩ ¼ W

D1 IN 4004 power diode

D2 BZT 03C 180 Zener diode

D3 BYX 42 1200R power diode

D4	BYX 42 1200R power diode
D5	IN 4004 power diode
C	200 μF 200 V electrolytic
T	IRF 641 TMOS power field effect transistor
L_s[†]	Inductance of Disole coils 337μH
R_s	Resistance of Disole coils 2.242Ω

The injector actuation solenoid may be considered as a series circuit of an inductance and a resistance[145]. Analysis of the effective RLC circuit (of the capacitor discharging through the coils of a solenoid) is described by Vieilledent[166] (with a better description of the background theory by Smith[167])[‡]. The analysis of this RLC circuit reveals that the roots of the characteristic equation are complex. The system is thus under-damped, which is desirable for a rapid current rise. The time to peak current is calculated to be 0.8 ms. In practice the peak current is limited by the value of the resistor R2. The rise to this peak current occurs within 0.15 ms of the trigger pulse.

The high voltage power supply was from mains via a variable auto-transformer (variac) and an isolating transformer. The variable auto-transformer enabled

---

[†] The inductance and resistance of the Disole were measured using a Wayne Kerr 4225 automatic LCR meter with the measurement frequency set to the recommended 1 kHz. The injector was assembled with the small armature and with the inner three coils connected in series.

continuously variable adjustment of the supply voltage. The power supply was converted to dc through a BR 254 full wave bridge rectifier. A 2000 μF 150 V capacitor was shunted across the load to filter out the ripple voltage. Provision was made to switch a circuit which discharges this capacitor through a 1 kΩ 10 W resistor. Thus the capacitor could safely be fully discharged before servicing the injector driver circuit.

In operation, the driver circuit was supplied with the high voltage to charge the capacitor. The start of the 12 V square timing pulse would switch the MOSFET on, thereby discharging the capacitor through the solenoid and R2 to ground. This discharging of the capacitor provided the high initial current required to rapidly actuate the solenoid. The resistor R1 provides resistance to recharging of the capacitor. Following the high current supplied by the capacitor a lower hold on current is supplied by the 13.8 V supply. This current holds the solenoid actuated until the MOSFET is switched off at the end of the 12 V square timing pulse. The decaying magnetic field in the solenoid stator causes a high transient reverse electro-motive force (e.m.f.). This is drained via D1. The zener diode D2 serves to protect the MOSFET drain from excessive voltage.

5.5 Injection timing circuit

The main requirement of the injection timing circuit was to be able to accurately set and record the timing and duration of the injection pulse. The first approach was to consider interfacing a computer to control the circuit. This was soon abandoned because it added unnecessary complexity to the system with no great advantage. Instead, a manually controllable circuit was devised as shown in Figure 5.6. The camshaft sensor (a slotted optical switch) was located at the rear end of the camshaft and was triggered by a slot in a disc attached to the camshaft. The slotted disc is normally used to trigger the start of petrol injection on the engine. The camshaft sensor was mounted so that it could be rotated about the camshaft axis to adjust the timing of the signal.

The pulse from the camshaft sensor triggered the start of the injection and a mono-stable multivibrator (74121) which provided a delay. The 5 kΩ multi-turn potentiometer enabled the duration of the delay to be adjusted between 1 ms and 20 ms. The injection pulse signal was inverted by the 7406 inverter. This signal then switched the BUK453 MOSFET to supply a 12 V square pulse of set timing and duration to the injector driver circuit.

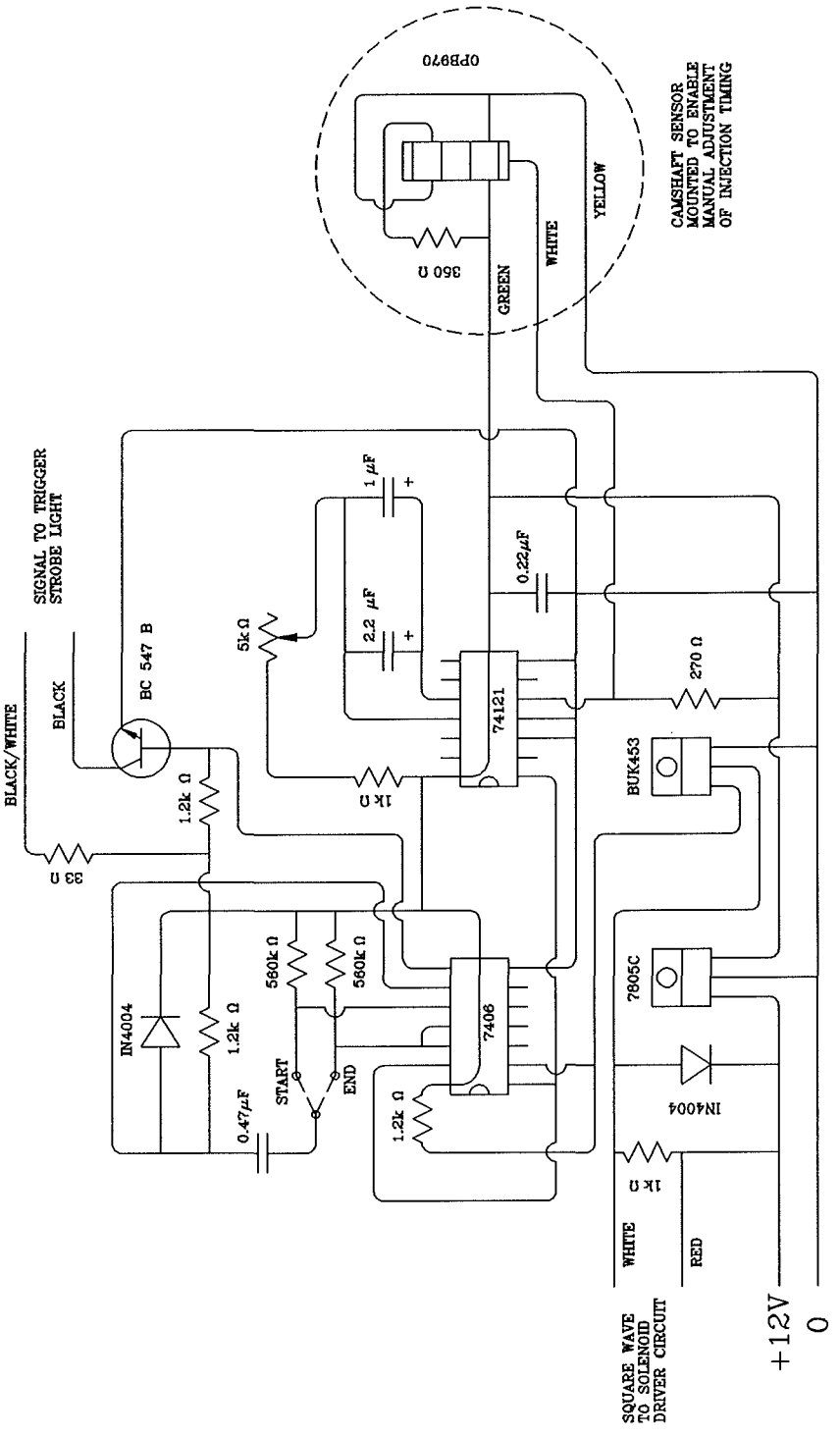

Figure 5.6 Injection timing circuit

In order to record accurately the precise timing and duration of the injection pulse, the circuit incorporated a trigger output for a stroboscope which flashed on the flywheel of the engine. The flywheel was marked in 1° increments and readings could be made to the nearest ½°. A switch was incorporated to enable triggering on either the start or the end of the injection pulse. The timing of the injection pulse was defined by the crank angle at the start of the pulse. The duration of the pulse was calculated from the engine speed and the angle between the start and end of the injection pulse.

5.6 Injector actuation testing

In order to assess the performance characteristics of the actuator and circuit, the injector actuation was tested in a bench test rig prior to final assembly. This bench rig was used to optimise the injector driver circuit and the injector armature configuration in order to provide the quickest travel times for valve opening and closing.

The injector was fitted with a modified needle and assembled without the base and nozzle. The modification to the needle was to enable a spring to be fitted to simulate the force acting to close the valve due to gas pressure. The injector assembly was mounted horizontally and a spring was fitted to supply a closing force of 40 N. The injector was connected to the injector driver circuit, the displacement transducer circuit and the water cooling lines (see Plate 5.1).

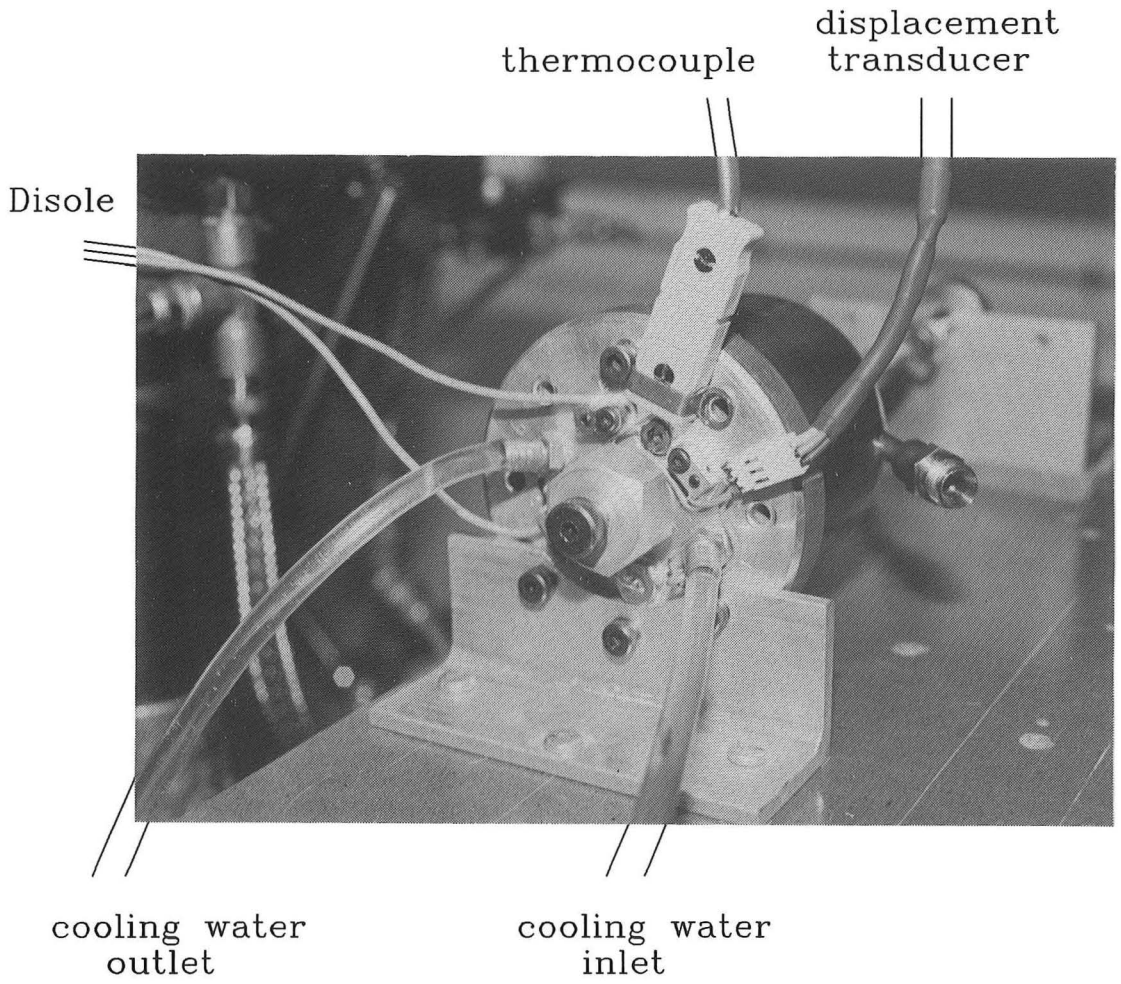

Plate 5.1 Injector installed on actuation test rig.

The displacement transducer output was displayed on a digital storage oscilloscope along with the voltage from the driver circuit resistor which indicated injector coil current. Tests were performed by motoring the Ricardo E6 engine to trigger the timing circuit and recording the resultant coil current and needle displacement on the oscilloscope. Traces captured on the oscilloscope were

transferred to the computer using the program RICARDO.BAS (Appendix E.1) for analysis and print-out.

The key parameters that were modified between injector actuation tests were:

a. Injector needle travel distance.

b. Minimum air gap between the Disole armature and stator.

c. Armature size and coil wiring.

d. Injector driver circuit components and supply voltage.

The injector needle travel distance was specified as 0.1 mm but testing showed that satisfactory needle travel performance could be attained for lifts in the order of 0.2 mm - 0.25 mm. Larger needle travel distances were tested and found to be detrimental to needle travel times. It was decided to determine the final optimization of needle lift distance during engine testing.

The modifications to the injector driver circuit were tested on a range of three different minimum air gaps and two armature sizes. The injector driver circuit thus determined is described in section 5.4. The best armature and coil configuration proved to be a small armature actuated by only the inner three coils.

The size of the minimum air gap had a great influence on the performance of the valve. A very small minimum air gap (0.2 mm) would cause the valve to hold on

for too long after the injection pulse had finished, giving an injection duration of 15 ms from a 2 ms injection pulse. A large minimum air gap (0.55 mm) gave a slower valve opening. A minimum air gap of 0.4 mm gave the best needle travel performance, providing an injection duration as low as 1 ms.

5.7 Actuated mass flow rate testing

The injector was tested for hydrogen mass flow rate under cycled actuation conditions prior to fitting to the engine. The experimental procedure was similar to that used for continuous flow mass flow rate testing (see section 4.6.3). The injector actuator was connected to the driver circuit and the injection frequency was controlled by controlling the engine speed. The experimental set-up is represented in Plate 5.2.

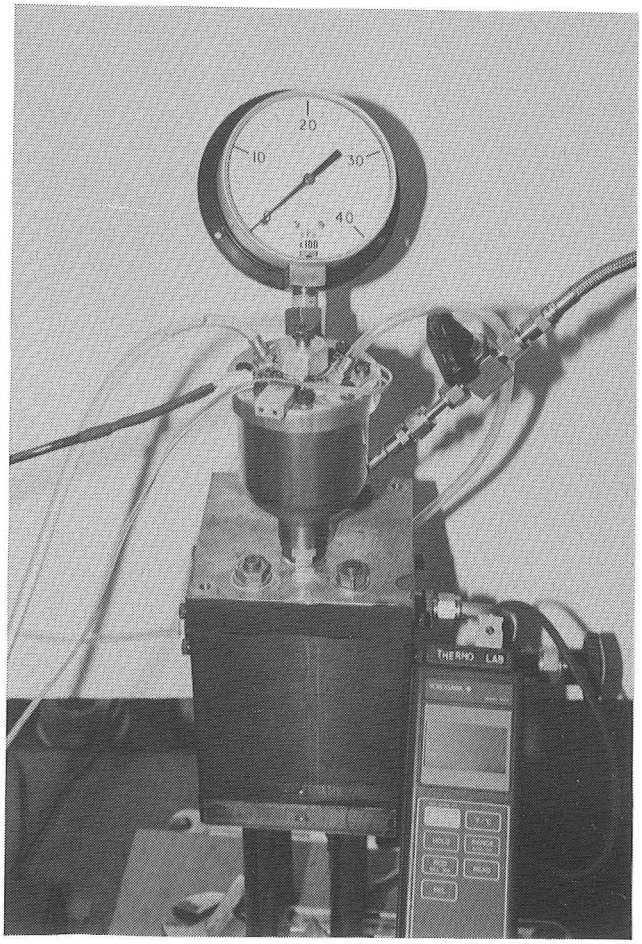

Plate 5.2 Injector set up for actuated mass flow rate testing.

The results of mass flow rate testing are shown in Figure 5.7. The valve lift was 0.25 mm and the engine speed was 15 rps (7.5 injections/sec). Further analysis revealed that the mass flow rate during injection was approximately constant at 6 g/s (over the current pulse duration range tested). Smaller mass flow rates could easily be achieved by reducing the valve lift distance. The optimum valve lift distance would be determined during engine testing.

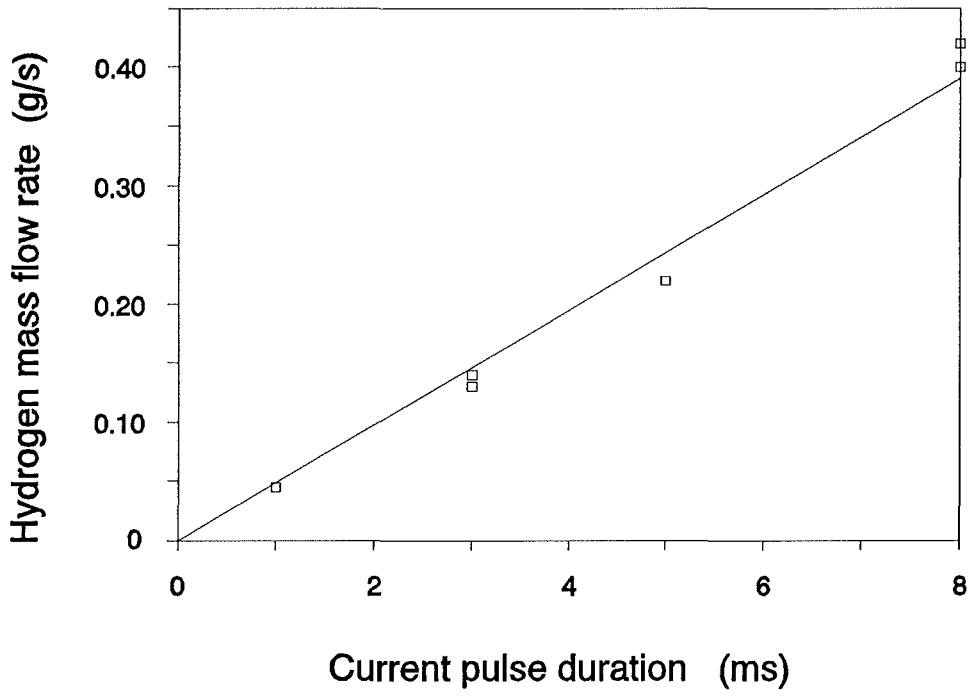

Figure 5.7 Actuated mass flow rate test results.

CHAPTER 6 ENGINE TEST CELL PREPARATION

This chapter describes the arrangement of the apparatus which was used to obtain the results of engine testing. The engine testing procedures and results are presented in chapters 7 and 8 respectively.

6.1 Engine modifications

Three items on the Ricardo E6 engine were modified in preparation for hydrogen engine testing. These modifications were:

a. The addition of an auxiliary M10 x 1 hole in the cylinder head to allow the installation of a pressure transducer.

b. The fabrication of a replacement camshaft cover incorporating a bracket to support the hydrogen injector.

c. The replacement of one of the crankshaft side covers with a safety burst disk in order to relieve pressure during a possible crank-case gas explosion.

6.1.1 Cylinder head

The standard cylinder head of the Ricardo E6 research engine has two M14 x 1.25 spark plug holes. Typically one of these is used for a spark plug and the other for a pressure transducer. For the purposes of this project it was necessary to site the pressure transducer in an alternative location so that the injector could be located in the auxiliary M14 hole. The engine manufacturers were contacted to find out if they could supply a cylinder head with three spark plug holes (two M14 x 1.25 and one M10 x 1). Such a cylinder head could be supplied but was prohibitively expensive†. Thus, modification of a spare standard cylinder head was undertaken. The geometries of the standard cylinder head and the adjacent camshaft housing were modelled using a three dimensional CAD system in order to determine the optimum site for the extra hole (Figure 6.1 and Plate 6.1). Van Aken[168] gives a detailed description of the errors associated with various cylinder head pressure transducer installations. The major requirements for the location of the pressure transducer are outlined in the documentation supplied with the AVL 8 QP 500c pressure transducer. The requirements for accurate combustion chamber pressure results are summarised as follows:

a. The sensing diaphragm area of the transducer should lie entirely over the combustion chamber cavity.

---

† In excess of £3900 - May 1991

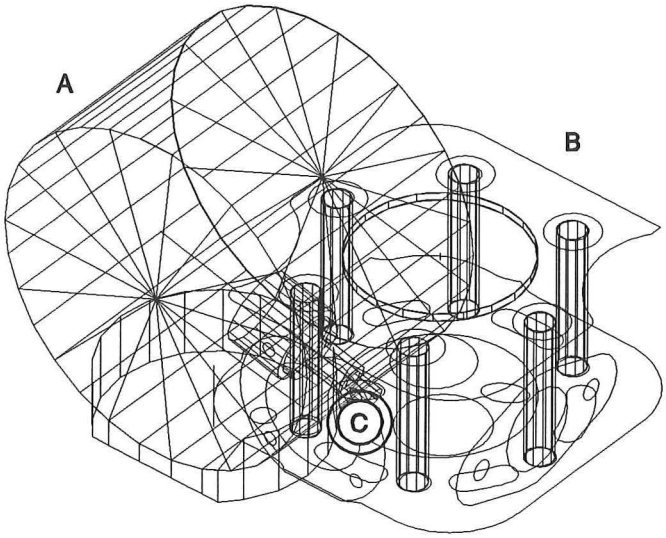

Figure 6.1 3-D wire-frame representation of cylinder head and camshaft housing

A - Camshaft housing
B - Cylinder head
C - Pressure transducer hole (drawing viewed along axis)

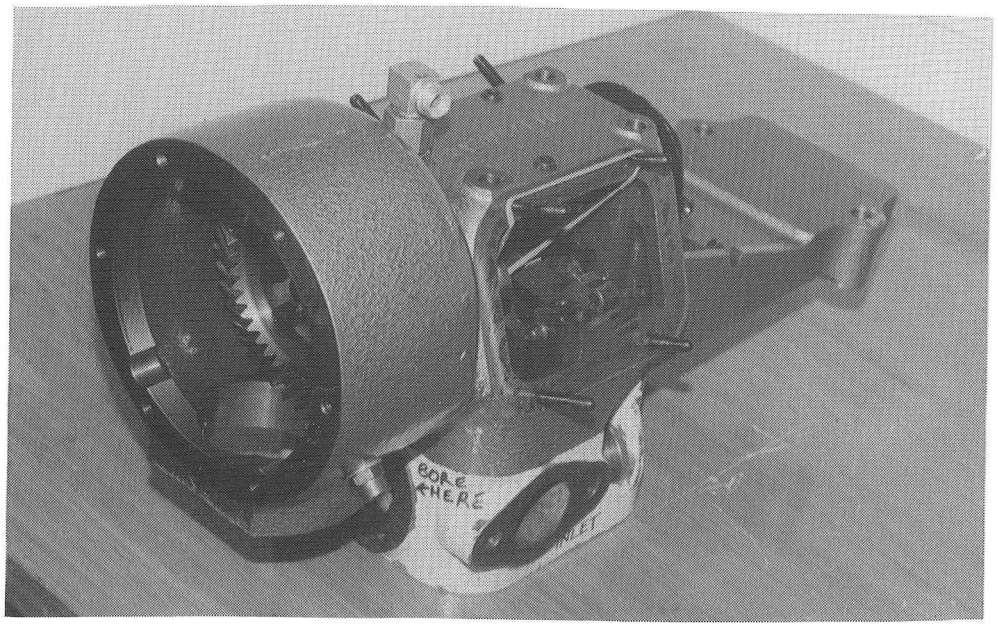

Plate 6.1 Cylinder head and camshaft housing.

b. The transducer should be located away from the exhaust valve in order to minimize thermal shock effects.

c. The axis of the pressure transducer should be as near to perpendicular to the internal face of the combustion chamber as possible.

d. Any connecting passage-way from the combustion chamber to the sensing diaphragm of the transducer should be minimal.

In addition to these requirements it was desirable to allow easy access for the removal of the pressure transducer. Whenever a pressure record was not required during engine testing, the transducer could then be replaced with a dummy plug in order to preserve the life of the transducer.

With consideration of the above requirements a sleeve was designed and welded into the cylinder head at a site determined using the CAD system. Because of space restrictions a special socket had to be manufactured to install and remove the pressure transducer. The details of the pressure transducer sleeve design are included in Appendix D.

Following the modifications to the cylinder head, the clearance volume was measured and the compression ratio setting micrometer recalibrated.

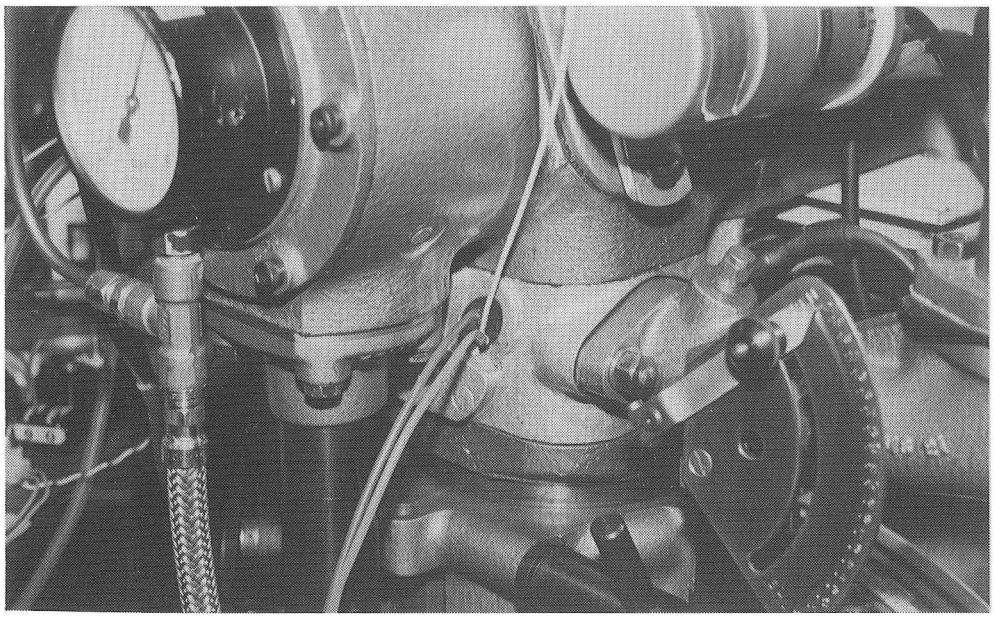

Plate 6.2 Pressure transducer installed on the engine

It was found after a period of operation, that the modified cylinder head had developed a leak. Water was leaking through a crack in the weld into the combustion chamber. The problem was traced to steel being mistakenly used as the sleeve material. Steel has a different coefficient of thermal expansion to cast iron[169] and the weld had cracked. Also, the weld was not of high integrity as the sleeve had been machined complete with the thread and the welder had to be careful to avoid destroying the thread or the valve seat inserts. Following consultation with a welder more experienced with cast iron, the original sleeve was removed and replaced with a cast iron one. Final internal machining of the sleeve was left until after welding and the valve seat inserts were replaced with weld metal. The resulting repair was very sound and no further problems have been encountered with the modification.

6.1.2 Camshaft cover

The mass and size of the injector caused some concern about the ability of the M14 threaded base to support the injector. It was decided to augment the support of the injector by supporting the top of the injector. The adjacent camshaft cover plate was replaced with a 6mm steel plate secured in place with countersunk cap screws instead of the usual studs and nuts. The injector was installed in the auxiliary M14 hole and measurements were taken to enable the design of a fixture on the camshaft cover plate, in a plane parallel to the top plane of the injector. The fixture was duly fabricated on the cover plate and an array of nine M8 holes machined in the face of the fixture. Two struts were made from 6mm x 25 mm mild steel to tie the top of the injector to the fixture. Steel washers were machined and used to fit the struts to the fixture so that they were aligned with the top of the injector. The complete injector installation on the engine, showing the modified camshaft cover and support struts, is shown in Plate 6.3.

6.1.3 Crank-case burst disk

Although no report of a crank-case explosion during hydrogen engine testing could be found it is conceivable that a combustible mixture could occur in the crank-case due to leakage of gas past the piston rings. For this to pose a safety hazard there must also be a potential source of ignition in the crank-case.

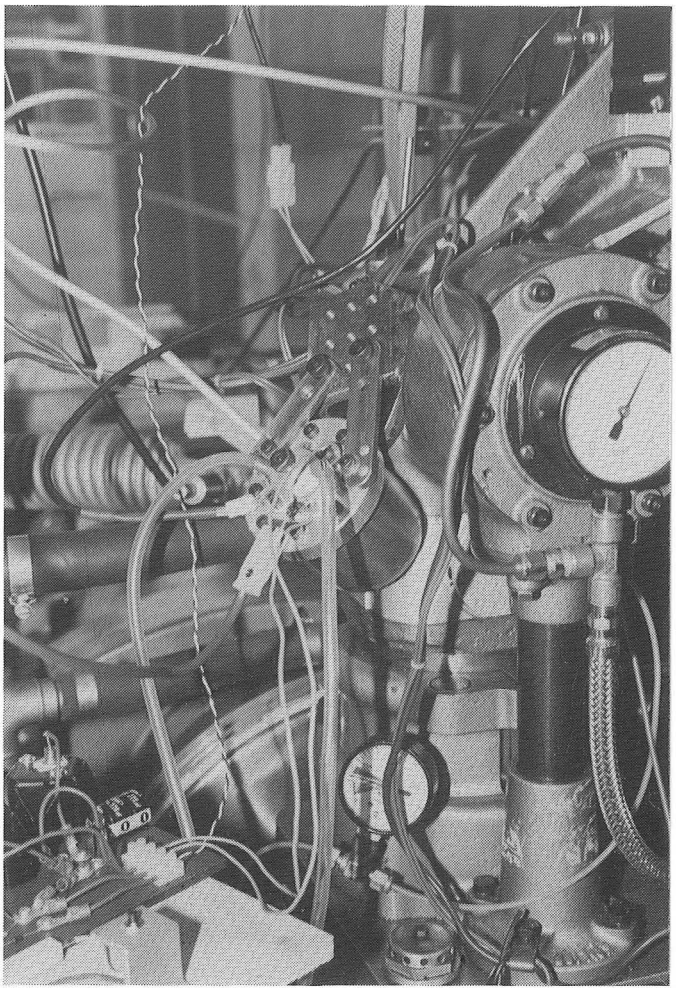

Plate 6.3 Hydrogen injector installed on the engine

Macdonald[170] took the precaution of purging the crank-case with air to avoid a possible build up of combustible mixture. The Ricardo E6 engine was equipped with a crank-case vent, so it was considered unlikely that a combustible mixture would occur in the crank-case. As an added precaution however, a burst disk arrangement was made to replace one of the crankcase side vents on the Ricardo. The burst disk was made from 1mm clear plastic sheet and was held in place by an 8mm steel plate surround as shown in Plate 6.4.

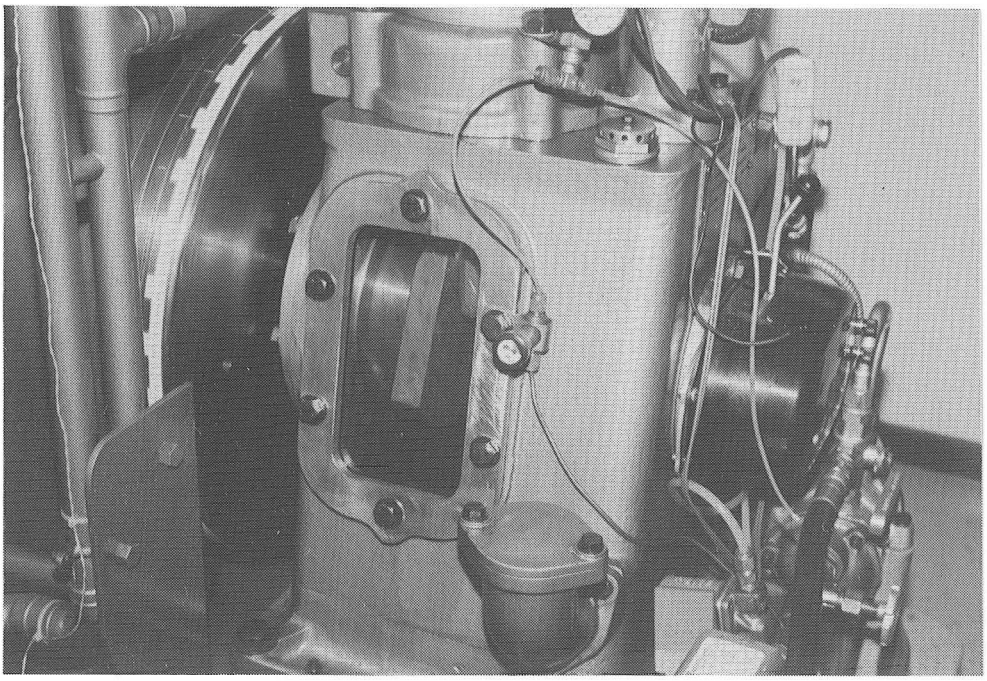

Plate 6.4 Crank-case burst disk

6.2 Safety system

Being odourless, colourless and potentially very dangerous, if a leak occurs in an enclosed space, some form of detection system was considered a sensible precaution for the safe use of hydrogen in the engine test cell. The engine test cell was fitted with a gas detector alarm system (Almaza Developments A200M

2-channel). This system utilises two gas sensitive semiconductor sensors (Figaro TGS 813). One sensor was mounted above the engine and the other was mounted above most of the hydrogen supply piping within the room. The alarm was calibrated by the manufacturer to activate when either sensor detected a level greater than 20% of the lower explosive limit of hydrogen in air. Upon sounding, the alarm would also activate relays to switch on a fan and switch off the hydrogen supply solenoid (Figure 6.2). When the alarm had de-actuated, the state of the fan and fuel supply solenoid would remain as activated until manually reset.

The operation of the safety system was put to the test numerous times during commissioning of the hydrogen supply system and in every case the fan quickly eliminated any hazard of a hydrogen explosion and the source of the leak could then be traced.

6.3 Fuel supply system

The recommendations of Segal *et al*[63] were considered when designing the fuel supply system for the Ricardo engine test cell. Calculations based on Segal's system suggested a minimum test duration of at least 1 hour 40 minutes between bottle changes. It was thought unnecessary to provide for such lengthy engine operation but it was considered important to allow space to manifold more bottles into the supply system if operating experience revealed this necessary. Initially,

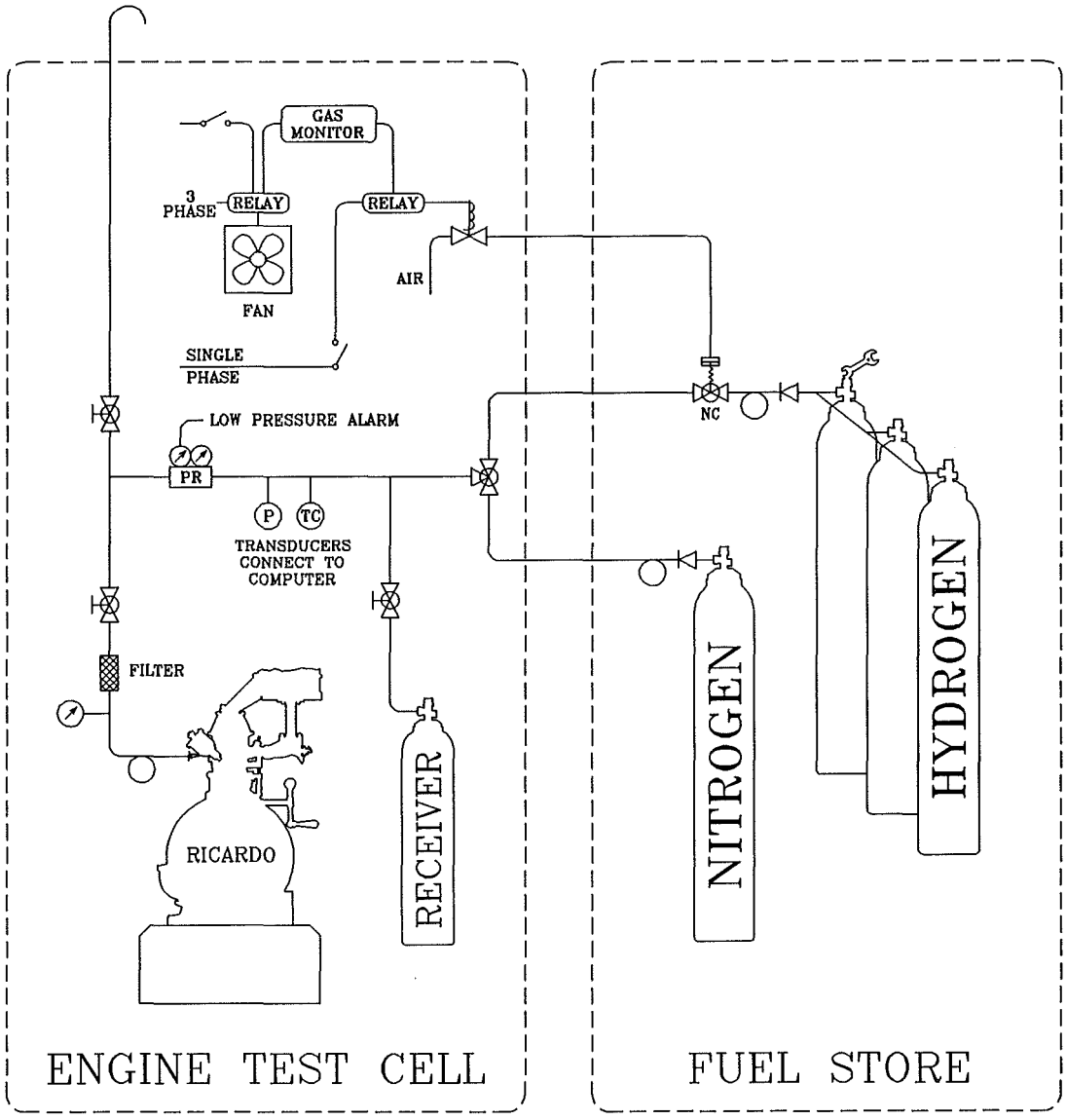

Figure 6.2 Hydrogen fuel supply system.

just one 5.8 m^3 hydrogen bottle was used. During engine testing it was found that three 5.8 m^3 hydrogen bottles manifolded together gave a sufficient length of engine test (1 hour minimum). The final configuration of the hydrogen supply system is shown in Figure 6.2. Many of the safety features of Segal's system were implemented for our test cell set-up. Features of the hydrogen supply system installed are detailed below.

a. A nitrogen supply was incorporated to purge the high pressure hydrogen line up to the engine.

b. The hydrogen storage bottles and nitrogen purge bottle were located outside the main building in a well ventilated storage building close to the engine test cell. This was not only a safe site for the storage of the gases but was most convenient for vehicle access to replace the bottles. The engine test cell was too crowded to consider housing the bottles inside and it would not be as safe as storing the bottles outside the building.

c. A normally closed air actuated ball valve on the hydrogen supply line allows for rapid and automatic isolation of the test cell from the supply in the event of a hydrogen leak. The air supply was via a normally closed solenoid valve. For the hydrogen supply to be on, both the air and power supplies to the solenoid must be on and the hydrogen gas sensors in the room must not be activated. If the gas sensors are

activated the hydrogen supply is automatically isolated and must be manually reset to recommence supply.

d. Inside the engine test cell room is a three position manual valve which is used to select hydrogen, nitrogen or off. This allows the rapid switching from nitrogen to hydrogen when commencing running the engine and switching back to nitrogen when engine testing is completed. The off position was selected to perform mass flow rate testing. With the receiver valve open, the transducers P and TC were monitored to provide data for the calculation of mass flow rate.

e. The pressure regulator incorporated a pressure switch at its outlet. The pressure switch was connected to sound an alarm and activate a flashing light when the pressure dropped below 70 bar. This precaution was taken because the injector design relied on the hydrogen supply pressure to close the valve. If a drop in supply pressure went unnoticed, the combustion chamber contents could flow back into the injector when the combustion chamber pressure exceeded the hydrogen supply pressure. This would cause contamination of the inside of the injector and could result in a combustion within the hydrogen supply system.

f. Following the pressure regulator there is a manual valve to allow the line to be vented outside the room. With the hydrogen supply isolated the supply line can still contain a significant quantity of hydrogen. In the

event of an emergency the hydrogen supply can be isolated and the line vented before purging with nitrogen. In practice it was also useful to be able to vent the line of nitrogen prior to dismantling the injector.

g. A manual shut off valve was mounted near the engine with a 60 micron filter and a pressure gauge between the valve and the engine. The filter was installed to prevent any particles causing damage to the injector seat. This isolation section of tubing between the valve and the engine was used to check the extent of any leakage through the injector. With nitrogen in the line and the engine stationary the valve was closed and any drop in pressure on the pressure gauge timed with a stopwatch. A "no leakage" condition was confirmed before each engine testing session. After each engine testing session the pressure drop (if any) was timed.

h. Loops were bent in the stainless steel supply tubing wherever relative movement of parts was apparent. Loops were used on the hydrogen and nitrogen bottle connections and at the connection to the injector. The connection to the injector required special consideration because the movement of the top end of the engine is considerable due to the compression ratio adjustment mechanism. A flexible high pressure hose seemed appropriate to use here but was not used because the teflon lined hoses available can leak hydrogen through the walls[63]. Instead of

a flexible hose, two loops of stainless steel tubing were used to connect to the injector.

i. Stainless steel tubing (¼") and stainless steel Swagelok fittings and Nupro valves were used throughout the high pressure gas system. The pressure switch used on the regulator and the pressure transducer were from Span Instruments (IPS-122 indicating pressure switch and SPT-100 pressure transducer respectively).

6.4 Instrumentation of the engine test cell

In order to make engine testing quick and reliable many of the transducers in the engine test cell were interfaced to a computer. A 386 personal computer was available for capturing, storing and processing information. One of the main requirements of the data acquisition was an ability for high-speed analogue to digital conversion. The two readings which required this high-speed conversion were from the piezo-electric pressure transducer channel and from the injector displacement transducer. Another requirement of the data acquisition system was to read in a number of other inputs at very much lower frequencies. These inputs were from thermocouples, a hydrogen pressure transducer and exhaust λ sensors.

Much of the standard instrumentation previously installed in the Ricardo E6 test cell was used unmodified. The development of a data acquisition system for hydrogen engine testing focused on reading data which could not be read manually or which would be error prone or time consuming if read manually.

The data acquisition system adopted for the engine test cell was a Keithley MetraByte DAS-20 with an EXP-20 multiplexer wired in through an STA-20 screw terminal accessory board. The DAS-20 data acquisition card was mounted in a full length expansion slot in the IBM 386 compatible computer. The STA-20 was used to enable easy connection of inputs to the DAS-20. The DAS-20 is a 12 bit A/D converter with direct memory access (DMA) capability enabling a maximum conversion rate of 100 kHz. There are eight programmable input voltage ranges between $\pm$50mV and $\pm$10V. The DAS-20 can be configured to accept either eight differential or sixteen single ended analogue inputs. For this work the DAS-20 was set for eight differential inputs, two of which were devoted to the connection of the EXP-20 multiplexer. Two of these channels were used to read data from the pen recorder outputs of a digital storage oscilloscope. The injector needle displacement transducer, piezo-electric pressure transducer and a trigger input (from the petrol injection circuit) utilized three other channels. A λ sensor in the exhaust was connected to one channel.

The EXP-20 enables 16 channels to be multiplexed into one DAS-20 channel. The EXP-20 is designed to be used for thermocouple inputs and it incorporates a cold junction compensation (CJC) sensor. The CJC sensor output runs

through a separate channel of the DAS-20. The EXP-20 was used for thermocouple inputs and the hydrogen pressure transducer input. Plan views of the STA-20 and EXP-20 connector boards are shown in Figure 6.3 and Figure 6.4 respectively. The connections, jumper positions and dip switch settings are typically as used for the engine testing.

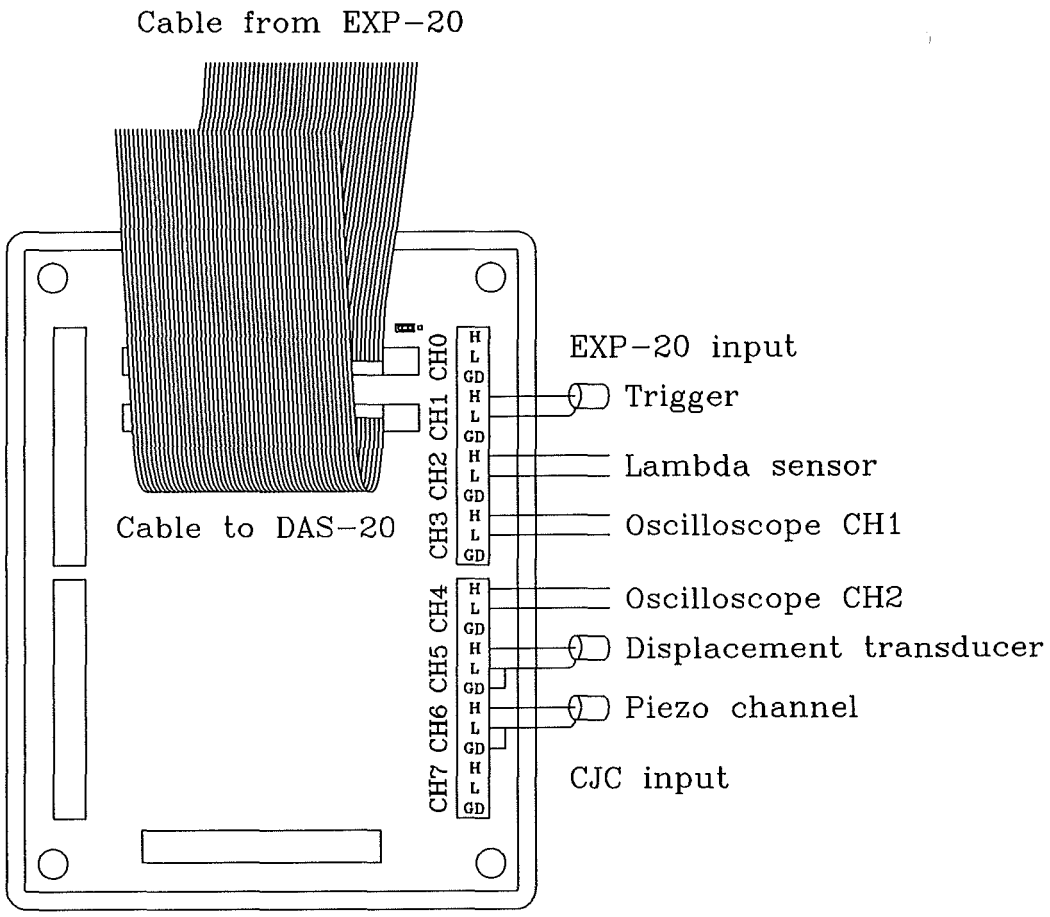

Figure 6.3 Screw Terminal Accessory board STA-20

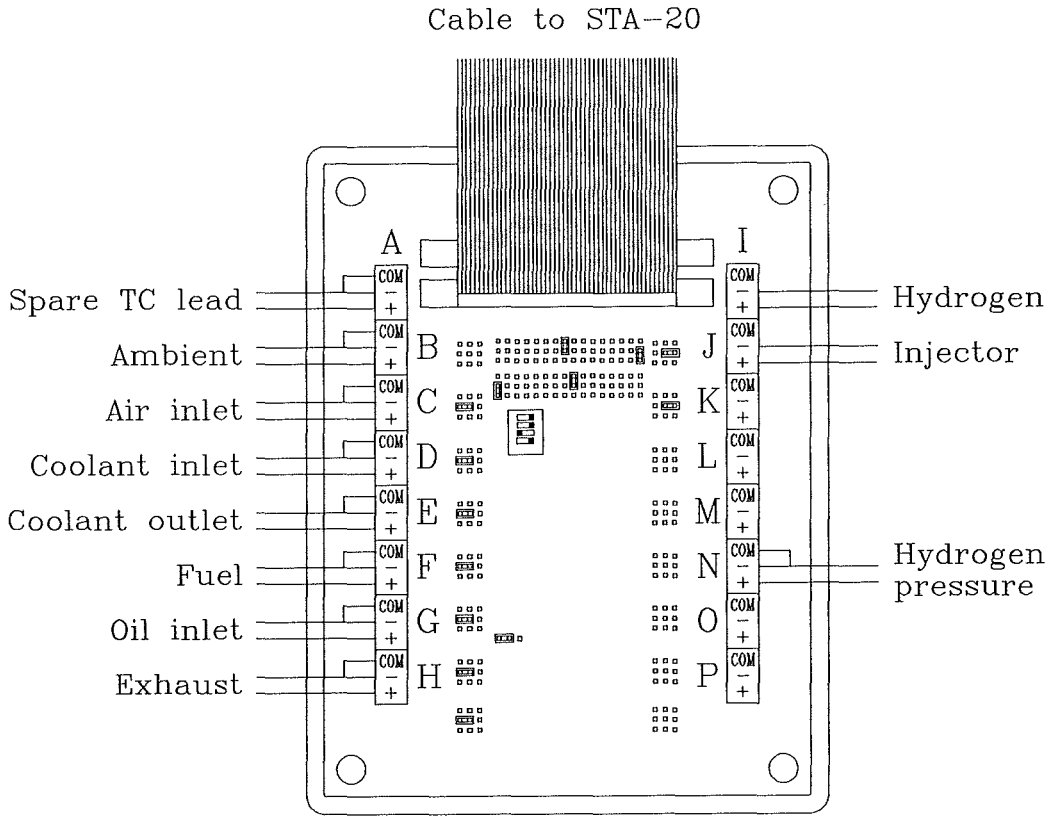

Figure 6.4 Expansion multiplexer board EXP-20 showing thermocouple and hydrogen pressure transducer connections.

CHAPTER 7 EXPERIMENTAL PROCEDURES

Further to the development of experimental apparatus detailed in previous chapters this section describes the procedures developed and used to establish the results of the engine test programme.

7.1 Engine operation

One hour before commencing engine testing on hydrogen the engine coolant and oil pumps and heaters were activated. The cooling water supplies to the injector and the piezo-electric pressure transducer were also turned on.

The compression ratio adjustment was set. The gasoline supply pump and injector were disconnected and the gasoline injection circuit was energized[†]. Approximately 10 minutes before starting the engine the power supply to the heated exhaust λ sensor was switched on.

The gasoline injection trigger, the piezo-electric pressure transducer output and the needle displacement transducer output were switched to the oscilloscope.

[†] The gasoline injection pulse was used as the trigger signal for combustion chamber pressure and injector needle lift data capture.

The computer program RICARDO.BAS was implemented and the configuration variables were set for the engine test to be performed (option 2 on the program menu). The thermocouple, hydrogen supply pressure and λ sensor data were then displayed on screen (option 3).

With the isolating shut off valve closed and the three way valve in the test cell off, the hydrogen and nitrogen cylinders were opened manually. The solenoid control valve was actuated, opening the isolating shut off valve. The test cell air conditioning unit and the ventilation fan were switched on.

The three way valve was turned to the nitrogen position and the regulator was adjusted to an outlet pressure of 80 bar.

The injector trigger circuit and the low pressure alarm were switched on.

The injector was tested for leakage as described in section 7.1.1.

The engine was motored up to speed then switched to fixed speed mode. The injector driver circuit, cooling fan and displacement transducer power supplies were switched on and the variac was adjusted to give 120 V dc across the output terminals of the bridge rectifier. The three way shut off valve was switched to hydrogen and the injection and ignition were adjusted until stable engine operation was achieved. The engine coolant and oil heaters were switched off and the valves connecting the hydrogen receiver were opened.

The air/fuel ratio was adjusted by varying the injection duration and noting the change in the exhaust temperature and the λ sensor voltage. For a given operating condition the ignition timing was adjusted to the minimum advance for best torque (MBT).

After the engine operating condition had stabilised, the thermocouple data and λ sensor data on the computer screen was saved to a file. The following data was then recorded manually:

- Compression ratio.
- Engine speed in rps.
- Barometric pressure in mm Hg.
- Injection start in °ATDC as read from the flywheel using the stroboscope.
- Injection end in °ATDC.
- Air flow meter manometer reading in mm water.
- Number of weights on the dynamometer.
- Dynamometer balance reading in N.
- Ignition timing in °ATDC.
- NO_x concentration in exhaust in parts per million (see section 7.1.2).
- Injector needle lift read in divisions from the oscilloscope. This reading was later scaled to mm.
- Injection duration setting read from a multi-turn dial on the duration adjustment potentiometer. This was later calibrated to give a relationship between the dial setting and injection duration in ms.

Menu option 5 was then selected in the RICARDO.BAS program. The needle displacement and piezo-electric pressure transducer signals, until now displayed on the oscilloscope, were switched along with the trigger signal to display needle displacement and combustion chamber pressure traces on the computer screen. The data for two consecutive cycles was captured and stored to a file for later analysis. Following data capture the signals were returned to the oscilloscope for continuous real time display.

The data required for calculation of the hydrogen mass flow rate was then recorded (as detailed in section 7.1.3).

Provided that there was sufficient fuel and the engine was functioning satisfactorily, the computer program configuration settings would be updated and another operating condition would be tested. Testing would proceed until the fuel supply pressure had decreased to near 80 bar or there was some malfunction with the test equipment.

The engine was shut down by closing the hydrogen receiver valves and switching the three way valve to nitrogen. Within a few seconds the engine would switch to motoring mode. The injector driver circuit was switched off and the engine motoring speed control turned to zero. The injector was then tested for leakage.

After switching off the low pressure alarm the three way valve was set to the off position and the pressure downstream of the valve was vented. If there was to be no further testing that day, the gas cylinders were shut down and all of the power supplies were switched off. The engine coolant and oil pumps were left on and the piezo-electric pressure transducer and injector cooling water lines were left running while the engine cooled.

7.1.1 Injector leakage testing

Prior to each series of engine test runs the injector was tested to verify that it did not leak. Upon failure of the injector, or following a series of tests, the injector would be tested again to determine the extent of any leakage. The test was performed when the engine was not running. The manual valve nearest the injector was turned off and the pressure drop (if any) was timed. Nitrogen was used for the leakage test to ensure that a combustible mixture did not build up in the engine and test cell. The volume of the injector, pressure gauge, filter and supply line, back as far as the valve was 93 ml. The leakage rate was determined by calculating the mass of nitrogen in the reference volume at the start and end of the timed period. The temperature of the nitrogen was assumed to equal the ambient temperature.

7.1.2 NO_x emission testing

It was initially envisaged that testing for the pollutant of oxides of nitrogen would be carried out using a Beckman chemiluminescent 951E NO_x analyzer. Unfortunately, the meter available was inoperable at the time of the engine testing. All other available options were considered for analysing the exhaust emissions and it was eventually decided to use Kitagawa length-of-stain type detector tubes. The Kitagawa system consists of a hand pump which is used to draw 100 ml of the sample gas through a slender glass tube. The tube contains chemicals which react with the gas to be detected (in this case NO_x) to change colour. The length of the stain in the tube then indicates the concentration of the detected gas in the sample.

The exhaust sample was taken from a ¼" stainless steel tube mounted in the exhaust pipe approximately 2 m from the engine. This distance was required to ensure that the exhaust gas had cooled sufficiently. The stainless steel tube was 3 m long to allow further cooling of the exhaust gas down to within the recommended range for the Kitagawa tubes (the instructions stated that no temperature correction was necessary at temperatures between 5°C and 45°C). A rubber hose was fitted to the end of the stainless tube to enable a Kitagawa tube to be inserted for testing.

After setting the engine operating conditions and taking all other readings a manual pump was used to draw exhaust gas through the hose. This was done

to ensure that the contents of the hose best represented the exhaust gases from the engine for that condition. The Kitagawa tube and pump were connected to the end of the hose and one full stroke of the pump was taken. The reading was then made in accordance with the instructions.

7.1.3 Hydrogen mass flow rate measurement

The mass flow rate of hydrogen into the engine was determined by recording the pressure and temperature changes from a reference supply volume (see Figure 6.2 page 116). The mass of hydrogen contained in the reference volume at any instant could be calculated from the hydrogen temperature and pressure.

The procedure developed for this test involved taking 100 readings of temperature and pressure over an 80 second period. These readings were timed and recorded via two channels of the data acquisition system. After the first 10 readings the small hydrogen receiver and engine were isolated from the main hydrogen supply. The main supply was reconnected either at the 90th reading or earlier if the pressure had fallen close to 80 bar. All the readings were written to a file for later processing to determine the mass flow rate. The mass flow rate of hydrogen was calculated using the QuickBASIC program MFRCALC.BAS.

Following the completion of the engine testing, personal communication with Sierens† highlighted a possible error in the mass flow rate measurement. Sierens used a similar configuration and method for measuring the mass flow rate of gaseous fuels. Sierens was concerned about the inaccuracy of assuming that the measurement of temperature and pressure in the pipe downstream of the hydrogen receiver‡ was representative of the conditions within the reference volume. In his work Sierens took measurements of temperature and pressure within the receiver.

It was decided to test the extent of the possible error by experiment. The following experiment was devised to compare the "as tested" mass flow rate with the mass flow rate calculated from steady state initial and final conditions.

An additional needle valve was installed in the hydrogen vent pipe to allow venting for a range of hydrogen mass flow rates. The mass flow rate sub-program of RICARDO.BAS was modified to allow the capture of 500 data points instead of the usual 100. After setting the needle valve on the vent and closing the vent shut off valve, the hydrogen receiver volume was isolated from the main supply cylinders and allowed to settle. The mass flow rate test proceeded as before but instead of re-engaging the main hydrogen supply at the 90th data point, the vent

---

† Roger Sierens[179], University of Gent, Belgium. Discussions held at the 9th World Hydrogen Energy Conference. 1992.

‡ The transducers were not installed in the receiver because it was hired from NZIG and could not be modified.

valve was quickly shut off. The subsequent data capture recorded the stabilising of the hydrogen temperature and pressure.

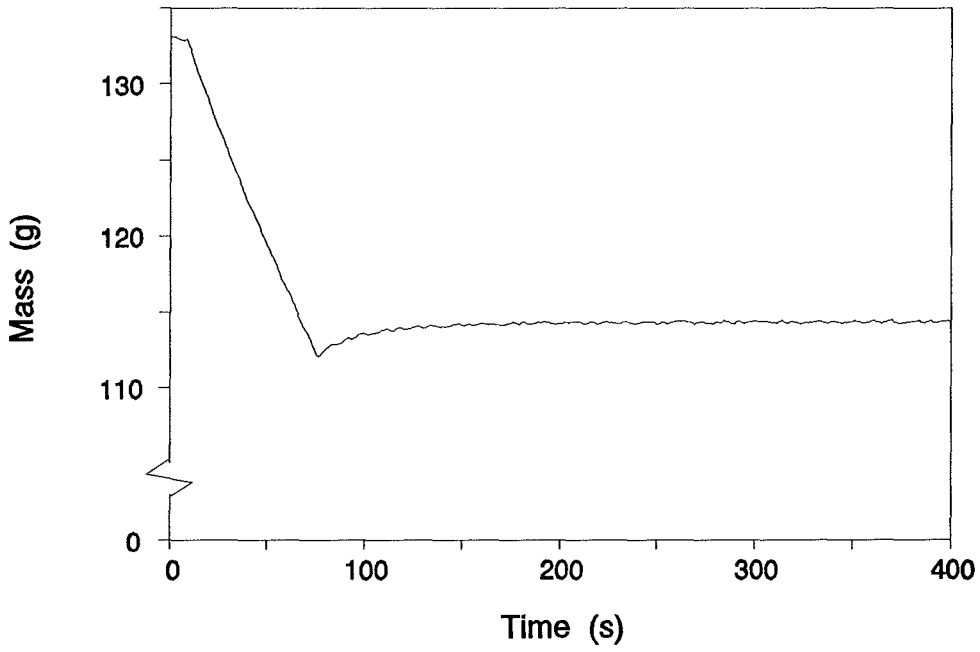

Figure 7.1 Typical mass-time record.

The data was processed using the Beattie-Bridgeman equation to give a record of the calculated mass of hydrogen within the reference volume. Figure 7.1 shows a typical mass-time record (test number 1). Note that the calculated mass appears to increase after the vent is closed. What actually happened was that the recorded temperature and pressure were changing as the conditions within the reference volume stabilised.

The mass flow rate was calculated in two ways:

a. Using a linear regression to determine the slope of the mass-time record. This was the method employed for the data produced from hydrogen engine testing.

b. From the initial and final steady state mass record and the duration of the venting. This method will give the best available indication of the actual mass flow rate.

A range of mass flow rates were tested representing those encountered during engine testing.

The results of these tests are shown in Table 7.1. Note that the ratio of actual MFR to regression calculated MFR is nearly constant. The actual MFR is on average an 8.4% reduction on the regression MFR. This calibration was applied to all of the mass flow rate test results.

Table 7.1 Results from mass flow rate method investigation.

Test number	Regression MFR g/s	Actual MFR g/s	Actual/Regression
1	0.304	0.278	0.914
2	0.211	0.194	0.919
3	0.134	0.123	0.918
4	0.091	0.083	0.912

7.2 Calibration of transducers

7.2.1 Injector needle displacement transducer

The calibration of the installed SOS displacement transducer was most easily verified by turning the adjustment screw by hand and recording the voltage displayed on the computer as read in by the DAS-20 A/D system (using menu option 1 on the computer program RICARDO.BAS). The eight equi-spaced cap screws on the top cap of the injector and points half way between these screws served as the necessary divisions for the calibration of the SOS in the assembled injector. The calibration graph for the displacement transducer is shown in Figure 7.2. The linear range of the displacement transducer output is between 0.15 V and 0.55 V.

7.2.2 Piezo-electric pressure transducer

The piezo-electric pressure transducer was calibrated using a specially modified Barnett dead weight tester. A piezo-electric pressure transducer only gives an output in response to a dynamic pressure input so static pressure calibration is inappropriate. The modifications to the dead weight tester were based on the work of Trolove[171]. Trolove attempted to simulate the rapid fluctuation in an engines combustion chamber pressure to calibrate the transducer. This was

found to be unnecessarily complex and the final configuration allowed only for the rapid release of a static pressure.

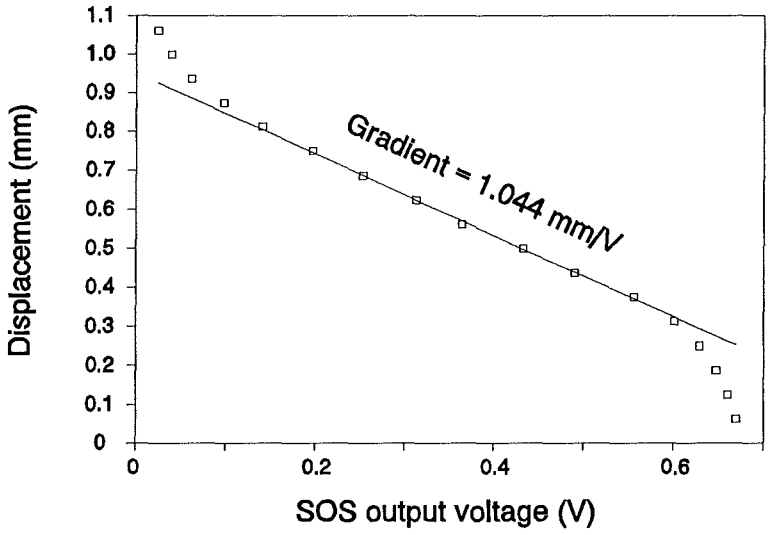

Figure 7.2 Slotted optical switch injector displacement transducer calibration.

A program was written to read voltages from the piezo-electric pressure transducer amplifier through a DAS-20 A/D board. The input was sampled at a rate of 1 kHz. The procedure was to apply the desired load, ground the piezo-channel input using a switch on the amplifier and then unload the transducer immediately after commencing the voltage reading. The program allowed for 1000 samples and the voltage noted was that of the maximum deviation found within those readings. This procedure was performed for a range of pressures from 0 to 135 bar in 5 bar increments. Results were graphed and the slope of the line of best fit calculated.

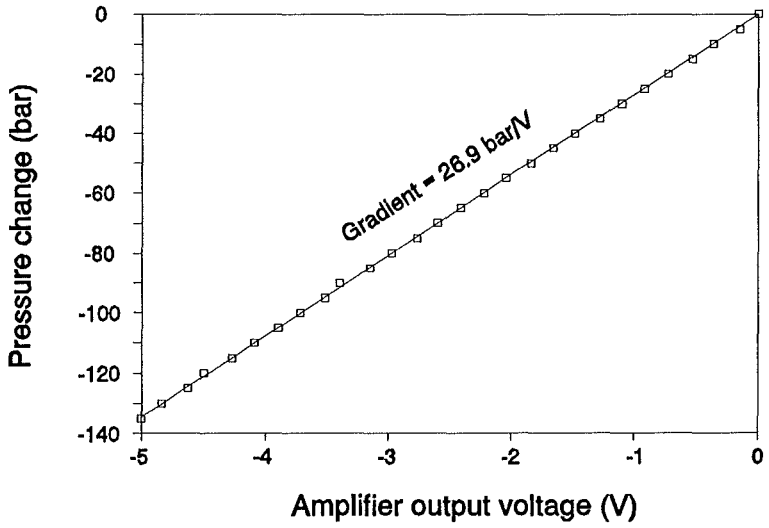

Figure 7.3 Piezo-electric pressure transducer calibration.

Because of the very low output levels from the piezo-electric pressure transducer, the output from the amplifier is very sensitive to small changes in the wiring and fittings connecting the transducer to the amplifier. Prior to assembly the connections were cleaned and dried. The calibration of the transducer was tested periodically and in particular after any interruption to the piezo-electric pressure transducer circuit or amplifier.

CHAPTER 8 PRESENTATION AND DISCUSSION OF RESULTS

During the development of the injector many experiments were performed to determine various parameters in order to define criteria for the next stage of the design. The results of these experiments have already been dealt with in previous chapters. This chapter details the results of experiments conducted on the Ricardo E6 research engine.

The Ricardo E6 engine was initially operated on 91 octane unleaded gasoline to establish the base line performance characteristics of the engine. The compression ratio was set to 8:1 (the highest useful compression ratio for this fuel) and the engine was operated for a range of throttle settings at speeds of 20 rps, 25 rps and 33.3 rps. The gasoline injection was adjusted to maintain the air/fuel ratio at stoichiometric for each test condition. This condition was established from the output of a λ sensor in the exhaust and later verified by calculation of the supplied air/fuel ratio. Ignition timing was set to the minimum advance for best torque.

Hydrogen engine testing was performed over the same range of engine speeds as for the gasoline engine tests. All of the hydrogen engine testing was done with the throttle wide open. Compression ratio settings of 8:1, 10:1 and 12:1 were tested.

8.1 Selected errors associated with results

8.1.1 Combustion chamber pressure

It was apparent from combustion chamber pressure data that the zero pressure voltage was prone to variation. This is a widely recognised problem with piezo-electric pressure transducers and elaborate multi-transducer installations have been used to solve the problem[19]. The raw voltage data captured from the piezo-channel amplifier was shifted to give zero volts corresponding to the mean pressure during the exhaust and inlet strokes. This data was then multiplied by the calibration constant (see section 7.2.2) and added to the barometric pressure to give the absolute pressure record.

The error associated with assuming the mean exhaust and inlet stroke pressure to be barometric has no effect on the main uses of the pressure data. Calculation of the maximum rate of pressure rise and the indicated power is not affected by the specification of the pressure datum. The only measurement made from the pressure data which is affected by a possible error in the datum specification is that of maximum absolute pressure. The extent of the datum error is only in the order of ± 1 bar and would have little effect on comparisons of maximum absolute pressure between different operating conditions.

Because of an upper limit on data array size it was necessary to come to a compromise between resolution and number of consecutive pressure cycles captured. It was decided to capture two consecutive cycles to provide sufficient resolution for analysis of combustion pressure vibration. More cycles of data would have been desirable to enable analysis of cyclic variability and to allow averaging for more representative analysis of peak pressure, maximum rate of pressure rise and indicated power.

8.1.2 Exhaust NO_x concentration measurement

The concentration of NO_x in the exhaust of the engine was determined using Kitagawa length-of-stain type detector tubes. The concentration of NO_x is indicated by the length of a stain caused by a chemical reaction between the contents of the tube and the NO_x as a sample of fixed volume (100 ml) is drawn through the tube. The scale on the tube is non-linear for concentrations below 800 ppm with divisions marked as indicated by data points in Figure 8.1.

With the divisions marked on the NO_x detector tube it was possible to read concentrations to the nearest 50 ppm for values less than 1000 ppm and to the nearest 100 ppm for values greater than 1000 ppm. The lower detectable limit of the Kitagawa NO_x detector tubes is 10 ppm.

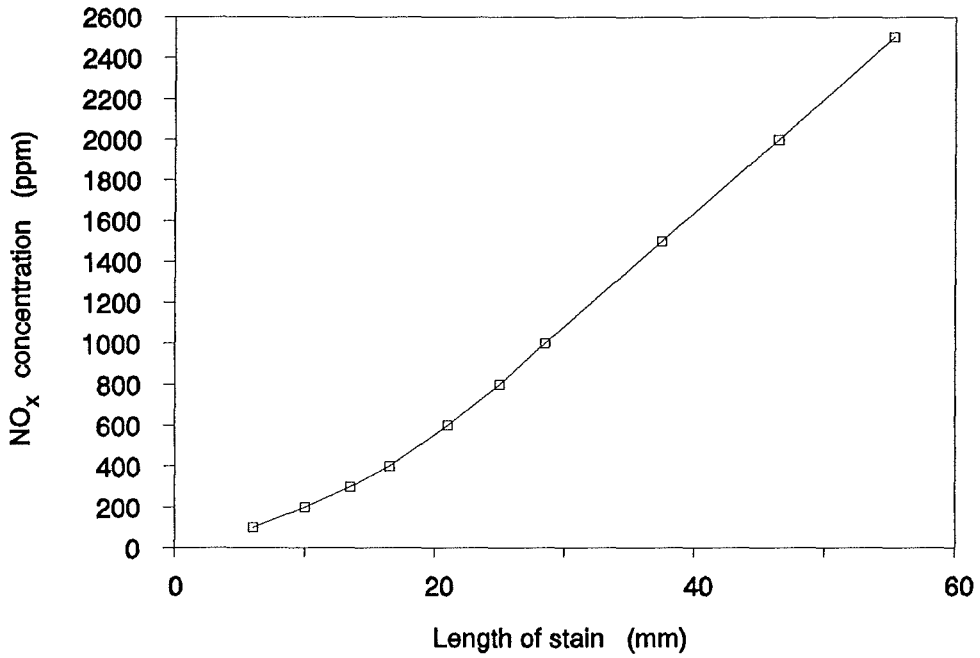

Figure 8.1 NO_x concentration as a function of the length of stain on a Kitagawa NO_x detector tube.

Whenever the concentration of NO_x in the exhaust exceeded the range of the detector tube (greater than 2500 ppm) a second measurement was taken using half a pump stroke (50 ml sample) and multiplying the result by 2. This approach, recommended by Kitagawa, doubles the possible error. The main region of interest when analysing engine performance was the transition from low to high NO_x production. The exact value of maximum NO_x production was of interest only, and considered of little importance to this investigation.

8.2 Hydrogen injector performance

8.2.1 Injector needle lift distance

The hydrogen injector was tested on the engine for a range of injector needle lift distances and opening durations. The minimum Disole armature-stator air gap was 0.4 mm (as determined in section 5.6). In order to provide for a range of injector needle lift distances a second needle 0.2 mm longer than the first was made. Adjustment of the injector needle lift was achieved by the installation of appropriate shims.

An injector needle lift distance of 0.2 mm was found to be suitable for a wide range of engine operation. The effective hydrogen mass flow rate when the valve was open 0.2 mm was approximately 4 g/s (based on the duration of the injection current pulse).

The upper limit of the injector current pulse duration for a given lift distance (Figure 8.2) represents near stoichiometric operation. Higher values of lift distance limited the operable range of λ as shown in Figure 8.3. The upper operating λ for a given lift distance is constrained by the minimum usable injector current pulse duration.

Operation of the injector with lift distances smaller than 0.2 mm was unnecessary with regard to the achievable range of λ. It was undesirable to operate the injector with very small lift distances because of the longer injection durations required for stoichiometric operation. The hydrogen injection must start late enough in the compression stroke to prevent pre-ignition and the injection duration must allow for adequate mixture formation before ignition. Hence, a long injection duration time will limit the maximum engine operating speed.

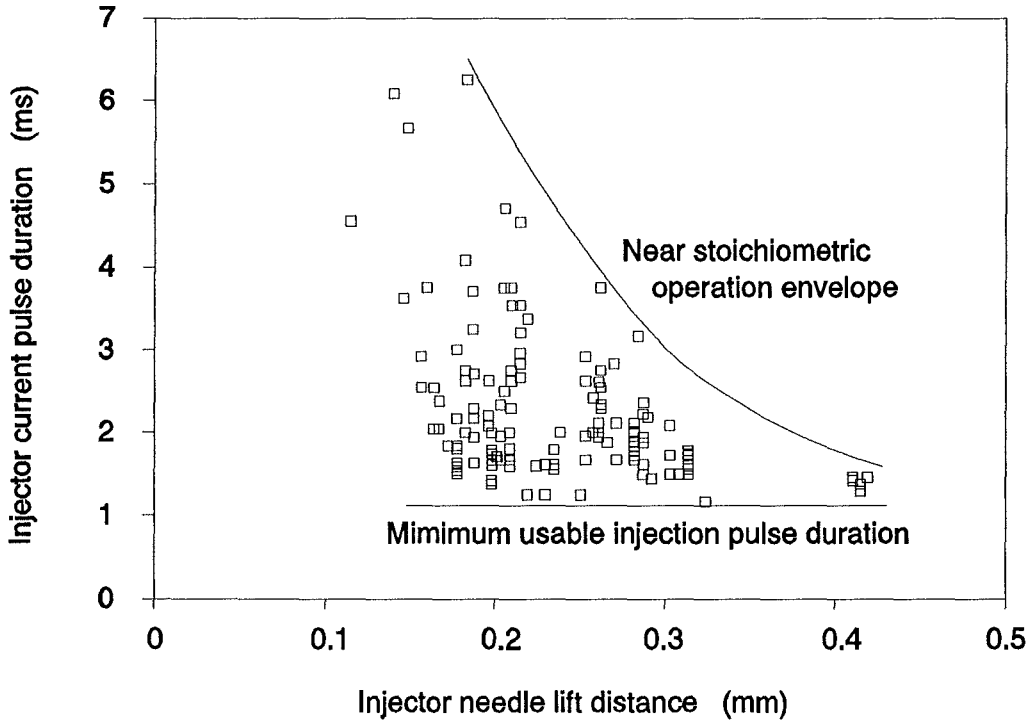

Figure 8.2 Injector current pulse duration vs injector needle lift distance.

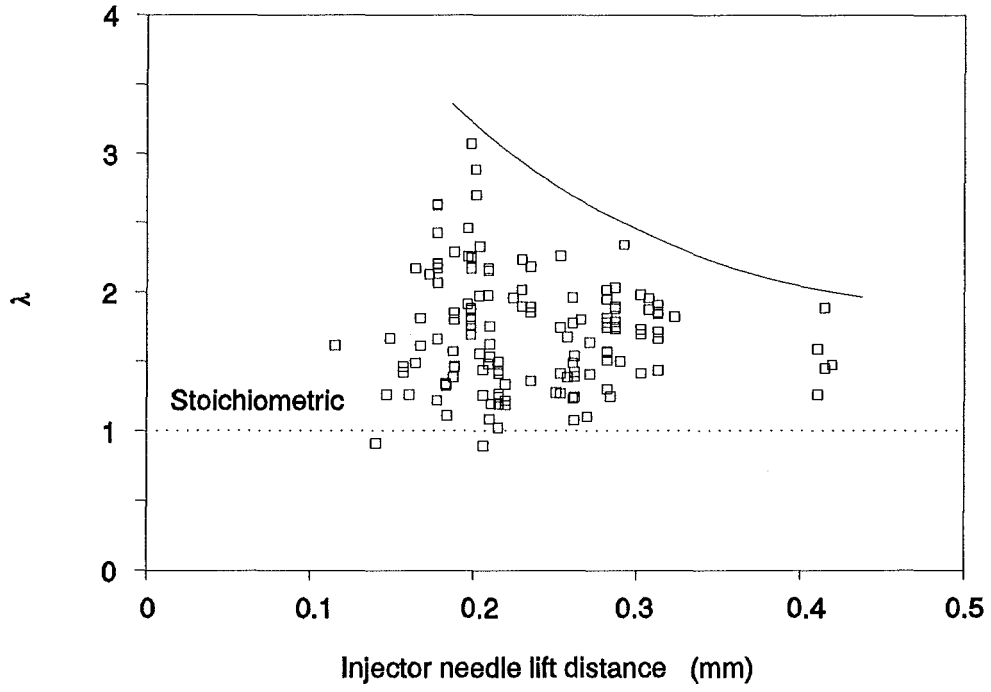

Figure 8.3 λ vs injector current pulse duration.

8.2.2 Injection duration variation

The duration of injection was controlled by varying the injector current pulse duration. The injector current pulse duration was calculated from a knowledge of the stroboscope/flywheel readings (for the injection start and end) and the engine rotational speed. The actual injection duration was calculated from the injector displacement transducer data. The data was analyzed using a spreadsheet to find the time between the injector being half-way opened and

being half-way closed (see Figure 8.4[†]). This definition of injection duration was chosen because it was concise and simple to calculate.

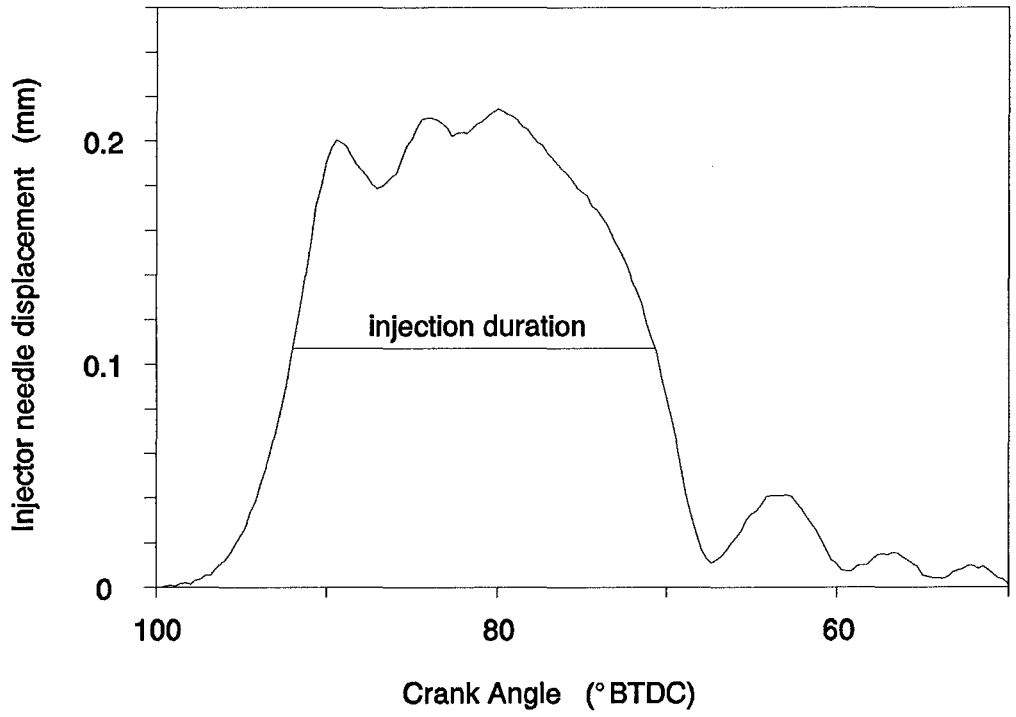

Figure 8.4 Actual injection duration definition.

The relationship between the current pulse duration and the actual injection duration is shown in Figure 8.5. For injector current pulse durations greater than 2.5 ms the actual injection duration closely follows a linear relationship with the current pulse duration. The increased deviation from this linear relationship for

---

[†] The injector current pulse for this particular example was from 100 °BTDC to 80 °BTDC. At 33.3 rps this equates to a time of 1.67 ms. The actual injection duration calculated as defined here was 1.89 ms.

values less than 2.5 ms is partially due to the greater variety of valve lift distances tested in this range.

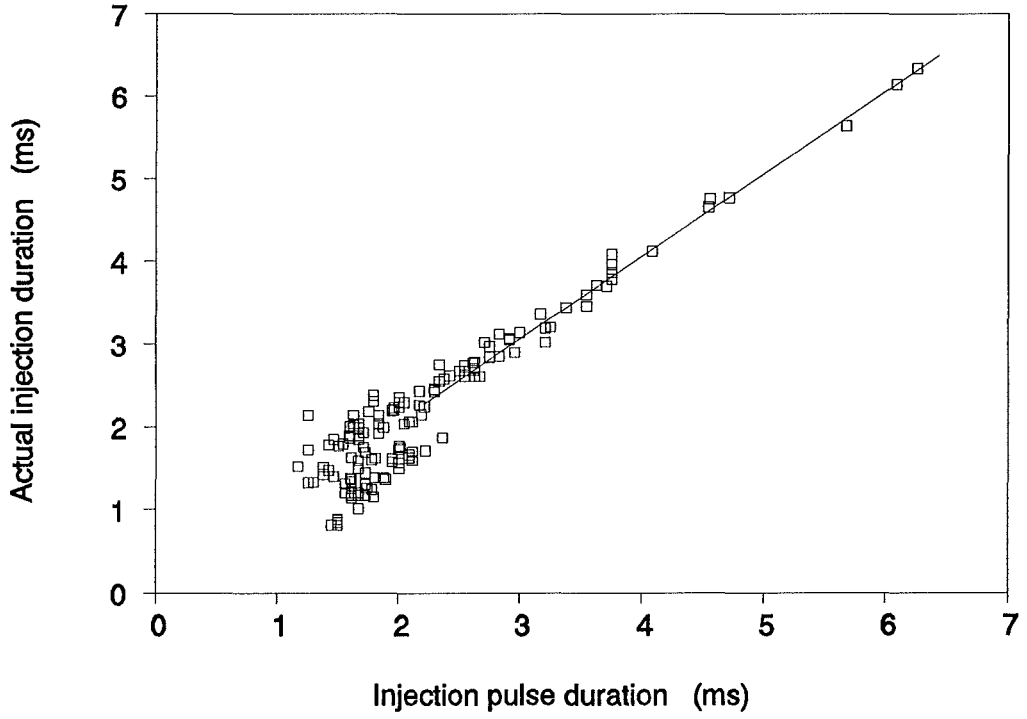

Figure 8.5 Actual injection duration vs injector current pulse duration.

Another reason for the discrepancy is the effect of the injector needle bouncing at the upper extreme of travel. For fine control adjustment of the injection duration in the region of 0.1 ms it was observed that a slight **decrease** in current pulse duration could result in an **increase** in the actual injection duration. The maximum injector needle displacement was observed to decrease, so the increase in actual injection duration was due to an absence of bounce to aid the

return travel of the needle. This effect was not noticeable for greater durations which allowed more than one bounce.

8.2.3 Injector durability

Operating the hydrogen injector during engine testing highlighted durability problems with the elastomeric seat. In most cases the engine was operated over a range of conditions until the elastomeric seat failed. The maximum duration of engine operation before seat failure was 2 hours 20 minutes. The average seat lifetime was greater than 30 minutes.

Injector seat failure was typically sudden and was identified by a rapid change in the displacement and pressure traces on the oscilloscope and an increase in exhaust gas temperature (the more extreme failures were accompanied by a significant reduction in air mass flow rate, indicating major hydrogen leakage during the inlet stroke). Failure of the elastomeric injector seat was occasionally so severe that pre-ignition would result (see Figure 8.6; CR = 8:1, engine speed = 33.3 rps). The level of leakage in this case has a similar effect to external mixture formation or low pressure internal mixture formation where pre-ignition may occur.

The extent of leakage through the injector following a failure was determined following the procedure detailed in section 7.1.1.

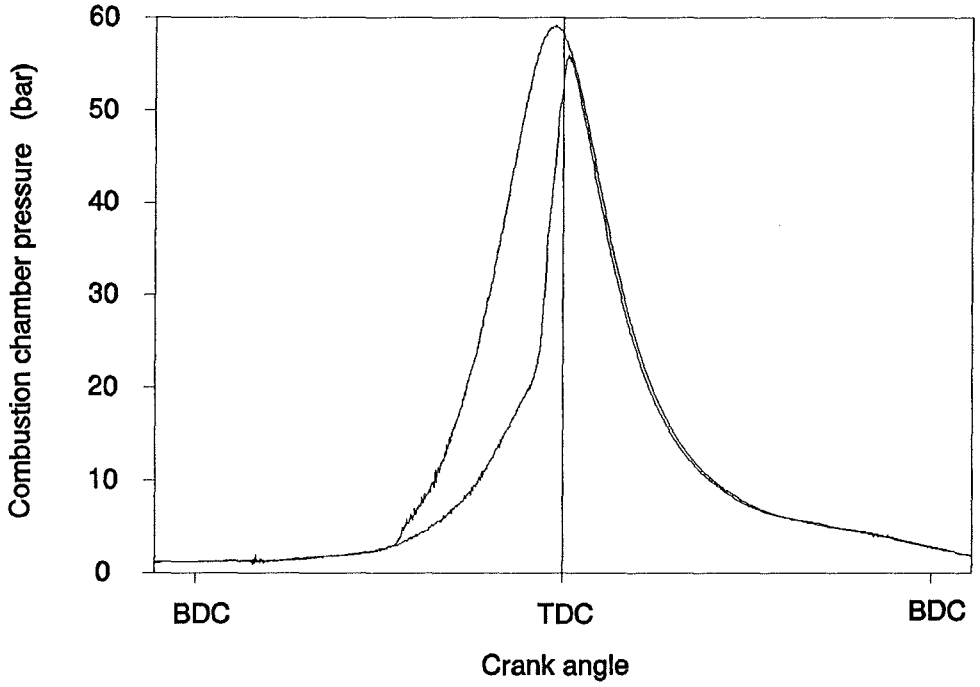

Figure 8.6 Pressure-crank angle diagrams showing a normal combustion and a pre-ignition resulting from injector seat failure.

Nitrogen leakage rates were obtained as the supply system pressure dropped from 80 to 50 bar.

Adiabatic flow was assumed (section 4.3)†, giving an estimate of the hydrogen leakage mass flow rate as:

$$H_2 \text{ MFR} = N_2 \text{ MFR} \times \sqrt{\frac{\text{molecular weight } H_2}{\text{molecular weight } N_2}} \qquad (8.1)$$

This calculation of hydrogen leakage mass flow rate under-estimates the actual rate during engine operation because the nitrogen leakage rate was determined over a range of pressure from 80 bar down to 50 bar. As the pressure decreases, so does the mass flow rate.

The hydrogen leakage rates calculated for the failed elastomeric seats were in the range 0.007 g/s to 0.46 g/s. The hydrogen leakage rate measured for the initial metal to metal injector needle-seat configuration was 0.0007 g/s (section 4.6.1). The failed elastomeric seats thus demonstrated at least an order of magnitude higher leakage mass flow rates than the metal to metal seat. However, due to the stable operation of the engine up until Quad-ring failure and the sudden deterioration upon failure, most of the hydrogen engine testing was performed with a sound leak-free injector seat. This was confirmed by the pre-failure shut-down and verification of zero leakage.

---

† Ratio of specific heats (γ) is approximately equal for hydrogen and nitrogen.

8.3 Engine performance

In order to compare gasoline fuelling with hydrogen fuelling of the engine over a range of operating conditions it was necessary to adopt a common abscissa unit for graphing. Graphing results against λ is suitable for hydrogen engine test data but not for gasoline engine test data (where λ is constant, $\lambda = 1$). Corrected brake power[†] (and BMEP) were adopted as the basis for comparison between hydrogen and gasoline engine testing.

8.3.1 Brake thermal efficiency

With similar compression ratio and engine speed settings the brake thermal efficiency achieved with hydrogen fuelling of the engine was not significantly different to that achieved with gasoline fuelling (Figure 8.7; compression ratio = 8:1, engine speed = 33.3 rps).

The anticipated gains in brake thermal efficiency at low loads due to reduced pumping losses associated with un-throttled operation were not apparent. Other researchers have reported gains in brake thermal efficiency of up to 100% at part

---

[†] Brake power data was corrected for ambient temperature and barometric pressure using the equation[150]:

$$BP_{corrected} = BP \times \frac{1.01325}{P_{barometric}} \times \sqrt{\frac{273.15 + T_{ambient}}{293.15}}$$

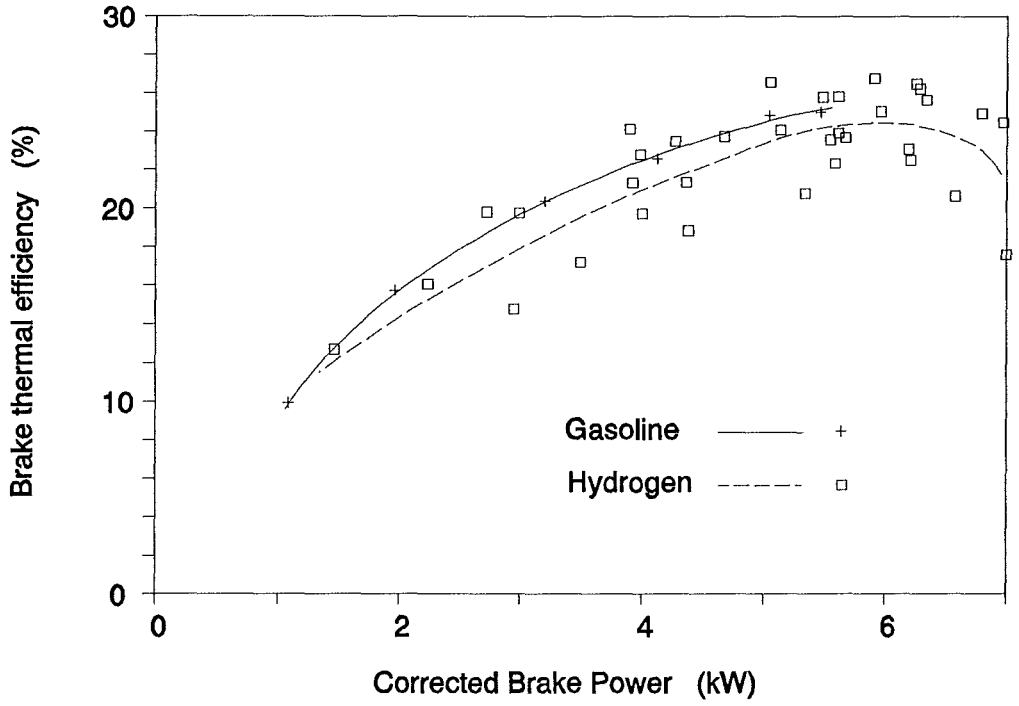

Figure 8.7 Brake thermal efficiency vs corrected brake power, hydrogen-gasoline comparison.

load (relative to gasoline)[68,100]. The relatively poor performance obtained here is thought to be largely due to inconsistent mixing of hydrogen at high λ (low load), particularly in the region of the spark plug. This would result in increased cycle to cycle combustion pressure variation. Hydrogen fuelling also promotes a higher heat loss to the combustion chamber walls[110]. It is thought that attention to cylinder head design with the relocation of the injector closer to the spark plug could improve brake thermal efficiency by allowing later injection to minimise the duration of the enhanced heat transfer and reduce cycle to cycle variation by providing better mixture formation in the vicinity of the spark plug.

Note that the peak corrected brake power obtained for wide open throttle stoichiometric gasoline operation is significantly lower than the peak power obtained from hydrogen operation. The increase in peak corrected power output is a result of the increase in charge energy due to direct injection of hydrogen (see Figure 3.1 page 27. There is a theoretical improvement in charge energy of 18% for internal mixture formation hydrogen fuelling compared to conventional gasoline fuelling.). Another factor contributing to improved power output is the much faster combustion of the hydrogen air charge (as indicated by the reduced ignition advance shown in Figure 8.15) yielding a pressure volume diagram which is closer to that described by the ideal otto cycle.

8.3.2 Compression ratio

Changing the compression ratio of the hydrogen fuelled engine can have a significant effect on the power output attainable. As the compression ratio was increased from 8:1 to 10:1 there was a measurable increase in power (see Figure 8.8; engine speed = 33.3 rps).

Increasing the compression ratio further to 12:1 had no appreciable effect on the corrected brake power.

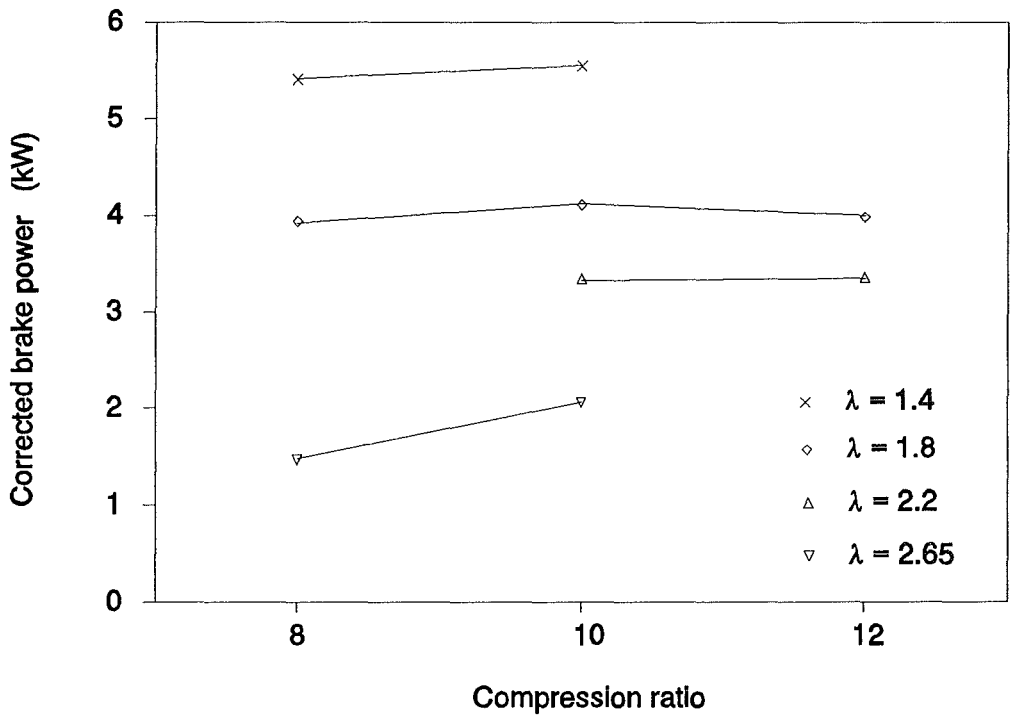

Figure 8.8 Effect of compression ratio on corrected brake power output for various λ.

Downs, Walsh and Wheeler[86] have presented results of highest useful compression ratio (HUCR[†]) determined from hydrogen fuelling of a Ricardo E6 research engine. They plotted HUCR against hydrogen consumption in lb/hr. To enable comparison with the results of the current work it was necessary to convert the hydrogen consumption data into λ. Downs, Walsh and Wheeler included a ccm (chemically correct mixture[‡]) reference point on the graph axis so it was possible to determine the mass flow rate of air. Being an external

---

† Highest useful compression ratio is defined as the compression ratio above which audible knocking combustion is apparent.

‡ Term for stoichiometric mixture.

mixture formation fuelling system it was necessary to consider the air displaced by hydrogen when calculating the mass flow rate of air. For this calculation it was assumed that the engine was operated with wide open throttle (WOT) and that the induced charge was at normal temperature and pressure (NTP). The converted results are shown in Figure 8.9. The engine was operated at 1500 rpm with oil and coolant temperatures of 60°C.

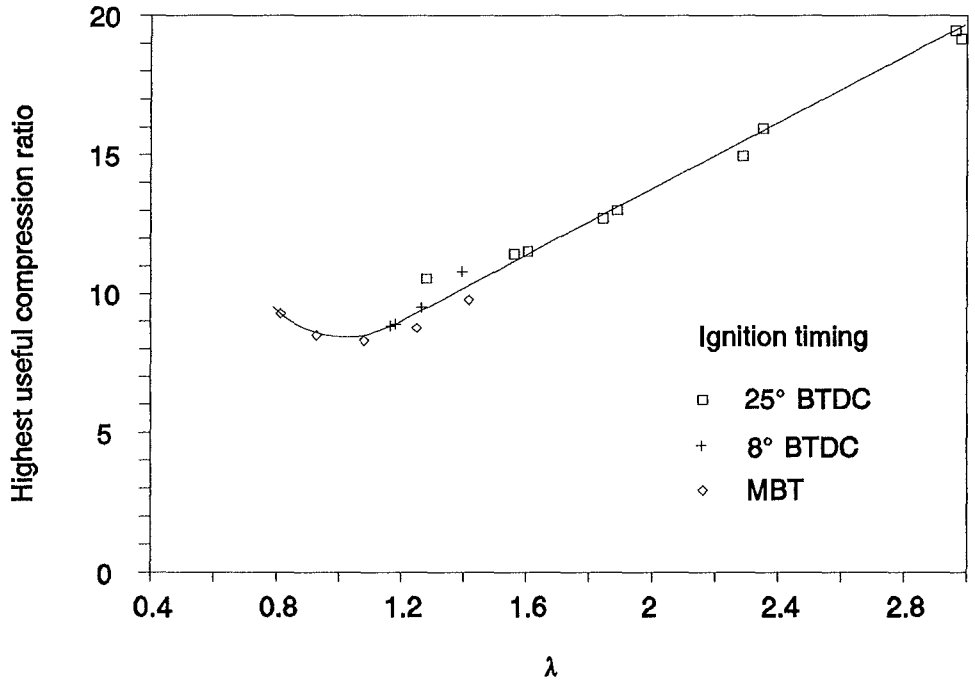

Figure 8.9 Highest useful compression ratio vs λ - results from Downs, Walsh and Wheeler[86].

From their results it is apparent that in order to operate a hydrogen fuelled Ricardo E6 engine, under stoichiometric conditions without knocking combustion, the compression ratio must be below 8:1. The engine may be operated at higher

compression ratios, but knocking would limit the engine to lean (and subsequent low power output) operation.

Combustion pressure vibration in the current work was identified from analysis of pressure-volume diagrams. The magnitude of combustion pressure vibration was grouped into three categories - smooth, moderate and severe. Examples of the pressure characteristic typical of each category are shown in Figure 8.10 (a - smooth, b - moderate and c - severe).

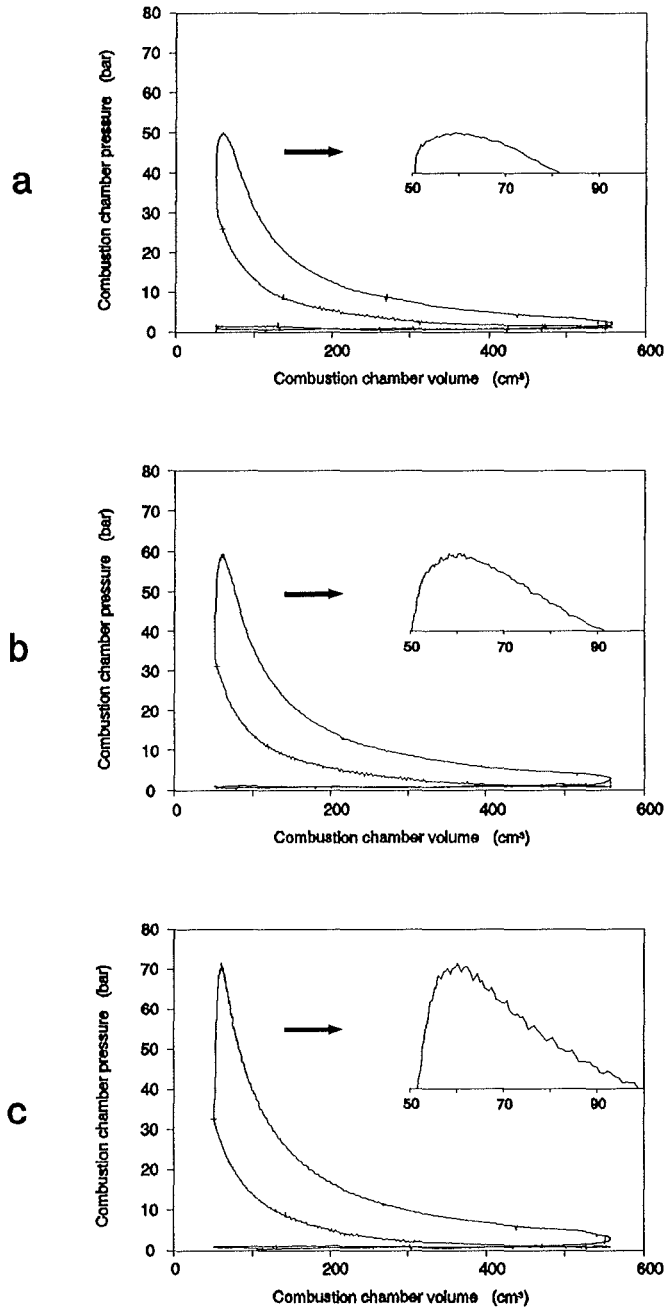

Figure 8.10 Pressure-volume diagrams illustrating combustion pressure vibration classification.

All three diagrams are from engine testing at a compression ratio of 10:1 and engine speed of 33.3 rps. Other operating parameters were:

a	$\lambda = 2$	MBT ignition timing = 13° BTDC
b	$\lambda = 1.5$	MBT ignition timing = 7° BTDC
c	$\lambda = 1.1$	MBT ignition timing = 0.5° BTDC

The grouped combustion pressure vibration data is presented in Figure 8.11.

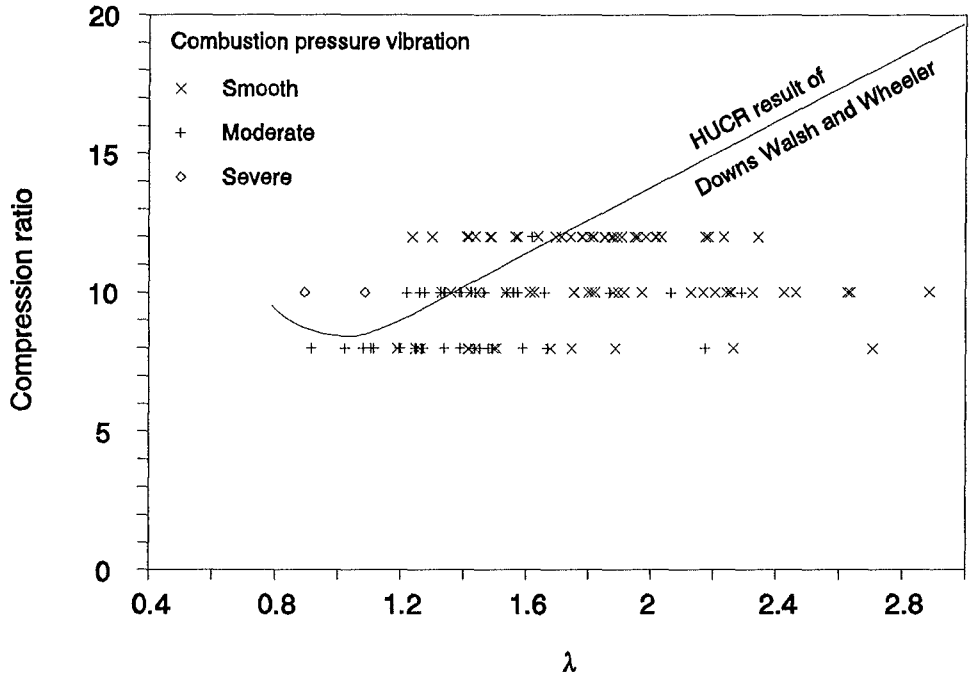

Figure 8.11 Magnitude of combustion pressure vibration plotted as a function of compression ratio and λ.

The results of Downs *et al* do not compare well with those obtained in the current research. At a compression ratio of 12:1 (engine speed 1500 rpm, coolant and oil temperatures 66°C and 61°C respectively - close to the operating conditions of Downs *et al*), smooth operation was possible down to λ of 1.2 whereas Downs *et al* suggest 1.6 to be the limit. This difference is thought to be due to the difference in the fuelling methods. In the work of Downs *et al* the hydrogen was supplied with the intake air, a method commonly associated with pre-ignition problems. The ear was used to determine the onset of audible knocking. The

knocking combustion noted by Downs *et al* may well have been due to pre-ignition instead of (or as well as) auto-ignition.

Suitably timed hydrogen direct injection eliminates the possibility of pre-ignition.

To ensure smooth combustion operation of a Ricardo E6 engine fuelled on hydrogen, the results shown in Figure 8.11 indicate that λ should be greater than 1.2. The data is insufficient to indicate any influence of compression ratio on this limit. Of the tests performed, only the two severe combustion pressure vibration results at the 10:1 compression ratio were accompanied by a distinctive highly audible knocking sound. This suggests that a compression ratio of 8:1 would allow satisfactory engine operation over a full range of λ down to 1.0 (stoichiometric).

8.3.3 NO_x emissions

A comparison between the measured NO_x emissions from hydrogen fuelling and gasoline fuelling of the engine are shown in Figure 8.12 (engine speed = 25 rps, compression ratios: gasoline 8:1, hydrogen 12:1). For low load operation, hydrogen produces negligible concentrations of NO_x in the exhaust. This is due to the reduced mixture strength resulting in lower flame temperatures.

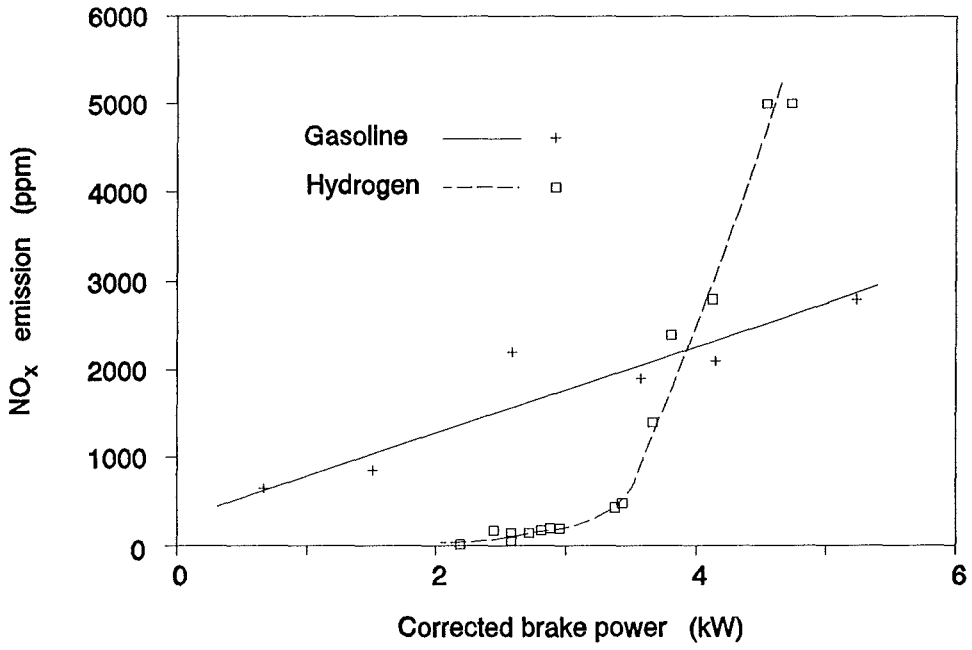

Figure 8.12 NO_x emissions - hydrogen fuelling compared to gasoline fuelling.

The exhaust gas temperatures corresponding to the data in Figure 8.12 are represented in Figure 8.13. Note that the exhaust gas temperatures are very much lower for hydrogen fuelling. The NO_x emission from hydrogen fuelling is significantly higher than that from gasoline fuelling for corrected brake power values greater than 4 kW. This is largely due to the difference in compression ratios. The higher compression ratio for hydrogen fuelling enhances NO_x production by increasing the peak flame temperature in the combustion chamber. The lower exhaust gas temperature for hydrogen indicates a more rapid cooling

of the charge, reducing the extent of NO_x dissociation back to N_2 and O_2 ("freezing out" the NO_x[19] - see section 2.1.1).

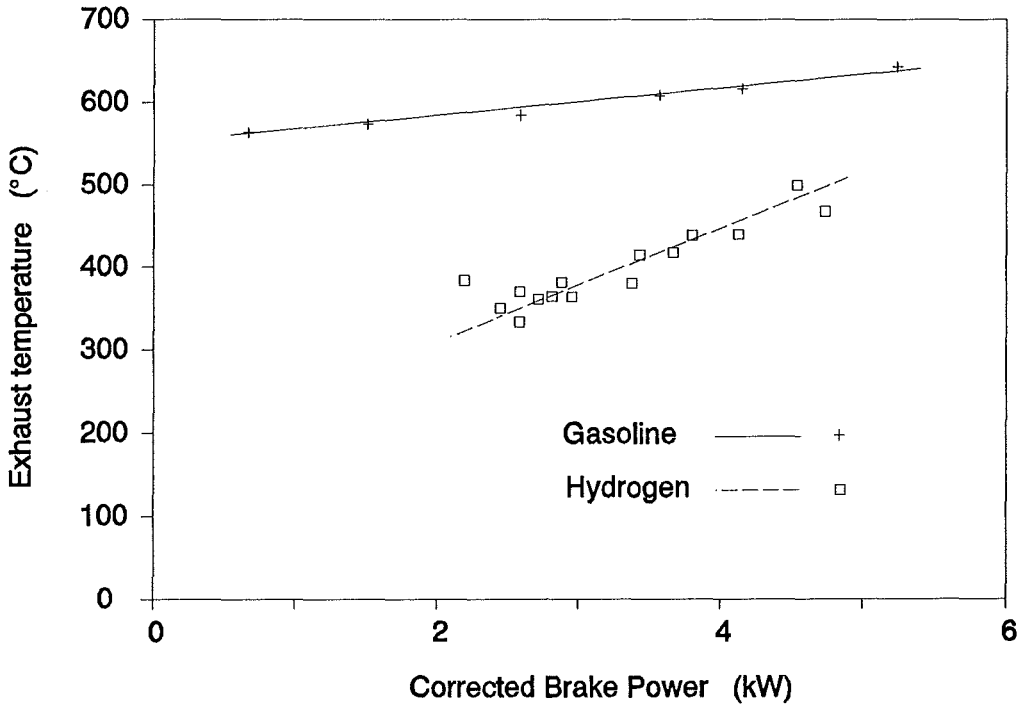

Figure 8.13 Exhaust temperature vs corrected brake power.

Another factor favouring the production of NO_x, for the moderate to high load hydrogen engine operation range, is that the load is regulated by controlling the λ. When λ is greater than 1 there is surplus air for the production of NO_x.

The NO_x emission from hydrogen engine operation is shown in Figure 8.14 as a function of λ. The NO_x emission falls to very small levels for operation with $\lambda >$ 1.8.

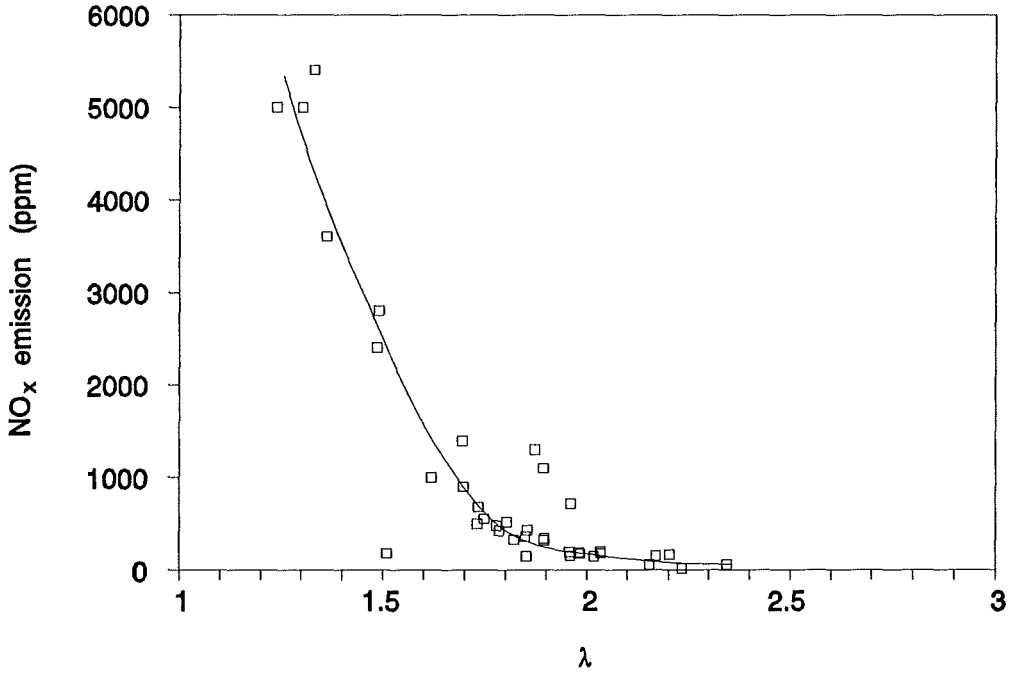

Figure 8.14 NO_x emission from hydrogen engine testing vs λ.

8.3.4 Ignition timing

The ignition timing was set to the minimum advance for best torque for all tests. The optimum advance for hydrogen fuelling was very much less than that for gasoline fuelling for equivalent brake mean effective pressure (Figure 8.15). This is due to the enhanced combustion properties of hydrogen.

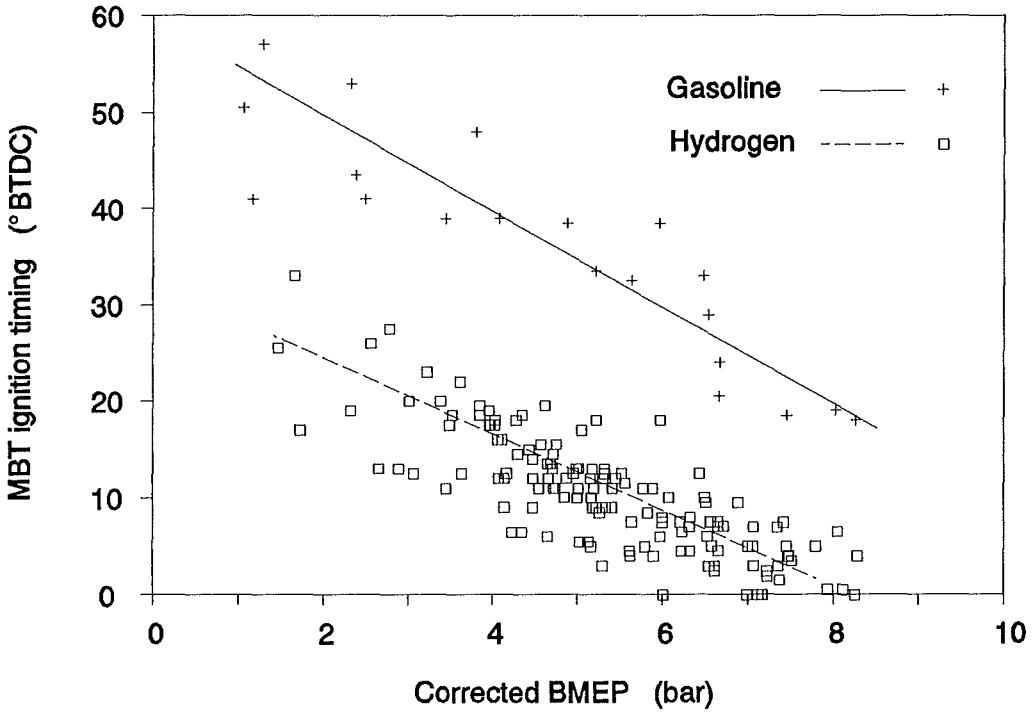

Figure 8.15 MBT Ignition timing vs corrected BMEP, hydrogen-gasoline comparison.

8.3.5 Hydrogen injection timing

For initial hydrogen engine tests the hydrogen injection timing was adjusted to give the best torque. Injection and ignition timing were adjusted alternately until the optimum torque was achieved for a given operating condition. After the first engine tests the average optimum injection timing (defined by the start of the injection pulse) was found to be 100 °BTDC. Injection earlier in the compression stroke could promote the occurrence of pre-ignition while later injection may not allow sufficient time for mixing of the charge. Small variations from this mean had

little effect on the power output performance of the engine so the injection start timing was fixed at 100 °BTDC for most of the engine testing.

It was considered important to determine the effect of injection timing on the emission of NO_x. The engine was operated at a fixed speed (25 rps) with λ = 2 while readings were taken for a range of injection timings.

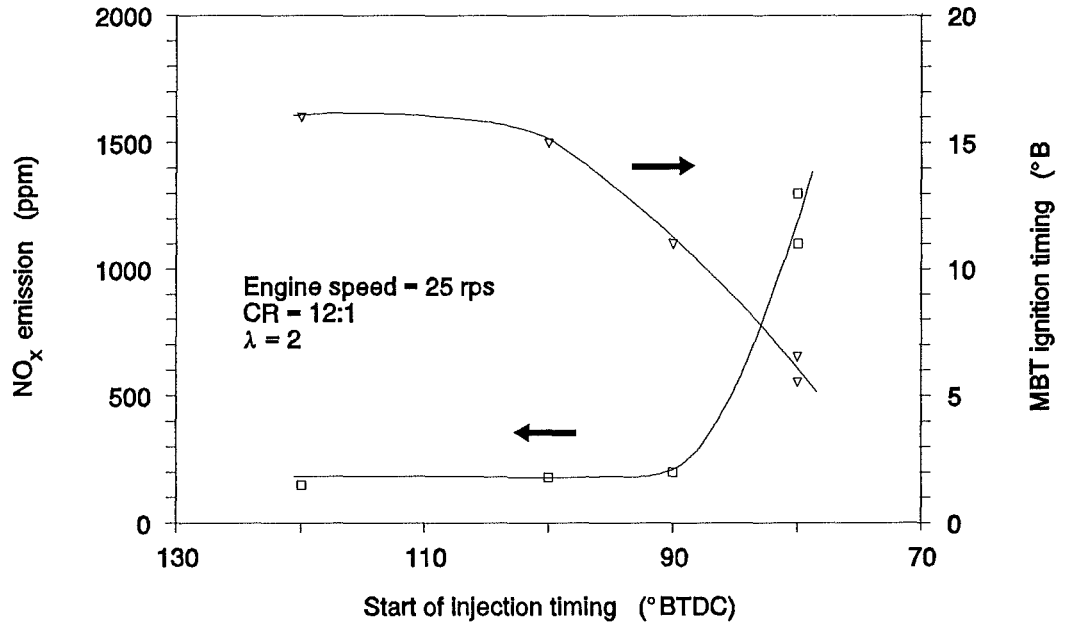

Figure 8.16 The effect of injection timing variation on NO_x emissions and MBT ignition timing.

The corrected brake power output was not significantly altered by the variation in injection timing over the range of operation detailed in Figure 8.16. The ignition timing was adjusted to give the best torque for each injection timing setting. The

injection pulse was 14 °CA long. It is apparent from Figure 8.16, that as the injection timing is retarded beyond 100 °BTDC so must the ignition timing be retarded. This suggests that a time in the order of 9 ms (the time between start of injection at 100 °BTDC and ignition at 15 °BTDC at 25 rps) between commencing injection and ignition is required for sufficient mixing of the charge to occur. This limits the extent to which the injection can be usefully retarded. The original intention of very late injection spanning the ignition period could therefore not be realised. In order to test very late injection it would be necessary to locate the injector outlet in close proximity to the spark plug. This would require a complete redesign of the cylinder head, including the overhead camshaft location.

It is thought that the large increase in the NO_x emissions for later injection timing (80 °BTDC) is due to combustion of a highly heterogeneous charge. It is thought that a significant proportion of the combustion occurs in regions of the charge which are richer than average (λ = 2). The flame temperature for these regions of combustion will be high, resulting in the higher NO_x production.

Homan *et al*[111] describe hydrogen direct injection into a CFR engine using two different types of cylinder head. The Otto head gives a similar configuration to that used on the Ricardo E6 engine where the injector and spark plug are diametrically opposite at either side of the combustion chamber. The CFR pre-chamber Diesel head was used to enable the location of the hydrogen injector in close proximity to a spark plug, thereby enabling successful ignition of

hydrogen injected very near to TDC. The optimum injection timing obtained with the Otto head is in close agreement with that determined in this work. Injecting into the pre-chamber Diesel head, Homan *et al* were able to identify a peak in NO_x production corresponding to injection starting at about 45 °BTDC (for λ = 1.9 - close to the operating condition for the data in Figure 8.16). Retarding the injection from this point resulted in a greatly reduced NO_x emission.

The mechanism for the reduction of NO_x emissions by injecting very near to top dead centre is the reduction of peak combustion chamber pressure (and temperature) by promoting combustion of the charge while injection is occurring.

8.3.6 Maximum rate of pressure rise during combustion

Analysis of the pressure crank angle data was performed to determine the maximum rate of pressure rise during combustion for each operating condition. A spreadsheet was used to identify and perform a linear regression on the region of greatest slope.

The practical upper limit to the maximum rate of pressure rise for a spark ignition engine is approximately 2.4 bar/°CA[172]. A more rapid pressure rise results in undesirable rough combustion. Compression ignition engines may operate effectively with rates of pressure rise as high as 7-8 bar/°CA[173].

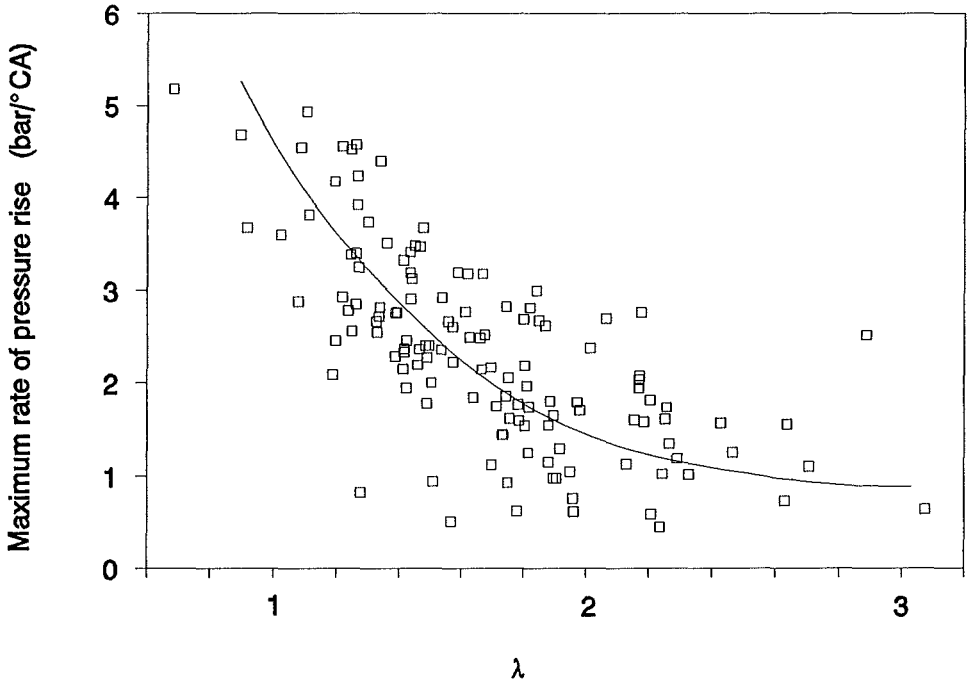

Figure 8.17 Maximum rate of pressure rise during combustion vs λ.

Maximum rate of pressure rise data is presented in Figure 8.17 as a function of λ. The large scatter of the data is a consequence of the small number of consecutive cycles sampled for the measurement (see section 8.1.1). Near stoichiometric conditions, the maximum rate of pressure rise is greater than that recommended for spark ignition engine operation, but well within the operable range for a compression ignition engine. The high maximum rates of pressure rise near stoichiometric operation correlate well with the region of knocking combustion described in section 8.3.2.

CHAPTER 9 CONCLUSIONS

The most favourable means of fuelling an internal combustion engine on hydrogen is by high pressure gaseous injection late in the compression stroke. Late injection of hydrogen overcomes the problem of pre-ignition. The high pressure direct injection of hydrogen has been successfully demonstrated using a specially designed high-speed electro-magnetically actuated injector to fuel a Ricardo E6 research engine.

Much of this project was devoted to the development of an injector to supply hydrogen under high pressure to the combustion chamber. The initial specification of the required hydrogen flow rate through the open injector was determined from a theoretical calculation of the fuel requirement of the Ricardo E6 engine. The hydrogen supply pressure of 80 bar was calculated to ensure sonic conditions through the injector nozzle. Sonic injection ensures a constant mass flow rate of hydrogen through the nozzle, irrespective of changing temperature and pressure conditions within the combustion chamber.

During the development of the injector numerous experiments were devised to test the performance of the injector and its components. Procedures were developed to determine the mass flow rate of hydrogen through the injector when

open, the leakage rate through the injector when closed and the forces exerted on the injector needle in either state.

The problem of sealing the injector was overcome by employing an elastomeric seal. The first attempt at this (using an O-ring seal) was disappointing - yielding very much lower mass flow rates than those predicted by sonic flow theory. By testing a solid replica of the O-ring sealed nozzle, the cause of the discrepancy was confirmed to be due to deformation of the O-ring causing a restriction of the flow area. A more rigidly constrained elastomeric seal design (using a Quad-ring seal) was tested and found to closely match the theoretical mass flow rate performance.

A special solenoid and a power supply circuit were developed to actuate the injector rapidly. The solenoid design was of a Disole (disk solenoid) configuration employing concentric coils in the face of a stator to attract a disk armature. The design parameters for the stator were determined using a computer program which was derived from a graphical solenoid design technique. The injector driver circuit used the principle of a capacitor discharge to force a rapid current rise (and subsequent magnetic field rise) in the solenoid coils, causing fast opening of the injector. The high initial current then decayed to a much smaller current supplied from a secondary power supply. This current was minimised to reduce power consumption and associated over-heating problems and to allow for rapid shut-off of the valve when the current was switched off. The actuation

solenoid and driver circuit proved satisfactory for actuating the injector over the required range of durations for the engine speeds tested.

The injector timing and duration were controlled using an adjustable delay circuit triggered from the rotation of the camshaft. The circuit was designed to enable accurate control of the injection and was equipped with a stroboscope output to provide an accurate means of setting or reading the injection timing. The injection timing circuit was most reliable and enabled precise control of the injection.

The rapid actuation performance of the injector was gauged from the output of an in-built optical displacement transducer based on a slotted optical switch. The rapid displacement response of the injector was the primary criteria for optimization of the solenoid and driver circuit parameters. The slotted optical switch was ideal as a displacement transducer, giving reliable and accurate output for the entire testing programme.

The engine test cell was fitted with a hydrogen supply system to enable safe and efficient engine testing. A nitrogen supply was incorporated for purging the engine supply piping during engine start up and shut down. A gas monitor was installed to warn of a build up of hydrogen in the room. If the concentration of hydrogen reached 20% of the lower explosive limit in air the alarm would sound and the monitor would actuate a fan and de-actuate the hydrogen supply valve. A low pressure alarm was fitted to the outlet of the hydrogen regulator to warn

if the hydrogen supply pressure dropped below 70 bar. It was essential to maintain the supply pressure greater than this to prevent possible damage to the injector from a back flow of combustion chamber gases. The hydrogen supply system proved to be very safe and reliable throughout the engine testing.

The cylinder head of the engine required modification to incorporate a pressure transducer. The cylinder head was modelled on a three dimensional CAD package to determine the optimum site for the additional port. The pressure transducer port was successfully designed and fabricated.

The original Ricardo engine instrumentation was augmented by the addition of a computer with a high-speed multi-channel data acquisition system. This system was configured and programmed to capture data from thermocouples, pressure transducers, an exhaust λ sensor and the injector needle displacement transducer. The pen recorder outputs of a digital storage oscilloscope were also interfaced to the computer via the data acquisition system. The data acquisition system enabled the capture of a wide range of data in a short time period, thereby reducing the possibility of manual reading errors and enabling more engine operating conditions to be tested per bottle change. The high-speed capture of combustion chamber pressure and injector needle lift data provided far greater cycle resolution than was possible by any other available means.

The measurement of the hydrogen mass flow rate during engine testing required careful consideration. The mass flow rate of hydrogen was inferred from the

change in pressure and temperature of hydrogen in a reference volume over time. The location of the pressure and temperature transducers relative to the reference volume was found to cause a discrepancy between measured and actual mass flow rates. This was compensated for by applying a calibration factor to the mass flow rate results.

The most appropriate value for the injector needle lift distance was found during engine testing to be in the order of 0.2 mm. A larger lift distance would limit the range of operating λ, while a smaller lift would limit the maximum engine rotational speed.

The use of an elastomeric seat to seal the injector was found to limit the operational life-time of the seal. Although most of the engine testing results were performed with a sound leak-free injector seal, some results were recorded indicating pre-ignition due to leakage of hydrogen through a failed elastomeric seat.

The hydrogen fuelled engine compared favourably with gasoline operation offering an increase in peak power output of more than 20% for similar engine speed, compression ratio and λ settings. Increasing the compression ratio of the hydrogen engine from 8:1 to 10:1 gave a further improvement in power output. Further increasing the compression ratio to 12:1 made no significant change to power output.

Analysis of combustion chamber pressure records revealed the occurrence of combustion pressure vibration when operating the engine for λ approaching 1. It was concluded that in order to avoid the problem of audible knocking combustion when fuelling the Ricardo E6 engine on hydrogen (for $\lambda \geq 1$) the compression ratio must be limited to 8:1. Knock-free operation was however possible for compression ratios of 10:1 and 12:1 with $\lambda \geq 1.2$.

The concentration of NO_x in the exhaust was very low for hydrogen engine operation leaner than $\lambda = 1.8$. Operation closer to stoichiometric increased NO_x concentrations to similar levels to those encountered with gasoline fuelling.

The maximum rate of pressure rise correlated well with the combustion pressure vibration and NO_x emissions over the range of λ tested. For operation approaching stoichiometric the increasing maximum rate of pressure rise relates well to the increases in undesirable combustion pressure vibration and NO_x emissions.

The optimum injection timing for best torque was determined from engine testing to start at approximately 100 °BTDC. During lean operation, later injection was found to greatly increase the concentration of NO_x in the exhaust. The mechanism for this increase was thought to be heterogenous charge combustion, where a significant proportion of the charge burns richer than the mean charge mixture strength, promoting a higher flame temperature.

The part load brake thermal efficiency results compared favourably with gasoline operation, but were disappointing compared to the results obtained by other hydrogen engine researchers. It is thought that the main reason for this lower level of performance is due to poor mixture formation at part load. Location of the injector closer to the spark plug is recommended as a means of enhancing brake thermal efficiency by optimizing mixture formation in the region of the spark plug. Cycle to cycle variation would be reduced. Relocation of the injector closer to the spark plug would also allow injection later in the compression stroke.

The application of a very late injection system would reduce the rate of pressure rise and allow knock-free operation at compression ratios higher than 8:1. Very late hydrogen injection is also considered as a promising means of reducing the NO_x concentration for high load operation.

ACKNOWLEDGEMENTS

The author wishes to acknowledge the assistance of the following individuals and organisations in helping to make this project a success.

Thanks to:

Roger Green (project supervisor) for initiating the project and providing tremendous technical guidance and administrative support during the project.

Ron Tinker (senior technical officer) for his high standard of technical input and assistance with the engine testing.

Trevor Brown (University data processing officer) for many discussions helping to formulate the ideas developed throughout the project.

The Minnesota Rubber Company for providing seating material samples and technical advice.

The University of Canterbury for providing the funding and facilities for this research.

The Chartered Institute of Transport for the award of the Research and Education Trust Board Scholarship 1990.

Electricorp Production and Appliance Wholesale for their generous contributions towards the authors living expenses.

REFERENCES

1. BOCKRIS, JOHN.O'M. Energy: the solar-hydrogen alternative. Australia and New Zealand Book Company. 1975.

2. HORD, J. PARRISH, W.R. VOTH, R.O. HUST, J.G. FLYNN, T.M. SINDT, C.F. OLIEN, N.A. Selected topics on hydrogen fuel. U.S.A. National Bureau of Standards. 1975.

3. MARCHETTI, C. Why Hydrogen?. *International Journal of Hydrogen Energy.* **vol.4 no.1** 1979. pp.1-5.

4. WINTER, C.-J. KLAIß, H. NITSCH, J. Hydrogen as an energy carrier: what is known? what do we need to learn?. *International Journal of Hydrogen Energy.* **vol.15 no.2** 1990. pp.79-91.

5. BILLINGS, ROGER.E. Survey of Hydrogen Energy Application Projects. *Billings Energy Corporation paper no. 76009 Submitted for 11th Intersociety Energy Conversion Engineering Conference.* 1976.

6. KELLEY, J.H. HAGLER JR, R. Storage, transmission and distribution of hydrogen. *World Hydrogen Energy Conference II Proceedings.* **vol.1** 1978. pp.25-53.
also published in:
International Journal of Hydrogen Energy. **vol.5 no.1** 1980. pp.35-54.

7. HORD, J. Is hydrogen a safe fuel?. *International Journal of Hydrogen Energy.* **vol.3 no.2** 1978. pp.157-176.

8. BOCKRIS, JOHN.O'M. Hydrogen: then and now. *World Hydrogen Energy Conference IV Proceedings.* **vol.1** 1984. pp.3-10.

9. ZWEIG, R.M. Health benefits derived from a planned hydrogen community. *World Hydrogen Energy Conference II Proceedings.* **vol.4** 1978. pp.2231-2245.

10. ZWEIG, R.M. Hydrogen-solution to the acid precipitation problem. *World Hydrogen Energy Conference V Proceedings.* **vol.4** 1984. pp.1901-1908.

11. SELVAM, P. Energy and the environment-an all time search. *International Journal of Hydrogen Energy.* **vol.16 no.1** 1991. pp.35-45.

12. BARBIR, F. VEZIROGLU, T.N. PLASS,JR. H.J. Environmental

damage due to fossil fuels use. *International Journal of Hydrogen Energy.* **vol.15 no.10** 1990. pp.739-749.

13. ZWEIG, R.M. Environmental impact of one year experience with a hydrogen bus. *World Hydrogen Energy Conference III Proceedings.* **vol.4** 1980. pp.2273-2285.

14. BACH, W. Fossil fuel resources and their impacts on environment and climate. *International Journal of Hydrogen Energy.* **vol.6 no.2** 1981. pp.185-201.

15. VEZIROGLU, T.N. GÜRKAN, I. PADKI, M.M. Remediation of greenhouse problem through replacement of fossil fuels by hydrogen. *International Journal of Hydrogen Energy.* **vol.14 no.4** 1989. pp.257-266.

16. PLASS,JR. H.J. BARBIR, F. MILLER, H.P. VEZIROGLU, T.N. Economics of hydrogen as a fuel for surface transportation. *International Journal of Hydrogen Energy.* **vol.15 no.9** 1990. pp.663-668.

17. BAKER, N.R. Oxides of nitrogen control techniques for appliance conversion to hydrogen fuel. SAE 749054. 1974. pp.463-467.

18. FLAGAN, RICHARD.C. SEINFELD, JOHN.H. Fundamentals of air pollution engineering. Prentice Hall. 1988. 542pp.

19. BENSON, ROWLAND.S. WHITEHOUSE, N.D. Internal Combustion Engines. 1st edition. Pergamon Press. 1979. 430pp.

20. NEWHALL, H.K. SHAHED, S.M. Kinetics of nitric oxide formation in high-pressure flames. *Thirteenth Symposium (International) on Combustion.* 1971. pp.381-389.

21. DE BOER, P.C.T. MCLEAN, W.J. HOMAN, H.S. Performance and emissions of hydrogen fueled internal combustion engines. *International Journal of Hydrogen Energy.* **vol.1 no.2** 1976. pp.153-172.

22. GRIFFITH, E.J. *Nature.* **248** 1974. p.458

23. GESSER, H.G. Letter to *New Scientist.* January 1989. p.82

24. SINCLAIR, L.A. WALLACE, J.S. Lean limit emissions of hydrogen-fuelled engines. *International Journal of Hydrogen Energy.* **vol.9 no.1** 1984. pp.123-128.

25. SWAIN, M.R. SWAIN, M.N. LEISZ, A. ADT, R.R. Hydrogen peroxide emissions for a hydrogen fueled engine. *International Journal of Hydrogen Energy.* **vol.15 no.4** 1990. pp.263-266.

26. ADT Jr, R.R. SWAIN, M.R. PAPPAS, J.M. U.S. Department of Energy/Alternative fuels contract No. EC-27CO3-1212. 1980.

27. FOWLES, GEORGE. COULSON, E.H. HOLT, CHARLES. The science masters' book - Chemistry. **series 4 pt.1** John Murray. 1964. 380pp.

28. HEYS, H.L. A new introduction to chemistry. George G.Harrap. 1945. 410pp.

29. PETERSEN, H.C. Does natural hydrogen exist?. *International Journal of Hydrogen Energy.* **vol.15 no.1** 1990. p.55

30. Solar hydrogen - energy carrier for the future. Companion brochure for an exhibition prepared by the German Aerospace Research Establishment (DLR), the Solar and Hydrogen Energy Research Center (ZSW) and the Ministry of Economic Affairs and Technology for the State of Baden-Württemburg, Federal Republic of Germany. 1990.

31. STEINBERG, MEYER CHENG, HSING.C. Modern and prospective technologies for hydrogen production from fossil fuels. *International Journal of Hydrogen Energy.* **vol.14 no.11** 1989. pp.797-820.

32. NIHOUS, G.C. MORI, Y. MASUTANI, S.M. VEGA, L.A. KINOSHITA, C.M. A strategy to reduce carbon dioxide emissions from hydrocarbon-fuelled power plants by pre-combustion reforming and deep ocean discharge of CO_2. *Proceedings of the 9th World Hydrogen Energy Conference.* **vol.3** 1992. pp.1733-1743.

33. SANDSTEDE, GERD Decomposition of hydrocarbons into hydrogen and carbon for the CO_2-free production of hydrogen. *Proceedings of the 9th World Hydrogen Energy Conference.* **vol.3** pp.1745-1753. 1992.

34. BROWN, THEODORE.L. LEMAY,JR. H.EUGENE Chemistry the central science. Prentice-Hall. 815p. 1977.

35. TENNAKONE, K. Hydrogen from brine electrolysis: a new approach. *International Journal of Hydrogen Energy.* **vol.14 no.9** 1989. pp.681-682.

36. WINTER, C.-J. FUCHS, M. HYSOLAR and solar-wasserstoff-bayern. *International Journal of Hydrogen Energy.* **vol.16 no.11** 1991. pp.723-734.

37. ESCHER, W.J.D. Technical discussion: comment on - The impracticability of large-scale generation of hydrogen from water photolysis by utilization of solar radiation. *International Journal of Hydrogen Energy.* **vol.5 no.2** 1980. pp.205-206.

38. GIACOMAZZI, G. Prospects for intercontinental seaborne transportation of hydrogen. *International Journal of Hydrogen Energy.* **vol.14 no.8** 1989. pp.603-616.

39. HIRAOKA, K. WATANABE, K. MORISHITA, T. NOMURA, M. KAN, S. IKAME, M. SENDA, T. Energy analysis and CO_2 emission evaluation of a solar hydrogen energy system for the transportation system in Japan - I. conceptual design of the system. *International Journal of Hydrogen Energy.* **vol.16 no.9** 1991. pp.631-638.

40. HIRAOKA, K. WATANABE, K. MORISHITA, T. NOMURA, M. KAN, S. IKAME, M. SENDA, T. Energy analysis and CO_2 emission evaluation of a solar hydrogen energy system for the transportation system in Japan - II. evaluation of the system. *International Journal of Hydrogen Energy.* **vol.16 no.11** 1991. pp.755-764.

41. WURSTER, R. The Euro-Quebec Hydro-Hydrogen Pilot Project EQHHPP. Hydrogen energy progress VIII. Proceedings of the 8th World Hydrogen Energy Conference. **vol.1** 1990. pp.59-70.

42. GRETZ, J. BASELT, J.P. ULLMANN, O. WENDT, H. The 100 MW Euro-Quebec hydro-hydrogen pilot project. *International Journal of Hydrogen Energy.* **vol.15 no.6** 1990. pp.419-424.

43. GRETZ, J. DROLET, B. KLUYSKENS, D. SANDMANN, F. ULLMANN, O. Phase II and phase III,0 of the 100 MW Euro-Quebec hydro-hydrogen pilot project EQHHPP. *Proceedings of the 9th World Hydrogen Energy Conference* **vol.3** 1992. pp.1821-1828.

44. The solar hydrogen energy world: a realistic vision. Poster presented by DFVLR (German aerospace) at the 8th World Hydrogen Energy Conference. 1990.

45. HANSON, J.A. FOSTER, R.W. ESCHER, W.J.D. TISON, R.R. Solar/hydrogen systems for the 1985-2000 time frame: a review and assessment. *International Journal of Hydrogen Energy.* **vol.7 no.1** 1982. pp.3-20.

46. CARPETIS, C. PESCHKA, W. A study on hydrogen storage by use of cryoadsorbents. *International Journal of Hydrogen Energy.* **vol.5 no.5** 1980. pp.539-554.

47. SMITH, E.M. Hydrogen in transportation. *Energy World.* **no.3** 1991. pp.11-13.

48. CARPETIS, C. Estimation of storage costs for large hydrogen storage facilities. *International Journal of Hydrogen Energy.* **vol.7 no.2** 1982. pp.191-203.

49. Matheson gas products, world leader in speciality gases and equipment. 1987 catalogue. 212pp.

50. SASTRI, M.V.C. Hydrogen energy-a prophesy come true. *International Journal of Hydrogen Energy*. **vol.5 no.4** 1980. pp.365-367.

51. SINOR, J.E. (CONSULTANTS INC.) The clean fuels report. **vol.2 no.3** 1990. p.111.

52. GARAT, A. Study of the possibilities of the conversion to hydrogen use of the natural gas pipeline network. *Hydrogen as an energy vector. Synopsis of results of the first programme on the production and utilization of hydrogen.* Commission of the European Communities. 1982. pp.548-569.

53. BRéELLE, Y. GELIN, P. MEYER, C. PETIT, G. Technico-economic study of distributing hydrogen for automotive vehicles. *International Journal of Hydrogen Energy.* **vol.4 no.4** 1979. pp.297-314.

54. HUSTON, E.LEE. Liquid and solid storage of hydrogen. *World Hydrogen Energy Conference V Proceedings*. **vol.3** 1984. pp.1171-1186.

55. LUCAS, G.G. RICHARDS, W.L. Mathematical modelling of hydrogen storage systems. *International Journal of Hydrogen Energy.* **vol.9 no.3** 1984. pp.225-231.

56. BERNAUER, O. Development of hydrogen-hydride technology in the F.R.G. *International Journal of Hydrogen Energy.* **vol.14 no.10** 1989. pp.727-735.

57. THIBAULT, J.J. The cryogenic storage of hydrogen. *World Hydrogen Energy Conference II Proceedings*. **vol.3** 1978. pp.1457-1473.

58. PRICE, ROBERT.O. Liquid hydrogen-an alternative aviation fuel. *International Journal of Hydrogen Energy.* **vol.16 no.8** 1991. pp.557-562.

59. LIN, F.N. MOORE, W.I. WALKER, S.W. Economics of liquid hydrogen from water electrolysis. *World Hydrogen Energy Conference V Proceedings*. **vol.1** 1984. pp.249-258.

60. KALANIDHI, A. Boil-off in long-term stored liquid hydrogen. *International Journal of Hydrogen Energy*. **vol.13 no.5** 1988. pp.311-313.

61. LODHI, M.A.K MIRES, R.W. How safe is the storage of liquid

hydrogen?. *International Journal of Hydrogen Energy.* **vol.14 no.1** 1989. pp.35-43.

62. CLEARY, MARGOT.KEAM. Great disasters of the 20th century. Bison books. 1990.

63. SEGAL, L. WALLACE, J.S. KEFFER, J.F. Safety considerations in the design of a gaseous hydrogen fuel supply for engine testing. *International Journal of Hydrogen Energy.* **vol.11 no.11** 1986. pp.737-743.

64. REIDER, R. EDESKUTY, F.D. Hydrogen safety problems. *International Journal of Hydrogen Energy.* **vol.4 no.1** 1979. pp.41-45.

65. DAS, L.M. Safety aspects of a hydrogen-fuelled engine system development. *International Journal of Hydrogen Energy.* **vol.16 no.9** 1991. pp.619-624.

66. KNOWLTON, R.E. An investigation of the safety aspects in the use of hydrogen as a ground transportation fuel. *International Journal of Hydrogen Energy.* **vol.9 no.1** 1984. pp.129-136.

67. KNOWLTON, R.E. An investigation into the safety aspects in the use of hydrogen as a ground transportation fuel. *World Hydrogen Energy Conference V Proceedings.* **vol.4** 1984. pp.1881-1892.

68. DELUCHI, M.A. Hydrogen vehicles: an evaluation of fuel storage, performance, safety, environmental impacts and cost. *International Journal of Hydrogen Energy.* **vol.14 no.2** 1989. pp.81-130.

69. FURUHAMA, S. State of the art and future trends in hydrogen-fuelled engines. *International Journal of Vehicle Design.* **vol.4 no.4** 1983. pp.359-385.

70. DAS, L.M. Hydrogen engines: a view of the past and a look into the future. *International Journal of Hydrogen Energy.* **vol.15 no.6** 1990. pp.425-443.

71. BINDON, J. HIND, J. SIMMONS, J. MAHLKNECHT, P. WILLIAMS, C. The development of a lean burning carburettor for a hydrogen-powered vehicle. *International Journal of Hydrogen Energy.* **vol.10 no.5** 1985. pp.297-304.

72. FRAME, GEORGE. A. VARDE, K.S. A study of combustion and engine performance using electronic hydrogen fuel injection. *World Hydrogen Energy Conference IV Proceedings.* **vol.3** 1982. pp.1021-1032.

73. MACCARLEY, C.A. VAN VORST, W.D. Electronic fuel injection techniques for hydrogen powered I.C. engines. *World Hydrogen Energy Conference II Proceedings.* **vol.5** 1978. pp.2747-2792.

74. FURUHAMA, S. YAMANE, K. YAMAGUCHI, I. Combustion improvement in a hydrogen fueled engine. *International Journal of Hydrogen Energy.* **vol.2 no.3** 1977. pp.329-340.

75. BINDER, K. WITHALM, G. Mixture formation and combustion in a hydrogen engine using hydrogen storage technology. *International Journal of Hydrogen Energy.* **vol.7 no.8** 1982. pp.651-659.
Repeated from:
Proceedings of the 3rd World Hydrogen Energy Conference. 1980. pp.1103-1117.

76. WATSON, HARRY.C. MILKINS, ERIC.E. Some problems and benefits from the hydrogen fueled spark ignition engine. *Proceedings of the 13th Intersociety Energy Conversion Engineering Conference.* Paper no. 789212. 1978. pp.1170-1177.

77. FURUHAMA, S. Technical note: two-stroke hydrogen injection engine. *International Journal of Hydrogen Energy.* **vol.4 no.6** 1979. pp.571-576.

78. An introduction to liquified petroleum gas. Second edition. The liquefied petroleum gas association of New Zealand (inc.) code of practice No.1 1985.

79. LEWIS, BERNARD VON ELBE, GUENTHER Combustion flames and explosions of gases. 2nd edition. Academic Press Inc. 1961.

80. DAS, L.M. Abnormal combustion in hydrogen engines: causes and remedies. *Proceedings of the Eighth World Hydrogen Energy Conference.* **vol.3** 1990. pp.1379-1397.

81. MACCARLEY, C.A. A study of factors influencing thermally induced backfiring in hydrogen fuelled engines, and methods for backfire control. SAE 819632. 1981. pp.1449-1453.

82. LUCAS, G.G. MORRIS, L.E. The backfire problem of the hydrogen engine. *Symposium - Universities Internal Combustion Engine Group, Kings College, London.* 1980. pp.191-206.

83. YAMAGUCHI, I. KIM, Y.K. TSURUGA, T. TAKISHITA, T. A study of abnormal combustions in hydrogen-fueled engines. *World Hydrogen Energy Conference III Proceedings.* **vol. 2** 1980. pp.1015-1025.

84. HII, S.E. Simulation of the residual gas ignition of hydrogen. *M.Eng.Sci Thesis,* University of Melbourne 1975.

85. GATHERCOLE, A.H. BINDON, J.P. ROBERTS, L.W. Detonation limited air fuel ratios in a conventional high speed spark ignition engine fueled with hydrogen. *The South African Mechanical Engineer* **vol.30 no.7** 1980. pp.257-263.

86. DOWNS, D. WALSH, A.D. WHEELER, R.W. A study of the reactions that lead to 'knock' in the spark-ignition engine. *Philosophical Transactions of the Royal Society.* **vol.243 A.870** 1951. pp.463-524

87. GAMMIE, M.A. BINDON, J.P. The effect of mixture strength and spark advance on detonation intensity in a small squish-chambered hydrogen fueled spark-ignition engine. *World Hydrogen Energy Conference III Proceedings.* **vol.2** 1980. pp.1001-1013.

88. GLASSON, NEIL. GREEN, ROGER. High pressure hydrogen injection. *Proceedings of the 9th World Hydrogen Energy Conference.* **vol.2** 1992. pp.1285-1294.

89. TAKIGUCHI, MASAAKI FURUHAMA, SHOICHI SUZUKI, TAKAYUKI TSUJITA, MAKOTO Combustion improvement of liquid hydrogen fueled engine for medium duty trucks. SAE 870535 1987. 11p.

90. TAKIGUCHI, M. PICHAINARONG, P. MATSUSHITA, T. FURUHAMA, S. Characteristics of combustion pressure vibration in hydrogen fuel injection hot surface ignition engines. SAE 871611 1987. 9p.

91. KING, R.O. HAYES, S.V. ALLAN, A.B. ANDERSON, R.W.P. WALKER, E.J. The hydrogen engine: combustion knock and related flame velocity. *Transactions of the Engineering Institute of Canada.* **vol.2 no.4** 1958. pp.143-148

92. PRABHUKUMAR, G.P. NAGALINGHAM, B. GOPALAKRISHNAN, K.V. Theoretical studies of a spark-ignited supercharged hydrogen engine. *International Journal of Hydrogen Energy.* **vol.10 no.6** 1985. pp.389-397.

93. NAGALINGAM, B. SCHMILLEN, KARL. DÜBEL, MARTIN. Performance of the supercharged spark ignition hydrogen engine. *Alternate Fuels for Spark Ignition Engines SP-559.* SAE 831688 1983. pp.97-105.

94. LYNCH, FRANK. Turbocharging the hydrogen-fueled internal combustion engine. *World Hydrogen Energy Conference III Proceedings.* **vol.4** 1980. pp.2257-2271.

95. FURUHAMA, S. HIRUMA, M. ENOMOTO, Y. Development of a liquid hydrogen car. *International Journal of Hydrogen Energy*. **vol.3 no.1** 1978. pp.61-81.

96. WOOLLEY, R.L. HENRIKSEN, D.L. Water induction in hydrogen-powered IC engines. *International Journal of Hydrogen Energy*. **vol.1 no.4** 1977. pp.401-412.

97. PRABHUKUMAR, G.P. SWAMINATHAN, S. NAGALINGHAM, B. Water induction studies in a hydrogen-diesel dual-fuel engine. *International Journal of Hydrogen Energy*. **vol.12 no.3** 1987. pp.177-186.

98. MISHCHENKO, A.I. The ways of the setting up of automobile-type hydrogen engine performance. *World Hydrogen Energy Conference V Proceedings*. **vol.4** 1984. pp.1529-1536.

99. LYNCH, F.E. Parallel induction: a simple fuel control method for hydrogen engines. *World Hydrogen Energy Conference IV Proceedings*. **vol. 3** 1982. pp.1033-1051.

100. WATSON, H.C. MILKINS, E.E. MARTIN, W.R.B. EDSELL, J. An Australian hydrogen car. *World Hydrogen Energy Conference V Proceedings*. **vol.4** 1984. pp.1549-1562.

101. MATHUR, H.B. DAS, L.M. Performance characteristics of a hydrogen fuelled S.I. engine using timed manifold injection. *International Journal of Hydrogen Energy*. **vol.16 no.2** 1991. pp.115-127.

102. MACCARLEY, C.A. VAN VORST, W.D. Electronic fuel injection techniques for hydrogen powered I.C. engines. *International Journal of Hydrogen Energy*. **vol.5 no.2** 1980. pp.179-203.

103. JING-DING, L. YING-QING, L. TIAN-SHEN, D. Improvement on the combustion of a hydrogen fueled engine. *International Journal of Hydrogen Energy*. **vol.11 no.10** 1986. pp.661-668.

104. NINOMIYA, YOSHINARI. HOSONO, YASUHARU. HASHIMOTO, HIROMASA. HIRUMA, MASARU. FURUHAMA, SHOICHI. NO_x control in LH_2-pump high pressure hydrogen injection engines. *Proceedings of the 9th World Hydrogen Energy Conference.* **vol.2** 1990. pp.1295-1304.

105. DAVIDSON, D. FAIRLIE, M. STUART, A.E. Development of a hydrogen-fuelled farm tractor. *International Journal of Hydrogen Energy*. **vol.11 no.1** 1986. pp.39-42.

106. SUZUKI, K. UCHIYAMA, Y. HAMA, J. Research of hydrogen fueled spark ignition engines. *World Hydrogen Energy Conference III Proceedings.* **vol.2** 1980. pp.1027-1039.

107. FURUHAMA, S. AZUMA, H. Hydrogen injection two-stroke spark ignition engine. *World Hydrogen Energy Conference II Proceedings.* **vol.4** 1978. pp.1851-1878.

108. WELCH, ALAN.B. WALLACE, JAMES.S. Development of a hydrogen injector for use in hydrogen-fuelled diesel engine research. *21st Intersociety Energy Conversion Engineering Conference.* Paper no. 869061 1986. pp.2110-2115.

109. KREPEC, T. GIANNACOPOULOS, T. MIELE, D. New electronically controlled hydrogen-gas injector development and testing. *International Journal of Hydrogen Energy.* **vol.12 no.12** 1987. pp.855-861.

110. PICHAINARONG, PICHAN. IWATA, TADASHI. FURUHAMA, SHOICHI. Study of thermodynamic analysis in hydrogen injection engines. *Proceedings of the 8th World Hydrogen Energy Conference.* **vol.3** 1990. pp.1275-1284.

111. HOMAN, H.S. DE BOER, P.C.T. MCLEAN, W.J. The effect of fuel injection on NOx emissions and undesirable combustion for hydrogen-fuelled piston engines. *International Journal of Hydrogen Energy.* **vol.8 no.2** 1983. pp.131-146.

112. GREEN, CHRIS.J. WALLACE, JAMES.S. Electrically actuated injectors for gaseous fuels. *Gaseous Fuels - Technology Performance and Emissions SAE SP-798.* SAE 892143 1989. pp.135-146.

113. FURUHAMA, S. HIRUMA, M. KOYANAGI, K. TOMISAWA, N. YAMAURA, K. The power system of a computer controlled hydrogen car - GH_2 injection and spark ignition engine with LH_2 tank and pump. *Proceedings of the Institution of Mechanical Engineers - Computers in Engine Technology* Paper no.C430/028 1991. pp.179-188.

114. FURUHAMA, S. KOBAYASHI, Y. A liquid hydrogen car with a two-stroke direct injection engine and LH_2-pump. *International Journal of Hydrogen Energy.* **vol.7 no.10** 1982. pp.809-820.

115. SORUSBAY, C. VEZIROGLU, T.N. Mixture formation techniques for hydrogen-fueled internal combustion engines. *Proceedings of the 7th World Hydrogen Energy Conference. 1988.* pp.1909-1921.

116. TAUBE, M. RIPPIN, D. KNECHT, W. HAKIMIFARD, D. MILISAVLJEVIC, B. GRUENENFELDER, N. A prototype truck

powered by hydrogen from organic liquid hydrides. *International Journal of Hydrogen Energy.* **vol.10 no.9** 1985. pp.595-599.

117. GREEN, R.K. Hydrogen fuelling of automotive engines. *Internal Daimler-Benz report.* October 1987.

118. GORDON, ROBERT Composite pressure vessels for gaseous hydrogen powered vehicles. *World Hydrogen Energy Conference V Proceedings.* **vol.3** 1984. pp.1225-1236.

119. POVEL, R. TöPLER, J. WITHALM, G. HALENE, C. Hydrogen drive in field testing. *Proceedings of the 5th World Hydrogen Energy Conference.* 1984. pp.1563-1577.

120. FEUCHT, F. HURICH, W. KOMOSCHINSKI, N. POVEL, R. Hydrogen drive for road vehicles-results from the fleet test run in Berlin. *Proceedings of the 6th World Hydrogen Energy Conference.* **vol.3** 1986. pp.1079-1086.

121. BUCHNER, H. BERNAUER, O. STRAUß, W. Development of high-temperature hydrides for vehicular applications. *World Hydrogen Energy Conference II Proceedings.* **vol.3** 1978. pp.1677-1689.

122. BUCHNER, H. POVEL, R. The Daimler-Benz hydride vehicle project. *International Journal of Hydrogen Energy.* **vol.7 no.3** 1982. pp.259-266.

123. BUCHNER, H. Hydrogen use-transportation fuel. *International Journal of Hydrogen Energy.* **vol.9 no.6** 1984. pp.501-514.

124. MARINESCU-PASOI, L. BEHRENS, U. LANGER, G. GRAMATTE, W. RASTOGI, A.K. SCHMITT, R.E. Hydrogen metal hydride storage with integrated catalytic recombiner for mobile application. *International Journal of Hydrogen Energy.* **vol.16 no.6** 1991. pp.407-412.

125. WITHALM, G. GELSE, W. The Mercedes-Benz hydrogen engine for application in a fleet vehicle. *World Hydrogen Energy Conference IV Proceedings.* 1986. pp.1185-1198.

126. PESCHKA, W. Liquid hydrogen pumps for automotive application. *International Journal of Hydrogen Energy.* **vol.15 no.11** 1990. pp.817-825.

127. KOBAYASHI, Y. FURUHAMA, S. IIDA, M. ENOMOTO, Y. LH_2-car with a two-stroke direct injection engine and LH_2-pump. *World Hydrogen Energy Conference III Proceedings.* **vol.2** 1980. pp.1087-1101.

128. CARPETIS, C. Comparison of the expenses required for the on-board fuel storage systems of hydrogen powered vehicles. *International Journal of Hydrogen Energy*. **vol.7 no.1** 1982. pp.61-77.

129. STEWART, WALTER.F. Operating experience with a liquid-hydrogen fueled buick and refuelling system. *World Hydrogen Energy Conference IV Proceedings*. **vol.3** 1982. pp.1071-1093.

130. PESCHKA, W. Operating characteristics of a LH_2-fuelled automotive vehicle and of a semi-automatic LH_2-refuelling station. *International Journal of Hydrogen Energy*. **vol.7 no.8** 1982. pp.661-669.

131. FURUHAMA, SHOICHI. SAKURAI, TAKEYASU. SHINDO, MASAHIKO. Study of evaporation loss of liquid hydrogen storage tank with LH_2-pump. *Proceedings of the 8th World Hydrogen Energy Conference.* **vol.3** 1990. pp.1087-1096.

132. PESCHKA, W. Liquid hydrogen fueled automotive vehicles in Germany-status and development. *International Journal of Hydrogen Energy.* **vol.11 no.11** 1986. pp.721-728.

133. PESCHKA, W. NIERATSCHKER, W. Experience and special aspects on mixture formation of an Otto engine converted for hydrogen operation. *International Journal of Hydrogen Energy*. **vol.11 no.10** 1986. pp.653-659.

134. FURUHAMA, S. MATUSHITA, T. NAKAJIMA, T. YAMAURA, K. Hydrogen injection spark ignition engine with LH_2 pump driven by high pressure hydrogen expander. *Proceedings of 7th World Hydrogen Energy Conference*. 1988. pp.1975-1987.

135. BILLINGS, R.E. BAKER, N. LYNCH, F. MACKAY, D. Ignition parameters of the hydrogen engine. SAE 749057 1974. pp.487-492.

136. IKEGAMI, M. MIWA, K. SHIOJI, M. A study of hydrogen fuelled compression ignition engines. *International Journal of Hydrogen Energy.* **vol.7 no.4** 1982. pp.341-353.

137. HOMAN, H.S. REYNOLDS, R.K. DE BOER, P.C.T. MCLEAN, W.J. Hydrogen-fueled diesel engine without timed ignition. *International Journal of Hydrogen Energy.* **vol.4 no.4** 1979. pp.315-325.

138. WONG, J.K.S. Compression ignition of hydrogen in a direct injection diesel engine modified to operate as a low-heat-rejection engine. *International Journal of Hydrogen Energy.* **vol.15 no.7** 1990. pp.507-514.

139. LAMBE, S.M. WATSON, H.C. MILKINS, E.E. Hydrogen engine with pilot diesel fuel ignition. *Proceedings of the 8th World Hydrogen Energy Conference.* **vol.3** 1990. pp.1333-1342.

140. ENOMOTO, K. FURUHAMA, S. KOBAYASHI, Y. Ignitability of hydrogen-air mixture by hot surfaces and hot gases. *World Hydrogen Energy Conference III Proceedings.* **vol.2** 1980. pp.1149-1163.

141. FURUHAMA, SHOICHI KOBAYASHI, YOSHIYUKI Development of a hot-surface-ignition hydrogen injection two-stroke engine. *World Hydrogen Energy Conference III Proceedings.* **vol.3** 1982. pp.1009-1020.
also appears in:
International Journal of Hydrogen Energy. **vol.9 no.3** 1984. pp.205-213.

142. FURUHAMA, S. FUKUMA, T. High output power hydrogen engine with high pressure fuel injection, hot surface ignition and turbocharging. *International Journal of Hydrogen Energy.* **vol.11 no.6** 1986. pp.399-407.

143. ROGERS, G.F.C. MAYHEW, Y.R. Thermodynamic and transport properties of fluids. Third edition. Basil Blackwell. 1980. 24pp.

144. SHAPIRO, ASCHER.H. The dynamics and thermodynamics of compressible fluid flow. **vol 1.** 1st edition. The Ronald Press Company. 1953. 647pp.

145. MACCARLEY, C.A. Development of a high speed injection valve for electronic hydrogen fuel injection. *World Hydrogen Energy Conference III Proceedings.* **vol.2** 1980. pp.1119-1133

146. LUCAS, G.G. EMTAGE, A.L. Microprocessor control of the hydrogen/petrol engine. IMechE paper no.C08/87. 1987. pp.231-240.

147. GREEN, R.K. GLASSON, N.D. Direct injector development for hydrogen fuelled internal combustion engines. *Proceedings of the 8th World Hydrogen Energy Conference.* **vol.3** 1990. pp.1285-1294.

148. VARDE, K.S. FRAME, G.A. Development of a high-pressure hydrogen injection for SI engine and results of engine behaviour. *International Journal of Hydrogen Energy.* **vol.10 no.11** 1985. pp.743-748.

149. FURUHAMA, S. Hydrogen engine systems for land vehicles *International Journal of Hydrogen Energy.* **vol.14 no.12** 1989. pp.907-913.

150. ADLER, U. (Editor in chief) Automotive handbook. Second edition. Robert Bosch GmbH. 1986. 707pp.

151. MAY, K.D. Advanced valve technology. *NASA SP-5019.* 1965. 102pp.

152. LEQUESNE, BRUNO Fast acting, long stroke, bistable solenoids with moving permanent magnets (part 1). *IEEE Transactions 88CH2565-0/88/0000-0142.* IEEE. 1988. pp.142-148.

153. STRATFORD, B.S. The calculation of the discharge coefficient of profiled choked nozzles and the optimum profile for absolute air flow measurement. *Journal of the Royal Aeronautical Society.* **vol.68** 1964. pp.237-245.

154. Ludowici (Australian distributor) Facts about heat and fluid resistant Viton fluoroelastomer. 1989.

155. Ludowici (Australian distributor) - DuPont Kalrez O-rings catalogue. 1989.

156. REID, ROBERT.C. PRAUSNITZ, JOHN.M. POLING, BRUCE.E. The properties of gases & liquids. 4th edition. McGraw Hill. 1987. 741pp.

157. WILHELM, EMMERICH. BATTINO, RUBEN. WILCOCK, ROBERT.J. Low pressure solubility of gases in liquid water. *Chemical Reviews.* **vol.77 no.2** 1977. pp.219-262.

158. WATSON, G.A. Flowmeter types and their usage. *Chartered Mechanical Engineer.* **no.2** 1978. pp.27-32.

159. HAYWARD, A.T.J. Flowmeters a basic guide and source book for users. Macmillan. 1979. 197pp.

160. ZAVIER, C.C. Charge stratification for an internal combustion engine. M.E. thesis. Department of Mechanical Engineering, University of Canterbury. 1991.

161. SEILLY, A.H. Helenoid actuators-a new concept in extremely fast acting solenoids. SAE 790119 1979. 11pp.

162. SEILLY, A.H. Colenoid actuators-further developments in extremely fast acting solenoids. SAE 810462 1981.

163. SCHECHTER, MICHAEL.M. Fast response multipole solenoids. SAE 820203 1982. pp.27-38.

164. KUSHIDA, TAKEO High speed, powerful and simple solenoid actuator "DISOLE" and its dynamic analysis results. SAE 850373 1985.

165. YANG, JEFFERSON.Y.S. Graphical technique simplifies solenoid design. *Machine Design*. **vol.57 no.16** 1985. pp.90-94.

166. VIEILLEDENT, E. Electronic fuel injection and emissions for two-stroke engines. *Design and Development of Small Internal Combustion Engines*. IMechE paper no. C118/78 1978. pp.223-229.

167. SMITH, RALPH.J. Circuits, devices and systems. Fourth edition. Wiley. 1984. 751pp.

168. VAN AKEN, C. Adapter errors in indicator diagrams of combustion engines. *Proceedings of The Institute of Mechanical Engineers.* **vol.191 no.8** 1977. pp.125-134.

169. DEUTSCHMAN, AARON.D. MICHELS, WALTER.J. WILSON, CHARLES.E. Machine design theory and practice. Macmillan publishing. 1975. 932pp.

170. MACDONALD, J.SCOTT Evaluation of the hydrogen-supplemented fuel concept with an experimental multicylinder engine. SAE 760101 1976. 16pp.

171. TROLOVE, H.P. Calibration of piezoelectric pressure transducers Department of Mechanical Engineering, University of Canterbury. Final year project **no.37** 1991. 50pp.

172. OBERT, EDWARD.F. Internal combustion engines and air pollution. 1st edition. New York. Intext Educational Publishers. 1973. 740pp.

173. KOWALEWICZ, ANDRZEJ. Combustion systems of high-speed piston I.C. engines. Elsezvier. 1984. 366pp.

174. MCCARTY, R.D. HORD, J. RODER, H.M. Selected properties of hydrogen (engineering design data). *United States Department of Commerce, National Bureau of Standards Monograph 168.* 1981.

175. RIVKIN, S.L. Thermodynamic properties of gases. 4th edition. Hemisphere Publishing Corporation. 1988. 295pp.

176. MORAN, M.J. SHAPIRO, H.N. Fundamentals of engineering thermodynamics. Wiley. 1988.

177. ROGERS, G.F.C. MAYHEW, Y.R. Engineering thermodynamics work and heat transfer. 3rd edition. Longman. 1980. 667pp.

178. BEATTIE, JAMES.A. BRIDGEMAN, OSCAR.C. A new equation of state for fluids. II. Application to helium, neon, argon, hydrogen,

nitrogen,oxygen, air and methane. *The journal of the American Chemical Society.* **vol.50 no.12** 1928. pp.3133-3138.

179. SIERENS, ROGER. Comparative tests on a S.I. engine fuelled with natural gas or hydrogen. *Personal communication 1992, submitted for presentation at the ASME Energy-sources Technology Conference, Houston, Texas. Jan.30-Feb.3 1993.*

180. KARLEKAR, B.V. Thermodynamics for engineers. Prentice Hall. 1983. 586pp.

181. KREYSZIG, ERWIN. Advanced engineering mathematics. Fifth edition. Wiley. 1983. 988pp.

182. Personal communication January 1992. Robert Bosch GmbH, Automotive Division, Customer Service, Stuttgart, GERMANY.

APPENDICES

APPENDIX A Properties of hydrogen

The various properties of hydrogen have been well documented. A list presented by Hord[7] giving various properties of para-hydrogen, methane and gasoline is summarised in Table A.1.

Para-hydrogen is hydrogen for which the spin of the nuclei of the adjacent atoms in the hydrogen molecule are in opposite directions[174]. In ortho-hydrogen molecules the nuclear spins of the atoms are in the same direction. Hydrogen consists of a mixture of these two configurations. The proportions of ortho-hydrogen and para-hydrogen in a mixture are temperature dependant. At normal temperature and pressure the equilibrium mixture of ortho-hydrogen and para-hydrogen is 75:25 (described as normal hydrogen). At very low temperatures (cryogenic) the equilibrium state is almost entirely para-hydrogen. The rate of conversion from para-hydrogen to ortho-hydrogen and vice-versa is very slow. For this reason the properties of para-hydrogen are entirely applicable for hydrogen from cryogenic storage being utilised at elevated temperature.

For all of the tests performed in the current study, the hydrogen was supplied from high pressure gaseous storage at ambient temperatures (normal hydrogen).

The properties of normal hydrogen are assumed to be approximately equal to those of para-hydrogen for the purposes of this study. Comparison of some of the properties with those for normal hydrogen[174] suggest that this assumption is valid.

Table A.1 Properties of hydrogen, methane and gasoline.

PROPERTY	UNITS	HYDROGEN	METHANE	GASOLINE
Molecular weight		2.016	16.043	~107.0
Normal boiling point temperature	K	20.268	111.632	310 to 478
Critical pressure	bar	12.928	45.988	24.8 to 27.4
Critical temperature	K	32.976	190.56	540 to 569
Density at critical point	kg/m^3	31.4	160.4	230
Density of liquid at NBP	kg/m^3	70.8	422.6	700[1]
Density of vapour at NBP	kg/m^3	1.34	1.82	4.5[1]
Density of gas at NTP	kg/m^3	0.083764	0.65119	4.4
Lower calorific value	kJ/kg	119930	50020	44500
Higher calorific value	kJ/kg	141860	55530	48000
Specific heat of NTP gas	kJ/kgK	14.89	2.22	1.62[1]
Specific heat of NBP liquid	kJ/kgK	9.69	3.5	2.2[1]
Ratio of specific heats of NTP gas		1.383	1.308	1.05[1]
Ratio of specific heats of NBP liquid		1.688	1.676	
Thermal conductivity of NTP gas	W/mK	0.1897	0.0330	0.0112
Adiabatic sound velocity in NTP gas	m/s	1294	448	154
Compressibility factor in NTP gas		1.0006	1.0243	1.0069
Compressibility factor in NBP liquid		0.01712	0.004145	0.00643[1]
Gas constant	kJ/kgK	4.124	0.5183	0.0780
Limits of flammability in air	% vol.	4.0 to 75	5.3 to 15.0	1.0 to 7.6
Limits of detonability in air	% vol.	18.3 to 59.0	6.3 to 13.5	1.1 to 3.3
Stoichiometric composition in air	% vol.	29.53	9.48	1.76
Minimum energy for ignition in air	mJ	0.02	0.29	0.24
Auto-ignition temperature	K	858	813	501 to 744
Flame temperature in air	K	2318	2148	2470
Proportion of thermal energy radiated from flame to surroundings	%	17 to 25	23 to 33	30 to 42
Burning velocity in NTP air	m/s	2.65 to 3.25	0.37 to 0.45	0.37 to 0.43
Detonation velocity in NTP air	km/s	1.48 to 2.15	1.39 to 1.64	1.4 to 1.7[2]
Diffusion coefficient in NTP air	cm^2/s	0.61	0.16	0.05
Diffusion velocity in NTP air	cm/s	≤2.00	≤0.51	≤0.17
Buoyant velocity in NTP air	m/s	1.2 to 9	0.8 to 6	non-buoyant
Maximum experimental safe gap in NTP air	cm	0.008	0.12	0.07
Quenching gap in NTP air	cm	0.064	0.203	0.2
Toxicity		non-toxic	non-toxic	slightly toxic

NBP = normal boiling point
NTP = 1 atmosphere (101.325 kPa) and 20°C (293.15 K)

The property values for gasoline were calculated from those of normal heptane and octane for the properties where values for gasoline were unavailable.

[1] At 1 atmosphere and 15.5°C
[2] Based on the properties of n-pentane and benzene.

Some of the properties of hydrogen given in Table A.1 are particularly relevant to the theoretical analysis of the flow of hydrogen through the injector and to the combustion of hydrogen in the engine. Two such properties are the ratio of specific heats and the stoichiometric composition of hydrogen in air. These properties are further detailed below:

A.1 Ratio of specific heats (cp/cv = γ)

The variation of γ with temperature is shown in Figure A.1[175,176]. In the range of interest for this work, the ratio of specific heats varies little from 1.4. Thus γ = 1.4 was accepted as a suitable approximation for the calculations in this work.

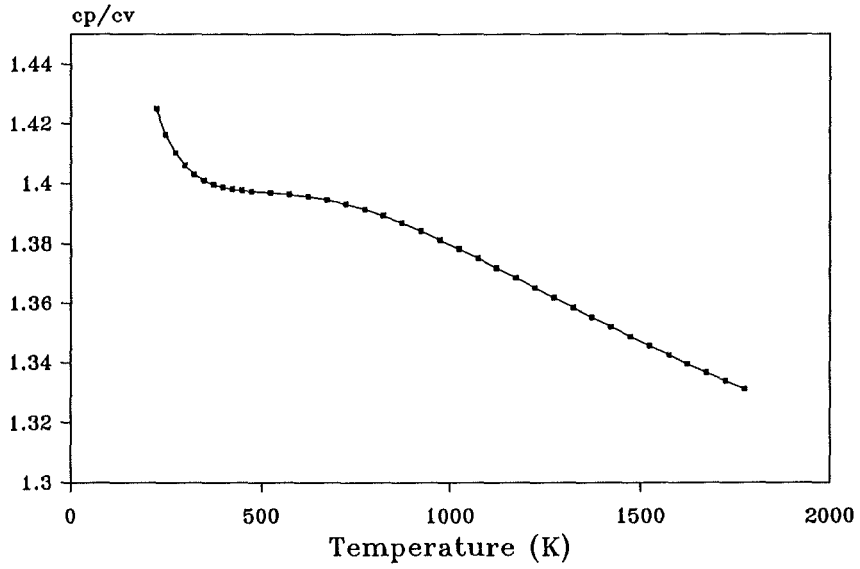

Figure A.1 Variation in ratio of specific heats (γ) with temperature.

A.2 Stoichiometric air/fuel ratio

The stoichiometric composition of hydrogen in air is given as a percentage by volume in Table A.1. For the calculations in chapter 4 the stoichiometric air/fuel ratio on a mass basis was required. This is most easily calculated from first principles.

Two parts of hydrogen react with one part of oxygen. The molecular weights of hydrogen and oxygen are 2.016 and 31.999 respectively.

Thus the mass of oxygen required to react with a unit mass of hydrogen is:

$$\frac{31.999}{2 \times 2.016} = 7.936 \qquad \textbf{(A.1)}$$

Oxygen accounts for 23.14% of air on a mass basis. The stoichiometric air/fuel ratio on a mass basis is therefore:

$$A/F_{stoic} = \frac{7.936}{0.2314} \qquad \textbf{(A.2)}$$

$$= 34.30$$

APPENDIX B Equations of State

Throughout this project the mass flow rate of a gas was often inferred from pressure and temperature changes in a fixed volume over time. Accurate calculation of specific volume from the pressure and temperature of a gas was thus very important.

A common first approximation is to assume ideal gas behaviour ($Pv = RT$). The error of this assumption is generally small when dealing with pressures and temperatures usually encountered in engineering[175]. The hydrogen mass flow rate tests during engine operation were likely to exhibit the greatest error from the ideal gas assumption because of the high pressures at relatively low temperatures.

There are a number of equations of state which can be used to calculate the PVT (pressure, volume and temperature) relationships of real gases - all of varying accuracy, applicability and complexity. Three of the most popular equations were assessed in order to determine the most suitable equation for this work.

B.1 Compressibility factors

A simple modification of the ideal gas equation can be used with appropriate compressibility factors (Z factors) to yield accurate PVT relationships. The Z factor is used in the equation Pv = ZRT. For given conditions the Z factor of a gas may be found from a chart or table or calculated from the equation:

$$Z = 1 + \frac{B}{v} + \frac{C}{v^2} + \frac{D}{v^3} + \ldots \qquad \textbf{(B.1)}$$

where B, C, D,... are the virial coefficients. In practice, only the B and C virial coefficients are used. The virial coefficients for a given gas are functions of absolute temperature only.

A compressibility factor chart and equations for determining the virial coefficients for hydrogen are described by McCarty, Hord and Roder[174] The compressibility factor chart would be very difficult to incorporate into a computer program. The computation of virial coefficients would be far more feasible to program.

B.2 van der Waals' equation

The ideal gas equation is based on the assumptions that gas molecules have zero volume, attractive forces between gas molecules are negligible and the gas

molecules are perfectly rigid and elastic[177]. Van der Waals' equation is a modification of the ideal gas equation to compensate for the inaccuracy of the first two of these assumptions. Van der Waals' equation is stated as:

$$\left(P + \frac{a}{v^2}\right)(v - b) = R\,T \qquad \textbf{(B.2)}$$

Where the a/v^2 term compensates for the attractive forces between molecules and the b term for the volume of the molecules. For hydrogen the constants are:

a	=	6028	Nm^4/kg^2
b	=	1.324×10^{-2}	m^3/kg
R	=	4.1243	kJ/kgK

where the units of the variables are:

P	-	Pa
v	-	m^3/kg
T	-	K

Van der Waals' equation is very easy to implement in a computer program.

B.3 Beattie-Bridgeman equation

The Beattie-Bridgeman equation of state is a fourth order equation and is most simply stated as:

$$P = \frac{R\,T\,(1-\epsilon)}{v^2}(v+B) - \frac{A}{v^2}$$

$$A = A_o\left(1 - \frac{a}{v}\right)$$

$$B = B_o\left(1 - \frac{b}{v}\right) \qquad \textbf{(B.3)}$$

$$\epsilon = \frac{c}{v\,T^3}$$

The constants for hydrogen are given by Beattie and Bridgeman[178] as:

A_o	=	0.1975	$atm.l^2/mol^2$
a	=	-0.00506	l/mol
B_o	=	0.02096	l/mol
b	=	-0.04359	l/mol
c	=	$0.0504x10^4$	$l/K^3.mol$
R	=	0.08206	$atm.l^2/K.mol^2$

where the units of the variables are:

P	-	atmospheres
v	-	l/mol
T	-	K

The Beattie-Bridgeman equation may be incorporated in a computer program most easily by employing a suitable numerical method.

B.4 Selection of the most appropriate technique

Of the three equations of state described above, van der Waals' equation is the simplest to incorporate in a program. The Beattie-Bridgeman and compressibility factor methods represent the PVT relationships of real gases better than the simpler van der Waals' equation.

The Beattie-Bridgeman equation has been tested recently by Sierens[179] in an application similar to that of the current work. Sierens concluded that the Beattie-Bridgeman equation was most applicable to the calculation of the specific volume of hydrogen for mass flow rate analysis. No reference to the use of compressibility factors for such work could be found. Thus the Beattie-Bridgeman equation was accepted for calculating the PVT relationship of hydrogen in the current work.

APPENDIX C Solenoid design computation

The initial design of the solenoid was undertaken using a graphical technique described by Yang[165]. Yang's method is for the design of a cylindrical solenoid but was applied in this case as an initial approximation of a disk solenoid (Disole). The Disole is assumed to offer superior performance to the standard cylindrical solenoid. This being the case, a Disole design based on the parameters of a cylindrical solenoid should easily match the performance of the cylindrical solenoid.

A Turbo Pascal program SOLENOID.PAS was digitised from Yang's graphical technique to enable the required iterations to be completed much faster and with less chance of error. Comparison with numerous manually calculated examples verified the program to be in close agreement with the graphical technique.

The following is the output from the program SOLENOID.PAS for a cylindrical solenoid to provide a 100 N force from a 12 V dc power supply. All other input variables were adjusted to give the optimum solution as shown in the output variables. The nomenclature is described by way of comments in the program listing which follows.

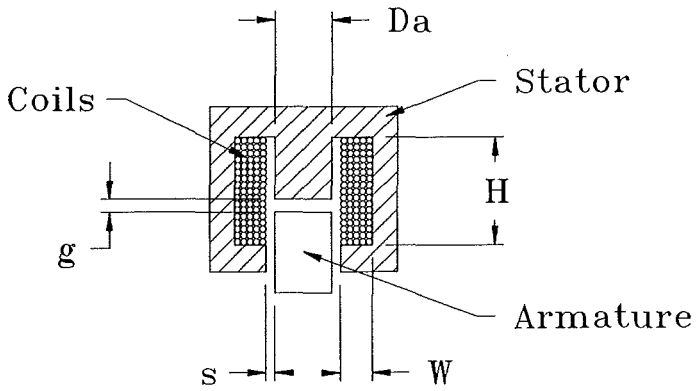

Figure C.1 Anatomy of a cylindrical solenoid

Input variables†

theta	(θ)	0.0
I		29.0
eta	(η)	0.60
HW	(H/W)	0.7
F		100.0
g		1.5
s		0.5
Bg	(B_g)	14.0
V		12.0

† Symbols in brackets are those used by Yang.

Output variables

Da	(D_a)	12.8
NI		27872
N		96
R		0.4
Dc	(D_c)	13.8
y1	(y_1)	2717
y2	(y_2)	125.7
y3	(y_3)	10.4
AWG		22
W		8.8
gamma1	(γ_1)	0.12
gamma2	(γ_2)	0.69
gamma3	(γ_3)	0.48
beta0	(β_0)	0.52
PeDa0	(($P_e/D_a)_0$)	0.041
Fbeta	(F_β)	1.123
Fp	(F_p)	0.947
Gbeta	(G_β)	1.487
Gp	(G_p)	0.63
beta	(β)	0.87
PeDa	(P_e/D_a)	0.024
alpha1	(α_1)	27

alpha2	(α_2)	0.023
Ba	(B)	16.1
Fr	(F_r)	99.59

The program was used to determine the input variables which would give the output resultant force close to that desired. The final output of the program shows that the computed resultant force Fr is very close to the initial required force of 100 N. The key parameters taken from this analysis and applied to the Disole design were the gauge of wire (22 AWG) and the number of turns of wire (96).

SOLENOID.PAS

```
program solenoid;
uses crt;
const
    mu  = 0.00319;      { Magnetic permeability of air (G/Oe)                }
    pi  = 3.1415927;
var
    Da          :real;    { Armature diameter (mm)                           }
    Dc          :real;    { Coil inside diameter (mm)                        }
    NI          :real;    { Magnetomotive force (ampere-turns)               }
    F           :real;    { Required force (Newtons)                         }
    Fr          :real;    { Calculated force delivered (Newtons)             }
    theta       :real;    { Armature cone angle (degrees)                    }
    H           :real;    { Coil height (mm)                                 }
    W           :real;    { Coil Width (mm)                                  }
    eta         :real;    { Solenoid efficiency                              }
    I           :real;    { Coil current (amperes)                           }
    V           :real;    { Operating voltage (Volts dc)                     }
    HW          :real;    { Height to width ratio of coil                    }
    R           :real;    { Resistance of coil (ohms)                        }
    g           :real;    { Working gap (mm)                                 }
    Bg          :real;    { Airgap magnetic flux density (kG)                }
    s           :real;    { Side gap allowance (mm)                          }
    N           :integer;         { Number of turns in coil                  }
    y1          :real;    { Factors for determining the wire size            }
    y2          :real;    { and width of the coil window                     }
    y3          :real;
    AWG         :integer;         { Wire size (American Wire Gauge)          }
    gamma1      :real;    { Calculated factors used to determine             }
    gamma2      :real;    { beta0, PeDa0, Fp, Fbeta, Gp and Gbeta            }
    gamma3      :real;
    beta0       :real;    { Reference value for beta                         }
    PeDa0       :real;    { Reference value for PeDa0                        }
    Fp          :real;    { Correction factors for PeDa0                     }
    Gp          :real;
    Fbeta       :real;    { Correction factors for beta0                     }
    Gbeta       :real;
    Beta        :real;    { ratio of useful to total airgap flux             }
    PeDa        :real;    { Effective magnetic permeance (Mx/A turn)         }
                          {       Armature diameter (mm)                     }

    alpha1      :real;    { Factors used to determine magnetic flux          }
    alpha2      :real;
    Ba          :real;    { Armature magnetic flux density (kG)              }
    cont        :boolean;         { Program flow control variable            }
    dfile       :text;    { Data file for input of default data.             }
```

```
    rfile       :text;    { Lotus.prn file for output of results.                }
    reply       :char;    { Reply to initial question on input data.             }
    resfile     :string[255];    { Path and filename of results file.            }
    saveres     :boolean;        { Ask if user wants to save results in a       }
                                 { lotus.Prn file for late analysis.            }


function power(x,y:real):real;      { Calculates x to the power of y }

begin
    power:=exp(y*ln(x));
end;                                { of function power }

procedure titlebox;                 { generates a title in a box.    }

var i    :integer;

begin
    clrscr;
    write('          '#201);
    for i:=1 to 47 do write(#205);
    writeln(#187);
    write('          '#186'       SOLENOID DESIGN ANALYSIS');
    writeln('          '#186);
    write('          '#200);
    for i:=1 to 47 do write(#205);
    writeln(#188);
end;

procedure initialize;

begin
    assign(dfile,'solenoid.dat');
    reset(dfile);
    readln(dfile,theta);
    readln(dfile,l);
    readln(dfile,eta);
    readln(dfile,HW);
    readln(dfile,F);
    readln(dfile,g);
    readln(dfile,s);
    readln(dfile,Bg);
    readln(dfile,V);

{  The following data was used in an example by Yang }
{    theta:=20;
    l:=1.5;
```

```
    eta:=0.65;
    HW:=8;
    F:=44.48;
    g:=2.54;
    s:=2.5;
    Bg:=9;
    V:=20;      }

end;

procedure askchange;

begin
    writeln;
    write('  The input variables for the solenoid design have');
    writeln(' been extracted from the file');
    writeln('  solenoid.dat.  Input variables are:');
    writeln;
    write('              solenoid armature cone angle  (degrees) ');
    writeln('    ',theta:3:1);
    write('              solenoid coil current         (amperes) ');
    writeln('    ',I:3:1);
    write('              solenoid magnetic efficiency            ');
    writeln('    ',eta:3:2);
    write('              coil window aspect ratio                ');
    writeln('    ',HW:3:1);
    write('              required force               (Newtons) ');
    writeln('    ',F:3:1);
    write('              air gap - required travel          (mm) ');
    writeln('    ',g:3:2);
    write('              side gap                           (mm) ');
    writeln('    ',s:3:2);
    write('              airgap magnetic flux density       (kG) ');
    writeln('    ',Bg:3:1);
    write('              solenoid driving voltage          (Vdc) ');
    writeln('    ',V:3:1);
    writeln;
    write('    do you wish to edit the default data ? (Y/N)  ');
    repeat
      reply:=upcase(readkey);
    until reply in ['Y','N'];
    clrscr;
end;

procedure change;

begin
```

```
cont:=false;
repeat
    clrscr;
    writeln; writeln; writeln;
    writeln('                current default settings');
    writeln;
write('          A. solenoid armature cone angle  (degrees) ');
writeln('   ',theta:3:1);
write('          B. solenoid coil current         (amperes) ');
writeln('   ',I:3:1);
write('          C. solenoid magnetic efficiency           ');
writeln('   ',eta:3:2);
write('          D. coil window aspect ratio               ');
writeln('   ',HW:3:1);
write('          E. required force               (Newtons) ');
writeln('   ',F:3:1);
write('          F. air gap - required travel      (mm) ');
writeln('   ',g:3:2);
write('          G. side gap                       (mm) ');
writeln('   ',s:3:2);
write('          H. airgap magnetic flux density   (kG) ');
writeln('   ',Bg:3:1);
write('          I. solenoid driving voltage       (Vdc) ');
writeln('   ',V:3:1);
    writeln; writeln;
    write('    select the parameter to be altered ( A - I ) ');
    write('or enter to finish editing  ');
    reply:=readkey;
    writeln;
    writeln;
    reply:=upcase(reply);
    write('    input new data value for ',reply,'  ');
    case reply of
        'A':readln(theta);      'B':readln(I);      'C':readln(eta);
        'D':readln(HW);         'E':readln(F);      'F':readln(g);
        'G':readln(s);          'H':readln(Bg);     'I':readln(V);
        #13:cont:=true;
    end;
until (cont=true);
clrscr;
write('     do you want to save the defaults for later runs ?');
write(' (y/n) ');
repeat
    reply:=upcase(readkey);
until reply in ['Y','N'];
if (reply='Y') then
begin
```

```
        rewrite(dfile);
        writeln(dfile,theta,'       theta');
        writeln(dfile,I,'       I');
        writeln(dfile,eta,'       eta');
        writeln(dfile,HW,'       HW');
        writeln(dfile,F,'       F');
        writeln(dfile,g,'       g');
        writeln(dfile,s,'       s');
        writeln(dfile,Bg,'       Bg');
        writeln(dfile,V,'       V');
        close(dfile);
    end;
    clrscr;
end;


procedure wiresize;

const
    lindat  : array[0..26,0..2] of real = (
      (18, -0.05103, 591.9537),
      (19, -0.04569, 473.8513),
      (20, -0.04003, 373.6492),
      (21, -0.03654, 297.4282),
      (22, -0.03271, 232.1511),
      (23, -0.02998, 187.7008),
      (24, -0.02670, 147.9395),
      (25, -0.02394, 117.3510),
      (26, -0.02122, 92.95330),
      (27, -0.01955, 74.38211),
      (28, -0.01728, 58.64072),
      (29, -0.01594, 47.10075),
      (30, -0.01436, 37.04016),
      (31, -0.01333, 29.51278),
      (32, -0.01207, 23.39545),
      (33, -0.01064, 19.00094),
      (34, -0.00964, 14.86701),
      (35, -0.00874, 11.77813),
      (36, -0.00803, 9.353371),
      (37, -0.00728, 7.248393),
      (38, -0.00688, 6.024298),
      (39, -0.00592, 4.601239),
      (40, -0.00564, 3.635610),
      (41, -0.00495, 2.943449),
      (42, -0.00468, 2.361872),
      (43, -0.00424, 1.838275),
      (44, -0.00408, 1.513078));
```

```
var
    count       :integer;
    diff        :array[0..26] of real;
    delta       :real;

begin
    for count:= 0 to 26 do
    diff[count]:=abs((y1*lindat[count,1]+lindat[count,2])-y2);
    count:=0;
    repeat
        count:=count+1;
        delta:=diff[count]-diff[count+1];
    until (delta<0);
    AWG:=round(lindat[count,0]);
end;

procedure winwidth;

var
    m           :real;
    c           :real;

begin
    case AWG of
        18:     m:=0.04921;
        19:     m:=0.04436;
        20:     m:=0.03878;
        21:     m:=0.03463;
        22:     m:=0.03133;
        23:     m:=0.02793;
        24:     m:=0.02509;
        25:     m:=0.02246;
        26:     m:=0.01993;
        27:     m:=0.01799;
        28:     m:=0.01606;
        29:     m:=0.01442;
        30:     m:=0.01302;
        31:     m:=0.01184;
        32:     m:=0.01066;
        33:     m:=0.009661;
        34:     m:=0.008661;
        35:     m:=0.007616;
        36:     m:=0.006570;
        37:     m:=0.005987;
        38:     m:=0.005404;
        39:     m:=0.004820;
        40:     m:=0.004237;
```

```
            41:     m:=0.003828;
            42:     m:=0.003419;
            43:     m:=0.003010;
            44:     m:=0.002601;
        end;
        m:=25.4*m;
        c:=0.50;
        W:=m*y3+c;
end;

procedure Ffactors;
const
    lindat  : array[1..12,1..5] of real = (
            ( 0.10 , 1.49 , 1.75 , 2.25 , 2.80 ),
            ( 0.15 , 1.29 , 1.45 , 1.71 , 1.98 ),
            ( 0.20 , 1.18 , 1.28 , 1.44 , 1.60 ),
            ( 0.25 , 1.11 , 1.17 , 1.27 , 1.35 ),
            ( 0.30 , 1.07 , 1.11 , 1.17 , 1.21 ),
            ( 0.35 , 1.04 , 1.06 , 1.09 , 1.12 ),
            ( 0.40 , 1.02 , 1.02 , 1.03 , 1.03 ),
            ( 0.50 , 1.00 , 0.99 , 0.97 , 0.95 ),
            ( 0.60 , 0.97 , 0.95 , 0.91 , 0.88 ),
            ( 0.70 , 0.95 , 0.93 , 0.88 , 0.84 ),
            ( 0.80 , 0.94 , 0.91 , 0.85 , 0.80 ),
            ( 1.00 , 0.93 , 0.89 , 0.82 , 0.75 ));

var
    a           :real;
    b           :real;
    c           :real;
    x           :array[1..3] of real;
    y1a         :real;
    y2a         :real;
    y3a         :real;
    yb          :array[1..3] of real;
    i,j,k       :integer;
    count       :integer;
    tmp         :integer;

begin
    if (gamma1<0.2) then
    begin
        x[1]:=  0.05;
        x[2]:=  0.1;
        x[3]:=  0.3;
        y1a:=1.4493*power(gamma2,3)-3.2252*sqr(gamma2)+2.4432*
            gamma2+0.4658;
```

```
        y2a:=1.6366*power(gamma2,3)-3.7817*sqr(gamma2)+3.002*
            gamma2+0.3073;
        y3a:=1.6043*power(gamma2,3)-3.9261*sqr(gamma2)+3.4548*
            gamma2+0.1296;
        yb[1]:=-14.3932*power(gamma2,5)+45.5233*power(gamma2,4)-
            55.4993*power(gamma2,3)+32.814*sqr(gamma2)-9.6975*
            gamma2+2.1827;
        yb[2]:=-18.8079*power(gamma2,5)+60.3299*power(gamma2,4)-
            75.0926*power(gamma2,3)+45.6979*sqr(gamma2)-13.9995*
            gamma2+2.7622;
        yb[3]:=-39.1204*power(gamma2,5)+122.5694*power(gamma2,4)-
            148.217*power(gamma2,3)+87.0833*sqr(gamma2)-25.567*
            gamma2+4.0722;
    end;
    if (gamma1>=0.2) then
    begin
        x[1]:=   0.1;
        x[2]:=   0.3;
        x[3]:=   0.6;
        y1a:=1.6366*power(gamma2,3)-3.7817*sqr(gamma2)+3.002*
            gamma2+0.3073;
        y2a:=1.6043*power(gamma2,3)-3.9261*sqr(gamma2)+3.4548*
            gamma2+0.1296;
        y3a:=1.4342*power(gamma2,3)-3.6986*sqr(gamma2)+3.5759*
            gamma2+0.0393;
        yb[1]:=-18.8079*power(gamma2,5)+60.3299*power(gamma2,4)-
            75.0926*power(gamma2,3)+45.6979*sqr(gamma2)-13.9995*
            gamma2+2.7622;
        yb[2]:=-39.1204*power(gamma2,5)+122.5694*power(gamma2,4)-
            148.217*power(gamma2,3)+87.0833*sqr(gamma2)-25.567*
            gamma2+4.0722;
        yb[3]:=-59.6147*power(gamma2,5)+186.9172*power(gamma2,4)-
            226.127*power(gamma2,3)+132.6086*sqr(gamma2)-38.5726*
            gamma2+5.5392;
    end;
    k:=0;
    repeat
         k:=k+1;
    until ((gamma2-lindat[k,1])<=0);
    for i:=1 to 3 do
    begin
        tmp:=round(x[i]*100);
        case tmp of
             5   :j:=2;
            10   :j:=3;
            30   :j:=4;
            60   :j:=5;
```

```
            end;
            yb[i]:=lindat[(k-1),j]+(lindat[k,j]-lindat[(k-1),j])*
                ((gamma2-lindat[k,1])/(lindat[k,1]-lindat[(k-1),1]));
        end;
        a:=((y2a-y3a)*(x[1]-x[2])-(y1a-y2a)*(x[2]-x[3]))/((x[2]*x[2]-x[3]*x[3])*(x[1]
          -x[2])-(x[1]*x[1]-x[2]*x[2])*(x[2]-x[3]));
        b:=((y2a-y3a)-a*(x[2]*x[2]-x[3]*x[3]))/(x[2]-x[3]);
        c:=y1a-a*x[1]*x[1]-b*x[1];
        Fbeta:=a*sqr(gamma1)+b*gamma1+c;

a:=((yb[2]-yb[3])*(x[1]-x[2])-(yb[1]-yb[2])*(x[2]-x[3]))/((x[2]*x[2]-x[3]*x[3])*(x
[1]-x[2])
          -(x[1]*x[1]-x[2]*x[2])*(x[2]-x[3]));
        b:=((yb[2]-yb[3])-a*(x[2]*x[2]-x[3]*x[3]))/(x[2]-x[3]);
        c:=yb[1]-a*x[1]*x[1]-b*x[1];
        Fp:=a*sqr(gamma1)+b*gamma1+c;
end;

procedure Gfactors;

var
        a    :real;
        b    :real;
        c    :real;
        x1   :real;
        x2   :real;
        x3   :real;
        y1a  :real;
        y2a  :real;
        y3a  :real;
        y1b  :real;
        y2b  :real;
        y3b  :real;

begin
        x1:=0.05;
        x2:=0.1;
        x3:=0.3;
        y1a:=-0.00014*power(gamma3,3)+0.005190*sqr(gamma3)-0.09275*
            gamma3+1.300474;
        y2a:=-0.00032*power(gamma3,3)+0.011442*sqr(gamma3)-0.16666*
            gamma3+1.507035;
        y3a:=-0.00186*power(gamma3,3)+0.047643*sqr(gamma3)-0.45694*
            gamma3+2.189623;
        y1b:=-0.00055*sqr(gamma3)+0.069444*gamma3+0.731111;
        y2b:=-0.00018*sqr(gamma3)+0.097592*gamma3+0.612592;
        y3b:=0.000555*sqr(gamma3)+0.157222*gamma3+0.362222;
```

```
    a:=((y2a-y3a)*(x1-x2)-(y1a-y2a)*(x2-x3))/((x2*x2-x3*x3)*(x1-x2)
      -(x1*x1-x2*x2)*(x2-x3));
    b:=((y2a-y3a)-a*(x2*x2-x3*x3))/(x2-x3);
    c:=y1a-a*x1*x1-b*x1;
    Gbeta:=a*sqr(gamma1)+b*gamma1+c;
    a:=((y2b-y3b)*(x1-x2)-(y1b-y2b)*(x2-x3))/((x2*x2-x3*x3)*(x1-x2)
      -(x1*x1-x2*x2)*(x2-x3));
    b:=((y2b-y3b)-a*(x2*x2-x3*x3))/(x2-x3);
    c:=y1b-a*x1*x1-b*x1;
    Gp:=a*sqr(gamma1)+b*gamma1+c;
end;

procedure Fluxdensity;

const
    lindat  : array[1..24,1..7] of real = (
    (  1.9, 1.80, 1.65, 1.44, 1.25, 0.98, 0.72  ),
    (  2.0, 1.93, 1.75, 1.50, 1.31, 1.00, 0.74  ),
    (  3.0, 3.09, 2.80, 2.32, 1.96, 1.47, 0.96  ),
    (  4.0, 4.09, 3.69, 3.14, 2.69, 2.01, 1.24  ),
    (  5.0, 5.06, 4.73, 4.14, 3.57, 2.68, 1.63  ),
    (  6.0, 6.10, 5.66, 5.02, 4.43, 3.40, 2.01  ),
    (  7.0, 7.14, 6.66, 5.97, 5.28, 4.14, 2.50  ),
    (  8.0, 8.18, 7.59, 6.86, 6.23, 4.81, 2.96  ),
    (  9.0, 9.08, 8.52, 7.75, 7.08, 5.56, 3.45  ),
    ( 10.0,10.09, 9.48, 8.57, 7.85, 6.30, 4.00  ),
    ( 12.0,12.07,11.27,10.13, 9.39, 7.67, 5.21  ),
    ( 14.0,13.64,12.69,11.37,10.58, 8.98, 6.38  ),
    ( 16.0,14.67,13.51,12.33,11.45, 9.88, 7.46  ),
    ( 18.0,15.36,14.15,13.02,12.09,10.68, 8.47  ),
    ( 20.0,15.90,14.54,13.47,12.66,11.32, 9.31  ),
    ( 25.0,16.60,15.18,14.18,13.43,12.43, 10.7  ),
    ( 30.0,17.03,15.56,14.56,13.87,13.10,11.63  ),
    ( 40.0,17.50,16.00,15.02,14.28,13.74,12.56  ),
    ( 50.0,17.80,16.29,15.27,14.54,14.05,13.12  ),
    ( 60.0,17.99,16.52,15.48,14.77,14.28,13.43  ),
    ( 70.0,18.17,16.70,15.66,14.95,14.49,13.70  ),
    ( 80.0,18.33,16.84,15.77,15.08,14.54,13.95  ),
    ( 90.0,18.45,16.96,15.83,15.18,14.67,14.10  ),
    (100.0,18.55,17.06,16.01,15.39,14.73,14.18  ));

var
    a     :real;
    b     :real;
    c     :real;
    x     :array[1..3] of real;
    y     :array[1..3] of real;
```

```
    i,j,k :integer;
    count :integer;
    tmp   :integer;
begin
    if (alpha2<=2.0) and (alpha2>=0.75) then
    begin
        x[1]:=0.5;
        x[2]:=1.0;
        x[3]:=2.0;
    end;
    if (alpha2<0.75) and (alpha2>=0.4) then
    begin
        x[1]:=1.0;
        x[2]:=0.5;
        x[3]:=0.3;
    end;
    if (alpha2<0.4) and (alpha2>=0.2) then
    begin
        x[1]:=0.5;
        x[2]:=0.3;
        x[3]:=0.1;
    end;
    if (alpha2<0.2) and (alpha2>=0.01) then
    begin
        x[1]:=0.3;
        x[2]:=0.1;
        x[3]:=0.01;
    end;
    k:=0;
    repeat
         k:=k+1;
    until ((alpha1-lindat[k,1])<=0);
    for i:=1 to 3 do
    begin
        tmp:=round(x[i]*100);
        case tmp of
              1 :j:=2;
             10 :j:=3;
             30 :j:=4;
             50 :j:=5;
            100 :j:=6;
            200 :j:=7;
        end;
        y[i]:=lindat[(k-1),j]+(lindat[k,j]-lindat[(k-1),j])*
              ((alpha1-lindat[k,1])/(lindat[k,1]-lindat[(k-1),1]));
    end;
    a:=((y[2]-y[3])*(x[1]-x[2])-(y[1]-y[2])*(x[2]-x[3]))/((x[2]*
```

```
      x[2]-x[3]*x[3])*(x[1]-x[2])-(x[1]*x[1]-x[2]*x[2])*(x[2]-x[3]));
    b:=((y[2]-y[3])-a*(x[2]*x[2]-x[3]*x[3]))/(x[2]-x[3]);
    c:=y[1]-a*x[1]*x[1]-b*x[1];
    Ba:=a*sqr(alpha2)+b*alpha2+c;
end;

procedure ansave;

var j    :integer;

begin
    saveres:=false;
    writeln;
    writeln;
    write('    do you wish to save the results in a lotus.Prn ');
    writeln('file ');
    write('    for later analysis ?(Y/n) ');
    repeat
        reply:=upcase(readkey);
    until reply in ['Y','N'];
    if (reply='Y') then
    begin
        write(' Y');
        writeln;
        write('    please enter the path and filename for the ');
        writeln('results. The extension .Prn');
        write('    is appended automatically.  ');
        Readln(resfile);
        for j:=1 to 255 do resfile[j]:=upcase(resfile[j]);
        assign(rfile,resfile+'.Prn');
        rewrite(rfile);
        saveres:=true;
    end;
    if saveres then
    begin
        writeln(rfile,'       Input variables');
        writeln(rfile);
        writeln(rfile,'theta ',theta:3:1);
        writeln(rfile,'I             ',I:3:1);
        writeln(rfile,'eta           ',eta:3:2);
        writeln(rfile,'HW            ',HW:3:1);
        writeln(rfile,'F             ',F:3:1);
        writeln(rfile,'g             ',g:3:1);
        writeln(rfile,'s             ',s:3:1);
        writeln(rfile,'Bg            ',Bg:3:1);
        writeln(rfile,'V             ',V:3:1);
        writeln(rfile);
```

```
        writeln(rfile,'       Output variables');
        writeln(rfile);
        writeln(rfile,'Da              ',Da:3:1);
        writeln(rfile,'NI              ',NI:6:0);
        writeln(rfile,'N               ',N:6);
        writeln(rfile,'R               ',R:3:1);
        writeln(rfile,'Dc              ',Dc:3:1);
        writeln(rfile,'y1              ',y1:6:0);
        writeln(rfile,'y2              ',y2:4:1);
        writeln(rfile,'y3              ',y3:3:1);
        writeln(rfile,'AWG             ',AWG:3);
        writeln(rfile,'W               ',W:3:1);
        writeln(rfile,'gamma1          ',gamma1:4:2);
        writeln(rfile,'gamma2          ',gamma2:4:2);
        writeln(rfile,'gamma3          ',gamma3:4:2);
        writeln(rfile,'beta0           ',beta0:4:2);
        writeln(rfile,'PeDa0           ',PeDa0:5:3);
        writeln(rfile,'Fbeta           ',Fbeta:4:3);
        writeln(rfile,'Fp              ',Fp:4:3);
        writeln(rfile,'Gbeta           ',Gbeta:4:3);
        writeln(rfile,'Gp              ',Gp:4:2);
        writeln(rfile,'beta  ',beta:4:2);
        writeln(rfile,'PeDa            ',PeDa:5:3);
        writeln(rfile,'alpha1          ',alpha1:4:0);
        writeln(rfile,'alpha2          ',alpha2:4:3);
        writeln(rfile,'Ba              ',Ba:4:1);
        writeln(rfile,'Fr              ',Fr:4:2);
        close(rfile);
    end;
    clrscr;
end;

procedure anscreen;

begin
    writeln('       Input variables ');
    writeln;
    write('      theta  ',theta:6:1,'       I       ',I:6:1);
    writeln('      eta     ',eta:6:2,'       HW      ',HW:6:1);
    write('      F       ',F:6:2,'       g       ',g:6:2);
    writeln('      s       ',s:6:2,'       Bg      ',Bg:6:1);
    writeln('      V       ',V:6:1);
    writeln;
    writeln('       Output variables');
    writeln;
    write('      Da      ',Da:6:1,'       NI      ',NI:6:0);
    writeln('      N       ',N:6,'       R       ',R:6:1);
```

```
    write('    Dc    ',Dc:6:1,'    y1    ',y1:6:0);
    writeln('    y2    ',y2:6:1,'    y3    ',y3:6:1);
    write('    AWG    ',AWG:6,'    W    ',W:6:1);
    writeln('    gamma1 ',gamma1:6:2,'    gamma2 ',gamma2:6:2);
    write('    gamma3 ',gamma3:6:2,'    beta0  ',beta0:6:2);
    writeln('    PeDa0  ',PeDa0:6:3,'    Fbeta  ',Fbeta:6:3);
    write('    Fp    ',Fp:6:3,'    Gbeta  ',Gbeta:6:3);
    writeln('    Gp    ',Gp:6:2,'    beta   ',beta:6:2);
    write('    PeDa   ',PeDa:6:3,'    alpha1 ',alpha1:6:0);
    writeln('    alpha2 ',alpha2:6:3,'    Ba    ',Ba:6:1);
    writeln('    Fr    ',Fr:6:2);
end;


begin
    titlebox;
    initialize;
    askchange;
    if reply='Y' then change;
    Da:=17.87*sqrt(F)/(Bg*cos(2*pi*theta/360));
    NI:=0.254*Bg*g*cos(2*pi*theta/360)/(mu*eta);
    N:=round(NI/I);
    R:=V/I;
    Dc:=s*2+Da;
    y1:=N/R*sqrt(N/HW);
    y2:=N*Dc/(R*25.4);
    y3:=0.886*sqrt(N/HW);
    wiresize;
    winwidth;
    H:=W*HW;
    gamma1:=g*sqr(cos(2*pi*theta/360))/Da;
    gamma2:=W/Da;
    gamma3:=H/Da;
    if gamma1>0.24 then PeDa0:=0.03675-0.03875*gamma1
    else
    PeDa0:=4864*power(gamma1,6)-5497*power(gamma1,5)+2479*
        power(gamma1,4)-570.9*power(gamma1,3)+71.47*sqr(gamma1)
        -4.832*gamma1+0.1859;
    beta0:=10*(127.5*power(gamma1,6)-203.6*power(gamma1,5)+126.2*
        power(gamma1,4)-39.78*power(gamma1,3)+7.134*sqr(gamma1)
        -0.836*gamma1+0.09651);
    Ffactors;
    Gfactors;
    Beta:=beta0*Fbeta*Gbeta;
    PeDa:=PeDa0*Fp*Gp;
    alpha1:=5.0127*PeDa*NI/Da;
    alpha2:=0.7977*PeDa*gamma2*(gamma3/gamma2+1);
```

```
    Fluxdensity;
    Fr:=4.448*0.454*sqr(Ba*Beta*(Da/25.4)*cos(2*pi*theta/360));
    ansave;
    anscreen;
    repeat until keypressed;
end.                {End of program  SOLENOID.PAS }
```

APPENDIX D Drawings of experimental apparatus

In this appendix the detail drawings of the experimental apparatus designed for the project are presented. Assembly drawings and descriptions of apparatus are included in chapters 4,5 and 6. The detail drawings of the initial manually adjustable injector are excluded from this appendix as they were superseded by the current design.

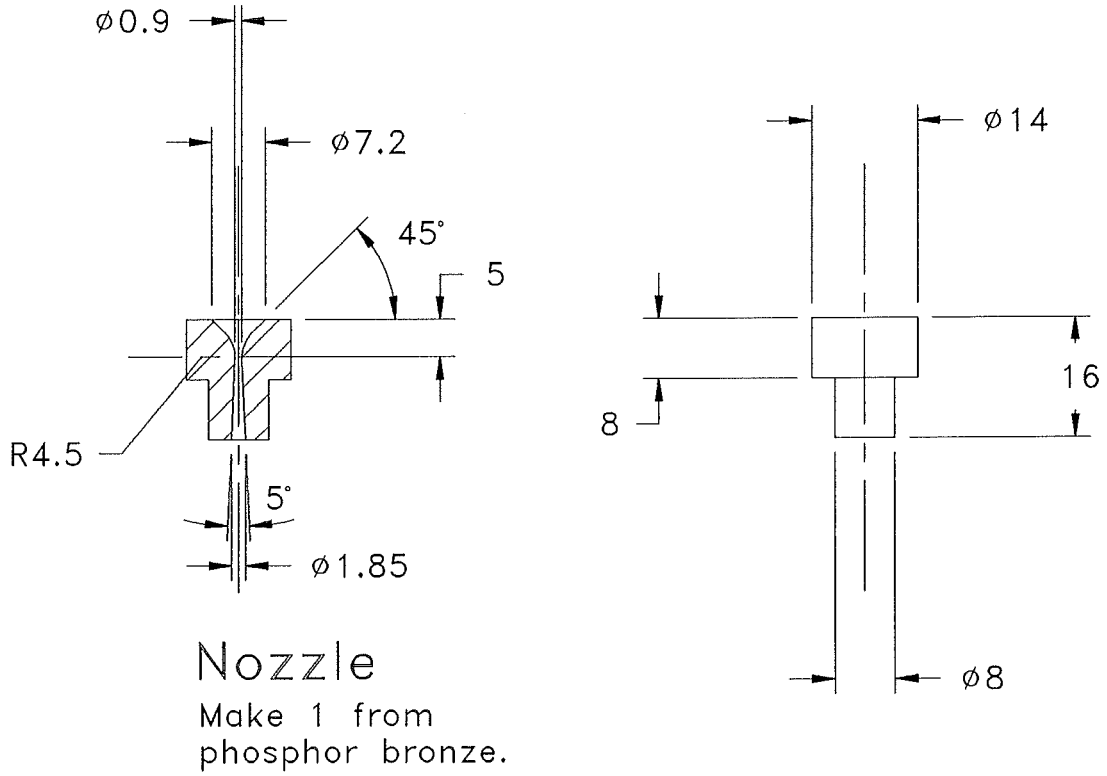

Figure D.1 Initial injector nozzle

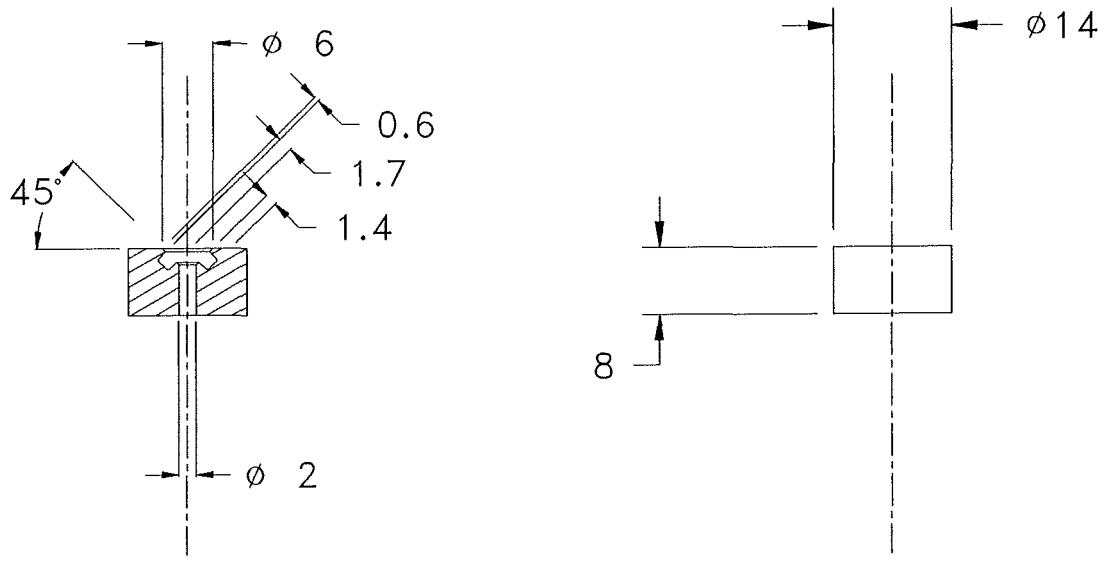

Figure D.2 O-ring nozzle

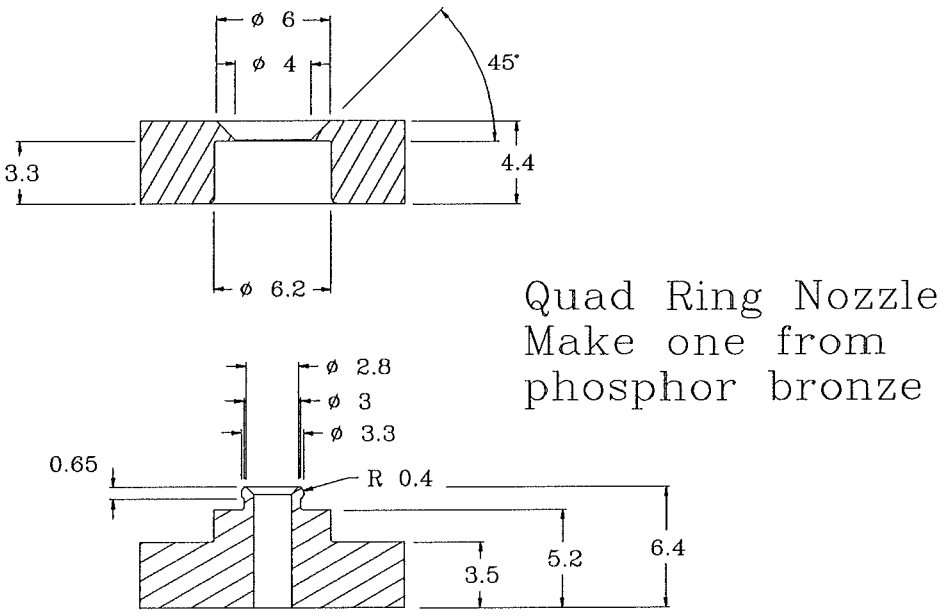

Figure D.3 Quad-ring nozzle

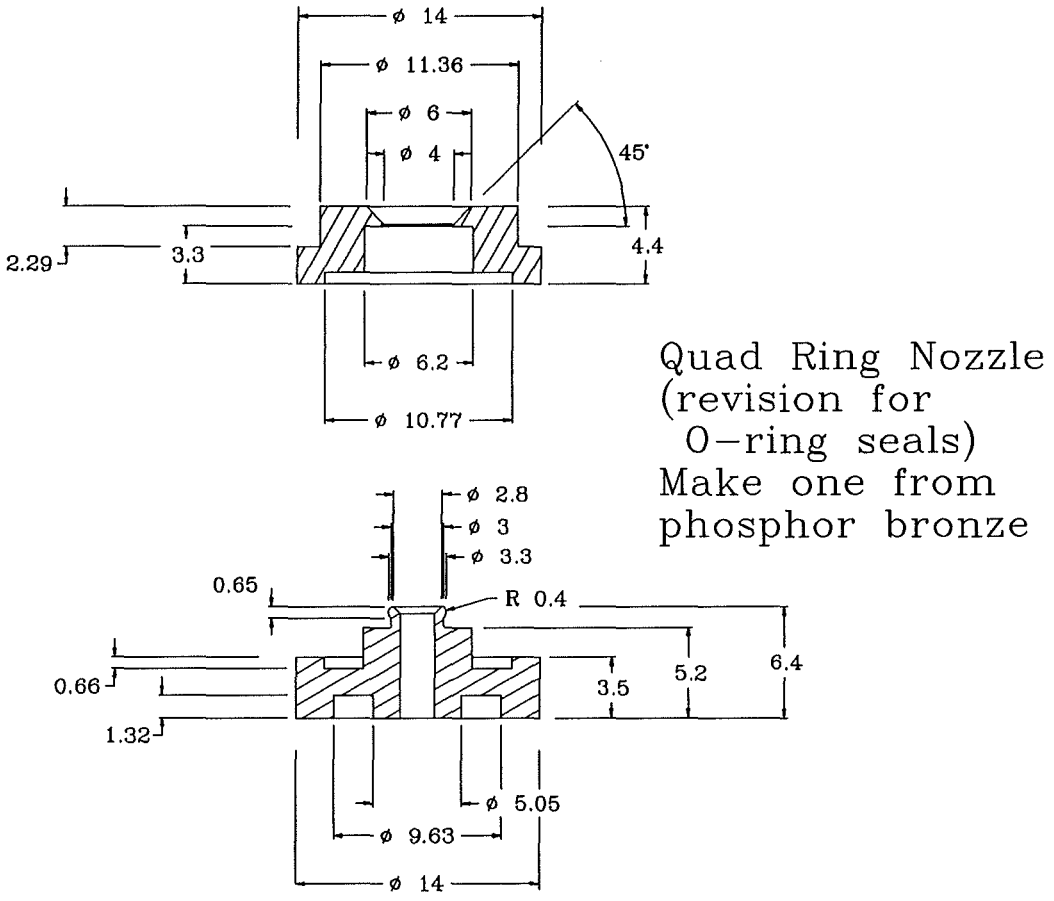

Figure D.4 Quad-ring nozzle modified for O-ring installation seals

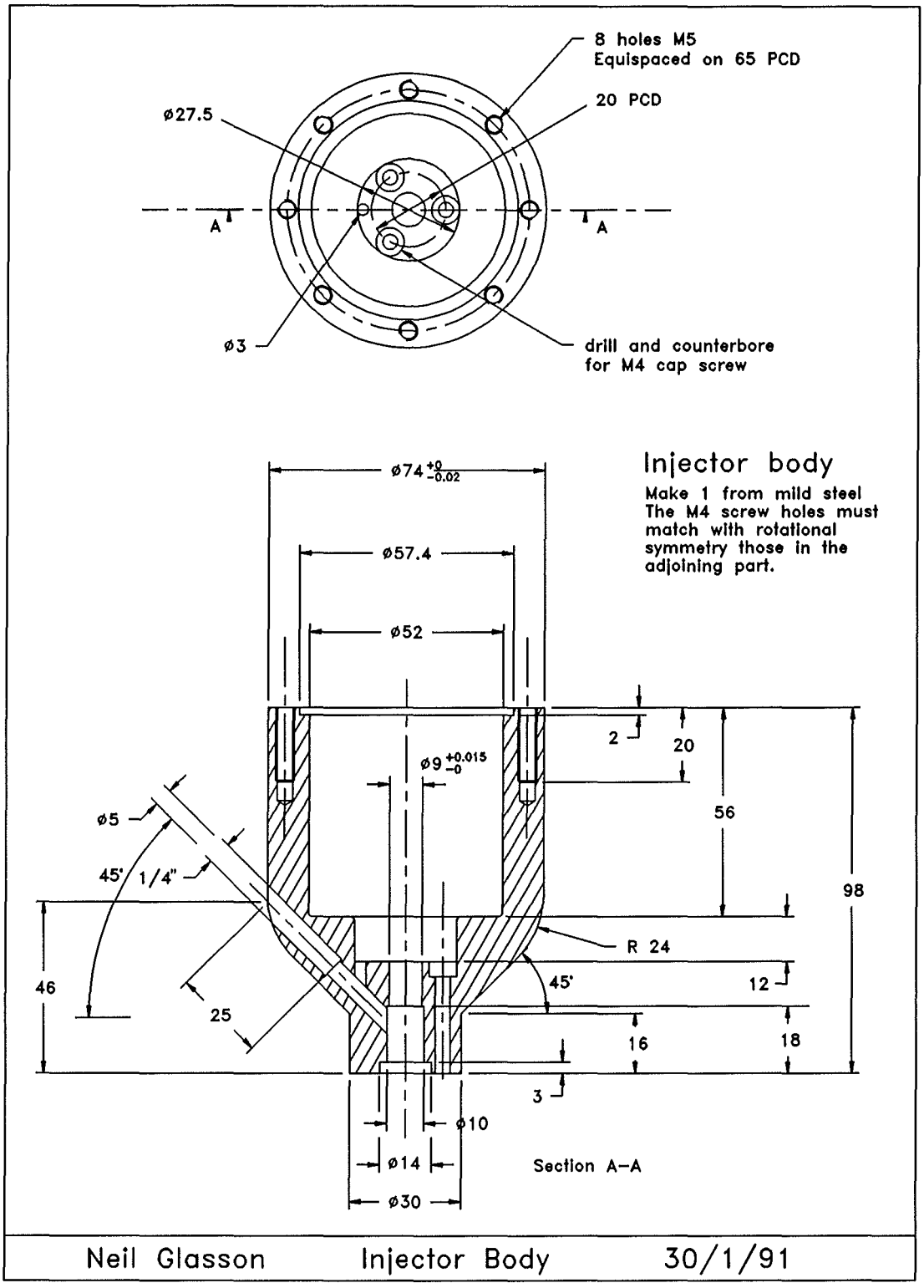

Figure D.5 Injector body

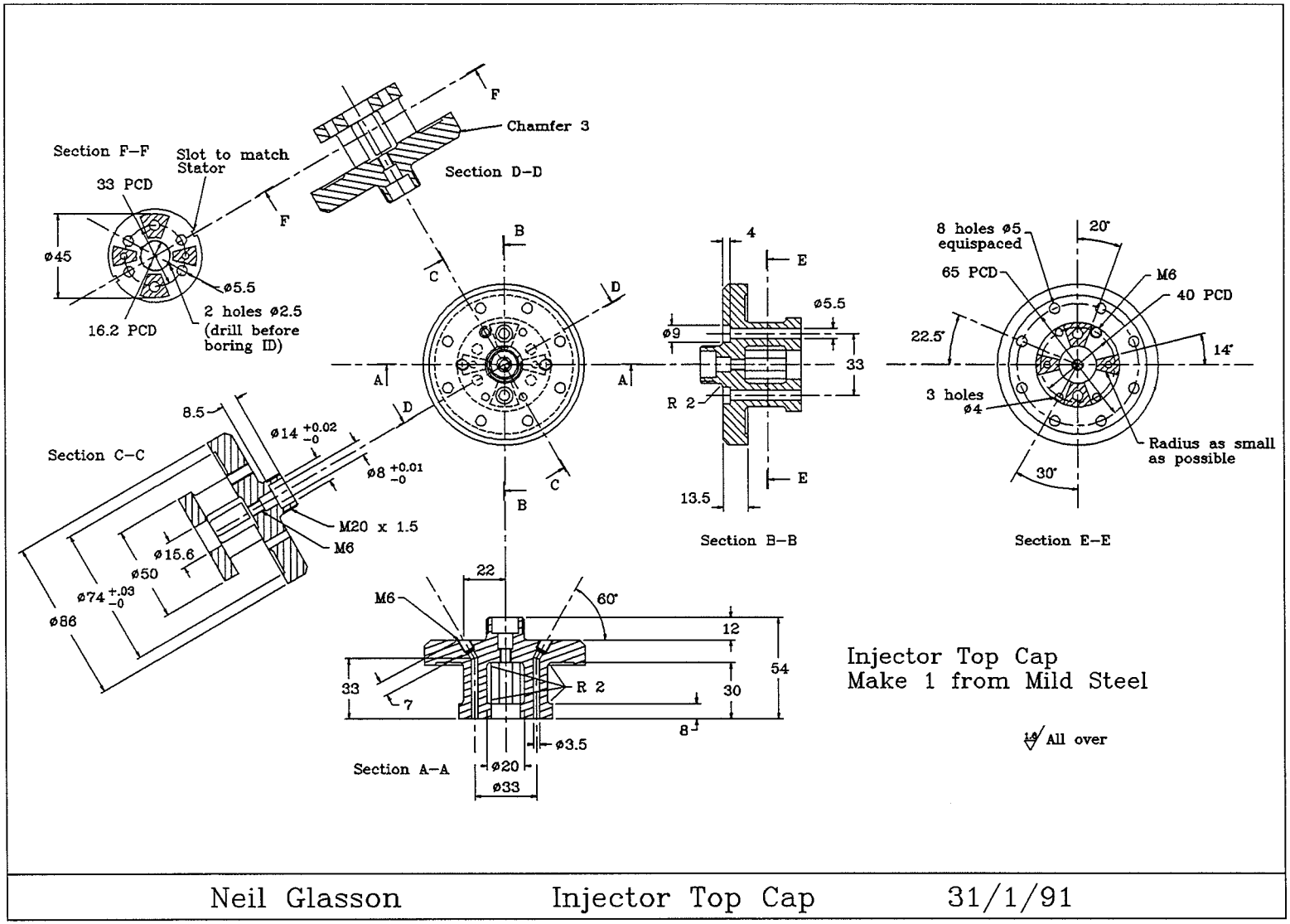

Neil Glasson	Injector Top Cap	31/1/91

Figure D.6 Injector top cap

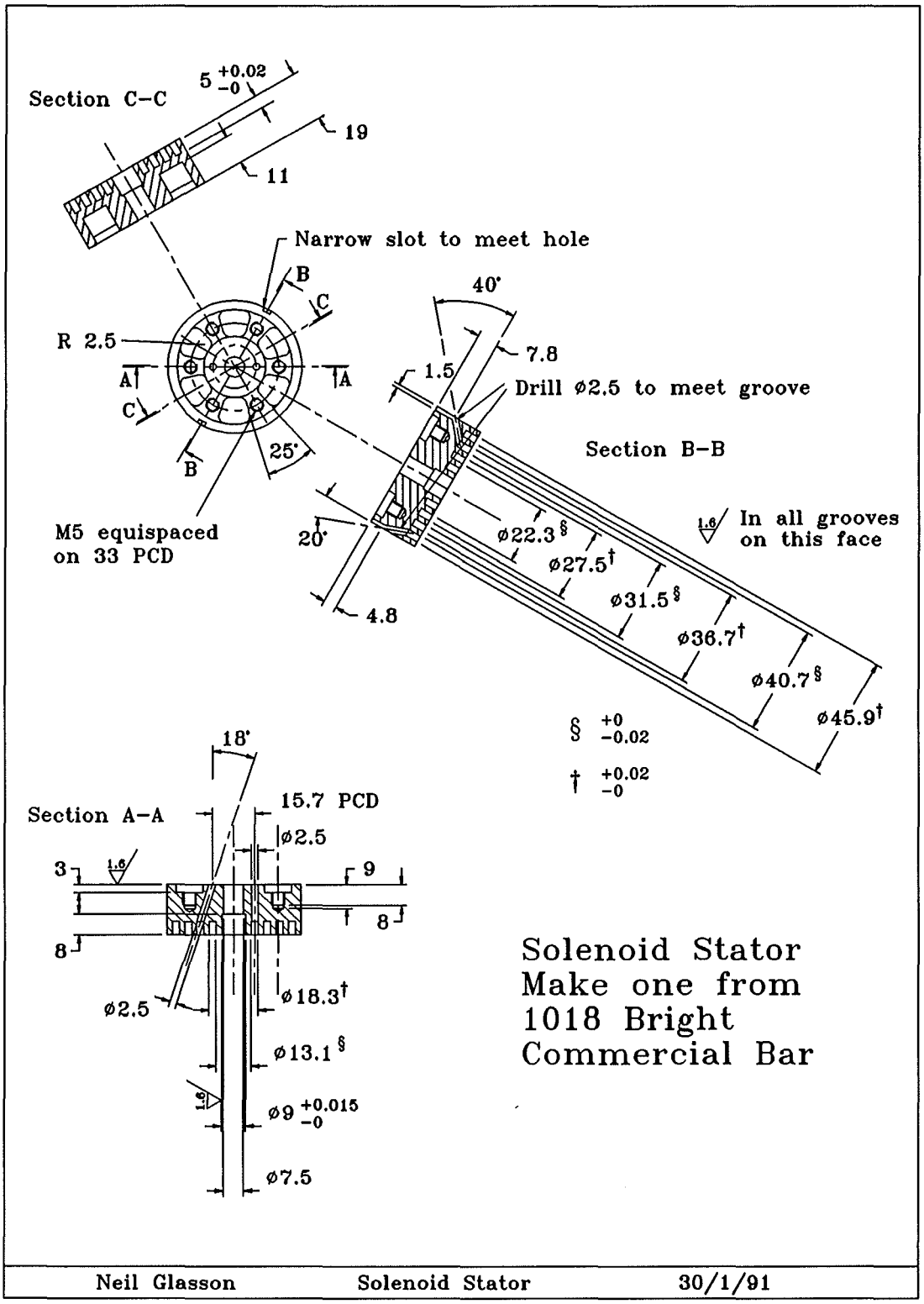

Figure D.7 Injector solenoid stator

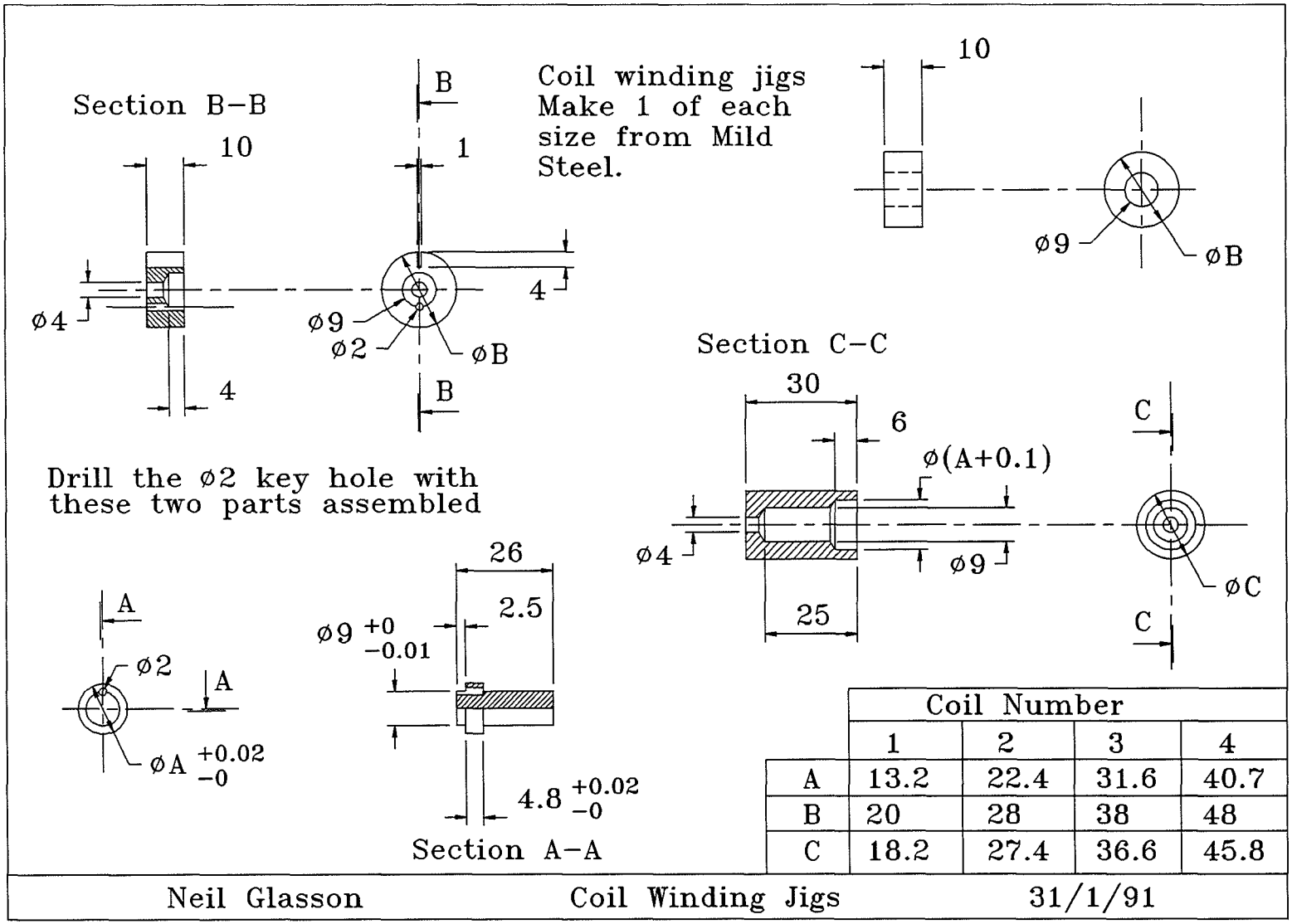

	Coil Number			
	1	2	3	4
A	13.2	22.4	31.6	40.7
B	20	28	38	48
C	18.2	27.4	36.6	45.8

Figure D.8 Jigs for winding solenoid coils

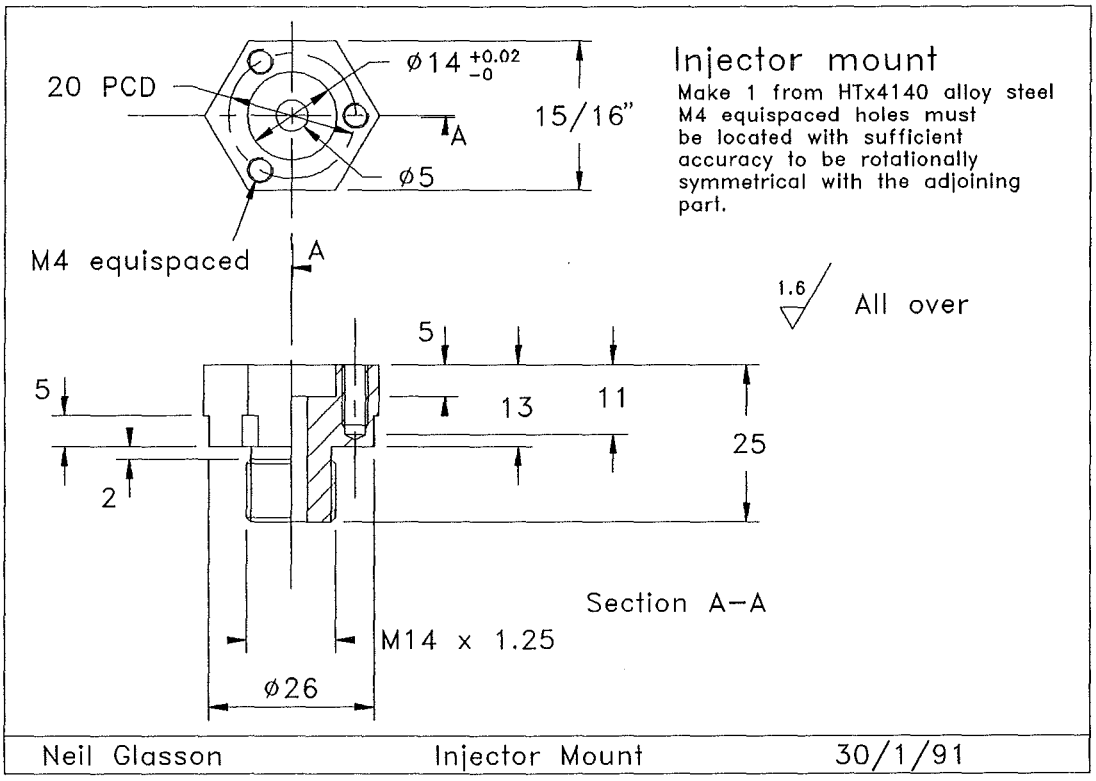

Figure D.9 Injector base

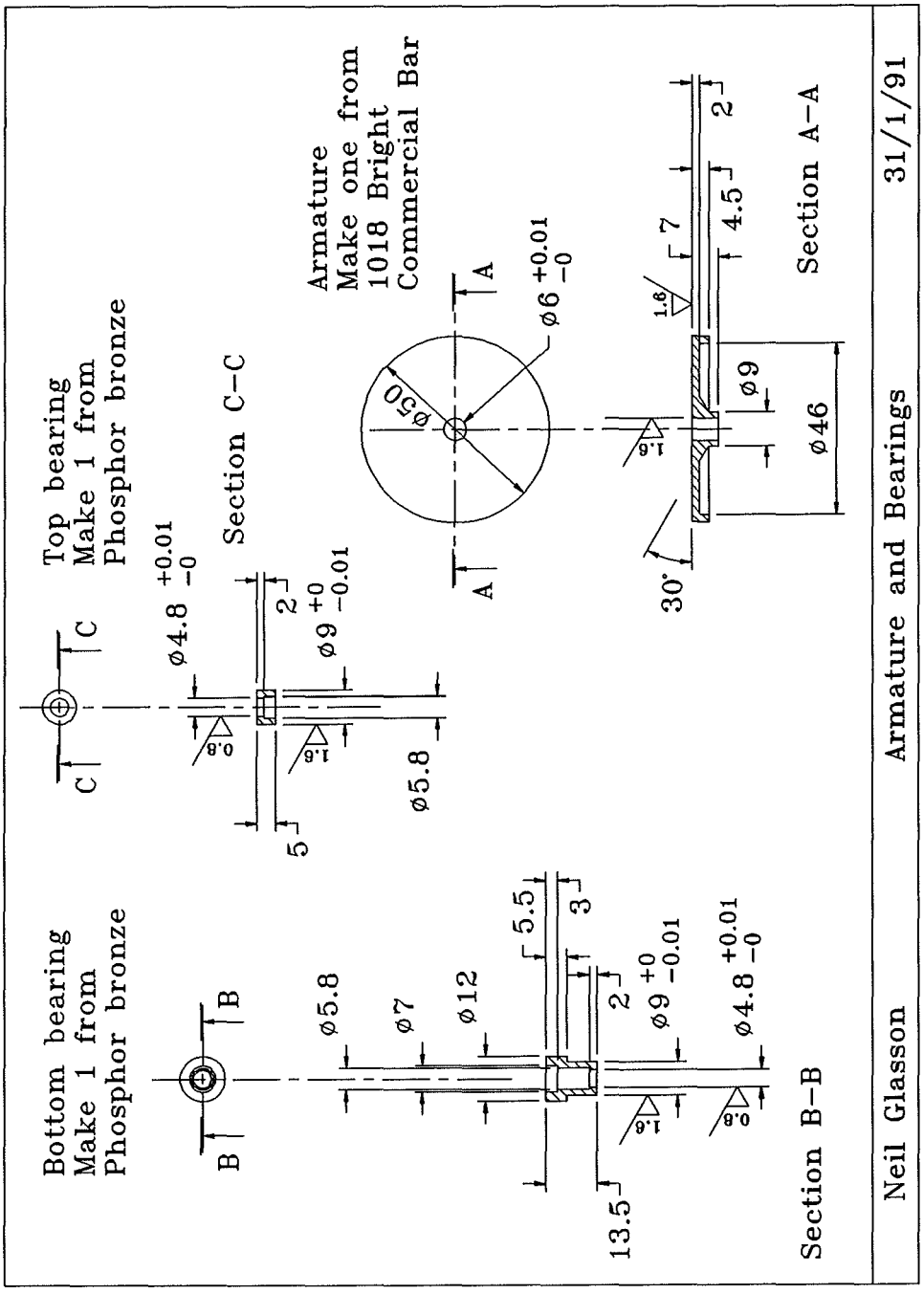

Figure D.10 Injector armature and bearings

Note that the final assembly tested on the engine employed a 40.7 mm diameter armature covering three energised coils.

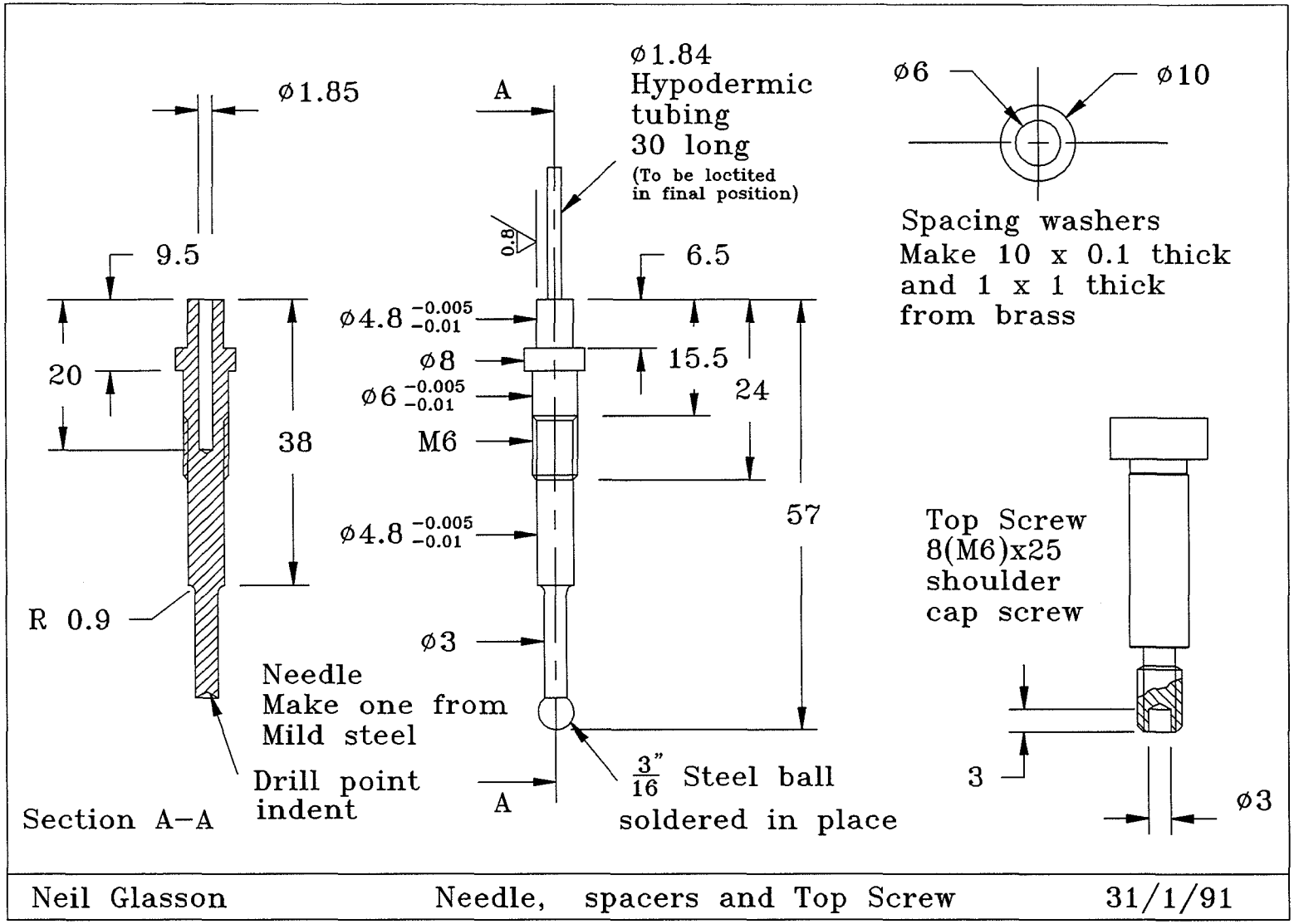

Figure D.11 Injector needle, spacers and top screw

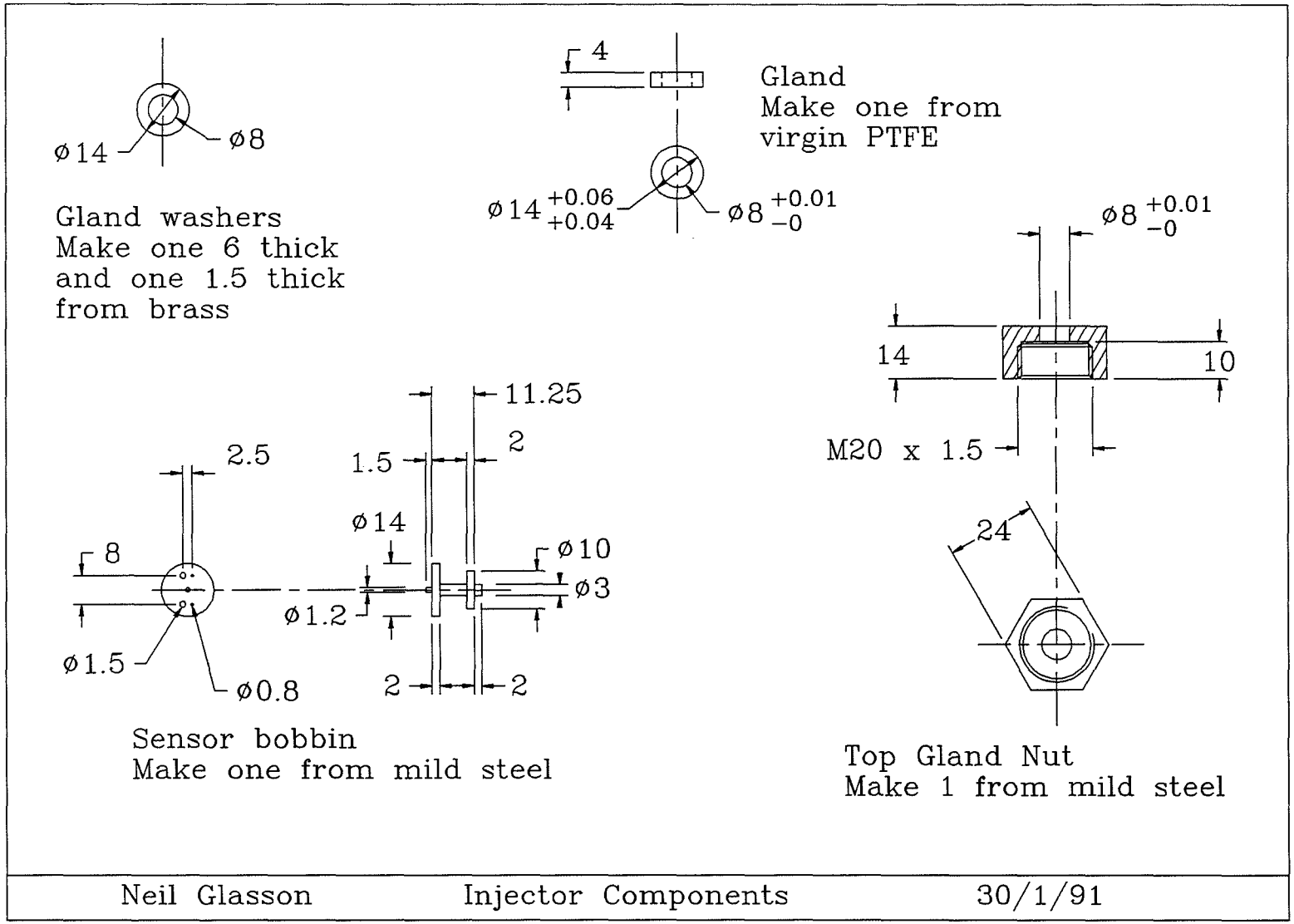

Figure D.12 Injector components

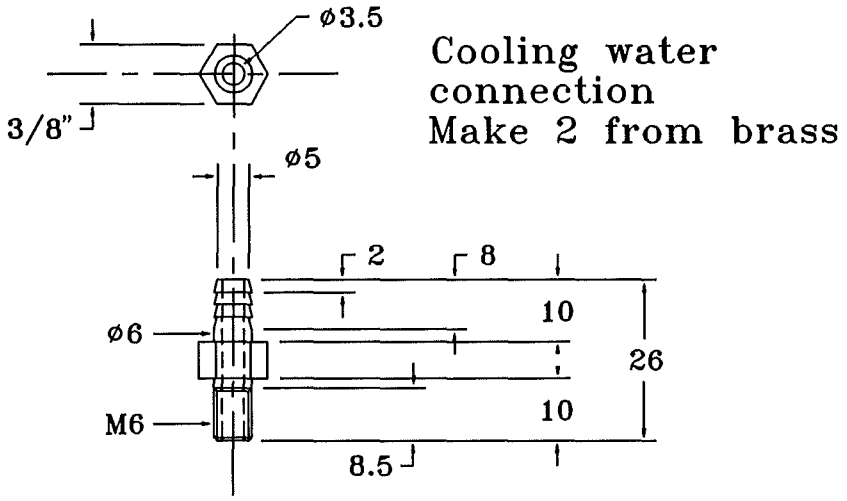

Figure D.13 Injector cooling water connection

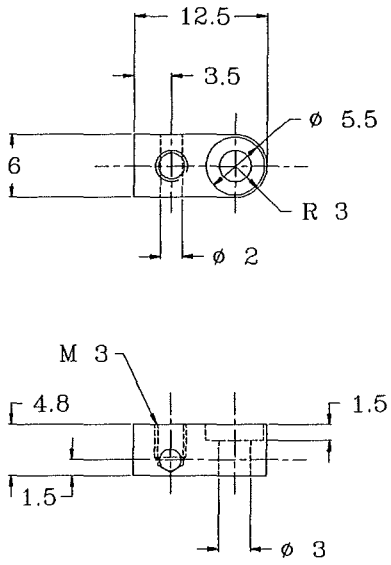

Electrical feedthrough
top connection
Make three from brass

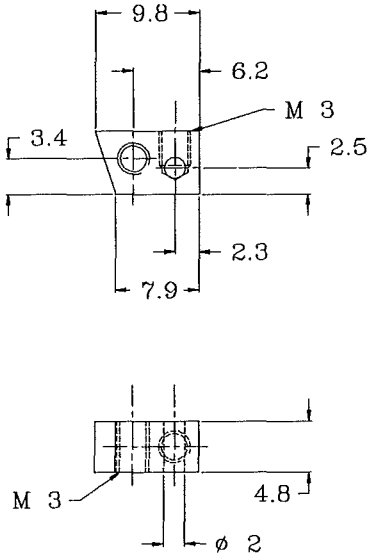

Electrical feedthrough
bottom connection
Make three from brass

Figure D.14 Electrical feed-through connections

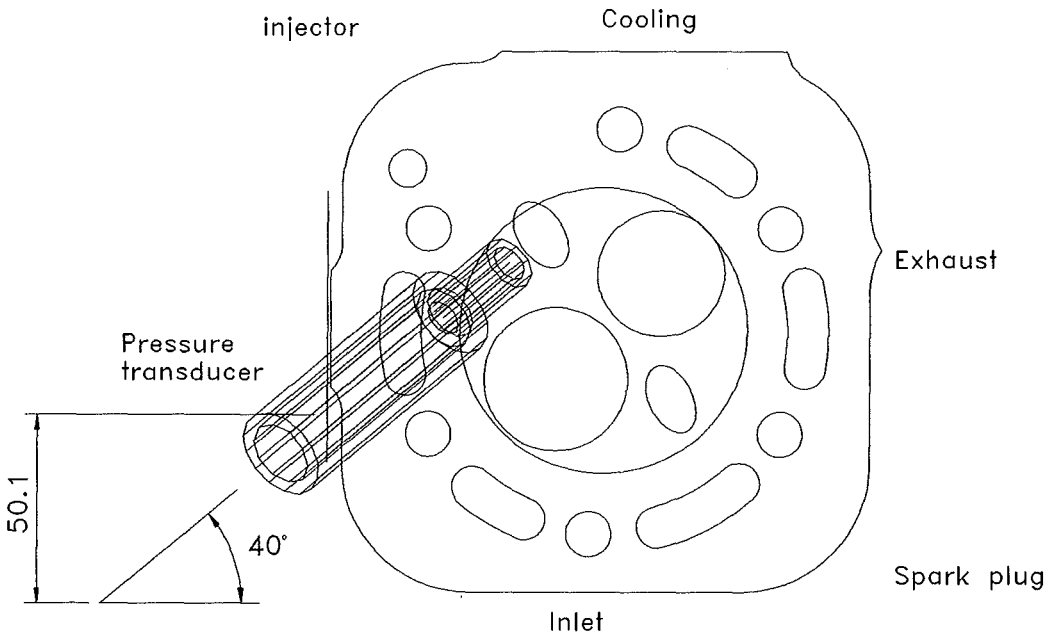

Figure D.15 Plan view of cylinder head modification.

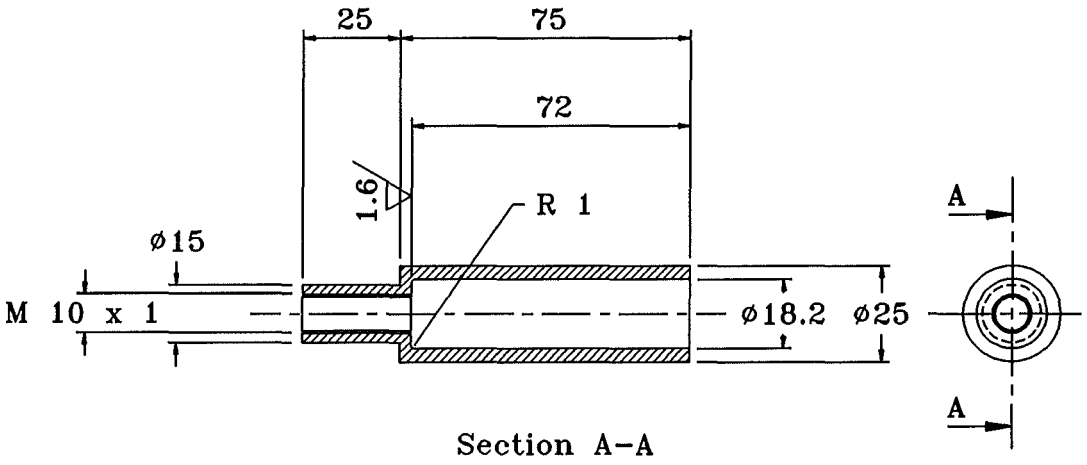

Spark plug hole sleeve
Make 1 from cast iron

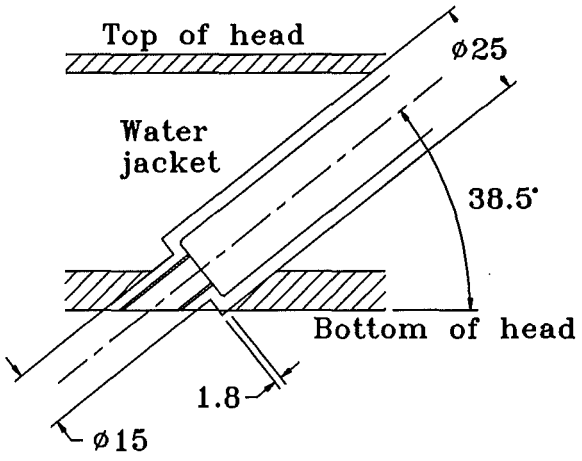

Detail of sleeve hole machined in head

Figure D.16 Detail of sleeve for cylinder head modification.

APPENDIX E Data acquisition and processing programs

The programs in this appendix were written in QuickBASIC 4.5. This was because the DAS-20 data acquisition system was supplied with a limited range of software support, Quickbasic 4.5 being the most advanced option for normal programming.

E.1 RICARDO.BAS

The program RICARDO.BAS was written to enable the collection of data during engine testing.

The program is menu driven and in operation displayed the engine test data on screen before saving to user specified files. Three data files were saved for each engine operating condition. The data saved in each of these files was as follows:

{filename}.TCD	steady state data of the various temperatures and the exhaust sensor readings.
{filename}.MFR	data of hydrogen supply temperature and pressure used in the calculation of the hydrogen mass flow rate.
{filename}.PIZ	cycle to cycle data from the piezo-electric pressure transducer and injector displacement transducer output

In addition to the primary functions of recording the above data the program incorporated two utility/debugging subroutines. One enabled the on screen display of the voltage at any particular DAS-20 channel and the other executed a data transfer from the digital storage oscilloscope to a computer file.

```
' RICARDO.BAS    A program written by Neil Glasson in November 1991,
    DIM T(9), DIO%(10), DT%(10000), CH%(10000), HPRES!(500), HTC!(500)
    COMMON SHARED DIO%(), DT%(), CH%()
    DECLARE SUB DAS20 (MODE%, BYVAL DUMMY%, FLAG%)
    DECLARE SUB ADDRESS (DMA%(), SAMP%, ADDR%)
    '$DYNAMIC
    ' Ask for twice as much memory as needed for the DMA transfer
    ' as an insufficiency in the PC DMA controller chip will cause
    ' DMA to "wrap around" to the beginning of a DMA page in the
    ' event that the DMA transfer reaches the end of a 64K DMA page
    ' in the PC's RAM.  Asking for twice as much memory insures that
    ' there will always be enough RAM to complete the transfer in one
    ' contiguous area of memory inside one DMA page.  For more
    ' information concerning the 8237 DMA controller chip, contact Intel
    ' Corporation for a more detailed data sheet.
    DIM DAT%(32766)
    ' The following variable definitions specify the number of
    ' consecutive samples to average for the respective measurement.
    NTC = 200  ' Number of data points to average for Thermocouples
    NPT = 200  ' Pressure transducer (hydrogen)
    NVL = 300  ' Variable Lambda (exhaust sensor)
    NFL = 200  ' Fixed Lambda
    NHMFR = 100         ' Number of data points for the calculation of
                        ' mass flow rate of hydrogen
    SCREEN 0, 0, 0: CLS : KEY OFF: WIDTH 80
    SAMP% = 10000
    CALL ADDRESS(DAT%(), SAMP%, APTR%)    ' Call sub.to calc. DMA
                                          ' address
    OPEN "DAS20.ADR" FOR INPUT AS #1
    INPUT #1, BASADR% ' initialize & declare CALL parameters
    CLOSE #1
    FLAG% = 0
    MD% = 0          ' Mode 0 = initialization
    DIO%(0) = BASADR% ' DAS-20 base address
    DIO%(1) = 7       ' DAS-20 Interrupt level 7
```

```
    DIO%(2) = 1        ' DAS-20 DMA level 1
    CALL DAS20(MD%, VARPTR(DIO%(0)), FLAG%)
    IF FLAG% <> 0 THEN PRINT "INSTALLATION ERROR"
    ' The EXP-20 output channel should be connected to
    ' DAS-20 channel #0 and the CJC channel to DAS-20 channel #7.
    OPEN "RICARDO.CFG" FOR INPUT AS #3
    INPUT #3, RPS!, CR!, FUEL%, OPTN%, CYCNO!, NDISP%, SAVEFNAM$
    CLOSE #3           ' Input variables from configuration file
    GOSUB 1100
    SCREEN 0      ' Set screen type to text mode only
50  COLOR 12      ' Set colour to light red
    WIDTH 40, 25 ' Set text format to 40 columns, 25 lines
    CLS
    PRINT "DATA ACQUISITION PROGRAM FOR HYDROGEN"
    PRINT "        RICARDO ENGINE TESTS "
    PRINT "     Neil Glasson December 1991 "
    PRINT
    COLOR 14      ' Change colour to yellow
    PRINT "  This program will record data from"
    PRINT "  user input and from the DAS-20 and"
    PRINT "    Exp-20 data acquisition system. "
    PRINT
    COLOR 11      ' Change colour to light cyan
    ' Print menu selection options on the screen
    PRINT "  1 Display a particular DAS-20 channel"
    PRINT "  2 View/modify input variables"
    PRINT "  3 Record and store data from engine"
    PRINT "  4 Record and store data from scope"
    PRINT "  5 Display piezo and lift data"
    PRINT "  6 Collect mass flow data"
    PRINT "  7 Exit"
    PRINT
    ' Request input from menu
    INPUT "  Make a selection from the menu "; REPLY$
    IF REPLY$ = "" THEN REPLY$ = "A"
    REP% = ASC(REPLY$)
    ' Perform action based on menu item selected
    IF REP% < 49 OR REP% > 55 THEN GOTO 50
    IF REP% = 49 THEN GOSUB 200     ' Display DAS-20 channel
    IF REP% = 50 THEN GOSUB 1600    ' View/modify input variables
    IF REP% = 51 THEN GOSUB 850     ' Record and store data from engine
    IF REP% = 52 THEN GOSUB 500     ' Record and store data from scope
    IF REP% = 53 THEN GOSUB 2100    ' Display piezo and lift data
    IF REP% = 54 THEN GOSUB 1900    ' Collect mass flow data
    IF REP% = 55 THEN END           ' End program
    GOTO 50                         ' Repeat menu display
    END                             ' End program
```

```
200  ' Read a DAS-20 channel and display data on screen
     MOD1 = 0
     GAIN% = 2
     CHANNEL% = 6
210  CLS
     COLOR 10
     PRINT " DISPLAY A PARTICULAR DAS-20 CHANNEL"
     N = 1000
     COLOR 11
     GAINR$(0) = "0 TO 10V"
     GAINR$(1) = "±10V"
     GAINR$(2) = "0 TO 10V"
     GAINR$(3) = "±5V"
     GAINR$(4) = "0 TO 1V"
     GAINR$(5) = "±0.5V"
     GAINR$(6) = "0 TO 100mV"
     GAINR$(7) = "±50mV"
     PRINT
     PRINT "        channel     "; CHANNEL%
     PRINT "        range       "; GAINR$(GAIN%)
     PRINT "        sample size "; N
     IF MOD1 = 1 THEN GOTO 300
     MOD1 = 1
     PRINT
     INPUT "Do you want to change these settings"; REPLY$
     IF REPLY$ = "" THEN REPLY$ = "a"
     REPLY% = ASC(REPLY$)
     IF REPLY% = 89 OR REPLY% = 121 THEN GOTO 290
     IF REPLY% <> 78 AND REPLY% <> 110 THEN GOTO 200
     ELSE GOTO 210
290  PRINT
     INPUT "Enter desired channel (1-6) "; CHANNEL%
     PRINT
     PRINT "     0  0 to 10V"
     PRINT "     1  ±10V"
     PRINT "     2  0 to 10V"
     PRINT "     3  ±5V"
     PRINT "     4  0 to 1V"
     PRINT "     5  ±0.5V"
     PRINT "     6  0 TO 100mV"
     PRINT "     7  ±50mV"
     PRINT
     INPUT "Select desired range from menu (0-7)"; GAIN%
     INPUT "Enter desired number of samples"; N
     GOTO 210
300  GOSUB 700
     LOCATE 10, 1
```

```
    PRINT
    PRINT "      DATA    ="
    COLOR 13
    LOCATE 11, 17
    PRINT USING "##.####"; VOLTS
    COLOR 11
    LOCATE 11, 26
    PRINT "VOLTS"
    LOCATE 23, 1
    PRINT "Press any key to return to main menu"
    IF INKEY$ = "" THEN GOTO 300
    RETURN
500  ' Set the queue
    MD% = 1
    DIO%(0) = 3
    DIO%(1) = 2  ' set to 1 for VC-6015 oscilloscope
    DIO%(2) = 2
    CALL DAS20(MD%, VARPTR(DIO%(0)), FLAG%)
    DIO%(0) = 4
    DIO%(1) = 2  ' set to 1 for VC-6015 oscilloscope
    DIO%(2) = 1
    CALL DAS20(MD%, VARPTR(DIO%(0)), FLAG%)
    CLS
    COLOR 10
    PRINT "   OSCILLOSCOPE DATA TRANSFER"
    PRINT
    COLOR 11
    PRINT "This section of the program will"
    PRINT "read both channels of information"
    PRINT "from the Hitachi VC-6041 digital"
    PRINT "storage oscilloscope and store "
    PRINT "the data in a user specified file."
    PRINT "Program was modified on 11/8/92 to"
    PRINT "accept input from VC-6015 Scope."
    ' This subroutine was originally written as a stand alone
    ' program (SCOPE.BAS), which was based on an earlier
    ' Turbo Pascal program (SCOPE.PAS) written for data capture
    ' from the VC-6014 oscilloscope via the lower speed DASH-8
    ' data acquisition system.
    PRINT
    PRINT "Connect the X and Y plotter"
    PRINT "outputs from the Scope to channels"
    PRINT "3 and 4 of the DAS-20 respectively."
    PRINT
    INPUT "Enter the filename "; FILENAME$
    PRINT
    IF FILENAME$ = "" THEN RETURN
```

```
    PRINT "Reading data"
    MD% = 24            ' Set A/D pacer clock
    DIO%(0) = 24847     ' First divisor
    DIO%(1) = 2         ' Second divisor set to 5 for VC-6015
    CALL DAS20(MD%, VARPTR(DIO%(0)), FLAG%)
    MD% = 4
    DIO%(0) = 2000
    DIO%(1) = VARPTR(DT%(0))
    DIO%(2) = 2
    DIO%(3) = 1         ' Unipolar or bipolar  set to 0 for VC 6041
    CALL DAS20(MD%, VARPTR(DIO%(0)), FLAG%)
    ' Stop internal timer if running (not always necessary)
    ' Needed if Internal timer was select (dio%(2) was a 1 or 2 for Mode 4
    MD% = 26
    DIO%(0) = 0         'Stop A/D Timer
    CALL DAS20(MD%, VARPTR(DIO%(0)), FLAG%)
    OPEN FILENAME$ FOR OUTPUT AS #2
    FOR I% = 0 TO 999
    J% = I% * 2
    CH2 = DT%(J%) * 10! / 4096
    CH1 = DT%(J% + 1) * 10! / 4096
    PRINT #2, USING " ##.### ##.### "; CH1; CH2
    NEXT I%
    CLOSE #2
    RETURN
600 ' Read the queue to check it
    MD% = 2
    DIO%(2) = 0
    WHILE DIO%(2) = 0
      DIO%(2) = 2
      CALL DAS20(MD%, VARPTR(DIO%(0)), FLAG%)
      PRINT USING "CHANNEL  ####  GAIN  #### "; DIO%(0); DIO%(1)
      DIO%(2) = 0
      CALL DAS20(MD%, VARPTR(DIO%(0)), FLAG%)
      PRINT USING "CHANNEL  ####  GAIN  #### "; DIO%(0); DIO%(1)
      PRINT USING "## DIO(2)"; DIO%(2)
    WEND
    RETURN
700 ' Routine to read a DAS-20 channel and return a voltage
    ' The inputs to this subroutine are DIO%(0) and DIO%(1).
    ' DIO%(0) specifies the instrument amplifier gain and range and
    ' DIO%(1) specifies the channel number to read.
    MD% = 3
    DIO%(0) = GAIN%
    DIO%(1) = CHANNEL%
    Z(0) = 10 / 4096
    Z(1) = 20 / 4096
```

```
    Z(2) = 10 / 4096
    Z(3) = 10 / 4096
    Z(4) = 1 / 4096
    Z(5) = 1 / 4096
    Z(6) = .1 / 4096
    Z(7) = .1 / 4096
    ZZ = Z(DIO%(0))
    VOLTS = 0
    FOR I% = 1 TO N
    DIO%(0) = GAIN%
    DIO%(1) = CHANNEL%
    CALL DAS20(MD%, VARPTR(DIO%(0)), FLAG%)
    VOLTS = VOLTS + DIO%(0) * ZZ
    NEXT I%
    VOLTS = VOLTS / N
    RETURN
800  ' Routine to read an Exp-20 channel and return a voltage
    Z(0) = 10 / 4096   ' 0 TO 10V
    Z(1) = 20 / 4096   ' ±10V
    Z(2) = 10 / 4096   ' 0 TO 10V
    Z(3) = 10 / 4096   ' ±5V
    Z(4) = 1 / 4096    ' 0 TO 1V
    Z(5) = 1 / 4096    ' ±0.5V
    Z(6) = .1 / 4096   ' 0 TO 100mV
    Z(7) = .1 / 4096   ' ±50mV
    ZZ! = Z(GAIN%)
    ' Digital outputs OP1-4 drive the EXP-20 sub-multiplexer address, so use
    ' mode 15 to set up the sub-multiplexer channel.
    MD% = 15
    DIO%(0) = EXPCHANL%      ' DAS-20 digital output to set EXP channel
    CALL DAS20(MD%, VARPTR(DIO%(0)), FLAG%)          ' address set
    IF FLAG% <> 0 THEN PRINT "ERROR IN EXP-20 CHANNEL NUMBER":
      END
    ' Now that channel is selected, perform A/D conversion using mode 3.
    VOLTS = 0
    FOR I% = 1 TO N
      MD% = 3: DIO%(0) = GAIN%: DIO%(1) = 0   ' do 1 A/D conversion
      CALL DAS20(MD%, VARPTR(DIO%(0)), FLAG%)
      VOLTS = VOLTS + DIO%(0) * ZZ!
    NEXT I%
    VOLTS = VOLTS / (N * GAINEXP%)
    RETURN
850  CLS
    COLOR 10
    PRINT "      STEADY STATE ENGINE DATA"
    PRINT
    COLOR 11
```

```
    ' Get gain setting of EXP-20
    AV = 100
    ' Initialize an integer array D%(15) to receive data
    ' Also initialize a corresponding real array to receive temperature data
890 ' Hydrogen supply pressure
    GAINEXP% = 100
    GAIN% = 0
    EXPCHANL% = 13
    N = NPT
    GOSUB 800
    LOCATE 3, 1
    PRINT USING "    HYDROGEN PRESSURE  = ###.# bar "; VOLTS *
      1319 - .5169
    ' Regression done from testing on 25/11/91. Results in SPANCAL.WK1
900 ' Get cold junction compensation temperature
    ' Output of CJC channel is scaled at 200mV/deg.C. This corresponds to
    ' 0.012207 °C/bit.
    ' Next get CJC data from this channel using Mode 3
    MD% = 3
    DIO%(0) = 2          ' DAS-20 gain X1 range unipolar 0 to 10 V
    DIO%(1) = 7          ' DAS-20 channel to convert
    CJC = 0
    N = NTC
    FOR I% = 1 TO N
    CALL DAS20(MD%, VARPTR(DIO%(0)), FLAG%)
    ' Change output in bits to real temperature
    CJC = CJC + DIO%(0) * .012207
    NEXT I%
    CJC = CJC / N
    ' Get the thermocouple data
    CH% = 0
    N = NTC
    GOSUB 1000
    ' This step is written as a subroutine so you can use it in your own
    ' programs by editing it out. Entry parameters are:-
    '   CH% - specifies DAS-20 channel that EXP-20 is connected to (0-7).
    '   D%(9) - integer data array to receive data from channels.
    '
    ' Convert data to volts and linearize
    ' AV = Gain setting on Dipswitch of EXP-20 (change to suit).
    FOR I% = 1 TO 6
    V = (D%(I%) / AV) * (1! / 4096!)
    GOSUB 1300
    T(I%) = TC
    NEXT I%
    V = (D%(7) / AV) * (10! / 4096!)
    GOSUB 1300
```

```
    T(I%) = TC
    FOR I% = 8 TO 9
    V = (D%(I%) / AV) * (1! / 4096!)
    GOSUB 1300
    T(I%) = TC
    NEXT I%
    ' Display temperature data
    TCPROBE$(1) = "AMBIENT          "
    TCPROBE$(2) = "AIR INLET        "
    TCPROBE$(3) = "COOLANT INLET    "
    TCPROBE$(4) = "COOLANT OUTLET   "
    TCPROBE$(5) = "GASOLINE         "
    TCPROBE$(6) = "OIL INLET        "
    TCPROBE$(7) = "EXHAUST          "
    TCPROBE$(8) = "HYDROGEN         "
    TCPROBE$(9) = "INJECTOR BASE    "
    LOCATE 6, 1
    FOR I% = 1 TO 9
    PRINT USING "##  &   = ###.# °C"; I%; TCPROBE$(I%); T(I%)
    NEXT I%
    LOCATE 15, 1
    PRINT USING "    CJC TEMPERATURE     = ###.# °C"; CJC
    ' read lambda probe results
    GAIN% = 2
    CHANNEL% = 1
    N = NVL
    GOSUB 700
    LAMVAR = VOLTS
    PRINT
    PRINT USING "    VARIABLE LAMBDA     = #.### Volts"; LAMVAR
    GAIN% = 4
    CHANNEL% = 2
    N = NFL
    GOSUB 700
    LAMFIXED = VOLTS
    PRINT
    PRINT USING "    FIXED LAMBDA        = #.### Volts"; LAMFIXED
    LOCATE 21, 1
    PRINT "     Press any key to continue "
    IF INKEY$ = "" THEN GOTO 890
980 LOCATE 21, 1
    PRINT USING "  Data will be saved to &.TCD "; SAVEFNAM$
    PRINT "  Press enter to continue or"
    INPUT "  M to return to main menu "; REPTCD$
    IF REPTCD$ = "" THEN GOTO 990
    IF REPTCD$ = "M" OR REPTCD$ = "m" THEN GOTO 999
    GOTO 980
```

```
990  OPEN (SAVEFNAM$ + ".TCD") FOR OUTPUT AS #5
     FOR I% = 1 TO 9
     PRINT #5, USING "  &    = ###.# °C"; TCPROBE$(I%); T(I%)
     NEXT I%
     PRINT #5, USING "    CJC TEMPERATURE     = ###.# °C"; CJC
     PRINT #5, USING "    VARIABLE LAMBDA     = #.### Volts"; LAMVAR
     PRINT #5, USING "    FIXED LAMBDA        = #.### Volts"; LAMFIXED
     CLOSE #5
999  RETURN
1000 ' Subroutine to convert EXP-20 channels to number of bits
     ' Select each EXP-20 channel in turn and convert it.
     ' Digital outputs OP1-4 drive the EXP-20 sub-multiplexer address, so use
     ' mode 15 to set up the sub-multiplexer channel.
     FOR MUX% = 1 TO 6          ' note use of integer index MUX%
     MD% = 15
     DIO%(0) = MUX%    ' DAS-20 digital output to set EXP channel
     CALL DAS20(MD%, VARPTR(DIO%(0)), FLAG%)         ' address set
     IF FLAG% <> 0 THEN PRINT "ERROR IN EXP-20 CHANNEL NUMBER":
       END
     J% = 0
     FOR I% = 1 TO 200
     J% = J% + 1
     NEXT I%
     ' Now that channel is selected, perform A/D conversion using mode 3.
     ' Transfer data to corresponding array element D%(MUX%)
     D&(MUX%) = 0
     FOR I% = 1 TO N
       MD% = 3: DIO%(0) = 5: DIO%(1) = 0  ' do 1 A/D conversion
       CALL DAS20(MD%, VARPTR(DIO%(0)), FLAG%)
       D&(MUX%) = D&(MUX%) + DIO%(0)
       IF FLAG% <> 0 THEN PRINT "ERROR IN PERFORMING A/D
         CONVERSION"
     NEXT I%
     D%(MUX%) = D&(MUX%) \ N
     ' Now repeat sequence for all other EXP-20 channels
     NEXT MUX%
     MUX% = 7    ' note use of integer index MUX%
     MD% = 15
     DIO%(0) = MUX%    ' DAS-20 digital output to set EXP channel
     CALL DAS20(MD%, VARPTR(DIO%(0)), FLAG%)        ' address set
     IF FLAG% <> 0 THEN PRINT "ERROR IN EXP-20 CHANNEL NUMBER":
        END
     ' Now that channel is selected, perform A/D conversion using mode 3.
     ' Transfer data to corresponding array element D%(MUX%)
     D&(MUX%) = 0
     FOR I% = 1 TO N
     MD% = 3: DIO%(0) = 3: DIO%(1) = 0  ' do 1 A/D conversion
```

```
    CALL DAS20(MD%, VARPTR(DIO%(0)), FLAG%)
    D&(MUX%) = D&(MUX%) + DIO%(0)
    IF FLAG% < > 0 THEN PRINT "ERROR IN PERFORMING A/D
      CONVERSION"
    NEXT I%
    D%(MUX%) = D&(MUX%) \ N
    FOR MUX% = 8 TO 9   ' note use of integer index MUX%
    MD% = 15
    DIO%(0) = MUX%    ' DAS-20 digital output to set EXP channel
    CALL DAS20(MD%, VARPTR(DIO%(0)), FLAG%)       ' address set
    IF FLAG% < > 0 THEN PRINT "ERROR IN EXP-20 CHANNEL NUMBER":
      END
    ' Now that channel is selected, perform A/D conversion using mode 3.
    ' Transfer data to corresponding array element D%(MUX%)
    D&(MUX%) = 0
    FOR I% = 1 TO N
      MD% = 3: DIO%(0) = 5: DIO%(1) = 0  ' do 1 A/D conversion
      CALL DAS20(MD%, VARPTR(DIO%(0)), FLAG%)
      D&(MUX%) = D&(MUX%) + DIO%(0)
      IF FLAG% < > 0 THEN PRINT "ERROR IN PERFORMING A/D
        CONVERSION"
    NEXT I%
    D%(MUX%) = D&(MUX%) \ N
    ' Now repeat sequence for all other EXP-20 channels
    NEXT MUX%
    ' All done - return from subroutine
    RETURN
1100 ' Table lookup data for K type thermocouple
    ' Run this subroutine only in the initialization section of a program
    ' Number of points, voltage step interval (mV), starting voltage (mV)
    DATA  309 ,  .2 , -6.6
    READ NK, SIK, SVK
    ' Temperature at -6.6mv, -6.4mV, -6.2mV etc.
1200
DATA -353.5,-249.3,-224.0,-207.6,-194.3,-182.8,-172.3,-162.8,-153.8,-145.4
DATA -137.3,-129.6,-122.3,-115.2,-108.3,-101.6, -95.1, -88.7, -82.5, -76.4
DATA  -70.4, -64.6, -58.8, -53.1, -47.5, -42.0, -36.6, -31.2, -25.9, -20.6
DATA  -15.4, -10.2,  -5.1,  -0.0,   5.0,  10.1,  15.1,  20.0,  25.0,  29.9
DATA   34.8,  39.7,  44.6,  49.5,  54.3,  59.1,  64.0,  68.8,  73.6,  78.4
DATA   83.2,  88.0,  92.9,  97.7, 102.5, 107.4, 112.2, 117.1, 122.0, 126.9
DATA  131.8, 136.7, 141.7, 146.6, 151.6, 156.5, 161.5, 166.5, 171.5, 176.5
DATA  181.6, 186.6, 191.6, 196.6, 201.6, 206.6, 211.6, 216.6, 221.5, 226.5
DATA  231.5, 236.4, 241.4, 246.3, 251.2, 256.1, 261.0, 265.9, 270.8, 275.6
DATA  280.5, 285.3, 290.2, 295.0, 299.8, 304.6, 309.4, 314.3, 319.1, 323.9
DATA  328.7, 333.4, 338.2, 343.0, 347.8, 352.6, 357.3, 362.1, 366.9, 371.6
DATA  376.4, 381.1, 385.9, 390.6, 395.4, 400.1, 404.8, 409.6, 414.3, 419.0
DATA  423.8, 428.5, 433.2, 437.9, 442.6, 447.3, 452.0, 456.8, 461.5, 466.2
```

```
DATA  470.9, 475.6, 480.3, 485.0, 489.7, 494.4, 499.1, 503.8, 508.5, 513.1
DATA  517.8, 522.5, 527.2, 531.9, 536.6, 541.3, 546.0, 550.7, 555.4, 560.0
DATA  564.7, 569.4, 574.1, 578.8, 583.5, 588.2, 592.9, 597.6, 602.3, 607.0
DATA  611.7, 616.4, 621.2, 625.9, 630.6, 635.3, 640.0, 644.8, 649.5, 654.2
DATA  658.9, 663.7, 668.4, 673.2, 677.9, 682.7, 687.4, 692.2, 696.9, 701.7
DATA  706.5, 711.3, 716.1, 720.8, 725.6, 730.4, 735.2, 740.0, 744.8, 749.7
DATA  754.5, 759.3, 764.1, 769.0, 773.8, 778.7, 783.5, 788.4, 793.3, 798.1
DATA  803.0, 807.9, 812.8, 817.7, 822.6, 827.5, 832.4, 837.3, 842.2, 847.2
DATA  852.1, 857.1, 862.0, 867.0, 872.0, 876.9, 881.9, 886.9, 891.9, 896.9
DATA  901.9, 906.9, 911.9, 916.9, 922.0, 927.0, 932.0, 937.1, 942.2, 947.2
DATA  952.3, 957.4, 962.5, 967.6, 972.7, 977.8, 982.9, 988.0, 993.1, 998.2
DATA 1003.4,1008.5,1013.7,1018.8,1024.0,1029.2,1034.4,1039.6,1044.8,1050.0
DATA 1055.2,1060.4,1065.6,1070.8,1076.1,1081.3,1086.6,1091.9,1097.2,1102.4
DATA 1107.7,1113.0,1118.3,1123.7,1129.0,1134.3,1139.7,1145.0,1150.4,1155.8
DATA 1161.2,1166.6,1172.0,1177.4,1182.9,1188.3,1193.8,1199.2,1204.7,1210.2
DATA 1215.7,1221.2,1226.8,1232.3,1237.9,1243.5,1249.1,1254.7,1260.3,1265.9
DATA 1271.6,1277.3,1282.9,1288.6,1294.3,1300.1,1305.8,1311.5,1317.3,1323.1
DATA 1328.9,1334.7,1340.5,1346.4,1352.2,1358.1,1363.9,1369.8,1375.7
    DIM TK(NK - 1): RESTORE 1200
    FOR I% = 0 TO NK - 1: READ TK(I%): NEXT I%
    RETURN
1300 ' Interpolation routine to find K thermocouple temperature
    ' Entry variables:-
    '    CJC = cold junction compensator temperature in deg. C.
    '     V = thermocouple voltage in volts
    ' Exit variables:-
    '     TC = temperature in degrees Centigrade
    '     TF = temperature in degrees Fahrenheit
    ' Execution time on std. IBM P.C. = 46 milliseconds
    ' Perform CJC compensation for K type
    VK = 1000 * V + 1! + (CJC - 25) * .0405    'VK in mV
    ' Find look up element
    EK = INT((VK - SVK) / SIK)
    IF EK < 0 THEN TC = TK(0): GOTO 1400
    ' If Out of bounds, round to lower limit
    IF EK > NK - 2 THEN TC = TK(NK - 1): GOTO 1400
    ' If Out of bounds, round to upper limit
    ' Do interpolation
    TC = TK(EK) + (TK(EK + 1) - TK(EK)) * (VK - EK * SIK - SVK) / SIK
    ' Temperature Centigrade
1400  RETURN
1500 ' Set programmable timer to output desired sample rate
    '       SAMPLE RATE = 5,000,000 / (DIO%(0) * DIO%(1))
    ' NOTE.. if DIO%(1) is 0 then only 16 bits of counter is used
    '       and SAMPLE RATE=5,000,000/dio%(0)
    DIO%(0) = 5000000 / SAMPRATE!
    DIO%(1) = 0                    ' since 0 16 bit counter used
```

```
    MD% = 24                    ' adc pacer timer set mode
    CALL DAS20(MD%, VARPTR(DIO%(0)), FLAG%)
    IF FLAG% <> 0 THEN PRINT "Error in setting timer. Error # "; FLAG%:
      STOP
    RETURN
1600 CLS
    COLOR 10
    GRPH$(1) = "Piezo"
    GRPH$(2) = "Valve lift"
    GRPH$(3) = "Both"
    FUELTYPE$(1) = "Petrol"
    FUELTYPE$(2) = "Hydrogen"
    PRINT "      VIEW/MODIFY INPUT VARIABLES"
    PRINT
    PRINT
    COLOR 11
    PRINT USING " 1  ENGINE SPEED       =  ##.# rev/s"; RPS!
    PRINT USING " 2  COMPRESSION RATIO  =  ##.#"; CR!
    PRINT USING " 3  FUEL               =  &"; FUELTYPE$(FUEL%)
    PRINT USING " 4  GRAPH DISPLAY      =  &"; GRPH$(OPTN%)
    PRINT USING " 5  NUMBER OF CYCLES   =  ##.#"; CYCNO!
    PRINT USING " 6  NUMBER OF DATA PTS =  #####"; NDISP%
    PRINT USING " 7  SAVE FILE NAME     =  &"; SAVEFNAM$
1650 LOCATE 19, 1
    PRINT "  Press enter to accept data or"
    INPUT "  Select an item to edit "; REPLY$
    PRINT
    IF REPLY$ = "" THEN REPLY% = 13: GOTO 1655
    REPLY% = ASC(REPLY$)
1655 IF REPLY% = 13 THEN GOTO 1700
    IF REPLY% < 49 OR REPLY% > 55 THEN GOTO 1650
    IF REPLY% = 49 THEN GOTO 1660
    IF REPLY% = 50 THEN GOTO 1670
    IF REPLY% = 51 THEN GOTO 1680
    IF REPLY% = 52 THEN GOTO 1690
    IF REPLY% = 53 THEN GOTO 1692
    IF REPLY% = 54 THEN GOTO 1694
    IF REPLY% = 55 THEN GOTO 1696
1660 INPUT "  Enter engine speed (rev/s) "; RPS!: GOTO 1600
1670 INPUT "  Enter compression ratio    "; CR!: GOTO 1600
1680 IF FUEL% = 1 THEN fueltemp% = 2
    IF FUEL% = 2 THEN fueltemp% = 1
    FUEL% = fueltemp%
    GOTO 1600
1690 IF OPTN% = 1 THEN OPTNTEMP% = 2
    IF OPTN% = 2 THEN OPTNTEMP% = 3
    IF OPTN% = 3 THEN OPTNTEMP% = 1
```

```
    OPTN% = OPTNTEMP%
    GOTO 1600
1692 LOCATE 22, 1
    PRINT "  Enter number of cycles to"
    INPUT "  display  (1-20)  "; CYCNO!
    IF CYCNO! < 1 OR CYCNO > 20 THEN GOTO 1692
    GOTO 1600
1694 LOCATE 22, 1
    PRINT "  Enter number of data points to display"
    INPUT "  from trigger  (200-10000)  "; NDISP%
    IF NDISP% < 200 OR NDISP% > 10000 THEN GOTO 1694
    GOTO 1600
1696 LOCATE 22, 1
    PRINT "  Enter file name for results "
    INPUT "  no extension is required   "; SAVEFNAM$
    GOTO 1600
1700 OPEN "RICARDO.CFG" FOR OUTPUT AS #5
    PRINT #5, RPS!; CR!; FUEL%, OPTN%, CYCNO!, NDISP%, SAVEFNAM$
    CLOSE #5
    RETURN
1900 COUNTER% = 1
1901 CLS
    PRINT " HYDROGEN MASS FLOW CALC"
    LOCATE 15, 1
    PRINT USING "  Data will be saved to &.MFR"; SAVEFNAM$
    PRINT "  Press enter to continue or M "
    INPUT "  to return to main menu "; REPMFR$
    IF REPMFR$ = "" THEN GOTO 1909
    IF REPMFR$ = "M" OR REPMFR$ = "m" THEN RETURN
    GOTO 1901
1909 STARTIME$ = TIME$ ' variable use to determine timing of samples
1910 GAINEXP% = 100
    GAIN% = 0
    EXPCHANL% = 13
    N = NPT
    GOSUB 800
    HPRES!(COUNTER%) = VOLTS * 1319 - .5169
    N = NTC
    EXPCHANL% = 8
    GAIN% = 5
    GOSUB 800
    V = VOLTS
    MD% = 3
    DIO%(0) = 2          ' DAS-20 gain X1 range unipolar 0 TO 10 V
    DIO%(1) = 7          ' DAS-20 channel to convert
    CJC = 0
    N = NTC
```

```
    FOR I% = 1 TO N
    CALL DAS20(MD%, VARPTR(DIO%(0)), FLAG%)
    ' Change output in bits to real temperature
    CJC = CJC + DIO%(0) * .012207
    NEXT I%
    CJC = CJC / N
    GOSUB 1300
    HTC!(COUNTER%) = TC
    LOCATE 10, 1
    PRINT USING " ##### press = ###.##  temp = ###.##";
      COUNTER%; HPRES!(COUNTER%); TC
    HKY = 1                      'This delay loop causes the temperature and
    FOR K% = 1 TO 20000          'pressure data to be captured at intervals of
    HKY = HKY * 1                ' approximately 0.84 seconds.
    NEXT K%                      ' The start and end times are recorded in the
                                 ' data file for calculating exact interval.
    COUNTER% = COUNTER% + 1
    IF INKEY$ = "" AND COUNTER% < (NHMFR + 1) GOTO 1910
    ENDTIME$ = TIME$      ' Variable used to determine timing of samples
    OPEN (SAVEFNAM$ + ".MFR") FOR OUTPUT AS #9 ' Open MFR data file
    PRINT #9, STARTIME$                ' Print start time to file
    FOR I% = 1 TO (COUNTER% - 1)       ' For the number of records taken
    PRINT #9, HPRES!(I%); HTC!(I%)     ' Print pressure and temperature
    NEXT I%                            ' records to file
    PRINT #9, ENDTIME$                 ' Print end time to file
    CLOSE #9                           ' Close MFR data file
2000 RETURN
2100 SCREEN 0
    WIDTH 40, 25
    CLS
    COLOR 10
    PRINT "      DISPLAY PIEZO AND LIFT DATA"
    PRINT
    PRINT
    COLOR 11
    IF OPTN% = 1 THEN L% = 6: U% = 3: C% = 1
    IF OPTN% = 2 THEN L% = 5: U% = 5: C% = 1
    IF OPTN% = 3 THEN L% = 6: U% = 3: C% = 2
2110 DIO%(0) = L%                  ' set channel
    DIO%(1) = U%                   ' set gain range
    DIO%(2) = C%                   ' set command
    MD% = 1                        ' mode 1 - set scan sequence
    CALL DAS20(MD%, VARPTR(DIO%(0)), FLAG%)
    IF FLAG% <> 0 THEN PRINT "Error #"; FLAG%; " in setting scan ": STOP
    IF C% = 2 THEN L% = 5: U% = 5: C% = 1: GOTO 2110
2200 SAMPRATE! = (RPS! * 10000) / (CYCNO! * 2)
    IF SAMPRATE! <= 100000 THEN GOTO 2210
```

```
    CYCNO! = RPS! / (20)
    PRINT
    PRINT USING "  Sorry only ##.# cycles "; CYCNO!
    PRINT USING "  can be stored at ##.# rev/s"; RPS!
    SAMPRATE! = 100000
    PRINT
    PRINT "  Press Enter to continue or "
    PRINT "  any other key to return to "
    INPUT "  the main menu  "; REPLY$
    IF REPLY$ <> CHR$(13) THEN GOTO 4000
2210 GOSUB 1500
    ' Analog trigger
    DIO%(0) = 4       ' channel 4
    DIO%(1) = 200     ' trigger level 1 volts
    DIO%(2) = 0       ' slope positive
    MD% = 16
    CALL DAS20(MD%, VARPTR(DIO%(0)), FLAG%)
    ' Now set A/D conversions and D.M.A. going using mode 6
    DIO%(0) = 10000     ' Total number of conversions
    DIO%(1) = APTR%     ' Memory segment to dump data
    DIO%(2) = 2         ' 0 =trigger external
                        ' 1 internal pace ,external gate
                        ' 2 internal pace start NOW
    DIO%(3) = 1         ' 1 = One shot and finish
                        ' 0 = Continuous scanning
    MD% = 6             ' mode 6 - A/D conversions using D.M.A.
    CALL DAS20(MD%, VARPTR(DIO%(0)), FLAG%)  ' set it going
    IF FLAG% <> 0 THEN PRINT "Error in mode 6 setup = "; FLAG%
    IF FLAG% = 62 THEN PRINT DIO%(1): STOP ' any errors?
    ' Set N = Total number of conversions requested
    N = DIO%(0)
    ' Retrieve data to arrays DT%(*) and CH%(*) using mode 13"
    MD% = 13
    DIO%(0) = 10000             ' number of words to transfer
    DIO%(1) = APTR%             ' memory segment to transfer from
    DIO%(2) = 0                 ' start transferring at conversion 0
    DIO%(5) = 1                 ' bipolar data
    DIO%(4) = VARPTR(CH%(0))          ' location of CH%(*) array
    DIO%(3) = VARPTR(DT%(0))          ' location of DT%(*) array
    CALL DAS20(MD%, VARPTR(DIO%(0)), FLAG%)    ' make transfer
    IF FLAG% <> 0 THEN PRINT "Mode 13 data transfer error # "; FLAG%:
       STOP
    ' save/display data
    MISPOINTS% = (SAMPRATE! / (RPS! * 360)) * (16 - RPS! * .133)
    SCREEN 9
    ' View port sized to proper scale for graph:
    VIEW (20, 2)-(620, 300), , 1
```

```
    WINDOW (MISPOINTS, -5)-(NDISP%, 5)
    VIEW PRINT 23 TO 24          ' Scroll printed output in
                                 ' rows 23 and 24.
    COLOR 14, 9
    CLS
    ADD% = 1
    IF OPTN% = 3 THEN ADD% = 2
    PRINT "Press any key to stop display"
    LOCATE 23, 30
    CYC! = CYCNO! * NDISP% / 10000
    PRINT USING " ##### data points  ##.# rev/s  ##.#  cycles ";
      NDISP%; RPS!; CYC!
    FOR J% = MISPOINTS% TO NDISP% - 2
       LINE (J%, DT%(J%) * 10! / 4086)-(J% + ADD%, DT%(J% + ADD%) *
         10! / 4096)
       LOCATE 23, 1
       IF INKEY$ <> "" THEN GOTO 3000
    NEXT J%                      ' point to the new point.
    GOTO 2200
3000 LOCATE 23, 1
    PRINT USING "  Data will be saved to &.PIZ              "; SAVEFNAM$
    INPUT "  Press enter to continue or M to return to main menu "; REPMFR$
    IF REPMFR$ = "" THEN GOTO 3100
    IF REPMFR$ = "M" OR REPMFR$ = "m" THEN GOTO 4000
    GOTO 3000
3100 OPEN (SAVEFNAM$ + ".PIZ") FOR OUTPUT AS #4
    IF OPTN% = 3 THEN GOTO 3990
    FOR I% = MISPOINTS% TO NDISP% - 2
    VOLTS = DT%(I%) * 10! / 4096
    PRINT #4, USING "#.###"; VOLTS
    NEXT I%
    CLOSE #4
    GOTO 4000
3990 FOR I% = MISPOINTS% TO (NDISP% - 2) / 2
    J% = I% * 2
    VOLTS1 = DT%(J%) * 10! / 4096
    VOLTS2 = DT%(J% + 1) * 10! / 4096
    PRINT #4, USING "#.###   #.###"; VOLTS1; VOLTS2
    NEXT I%
    CLOSE #4
4000 SCREEN 0
    RETURN

SUB ADDRESS (DMA%(), SAMP%, ADDR%)
'  SUBROUTINE TO ALLOCATE SPACE FOR DMA TRANSFERS...
DIM a AS LONG
DIM b AS LONG
```

```
    CLS
    s = VARSEG(DMA%(0))       'GET SEGMENT ADDRESS
    o = VARPTR(DMA%(0))       'GET SEGMENT OFFSET
    IF o < 0 THEN o = o + 65536
    IF s < 0 THEN s = s + 65536
    a = s * 16 + o
    page = INT(a / 65536)
    REM   See if there will be a DMA WRAP AROUND
    b = a - (page * 65536)
    b = b + SAMP% * 2
    IF b > 65535 THEN
        a = (page + 1) * 65535
    END IF
    a = INT(a / 16)
    IF a > 32767 THEN
        ADDR% = a - 65536
    ELSE
        ADDR% = a
    END IF
END SUB
```

E.2 MFRCALC.BAS

```
' This program was written by Neil Glasson to calculate
' mass flow rates of hydrogen from engine test data. 1/8/92
' The mass flow rate data {filename}.MFR written from
' the program RICARDO.BAS was modified to include barometric
' pressure before being read as input to this program.
' This program calculates the mass flow rate by the linear
' regression of mass-time data. The Beattie-Bridgeman equation
' of state was used to determine the mass data from recorded
' pressure and temperature data. The output data is: engine
' test number, mass flow rate and R-squared value (indicating
' the validity of a linear regression).
      CLS
      DIM PRESS(1 TO 550)       ' pressure
      DIM TEMP(1 TO 550)        ' temperature
      DIM SPVOL(1 TO 550)       ' specific volume
      DIM MASS(1 TO 550)        ' mass
      DIM TIME(1 TO 550)        ' time
      DIM MASSPRED(1 TO 550)      ' mass predicted from linear regression
      DIM FILENO$(1 TO 550)     ' engine test number
      OPEN "d:\mfr\h2nos.dat" FOR INPUT AS #1
      K = 1
      DO WHILE NOT EOF(1)
          INPUT #1, FILENO$(K)          ' read in numbers indicating engine
          K = K + 1                     ' test runs to be analyzed
      LOOP
      CLOSE #1
      L = 1
      OPEN "d:\mfr\results.dat" FOR OUTPUT AS #2
200    V = .3
      STARTPNT = 20
      ENDPNT = 80
      OPEN "d:\mfr\h2" + FILENO$(L) + ".mfr" FOR INPUT AS #3
      INPUT #3, BARO!  ' input barometric pressure
      INPUT #3, STARTHOUR, STARTMIN, STARTSEC ' test start time
      I = 1
500    INPUT #3, PRESS(I), TEMP(I)  ' input pressure, temperature data
      PRESS(I) = 100 * (PRESS(I) + 1.01325 * BARO! / 760)
      TEMP(I) = 273.15 + TEMP(I)
      I = I + 1
      IF I < 101 THEN GOTO 500
      INPUT #3, ENDHOUR, ENDMIN, ENDSEC             ' test end time
```

```
      CLOSE #3
      STARTIME = STARTHOUR * 3600 + STARTMIN * 60 + STARTSEC
      ENDTIME = ENDHOUR * 3600 + ENDMIN * 60 + ENDSEC
      DURATION = ENDTIME - STARTIME          ' test duration
      INCREMENT = DURATION / (I - 1)         ' incremental time
      Ao = 20.0117                 ' Beattie-Bridgeman equation constants for
      a = -.00506                  ' hydrogen.  Calculated by Beattie and
      Bo = .02096                  ' Bridgeman[178].  Given here for more
      b = -.04359                  ' familiar units as specified by Karlekar[180]
      c = 504
      R = 8.31434                  ' gas constant for hydrogen
      MOLMASS = 2.016              ' molecular mass of hydrogen
      VOLUME = 15.418              ' litres
      ACCURACY = .00001#           ' tolerance for Newton's method
      TIME(STARTPNT) = 0
      J = STARTPNT - 1
600    J = J + 1
      v1 = V
      IF J > ENDPNT THEN GOTO 3000
      IF J > STARTPNT THEN TIME(J) = TIME(J - 1) + INCREMENT
      P = PRESS(J)
      T = TEMP(J)
      c1 = -P
      c2 = R * T
      c3 = R * T * Bo - R * c / T ^ 2 - Ao
      c4 = -R * T * Bo * b - R * Bo * c / T ^ 2 - Ao * a
      c5 = R * Bo * b * c / T ^ 2
      ' using Newton's method to solve the Beattie-Bridgeman equation
1000   f = c1 * v1 ^ 4 + c2 * v1 ^ 3 + c3 * v1 ^ 2 + c4 * v1 + c5
      df = 4 * c1 * v1 ^ 3 + 3 * c2 * v1 ^ 2 + 2 * c3 * v1 + c4
      v2 = v1 - f / df
      IF ABS(v2 - v1) < ACCURACY THEN GOTO 2000
      v1 = v2
      GOTO 1000
2000   VSPEC = v1
      ' having found the molar specific volume
      MASS(J) = VOLUME * MOLMASS / VSPEC
      GOTO 600
3000   ' linear regression analysis
      ' as described in Kreysig[181] pg 985
      N = ENDPNT - STARTPNT + 1
      I = STARTPNT
      SUMTIME = 0
      SUMMASS = 0
      SUMTIME2 = 0
      SUMTMASS = 0
4000   SUMTIME = SUMTIME + TIME(I)
```

```
      SUMMASS = SUMMASS + MASS(I)
      SUMTIME2 = SUMTIME2 + TIME(I) ^ 2
      SUMTMASS = SUMTMASS + TIME(I) * MASS(I)
      I = I + 1
      IF I < ENDPNT + 1 THEN GOTO 4000
      S12 = 1 / (N - 1) * (SUMTIME2 - (1 / N) * SUMTIME ^ 2)
      STM = 1 / (N - 1) * (SUMTMASS - (1 / N) * SUMTIME * SUMMASS)
      MFR = -STM / S12
      I = STARTPNT - 1
      RESUMSQR = 0
      TOTSMSQR = 0
5000   I = I + 1
      MASSPRED(I) = -MFR * TIME(I) + MFR * SUMTIME/N + SUMMASS/N
      RESUMSQR = RESUMSQR + (MASS(I) - MASSPRED(I)) ^ 2
      TOTSMSQR = TOTSMSQR + (MASSPRED(I) - SUMMASS / N) ^ 2
      IF I < ENDPNT THEN GOTO 5000
      RSQUARED = 1 - RESUMSQR / TOTSMSQR
      IF MFR < .05 OR RSQUARED < .98 THEN PRINT #2, : GOTO 5500
      PRINT #2, FILENO$(L), MFR, RSQUARED  ' write results to file
5500   PRINT FILENO$(L)
      L = L + 1
      IF FILENO$(L) <> "140" THEN GOTO 200
      CLOSE #2
```

E.3 RICLABH2.BAS

```
' Program to perform calculations for experimental runs on
' the Ricardo E6 spark ignition engine  H.J.Anink. May 1986
' Converted from Basica to Quickbasic 4.5 in Dec 1991 and
' modified for hydrogen engine calculations.
    DIM INJSTRT(30), ATEMP(30), AMTER(30), TIME(30), LOAD(30), BAL(30)
    DIM RPS(30), IGN(30), EXT(30), TORQUE(30), POWER(30), TC(30)
    DIM FC(30), SFC(30), AIRFL(30), AIRFU(30), BTE(30), INJEND(30)
    DIM MFROPEN(30)
    LCV = 119930! ' in gasoline program LCV = 44700!: SG = 0.73
    CLS
    PRINT "Ricardo E6 hydrogen engine test result analysis"
    GOSUB 1000          ' load lookup table for air mass flow meter correction
                        ' factors
100  LOCATE 10, 1
    DAT$ = DATE$
    INPUT "No of runs----------"; NRUNS
    INPUT "BAROMETRIC PRESSURE (mm Hg)-------"; ATM
    PRINT : INPUT "ARE THESE ENTRIES CORRECT Y/N"; B$
    IF B$ = "N" OR B$ = "n" THEN 100
    FOR N = 1 TO NRUNS
    ' input the engine test data
200  PRINT : PRINT : PRINT
    PRINT "Run No."; N: PRINT
    INPUT "ENGINE SPEED   RPS ----------"; RPS(N)
    INPUT "INJECTOR START  °ATDC ----------"; INJSTRT(N)
    INJSTRT(N) = 360 - INJSTRT(N)
    INPUT "INJECTOR END  °ATDC ----------"; INJEND(N)
    INJEND(N) = 360 - INJEND(N)
    INJDUR(N) = 1000 * ((INJSTRT(N) - INJEND(N)) / 360) / RPS(N)
    INPUT "FUEL FLOW RATE  g/s ----------"; FC(N)
    MFROPEN(N) = FC(N) / ((INJSTRT(N) - INJEND(N)) / 720)
    INPUT "AIR TEMPERATURE  °C ----------"; ATEMP(N)
    GOSUB 2000    ' find air mass flow meter correction factor
    PRINT "AIR TEMPERATURE CORRECTION FACTOR "; TC(N)
    INPUT "AIRMETER MANOMETER   mm ----------"; AMTER(N)
    INPUT "NUMBER OF WEIGHTS ----------"; LOAD(N)
    INPUT "SPRING BALANCE   N ----------"; BAL(N)
    INPUT "IGNITION TIMING  °ATDC ----------"; IGN(N)
    IGN(N) = 360 - IGN(N)
    INPUT "EXHAUST TEMPERATURE  °C ----------"; EXT(N)
    PRINT : INPUT "ARE THESE ENTRIES CORRECT"; A$
```

```
    IF A$ = "N" OR A$ = "n" THEN 200
    NEXT N
    CLS
    PRINT "Results being written to file"
    FOR N = 1 TO NRUNS
    X = 20.15 * LOAD(N) - BAL(N)
    TORQUE(N) = X * .457
    POWER(N) = X * RPS(N) / 348.1
    SFC(N) = (FC(N) * 3.6 / POWER(N))
    VOL = TC(N) * .000077 * AMTER(N) * 3600
    AIRFL(N) = VOL * (273.15 / (273.15 + ATEMP(N))) * (ATM / 760) * 1.293
    AIRFL(N) = AIRFL(N) * 1000 / 3600
    AIRFU(N) = AIRFL(N) / FC(N)
    LAMBDA(N) = AIRFU(N) / 34.3
    BTE(N) = POWER(N) * 360000! / (FC(N) * 3.6 * LCV)
    NEXT N
    OPEN "C:\WORK\TEMP.CLC" FOR OUTPUT AS #1
    FOR N = 1 TO NRUNS
    PRINT #1, 1.01325 * (ATM / 760)     ' barometric pressure
    PRINT #1, RPS                       ' engine speed
    PRINT #1, INJSTRT(N)                ' injector pulse start
    PRINT #1, INJEND(N)                 ' injector pulse end
    PRINT #1, FC(N)                     ' fuel mass flow rate
    PRINT #1, ATEMP(N)                  ' inlet air temperature
    PRINT #1, AMTER(N)                  ' air flow meter manometer reading
    PRINT #1, LOAD(N)                   ' number of weights on
                                        ' dynamometer
    PRINT #1, BAL(N)                    ' balance reading on dynamometer
    PRINT #1, IGN(N)                    ' ignition timing
    PRINT #1, EXT(N)                    ' exhaust temperature
    PRINT #1, TORQUE(N)                 ' torque
    PRINT #1, POWER(N)                  ' brake power
    PRINT #1, SFC(N)                    ' brake specific fuel consumption
    PRINT #1, AIRFL(N)                  ' air mass flow rate
    PRINT #1, AIRFU(N)                  ' air/fuel ratio
    PRINT #1, LAMBDA(N)                 ' λ
    PRINT #1, BTE(N)                    ' brake thermal efficiency
    PRINT #1, INJDUR(N)                 ' injection pulse duration
    PRINT #1, MFROPEN(N)                ' mass flow rate during injection
                                        ' pulse
    PRINT #1, CHR$(12)
    NEXT N
    CLOSE #1
    END
1000 DATA 31,1,10                   ' data for viscous flow air meter temperature
    READ NAC, SIAC, SVAC            ' correction factor calculation
1100 DATA 1.027,1.024,1.022,1.019,1.016,1.013,1.011,1.008,1.005,1.003,1.000
```

```
    DATA .997,.995,.992,.99,.987,.984,.982,.979,.977,.974,.972,.969,.967
    DATA .964,.962,.959,.957,.955,.952,.950
    DIM ACF(NAC - 1): RESTORE 1100
    FOR I% = 0 TO NAC - 1: READ ACF(I%): NEXT I%
    RETURN
2000 ATC = INT((ATEMP(N) - SVAC) / SIAC)
    TC(N) = ACF(ATC) + (ACF(ATC + 1) - ACF(ATC)) * (ATEMP(N) - ATC *
      SIAC - SVAC) / SIAC
    RETURN
```

E.4 ANALYSIS.BAS

```
' Program written in March 1992 for the analysis of combustion
' chamber pressure and valve needle displacement data. The program
' reads data from the {filename}.PIZ files written from RICARDO.BAS
' and displays the data graphically on screen. The data point numbers
' corresponding to probable ignition timing spikes on the displacement
' trace are then presented for user verification. The program
' computes the crank angle associated with each data point. This
' information is used to calculate pressure-volume data which is
' displayed on screen and written to a data file. The pressure-volume
' data is also used to calculate the indicated mean effective pressure,
' peak pressure and related information. This data is written to a
' separate data file.
    DECLARE FUNCTION ASIN! (ANG!) ' declare the inverse sine function
    DIM PIZ!(1 TO 5000), LIFT!(1 TO 5000), IGNPOINT%(1 TO 100)
    DIM RADCA!(1 TO 5000), VOLUME!(1 TO 5000)
    CLS   ' input information on the engine test
    INPUT "ENTER THE HYDROGEN ENGINE RUN NUMBER "; RUNNO$
    INPUT "ENTER THE ENGINE SPEED IN RPS        "; RPS!
    INPUT "ENTER THE IGNITION TIMING BTDC       "; BTDC!
    OPEN "A:\H2" + RUNNO$ + ".PIZ" FOR INPUT AS #1
    DATANO% = 1
    DO WHILE NOT EOF(1) AND DATANO% < = 5000
    INPUT #1, PIZ!(DATANO%), LIFT!(DATANO%)
    DATANO% = DATANO% + 1
    LOOP
    CLOSE #1
    REM SCREEN 9                        ' this setup for EGA screen
    SCREEN 3                            ' this setup for HERC screen
    ' View port sized to proper scale for graph:
    REM VIEW (20,2)-(640,200), , 1      ' this setup for EGA screen
    VIEW (20, 2)-(710, 160)             ' this setup for HERC screen
    WINDOW (0, 0)-(5000, 5)
    VIEW PRINT 16 TO 24                 ' Scroll printed output in
                                        ' rows 23 and 24.
    REM COLOR 14, 9
    CLS
    FOR I% = 0 TO 10
    LINE (I% * 500, 0)-(I% * 500, 5)
    REM ,4
    NEXT I%
    FOR j% = 1 TO DATANO%
```

```
      LINE (j%, LIFT!(j%))-(j% + 1, LIFT!(j% + 1))
   NEXT j%                          ' point to the new point.
50  LOCATE 16, 1
   ' test for spikes in the valve needle displacement trace
   INPUT "ENTER IGNITION POINT TOLERANCE "; TOL!
   j% = 0
   FOR I% = 2 TO 5000
   IF (LIFT!(I% - 1) - LIFT!(I%)) > TOL! THEN j% = j% + 1:
     IGNPOINT%(j%) = I%
   IF j% = 99 GOTO 100
   NEXT I%
100  FOR I% = 1 TO j%
   PRINT I%, IGNPOINT%(I%)
   IF I% MOD 7 = 0 THEN INPUT "PRESS A KEY TO CONTINUE"; a$
   NEXT I%
150  LOCATE 23, 1
   INPUT "PRESS C TO CONTINUE OR R TO RECALCULATE"; REPLY$
   IF REPLY$ = "C" OR REPLY$ = "c" THEN GOTO 200
   IF REPLY$ = "R" OR REPLY$ = "r" THEN GOTO 50
   GOTO 150
   ' prompt user for input of ignition spike location
200  INPUT "ENTER THE FIRST  IGNITION DATA POINT NUMBER"; FST%
   INPUT "ENTER THE SECOND IGNITION DATA POINT NUMBER"; SEC%
   FSTPNT% = IGNPOINT%(FST%)
   SECPNT% = IGNPOINT%(SEC%)
   CLS
   PI# = 3.1415927#
   CYCL% = SECPNT% - FSTPNT%
   INCR# = (4 * PI#) / CYCL%  ' crank angle increment in radians
   BTDCRAD! = (BTDC! * (2 * PI#)) / 360  ' data capture start angle
   RADCA!(1) = 2 * PI# - INCR# * FSTPNT% - BTDCRAD!
   FOR I% = 1 TO DATANO%
   VOLUME!(I%) = 1000000! * (.0000507# + (PI# * (.0762 * .0762) / 4) *
     (.2965625# - .241 * SIN(PI# - (ASIN!(.0555625# * SIN(RADCA!(I%))
     / .241)) - RADCA!(I%)) / SIN(RADCA!(I%))))
   IF RADCA!(I%) > 4 * PI# THEN RADCA!(I%) = RADCA!(I%) - 4 * PI#
   RADCA!(I% + 1) = RADCA!(I%) + INCR#
   NEXT I%
   DIVNO% = 0
   SUM! = 0
   FOR I% = 1 TO DATANO%
   IF ((0 < RADCA!(I%)) AND (RADCA!(I%) < PI#)) OR ((3.1 * PI# <
     RADCA!(I%)) AND (RADCA!(I%) < 4 * PI#)) THEN SUM! = SUM! +
     PIZ!(I%) * 27: DIVNO% = DIVNO% + 1
   NEXT I%
   POFFSET! = (SUM! / DIVNO%) - 1
   FOR I% = 1 TO DATANO%
```

```
PIZ!(I%) = PIZ!(I%) * 27 - POFFSET!
NEXT I%
VIEW (1, 1)-(710, 200)
WINDOW (0, 0)-(600, 80)
VIEW PRINT 20 TO 24          ' Scroll printed output in
                             ' rows 23 and 24.
CLS
FOR I% = 1 TO DATANO% - 1  ' display P-V diagram
LINE (VOLUME!(I%), PIZ!(I%))-(VOLUME!(I% + 1), PIZ!(I% + 1))
NEXT I%
' Calculate area of P-V diagram and find peak pressures
WORK1! = 0  'for first cycle
PEAK1! = 0
FOR I% = 2 TO CYCL%
IF 0 <= RADCA!(I%) AND RADCA!(I%) <= PI# THEN SIGN! = .1
IF PI# < RADCA!(I%) AND RADCA!(I%) <= 2 * PI# THEN SIGN! = -.1
IF 2 * PI# < RADCA!(I%) AND RADCA!(I%) <= 3 * PI# THEN SIGN! = .1
IF 3 * PI# < RADCA!(I%) AND RADCA!(I%) < 4 * PI# THEN SIGN! = -.1
WORK1! = WORK1! + SIGN! * ABS(VOLUME(I%) - VOLUME(I% - 1)) *
  (PIZ!(I%) + PIZ(I% - 1)) / 2
IF PIZ!(I%) > PEAK1! THEN PEAK1! = PIZ!(I%)
NEXT I%
WORK2! = 0  ' for second cycle
PEAK2! = 0
STARTNO% = DATANO% - CYCL% + 1
FOR I% = STARTNO% TO DATANO%
IF 0 <= RADCA!(I%) AND RADCA!(I%) <= PI# THEN SIGN! = .1
IF PI# < RADCA!(I%) AND RADCA!(I%) <= 2 * PI# THEN SIGN! = -.1
IF 2 * PI# < RADCA!(I%) AND RADCA!(I%) <= 3 * PI# THEN SIGN! = .1
IF 3 * PI# < RADCA!(I%) AND RADCA!(I%) < 4 * PI# THEN SIGN! = -.1
WORK2! = WORK2! + SIGN! * ABS(VOLUME(I%) - VOLUME(I% - 1)) *
  (PIZ!(I%) + PIZ(I% - 1)) / 2
IF PIZ!(I%) > PEAK2! THEN PEAK2! = PIZ!(I%)
NEXT I%
PEAKMAX! = PEAK1!
IF PEAK2! > PEAK1! THEN PEAKMAX! = PEAK2!
PEAKBOTH! = (PEAK1! + PEAK2!) / 2
WORKBOTH! = (WORK1! + WORK2!) / 2
IMEP1! = .00001 * WORK1! / .000507#
IMEP2! = .00001 * WORK2! / .000507#
IMEPMAX! = IMEP1!
IF IMEP2! > IMEP1! THEN IMEPMAX! = IMEP2!
IMEPBOTH! = .00001 * WORKBOTH! / .000507#
IP1! = .001 * (RPS / 2) * WORK1!
IP2! = .001 * (RPS / 2) * WORK2!
IPMAX! = IP1!
IF IP2! > IP1! THEN IPMAX! = IP2!
```

```
    IPBOTH! = .001 * (RPS / 2) * WORKBOTH!
    OPEN "D:\WORK\H2" + RUNNO$ + ".IPD" FOR OUTPUT AS #2
    PRINT #2, IMEP1!              ' IMEP of first cycle
    PRINT #2, IMEP2!              ' IMEP of second cycle
    PRINT #2, IMEPMAX!            ' maximum IMEP
    PRINT #2, IMEPBOTH!           ' average IMEP
    PRINT #2, IP1!                ' indicated power of first cycle
    PRINT #2, IP2!                ' indicated power of second cycle
    PRINT #2, IPMAX!              ' maximum indicated power
    PRINT #2, IPBOTH!             ' average indicated power
    PRINT #2, PEAK1!              ' peak pressure of first cycle
    PRINT #2, PEAK2!              ' peak pressure of second cycle
    PRINT #2, PEAKMAX!            ' maximum peak pressure
    PRINT #2, PEAKBOTH!           ' average peak pressure
    PRINT #2, FSTPNT%             ' first ignition spike data point
    PRINT #2, SECPNT%             ' second ignition spike data point
    CLOSE #2
    ' write P-V data to file indicating ignition points
    OPEN "D:\WORK\H2" + RUNNO$ + ".PVD" FOR OUTPUT AS #3
    FOR I% = 1 TO DATANO% - 1
    IF I% = FSTPNT% THEN PRINT #3, PIZ!(I%), VOLUME!(I%), PIZ!(I%):
      GOTO 2000
    IF I% = SECPNT% THEN PRINT #3, PIZ!(I%), VOLUME!(I%), PIZ!(I%):
      GOTO 2000
    PRINT #3, PIZ!(I%), VOLUME!(I%)
2000 NEXT I%
    CLOSE #3
9999

    FUNCTION ASIN! (ANG!)
      ASIN! = ATN(ANG! / (SQR(-ANG! * ANG! + 1)))
    END FUNCTION
```

APPENDIX F Performance of a Bosch gasoline injector

During the testing of the hydrogen injector it was considered useful to compare the performance of the injector with that of a commercially available gasoline injector. Little information was available on the performance of gasoline injectors so an experiment was devised to test an injector. As with the hydrogen injector, the performance of the gasoline injector was determined by recording the valve displacement response.

The injector used for the test was a Bosch gasoline injector, part number 0 280 150 201† which is specified for vehicles such as the BMW 733i. Bosch[182] provided the following details for this injector:

Operating voltage	12 V with 6 Ω resistor
Valve lift	0.1 mm
Flow rate at P = 300 kPa:	
236 cm^3/min with valve permanent open	
6.9 cm^3/1000 openings with time of opening signal ti = 2.5 ms	
Maximum time of 1.8 ms for opening	
Maximum time of 0.9 ms for closing	

† This injector is similar to the injector used on the Ricardo E6 gasoline engine (0 280 150 151). The operational specifications are identical.

A slotted optical switch (SOS) of the same type used for the hydrogen injector displacement transducer (General Instruments MST8) was used to signal the injector needle displacement. A 0.1 mm thick stainless steel flag was attached to the end of the valve needle with high strength epoxy resin so that it intersected the light beam of the SOS. The size of the 0.1 mm shim flag was minimised to ensure that it would not significantly affect the response of the needle. The test injector layout is shown in Figure F.1 with the SOS positioned so as not to be affected by the gasoline spray. The SOS location clamp is omitted from the drawing for clarity.

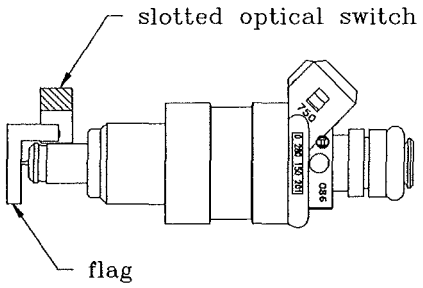

Figure F.1 Bosch injector configured for response testing.

The injector was tested both dry, and with gasoline supplied at a pressure of 2 bar from the Ricardo E6 engine fuel pump. The gasoline injector was actuated with the Ricardo injector circuit and was later tested with the hydrogen injector circuit for comparison. The signal conditioning and data acquisition system used for measuring displacement response was identical to that used for the hydrogen injector.

F.1 Injector test method

The position of the SOS was adjusted to give an output of 0.4 V with the injector closed. The output of the transducer would then decrease within the linear range as the valve opened.

Tests were performed over a range of injection pulse durations from 1ms to 6ms, corresponding to the range of durations tested on the hydrogen injector prior to engine testing.

With the Ricardo motoring in fixed speed mode to supply the injection pulse and fuel, the injector needle displacement was monitored on an oscilloscope. The voltage across the injector terminals was also displayed to indicate the relationship between the injection voltage pulse and the needle motion. When the hydrogen injector circuit was used, the solenoid current was recorded instead of the voltage. The injector was supported above a tray to collect the injected gasoline.

The displacement and voltage traces from the gasoline injector tests were transferred from the oscilloscope to a computer via a DAS-20 data acquisition system. The data was scaled to represent the appropriate units and graphs were produced.

F.2 Results and discussion

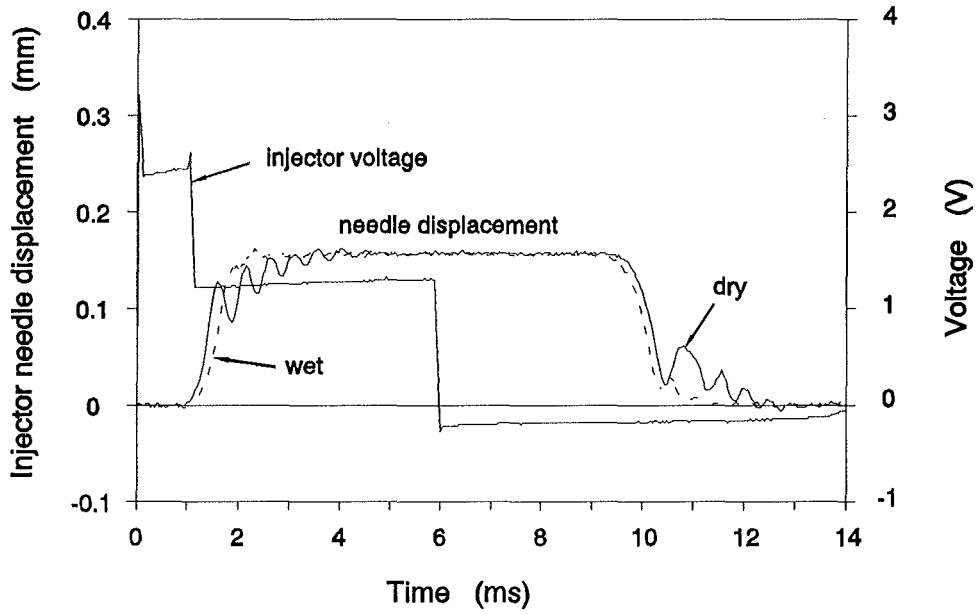

Figure F.2 Bosch gasoline injector response to a 6 ms pulse from the Ricardo injector circuit.

For the initial gasoline injector tests a pulse of 6 ms duration was supplied from the Ricardo injector circuit. The results of both wet and dry injection tests are shown in Figure F.2. The negative voltage which follows the 6 ms pulse is caused by the decay of the magnetic field in the solenoid setting up a reverse e.m.f. Operation of the valve without gasoline (dry) results in significant bouncing of the valve needle at both extremes of travel. When operated with gasoline (wet) this needle bounce is very much reduced due to fluid damping. The slower valve opening and the more rapid valve closing for the wet injection is consistent with

the additional force acting to close the needle due to the pressure of the gasoline.

The gasoline injector opening and closing times are approximately 1 ms and the delay between the start of the voltage pulse and full valve opening is close to 2 ms. There is considerable delay between the end of the voltage pulse and the completion of injection - in the order of 4 ms. Thus a 6 ms pulse results in a valve opening duration of more than 8 ms.

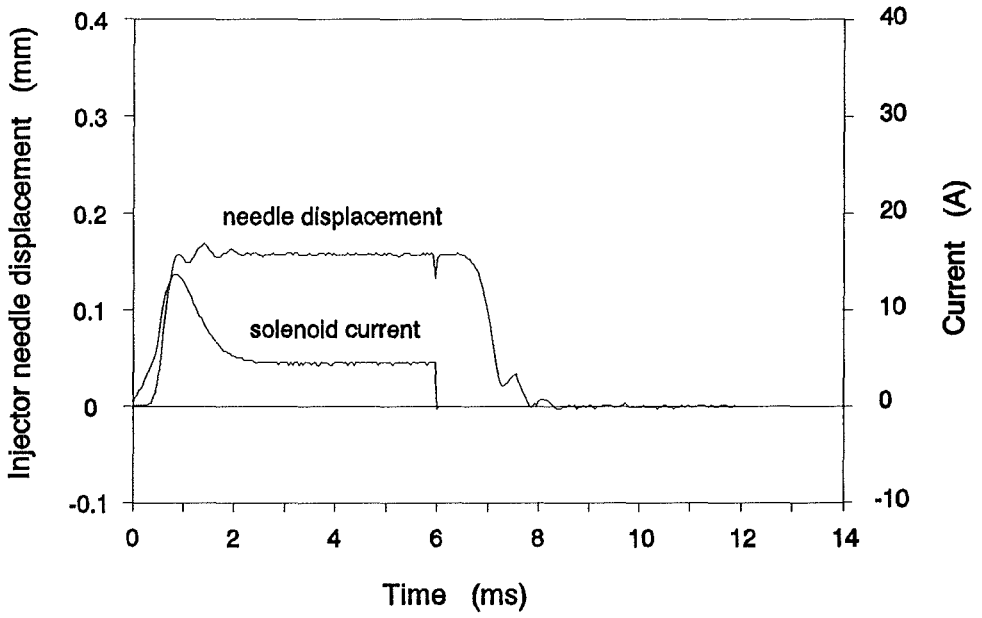

Figure F.3 Bosch gasoline injector response to a 6 ms pulse from the hydrogen injector circuit.

The gasoline injector was tested with gasoline flow for a range of injection durations using both the Ricardo injector circuit and the hydrogen injector circuit. Figure F.3 shows the result of testing the gasoline injector with a 6 ms duration pulse from the hydrogen injector circuit. The solenoid current trace is different

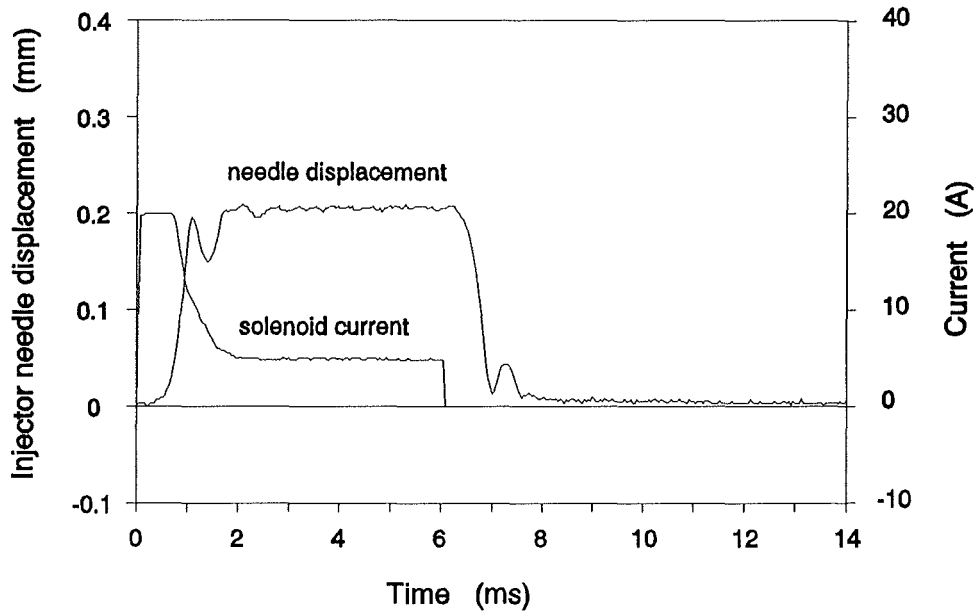

Figure F.4 Hydrogen injector response to a 6 ms pulse from the hydrogen injector circuit.

to that typical for hydrogen injection (Figure F.4) because the high voltage DC supply to the hydrogen injector circuit was greatly reduced for driving the gasoline injector. The voltage was set at 40 V for the gasoline injector whereas the voltage for the hydrogen injector was 120 V. The reason for the reduced voltage was to avoid overheating of the gasoline injector. During initial testing of the gasoline injector the voltage was gradually increased to 40 V where the injector response performance approximated that of the hydrogen injector (Figure F.4).

Comparing the results from testing the gasoline injector with the two different circuits (Figure F.2 vs Figure F.3) it can be seen that the hydrogen injector circuit

greatly enhances the response performance of the injector. The most significant difference between the two results is the great reduction in the valve closing delay. This is largely due to a design feature of the hydrogen injector circuit which rapidly drains the reverse e.m.f., thereby enhancing the magnetic field collapse. The hydrogen injector circuit also enhances the opening response of the gasoline injector due to the high initial current supply.

The bouncing of the hydrogen injector needle at the extremes of travel is more pronounced than for the gasoline injector tested with gasoline flow. This is due to the absence of liquid damping in the hydrogen injector.

Figure F.5 shows the response of the gasoline injector to the minimum injection pulse duration setting from the Ricardo injector circuit. The actual injection duration is more than twice the duration of the voltage pulse. A similar duration pulse to the hydrogen injector (Figure F.6) results in an injection duration very similar in length to the driving pulse. The response of the hydrogen injector is thus close to ideal, with an approximately linear relationship between injector driving pulse duration and injection duration.

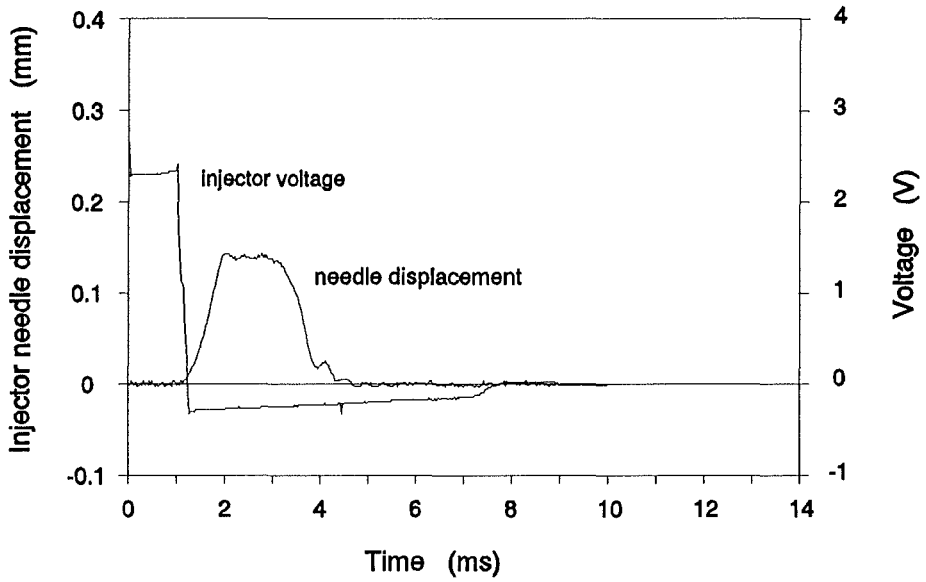

Figure F.5 Bosch gasoline injector response to the minimum duration pulse from the Ricardo injector circuit.

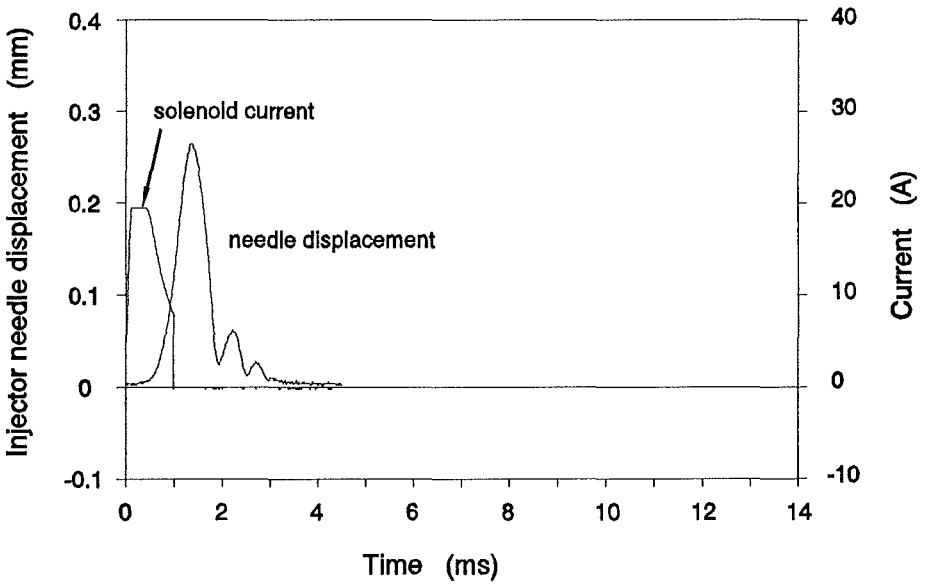

Figure F.6 Hydrogen injector response to a 1 ms pulse from the hydrogen injector circuit.

F.3 Conclusions

The performance of the injector developed for fuelling the Ricardo E6 engine on hydrogen compares favourably with the performance of a Bosch injector designed for gasoline operation.

The hydrogen injector needle bounces more than the gasoline injector needle at the extremes of travel. The likely reason for this is the absence of liquid damping in the hydrogen injector.

The circuit developed to drive the hydrogen injector gives much improved performance to the gasoline injector response. When driven by the hydrogen injector circuit, the gasoline injector demonstrated very similar response characteristics to those of the hydrogen injector.

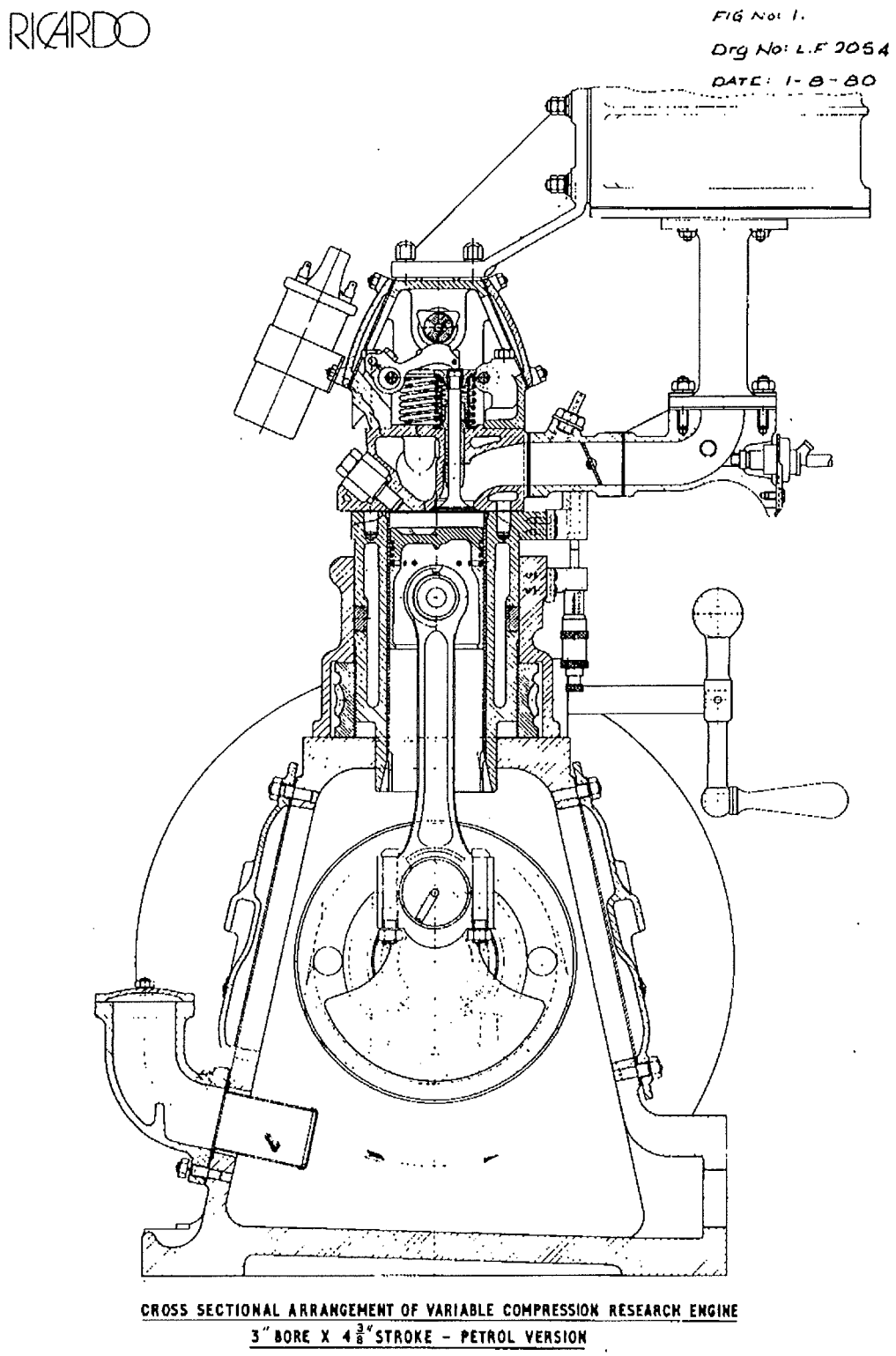

Figure G.1 Cross sectional arrangement of a Ricardo E6 variable compression research engine.

APPENDIX G Ricardo E6/Mk6 variable compression engine specification

Serial number	138/82
Number of cylinders	1
Bore	76.2 mm
Stroke	111 mm
Connecting rod length	241 mm
Swept volume	507 cm^3
Compression ratio	variable 4.5:1 - 20:1
Valve timing	
Inlet opens	8° BTDC
Inlet closes	36° ABDC
Exhaust opens	42° BBDC
Exhaust closes	8° ATDC
Gasoline pump	Bosch 0580 464 008, 12 volt
Petrol Injector	Bosch 0280 150 151
Air meter	Alcock Viscous Flow Type Serial No. 1092 V
Ignition	Lumenition MK 16
Coil	Lucas Sports Coil, No. 21949602 Li
Spark plug	Lodge HNP, 0.6 mm gap specified. Champion L54R (0.5 mm gap) used for hydrogen engine testing.
Dynamometer	BKB Swinging field 400 volt DC Serial No. 55077-3
Thermocouples	K-type